2011

Development, Evaluation and Implementation of Sensor Techniques for Bridges Critical to the National Transportation System

Ursula Mercedes Deza
Iowa State University

Development, evaluation and implementation of sensor techniques for bridges critical to the national transportation system

by

Ursula M. Deza

A dissertation submitted to the graduate faculty

in partial fulfillment of the requirements for the degree of

DOCTOR OF PHILOSOPHY

Major: Civil Engineering (Structural Engineering)

Program of Study Committee:
Terry J. Wipf, Co-major Professor
Brent M. Phares, Co-major Professor
F. Wayne Klaiber
Loren W. Zachary
Douglas D. Stokke

Iowa State University

Ames, Iowa

2011

TABLE OF CONTENTS

LIST OF FIGURES

LIST OF TABLES

ABSTRACT

The evolution of structural materials and sensor technology has impacted the bridge industry by improving the robustness of the highway network and providing behavior based condition assessments. During the last decades, conventional materials have been supplemented with state-of-the-art materials (e.g., carbon and fiber based, ultra-high performance concrete, etc.). The evolution of smart or intelligent structures by incorporating systems to quantify performance will continue to revolutionize the bridge industry. While laboratory and field applications have indicated that smart materials are appropriate for bridge applications, additional investigations regarding sensor installation, deployment and data reduction are still needed. The work described herein is a collection of field and laboratory tests in which sensors were applied to verify structural and material behavior and develop smart members for integration as part of a structural health monitoring system for bridge superstructures.

Three projects are presented in which new materials and unique structures were evaluated using specialized sensors and monitoring techniques. Two basket-handle arch pedestrian bridges with high-strength steel hanger rods supporting a pre-cast, post-tensioned concrete panel deck system were monitored to prevent deck cracks in the vicinity of the hanger rods. Fiber optic sensors and externally mounted accelerometers were attached to the hanger rods to indirectly determine the tensile forces during incremental construction stages and in service conditions. For the second project, a three-span prestressed concrete (PC) girder, composite deck bridge was monitored and evaluated. One end span consisted of composite FRP deck panels and was compared to the opposite cast-in-place reinforced concrete deck end span. Strategically placed transducers measured strain levels on the PC girders and the FRR panels from controlled live and ambient traffic loadings to determine the degree of composite action, load distribution, and maximum in-service strains. A FRP panel temporary bypass bridge was evaluated as a replacement to typical steel temporary bridges as part of the third project. The research focused on the design, fabrication, construction and load testing of this state-of-the-art bridge. This bridge was instrumented with transducers for measuring deflections and loaded with a static truck at pertinent locations to evaluate its performance.

A five year research plan was established to develop a conceptual smart timber bridge made of glued laminated (glulam) stringers and a transverse glulam deck. Both stock and custom fiber optic sensor packages were implemented to quantify the structural response. The first of multiple phases of

this national five year plan includes the development of an efficient structural health monitoring system and a smart timber bridge field demonstration. To support these goals, two types of FBG sensors packages were developed, the first evaluated the structural strain response and the second isolated the sensor from mechanical strain for detecting deterioration parameters (e.g., moisture content, corrosion, wood deterioration, etc.). Techniques were developed for embedding and attaching the FBG sensor packages to glulam specimens. Small scale specimens were instrumented with the custom FBG sensor packages and tested under a range of temperature and loading conditions to determine sensor viability. A full scale glulam beam was instrumented with similar FBG sensor packages to demonstrate applicability and evaluate performance at service level proportions.

From this work, the following contributions in structural bridge monitoring were added to the state-of-the-art:

- Application of FBG sensors and accelerometers to monitor the structural behavior of a bridge during construction.
- Applied testing of non-traditional FRP deck panels to validate composite action.
- Initial development of a smart timber bridge structural health monitoring system.
- Development of FBG sensor packages for implementation in glulam members as part of a smart timber bridge.

CHAPTER 1. INTRODUCTION

1.1. GENERAL BACKGROUND

National Bridge Inspection Standards (NBIS) have been in place since 1968. Among other responsibilities, the NBIS establishes the inspection requirements for highway bridge type and frequency, and related management activities (e.g., organizational responsibilities, personal qualifications, need for quality control and assurance, etc.) (Ampalli, 2010). The data held by the National Bridge Inventory (NBI) contain a complete source of long-term information; however, the lack of details has made these data insufficient for long-term life-cycle decision support (Chase and Ghasemi, 2003). Several research and technology programs developed by government agencies have highlighted fundamental changes for evaluating and constructing highway bridges, while reducing the number of substandard or deficient bridges in the future. In 2005, the American Association of State Highway and Transportation Officials (AASHTO) prescribed the top Grand Challenges related to bridge infrastructure problems. Two of those challenges are the need for new materials and approaches to construction and repair, and new methods to remotely and continuously monitor structural health and condition.

Most engineers report on the bridge condition based on visual observations and supported by theoretical analysis, valid for common bridge types. To determine the capacity of in-service bridges, a more effective evaluation may be required. Structural monitoring has emerged as an accurate method to evaluate the current condition of in-service bridges. With the use of advanced technology, including sensors, data acquisition equipment and data processing methods, structural monitoring has been demonstrated as an effective tool for determining bridge condition. Some typical applications of structural monitoring used by bridge engineers include:

- Re-evaluating older bridges based on new design and load evaluation specifications.
- Determining capacity for bridges with unknown or insufficient design or construction data.
- Evaluating the need to impose temporary load restrictions on damaged bridges.
- Reducing the number of bridges restricting a reasonable flow of overweight trucks.
- Verifying effectiveness of new strengthening techniques.
- Removing load restriction imposed on additional bridges due to implementation of new weight laws.

- Determining the behavior of bridges under unusually heavy loads (super loads) with calculated load rating below anticipated capacity needs.
- Monitoring critical bridge members during construction, particularly when unique construction procedures are used.
- Monitoring bridges composed of new materials or unique structural systems for which no design specifications exist.

Generally, public and private agencies have recognized the need for using bridge monitoring to support inspection and design reporting and management decisions.

While structural monitoring only diagnoses the current condition of the structure for immediate management decisions, structural health monitoring (SHM) provides the condition of a structure continuously during its service life (diagnosis) and indicates the evolution of the damage and the residual life (prognosis) of individual members and the entire structure (Balagueas et al., 2006). SHM has the capability to evaluate the structure condition modified by continuous usage and other environmental and accidental factors. During continuous monitoring, SHM can alert when the structure passes from the design domain to early deterioration or damage. The results of the reported evaluations can also be used for design considerations and management decisions not only for individual structures but also as part of a highway bridge network.

In the past century, various forms of structural health monitoring (SHM) have been used to understand the behavior and potential damage and/or deterioration of an entire structure or individual bridge members under ambient loads over time (e.g., construction, traffic, wind, earthquake, etc.) (Brownjohn, 2007; Carder, 1937; University of Washington, 1954). With the use of computer-based systems, advanced sensing technologies, and communications in the last two decades, SHM has enabled bridge engineers to continuously monitor and evaluate a bridge or bridge members for extended periods (i.e., months, years) (Doornink, 2006). The recent technological advances and proven reliability of the SHM techniques have increased the confidence of bridge owners for investing in and implementing these systems.

The success of bridge monitoring and SHM systems relies not only on the efficiency of their real-time monitoring and reporting systems but also the utilized sensing and measuring technologies. Sensors are mechanical devices that respond to physical stimuli (e.g., light, sound waves,

temperature, particular motion, etc.) and transmit that resulting energy (e.g., mechanical strain, load, pressure, etc.). There are many sensor types available on the market, such as electrical strain gages and transducers, fiber optics, dielectric measurement sensors, piezoelectric materials and micro-electromechanical systems (MEMS). Relatively recently, nanotechnology has been applied to MEMS technology and has resulted in nanoelectromechanical systems (NEMS). Sensor selection depends on the resolution, evaluation period, and level of damage detection and automation of the bridge monitoring system.

The evolution of advanced materials has impacted bridge engineering recently. To improve the bridge network, conventional have been replaced by high performance materials (e.g., composite materials, fiber reinforced polymer (FRP), etc.) that allow structures to be created with properties adapted to specific uses. Materials and structures have also been developed with the capability of sensing, diagnosing and actuating to perform their design function (Srinivasan and McFarland, 2001; Balagueas, 2006). The levels of the material "intelligence" correspond to the existence of either one, or two or three qualities (i.e., sensing, diagnosing, actuating). Most smart or intelligent materials and/or structures have the capability to respond to a changing external environment (e.g., load or shape change) as well as to a changing internal environment (e.g., damage or failure) (Chopra, 2002). The majority of achievements in smart structures involve the integration of sensing systems (e.g., fiber optic sensors, MEMS, etc.). Demonstrations on field tests reported on several bridge structures have proved that smart materials are suitable to be used under service conditions. More investigations regarding sensor installation techniques and aging characteristics, feasibility of repairing techniques for embedded sensors and materials, verification of damage detection methods and communication systems are still in progress.

1.2. RESEARCH OBJECTIVE AND APPROACHES

The main objective of this dissertation was to study the development, evaluation, and implementation of sensor techniques for bridges critical to the national transportation system. This study includes field and laboratory tests in which sensors have been integrated into structural members for bridge performance quantification. In this context, the structural monitoring of two pedestrian bridges, one highway bridge composed of FRP composites and one FRP temporary bypass bridge, as well as development of a conceptual smart timber bridge research plan and implementation of initial tasks within the plan to smart timber members for long-term monitoring, were conducted.

Three steel basket-handle arch pedestrian bridges constructed by the Iowa Department of Transportation (Iowa DOT) over Interstate 235 (I-235) in Des Moines had hanger systems consisting of high-strength threaded steel rods to support a precast, post-tensioned concrete deck system. Challenging construction practices, initially implemented on the first of the three bridges, caused premature cracking of precast elements. Subsequently, a unique monitoring system using optical fiber Bragg grating (FBG) sensors for strain detection was developed, and integrated into the construction process, to monitor arch hanger forces in real time during concrete deck installation on the second and third bridges. Alternatively, the hangers were instrumented with externally-mounted accelerometers used to monitor free vibration during the incremental assembling of the hangers and concrete panels.

For the second project, monitoring and evaluation of the three-span Bettendorf Bridge was conducted. The eastern bridge span was constructed with pultruded FRP panel deck compositely with prestressed girders, the first of its type in the U.S. The structural performance of the state-of-the-art system was investigated and compared to the western bridge span constructed with conventional reinforced concrete deck also composite with prestressed girders. The performance of the bridge was evaluated during two short-term field tests and also through long-term monitoring. For the third project, a FRP temporary bypass bridge was evaluated as a replacement of steel temporary bridges. The research comprised of the design, fabrication of FRP panels, construction and load testing of this novel bridge. Prior to field implementation, this bridge was instrumented with transducers for measuring deflections and loaded with a static truck at pertinent locations to evaluate its performance.

The fourth project was related to the development of a smart timber bridge for monitoring long-term performance. A national five-year research plan and the first phase of that plan were completed. The first phase consisted of the development of techniques for embedding fiber optic sensors (FOSs) in glulam timber members for detecting structural and non-structural bridge attributes. Both small scale glulam member and glulam girder testing were performed in the laboratory.

1.3. OUTLINE OF THE DISSERTATION

The content of this dissertation is organized as follows:

- In Chapter 2, a review of literature is presented for bridge monitoring, bridge structural health monitoring and related sensors and sensing systems.

- Chapter 3 presents the construction, monitoring and evaluation of two steel basket-handle arch pedestrian bridges constructed with a hanger system and precast deck system (Refereed Proceeding Paper presented also presented at the 2007 Transportation Research Board 86th Annual Meeting [1]).
- The performance evaluation of a FRP deck composite with prestressed girders bridge and a FRP temporary bypass bridge is presented in Chapter 4 (Refereed Proceeding Paper presented at the 2009 Transportation Research Board 88th Annual Meeting[2])
- A 5-year research plan of the Smart Timber Bridge is presented in Chapter 5 (Refereed Report currently in editing by USDA Forest Service, Forest Product Laboratory[3]).
- The peer-reviewed report on the evaluation of techniques for embedding and attaching FBG sensors to glulam bridge members is presented in Chapter 6 (Refereed report in preparation).
- To conclude this work, a general discussion, conclusions, and recommendation for future work are presented in Chapter 7.

[1] *LaViolette, M.D., Deza, U., Wipf, T. J., Phares, B. M. and Abu-Hawash, A. H. "Construction, Monitoring and Evaluation of a Pedestrian Arch Bridge with Precast Deck System". Transportation Research Board, 86th Annual Meeting Compendium of Papers DVD, Journal of the Transportation Research Board, Washington, D. C. 2007, pp. 17.*

[2] *Lee, Y. S., Hosteng, T., Deza, U., Wipf, T. J., Phares, B. M., Wood, D. and Klaiber, F. Wayne. "Structural Field Testing and Evaluation of Two Demonstration FRP Deck Bridges: Case Studies on FRP Panel Deck Bridge and Temporary Bypass Bridge", Transportation Research Board, 88th Annual Meeting Compendium of Papers DVD, Journal of the Transportation Research Board, Washington, D. C. 2009, pp. 19.*

[3] *Deza, U., Phares, B. M. and Wipf, T. J. "Development of Smart Timber Bridge—A Five Year Flan", General Technical Report, FPL-GTR-___, United States Department of Agriculture/Forest Products Laboratory (accepted for publication and currently in editing, pp. 18.*

CHAPTER 2. LITERATURE REVIEW

This chapter presents a synopsis of previously applied structural bridge monitoring for in-service and newly constructed bridges. An introduction to the national bridge agenda is presented to inform the status of the bridge inspection and management to ensure the users' safety and determine the condition of the bridge inventory. Strategic plans for improving the bridge network and developing the bridge of the future are also included. An overview of the bridge monitoring and structural health monitoring (SHM) for field evaluation are presented. As part of the SHM development, current sensor technologies with proven laboratory and field applications are summarized. To complete the review, the development of some the most recent smart structures are presented.

2.1. STATE OF THE NATIONAL BRIDGE AGENDA

With the tragic collapse of the suspension Silver Bridge over the Ohio River in 1967, the need for a national policy for bridge inspection and maintenance practices was highlighted by the Bureau of Public Roads (now the Federal Highway Administration (FHWA)). The following year, the U. S. congress approved the National Bridge Inspection Standards (NBIS) to regulate minimum requirements for inspection and evaluation of highway bridges (Lichtenstein, 1993). The standards set requirements for type and frequency of bridge inspections, reporting, need for quality control, and follow-up procedures to address critical findings resulting from inspections (Ampalli, 2010). These data are maintained by the National Bridge Inventory (NBI) and utilized by the Federal Highway Administration (FHWA) for network-level condition assessment and allocation of program funds. Currently, most transportation agencies and private owners exceed minimum NBIS and federal mandates collecting additional information to improve their bridge management programs (King et al, 2007). As previously noted, visual inspections are relied upon for managing and administering a national bridge program intended to identify the general condition of the bridge inventory. However, the NBI data do not contained specific bridge behavior and performance information for elaborating detailed bridge maintenance plans (Chase, 2005). In this context, there is a need to accurately quantify the operational performance of highway bridges using monitoring bridge techniques to support bridge management decisions.

In the current US highway system, 50% of bridges in service were constructed before 1970 and approximately 25% of the total bridge network (604,485 bridges) requires repair, rehabilitation or

reconstruction (NBI, 2010). With the given number of bridges that require rehabilitation or replacement, the resources to carry out this magnitude of work fall significantly short. In an effort to overcome this deficit and best prioritize the placement of available founds, the FHWA constantly supports research and technological efforts focused on both short-term and long-term solutions whether repair, rehabilitation or new construction of bridges are required (Friedland and Small, 2003). Traditionally, the FHWA has worked closely with federal, state and private agencies (e.g., the American Association of State Highway Transportation Officials (AASHTO), the Transportation Research Board (TRB), National Cooperative Highway Research Program (NCHRP), etc.) and academia to develop bridge research programs. The results of these partnerships are to renovate the bridge network while reducing the numbers of deficient bridges and developing best management practices for bridge owners.

In 2003, the FHWA proposed a research and technology program for developing the "bridge of the future" (Chase and Ghasemi, 2003). This program focused on the development of newly constructed bridge systems composed of high-performance materials and cost-effective pre-fabricated construction techniques to provide long-term bridge performance. Four critical elements were identified to achieve this futuristic bridge including gathering information (monitoring for obtaining reliable data), effective work force (training and professional development), technology (materials and structural bridge systems) and deployment of new bridges. Among the four elements, obtaining bridge condition information was of special interest for this review. Though the NBI contains long-term nationwide bridge information, the nature of this information is insufficient to determine quantitative long-term life-cycle decisions of any particular bridge because the structural performance is not appraised. In response, a Long-Term Bridge Performance (LTBP) program was developed to construct a database with detailed information for bridge management decisions (Chase and Ghasemi, 2003). In the first phase of the LTBP program, detailed inspections and periodic evaluations are planned to be implemented on a representative bridge sample to monitor performance over a minimum of 20 years. The obtained information is intended to improve design methods, predictive models and bridge management systems. The second phase of the LTBP program includes the long-term structural monitoring of a group of the previously selected bridges to obtain real time bridge performance data. To perform these monitoring activities, the program supports the use of new evaluation technologies including sensor installations, data acquisition systems and software for interpreting condition data. In addition, the LTBP program included a plan for detailed forensic autopsies of a group of decommissioned bridges to document the degree of corrosion, overload

effects and other deterioration processes. Currently, a LTBP pilot study is been conducted to "validate the methods and protocols developed for data collection under the developmental phase of the program (LTBP News, 2010)." Seven states including New York, New Jersey, Florida, California, Utah, Virginia and Minnesota have been selected for the pilot program to investigate the validity of the protocols in a variety of bridge structures and weather conditions. The final LTBP protocol will be determined by the experiences and results obtained from inspecting, instrumenting, testing, and monitoring of the selected bridges.

As a part of the LTBP program, sensing systems and measurement technologies were identified as relevant to not only provide quantitative bridge data but also support the bridge level management decisions for repairing and/or replacing bridges. In Table 2.1 (Chase, 2005), an extract of the main measurement needs not covered by the visual inspection practices used during the NBI bridge inspection are listed. Parameters to measure bridge performance were focused upon quantifying damage, deterioration and traffic operation.

Table 2.1. An Extract of the "Sensing and Measurement Needs" by Chase, 2005

Damage	Deterioration	Operation
Impact	Corrosion	Traffic counts
Overload	Fatigue	Weight of trucks
Scour	Water absorption	Maximum stress
Seismic	Loss of prestressed force	Deflection
Microcracking	Unintended structural behavior	Displacement
Settlement	Chemical changes (e.g., alkali silica reaction, diesel exhaust fluid)	
Movement		
Lack of movement		

In practice, some of the main adopted technologies include the following (Chase, 2005):

- Global health monitoring installed on long span bridges (i.e., Commodore Barry Bridge over the Delaware River in Pennsylvania). A unique application consists of the evaluation of tension elements to quantifiy unexpected bending stresses caused by solar radiation exposure. This monitoring system has demonstrated to be an effective tool for bridge owners providing the overall real time evaluation of the bridge condition.
- Due to the brittle fracture of a welded plate girder in Wisconsin (2001), fracture critical steel bridges have been monitored for fatigue and vulnerability to fracture. Portable, battery powered

data acquisition systems have been implemented for detecting and measuring fatigue and fracture vulnerability. These systems are designed to detect rapid changes in structural stiffness resulting from crack propagation in in-service structures by monitoring the fundamental frequencies of the members.

- To evaluate the performance of bridges due to service loads, smart structures for collecting information and preventing damage were proposed. As an example, smart bridge bearings were developed using multi-axis fiber optic strain sensors to quantify stress levels, load distribution, stiffness changes, etc.
- Mounted accelerometers have been installed on in-service prestressed concrete bridges to witness strand failure due to undetected corrosion. The accelerometers are strategically installed near the tensioned strands to detect sudden stress waves due to the energy release at the moment of wire breakage. This information can be relayed to the bridge owner alerting of the otherwise undetected strand deterioration, thereby preventing a catastrophic failure.

The innumerable applications for sensing and measurement technologies for highway bridges already available can provide quantitative and objective information to augment the "current subjectively based bridge management systems" (Chase, 2005). The United States National Academies of Science and Engineering has also recommended and highlighted the immediate implementation of sensing and measurement technologies for best bridge management practices.

In 2005, AASHTO Highway Subcommittee on Bridges and Structures developed a bridge engineering plan composed of seven grand "challenges" focused on extending service life, optimizing structural systems, accelerating bridge construction, advancing AASHTO specifications, monitoring bridge conditions, contributing to the national policy and managing knowledge (AASHTO HSOBS, 2005). By monitoring bridge condition, relevant for this study, the bridge performance is assessed by gathering information from critical structural members to determine the health of the entire structure. These resulting monitoring systems and strategies are integrated to aid in the management of existing bridges thereby improving the long-term performance and credibility of the inspection reports. Note that the bridge monitoring systems would not necessarily be continuous. Some of the important activities/areas for research include:

- The evaluation and identification of available technologies.
- Identification of the type of structures to be assessed and the data to be collected

- Deployment and cost/benefits of the most promising monitoring technologies and assessment of the systems in the short-term (in 2 to 3 years), with the deployment of multiple integrated health assessment systems in the long term (longer than 5 years).

The "2005 Grand Challenges" work has focused on the development of system fracture analysis methods for fracture critical steel bridges, new LRFD design specifications for tunnels, self-consolidated concrete (SCC) in cast-in-place bridges and accelerated bridge construction (ABC) connections in moderate to high seismic regions (Thompson, 2010). Monitoring bridge condition evaluations are forthcoming.

Though existing inspection and evaluation programs have demonstrated to be adequate to ensure the public safety (Alampalli, 2010), however, management decisions based solely on qualitative visual inspections do not consider the quantitative structural performance of any particular bridge. The use of new and advanced technologies to monitor the bridge structural response can supplement inspections and develop performance based management methods.

2.2. STRUCTURAL BRIDGE MONITORING

At the basic level, frequent visual examination and evaluation of the bridge structural condition (e.g., detection of cracking, spalling, corrosion, measurement of moisture content levels, deformations, etc) can be considered a form of structural bridge monitoring. However, monitoring the health of bridge structures usually involves the use of instrumentation, field load testing and the collection and processing of data for determining the current condition of the bridge on an ongoing basis.

According to Brownjohn (2007), the vibration evaluation of two bridges near San Francisco, California, was one of the first bridge monitoring tests ever reported. In both tests, conducted by the United States Coast and Geodetic Survay, natural vibration data of the Oakland Bay Bridge and Golden Gate Bridge were obtained to determine the probabilities of damage caused by resonance between the ground and the structure from a seismic event (Carder, 1937). The typical instrumental equipment utilized for the study of both bridges consisted of two survey vibration meters set at right angles and a spring recorder. In addition, a Wood-Anderson seismometer was utilized for detecting large magnifications. Natural forces such as wind, moving water, traffic and equipment at work were

utilized to incite the structural members. The instrumental equipment was located on several piers and at mid span to measure amplitudes and periods. Several tests were performed during the construction and after the completion of the bridges for a span of three years. From the vibration data, changes in the amplitudes and periods of bridge members and towers were observed during the construction. Comparisons of the amplitudes for any given bridge member at different stages of the construction was not possible due to the varying material and boundary conditions. While describing the dynamic properties, the behavior of the bridge structures during an earthquake could not be directly answered from the collected data, rather the data only described the fundamental behavior under ambient excitation.

Prior to its collapse in 1940, the first Tacoma Narrows Bridge was monitored by University of Washington (Farquharson, 1954) focusing on vibration measurements induced by wind. Since the Tacoma Narrows failure, most long-span suspension bridges have been monitored to determine susceptibility to wind-induced response and associated instability (Brownjohn, 2007). The evaluation of the in-service bridge integrity can verify not only the safety of end users but also provide data to assist in the programming of bridge maintenance activities for preventing catastrophic failures.

Over the last four decades, bridge conditions have been appraised by using visual inspections as stipulated in the NBI standards. While the inspection methods are cost effective and readily applied, the obtained results have been shown to contain some inconsistencies and erroneous evaluations (Moore et al, 2001). Inspection techniques have been enhanced by the implementation non-destructive testing techniques (e.g., penetrating dye testing, ultrasonic testing, acoustic emission, radiography, etc.) to verify and/or quantify the level of deterioration (Ghorbanpoor et al, 2003).

Non-destructive load testing is another means to assess bridge performance and/or deterioration. Due to the increasing traffic loads and aging bridge network, non-destructive load testing has been utilized to evaluate bridge components and system performance under a known live load as an alternative evaluation to analytical load for bridge rating (Lichtenstein et al, 1998). Two types of non-destructive bridge loading are diagnostic and proof tests. While diagnostic bridge tests are conducted to measure the bridge response under known loads, and evaluate other associate bridge performance parameters, proof tests are used to verify the maximum safe load capacity of the bridge for a linear elastic performance (Faber et al, 2000).. Diagnostic tests have been utilized as a tool for bridge rating applications to evaluate the bridge performance during last three decades (Jauregui,

2001). From these evaluations, the in-service strength behavior of several bridges have been favorably influenced by bridge factors such as unintended composite action, flexural participation of parapets and curbs, and bearing restrain, among many others.

In late 1990's, a bridge diagnostic loading testing program was developed by the Iowa Department of Transportation (DOT), with the support of the Bridge Engineering Center at Iowa State University (Iowa DOT News, 2010). The program has established the use of bridge load tests to re-evaluate aging bridges under new specifications, determine the capacity of in-service bridges subjected to heavy truck loads, impose or remove load restriction due to load rating evaluations and verify the use of new strengthening techniques, among many others. To enhance conventional analysis techniques, the bridge testing program also supports the use of new technologies for load testing. A typical bridge load test consists of a temporarily placed data acquisition system with incorporated software to record and visualize real time data due to the applied known truck load. The strain transducers are placed at key locations and a controlled load truck (state legal vehicle for load rating) crosses the bridge at a crawl speed (Phares et al, 2003).

Other forms of bridge monitoring and SHM systems have been developed and used to assess bridge structural conditions during the past century. Definitions of SHM have taken many forms, including an overlap with non-destructive evaluation (NDE). While the traditional NDE techniques directly measure the physical condition of the structure at a localized level, SHM evaluates the global performance of the structure based on strategically placed localized measurements. Another definition of SHM, given by Balageas et al (2006), establishes that "SHM aims to give, at every moment during the life of a structure, a diagnosis of the "state" of the constituent materials, of the different parts, and of the full assembly of these parts constituting the structure as a whole". In contrast to the NDE, SHM has capabilities to continuously evaluate the structure conditions which can be modified by frequent usage and other environmental and accidental factors. The SHM system can issue an alert when the structure experiences early deterioration, catalog the evolution of damage and estimate residual service life. The results of the reported evaluations can also be used for the development of design specifications and extrapolated for management decisions not only in local structures but as part of larger systems.

The advances in computer and internet technologies have influenced the rapid evolution of the monitoring concepts in the last decade. In response, new monitoring techniques have improved the

planning of maintenance, repair and replacement of existing and newly constructed structures (Frangopol et al, 2008). According to Ross and Matthews (1995) and Mita (1999), there are several cases in which structural monitoring of civil infrastructures may be required; common applications have included the modification of an existing structure, novel construction systems, fatigue assessment and structures subjected to long term movement or degradation of materials, in particular. Though SHM systems provide real time monitoring and reporting and require minimal labor once installed; technical issues related to sensor calibration, damage and structural characterization as well as cost have hampered wider implementation. Improvements in the sensor integrity, data reduction and sensor/structure interaction are needed before extensive implementation is warranted.

2.3. SENSOR INSTRUMENTATION FOR STRUCTURAL BRIDGE MONITORING

Existing and recently developed sensors available on the market such as strain gages, fiber optic sensors (FOSs), dielectric measurement sensors, piezoelectric materials, and microelectromechanical systems (MEMS) sensors, have been used for bridge monitoring purposes in the last decades. Two types of strain gages are electrical resistance strain gages and vibrating wire strain gages. Both gages types are relatively easy to be either embedded or attached to structural members for measuring strains from quasi-static and dynamic events. However, both sensors are not durable and fragile, and upon loading have signal drift over time which limits the use of these sensors to only quasi-static strain measurements for short-term evaluation (Ko et al, 2005). In an effort to incorporate sensors with higher reliability and greater range of application for structural bridge monitoring and SHM systems, the use of fiber optics, piezoelectric and MEMS sensors have been pursued. The listed sensors have successfully been used in various fields including aerospace and automation industry and have been gradually incorporated into the civil infrastructures. A description of previous research and development of each sensor type as related to the implementation to bridge structures is presented in the following sections.

Fiber Optic Sensors: Development and Applications.

A Fiber Bragg Grating (FBG) is typically characterized as a periodic perturbation of the refractive index along an optical fiber length known as the grating length (Hill and Metlz, 1997). Grating writing techniques have evolved from the internal laser writing (Hill et al, 1978) and transverse holographic methods (Metlz et al, 1989) to the phase mask method (Hill, 1993). FBG sensors are categorized as spectrometric sensors which detect wavelength changes in guided light inside the fiber.

Upon loading, the sensor grating pitch spacing is altered reflecting a different wavelength, linearly proportional to strain levels. Some positive FBG sensor characteristics are immunity to electromagnetic interference, dielectric (passive), light weight, small size with large bandwidth and high sensitivity-temperature performance (Udd, 1991). These sensors are easily installed and optically multiplexed. Though, FBG sensors for measuring strain and temperature are commercially available, FBG sensors can be written to detect other factors associated with structure behavior and usage (e.g., concrete moisture, corrosion, etc.).

An early National Science Foundation investigation involving the use of FBG sensors to characterize strain and/or stress in concrete civil structures was carried out in a three phased laboratory testing program (Nawy et al (1994)). In Phase I, sensor response when embedded into a small scale structural concrete prism tested in bending was performed. The second phase comprised of theoretical evaluation and experimental calibration of FBG sensors for strain measurement in structural components. A selected FBG sensor package, bonded to steel reinforcement, was embedded into small reinforced concrete specimens to provide maximum strain transference. The FBG sensor strain measurements were comparable to values recorded by electrical resistance strain gages. In Phase III, large scale specimens, composed of reinforce concrete girders, pretressed concrete beams and composite beams, were internally instrumented at mid span and tested to failure. In addition to the FBGs, mechanical extensometers composed of dial gages were installed for obtaining deformation upon loading. From the information gathered, guidelines and criteria for field implementation and usage of the selected fiber optic strain sensors was presented. In this investigation, the laboratory results concluded that the FBG sensor system has the advantage of measuring average strains in beams when comparing to the beam deformations at service levels. FBG sensors conformed to the deformed beam while covering any desired gage length; the average strain measurements at the post-cracking stages were reliable. More sensor development regarding proper packaging and installation techniques were proposed for further application in reinforced concrete beams.

FBG sensors have been implemented in different civil structural members with some success (e.g., in concrete, on steel and fiber reinforced polymer (FRP) reinforcement, steel girders, etc.) (Vohra et al, 1999, Tennyson et 2001, Casas et al, 2003, Li et al, 2004)). Although, the small bare FBG sensors are easy to install, they can be easily damaged when not handled with care. To increase

the durability, either recoating the bare fiber or providing a protective packaging is recommended to minimize damage and extend the FBG sensor life (Lin et al, 2005).

In health monitoring systems developed in Japan, FBG sensors were embedded in FRP composite for damage prevention (Satori et al, 2001). These sensors were fabricated with 40-μm diameter optical fibers, coated with polyimide and heat treated at 300^{o}C (572^{o}F). After the high temperature treatment, the retained mechanical strength and reflectivity were verified. The resulting package, consisting of the FRP protective covering and the FBG strain gage were attached to the structure of interest using a surface epoxy. From the temperature and tensile test evaluations, the coated and packaged FBG sensors were recommended to be implemented in health monitoring systems for sensing strains or temperatures.

In one study, three techniques for packaging bare FBG sensors, which included the preparation of nickel recoating, quartz glue and steel tube packaging with 1- and 2-mm wall thickness, were evaluated (Lin et al, 2005). The bonding effect was studied to understand the strain transmission between the FBG sensor, either with or without packaging, and its host member material (specimen). In each case, the experimental results were compared to finite element model (FEM) results to verify that the bare FBG sensors attached with different adhesive thicknesses and material packages did not modify the strain transmission rates.

The thermo-optic and photo-elastic effects of packaging materials on the FBG sensor performance were investigated by Hao et al (2006). Polymethyl methacrylate (PMMA) and carbon fiber reinforced composite (C-FRC) were selected as packaging materials for their high thermal expansion and high tensile strength coefficients, respectively. While the PMMA package allowed the FBG sensor high sensitivity to thermal variations, the C-FRC package had lower influence on the FBG sensors with respect to thermal effects. In contrast to the C-FRC package, the PMMA sensor package demonstrated to have poor sensitivity to stress response. Other variation of the C-FRC package was the fiber orientation; when C-FRC package was orientated 90^{o} with respect to the bare FBG sensor, the thermal expansion coefficient was five times larger than the bare fiber value. In conclusion, the C-FRC package with 0^{o} orientation was recommended for strain/strength evaluations; while the PMMA package was suitable for measuring temperature effects.

In Singapore, three types of FBG sensors were developed and deployed to measure temperatures, strains and temperature-compensated strains on reinforced concrete highway bridges (Moyo et al,

2005). The temperature sensor consisted of a 35 mm (1.4 in.) long tube that isolated the FBG sensor from external stress while increasing the temperature sensing range. The FBG strain sensor was packaged with 50-mm (2-in.) carbon composite layers. The temperature-compensated FBG strain sensor consisted of combination of one temperature sensor and one strain sensor inserted into a custom designed dumbbell. The temperature FBG sensor was set loose on the specimen while the strain FBG sensor was bonded to the inner surface of the dumbbell. Specimens were instrumented with three FBG sensors and electrical resistance strain gages for comparison. The FBG sensors that were protected during casting and isolated from pressure effects survived installation highlighting the need for proper packaging. Tests for tensile, bending and dynamic loading effects, and temperature were conducted with sensors attached to steel reinforcement and embedded in reinforced concrete beams. The surviving sensors provided accurate strain and temperature measurements. These developed FBG sensors demonstrated viability for use in both short term load tests and long term structural health monitoring.

Weldable strain and temperature FBG sensors were prepared for structural health monitoring of steel bridges in Portugal (Barbosa et al, 2008). The packaging process consisted of embedding the bare FBG sensor in a stainless steel capillary tube bonded with a thermal curing epoxy. Each steel tube was laser welded to a 45 x 15 x 0.3 mm stainless steel base which was spot welded to the steel structure at determined locations thereby attaching the prepared packages. At each ingress/egress, fibers were protected with standard 990 μm buffers. Additionally, each input/output fiber was covered by a 3-mm PVC tube containing an internal stainless steel coil. Stainless steel caps for protecting the weldable strain and temperature FBG sensors were welded to the steel bridge structure. Both weldable FBG strain and temperature sensors were laboratory calibrated before being deployed. Only laboratory test results were reported. The FBG sensors were shown to be stable and reliable under cyclic loading.

The development of two packages for strain measurement using bare FBG strain sensors and composite materials was presented by Gangopadhyay et al (2009). Only laboratory tests were presented for the FBG sensor packaged with a two part epoxy resin. The packaged FBG sensor was installed on a steel cantilever beam with electrical resistance strain gages and a bare FBG sensor for comparing tensile test results. In addition, X-ray diffraction profile, thermo gravimetric analysis, differential analysis and scanning electron microscope for epoxy polymer resin were performed to ensure the bonding and confirm the packaging performance. From the experiments, the use of a thin

layer of adhesive, a high modulus coating material and a sufficient embedment length were recommended for packaging.

Piezoelectric Sensors: Development and Applications.

Piezoelectric sensors rely on the piezoelectric effect discovered by the Curie brothers in the late 19th century. Piezoelectric materials have capabilities to transform mechanical energy input or applied pressure into proportional electrical output or charges (Piezocryst, 2010). Piezoelectric sensors are used for determining pressure, acceleration, strain or force in quality assurance, process control and development in various industries including applications in SHM systems (Guy and Monnier, 2006). Piezoelectric sensing techniques are grouped in three categories: acoustic emission, acoustic-ultrasonic using piezoelectric transducers and electromechanical impedance.

Acoustic Emission. In the acoustic emission (AE) technique, piezoelectric sensors are embedded into materials as AE detectors to evaluate material physical parameters and damage mechanisms. AE can also be used as an on-line non-destructive testing (NDT) technique. The AE technique can be explained as the energy released in waves resulting from a rapid change in its structural behavior that when amplified provide the so-called acoustic emission signal. AE techniques have been applied in the aerospace, particularly in air safety, and NDT for bridge damage detection. Applications for bridge SHM have been limited because of the lack of a standardized defect classification and a shortage of developed software (Geng, 2004).

An example of AE technology being used for a bridge application was a non-destructive evaluation of the cable stayed Varina-Enon Bridge, Richmond, Virginia (Parmar and Sharp, 2010). Using AE techniques, active defects such as corrosion, crack expansion and rubbing and wire breaks were investigated on a single stay-cable and anchorage points. The testing program consisted of short period tests performed during low traffic volumes (acoustically quiet) and high traffic volumes (acoustically noisy). The source and location of the acoustic event were determined with specific software. When testing, AE events were generated inside the pylon near the saddle region. Despite the AE responses from the stay-cable, the recorded data did not contain any signal of damaged or broken cable strands during the testing period. The recorded AE signals were attributed to the higher winds or blowing debris striking the cable and /or anchorage region. Follow up periodic AE tests were recommended for crack detection and/or propagation. From this study, AE were recommended to complement traditional inspection methods.

Acoustic-Ultrasonic. Traditional ultrasonic non-destructive evaluation techniques experience problems associated with factors such as reproducibility of acoustic coupling, accessibility of the structure and materials with poor-signal-to-noise ratio (Guy and Monnier, 2006). To overcome some of these limitations, piezoelectric sensors have to be embedded into or bonded to the members to be evaluated. Under these conditions, these sensors can be used to monitor the integrity of composite materials from their curing process through the entire life cycle.

In research conducted by Shiotani et al (2009), twenty eight frequency acoustic emission sensors were installed on a 135 ft (45 m) single span concrete bridge to determine the area of potential damage (crack locations). Though the AE technique provided indices that did not correlated with the degree of known damage, the obtained data suggested that parts of the concrete structure were in need of supplementary investigations. Additional ultrasonic examinations were conducted near sources of deterioration or damage (e.g., concrete cracks, friction between the tendon ducts, etc.). Nine AE sensors were installed under the previously examined concrete slab to measure surface wave transmission using an acoustic ultrasonic technique. Obtained velocities were low, indicating that concrete possessed either poor quality or extensive damage. These results confirmed the AE technique diagnostic. However, characterizations to determine the crack depth using analytical evaluations needed further study. Both AE and the ultrasonic techniques showed potential as a global monitoring method for examining large concrete structures using limited number of sensors.

Electromechanical Impedance (EMI). Piezoelectric sensors can be used in an active way to produce and detect high-frequency vibrations. When applying an alternating voltage, the piezoelectric sensor attached to a structural member generates strain parallel to the member surface. The sensor response is analyzed using an electromechanical impedance (EMI) method (Guirgiutiu and Rogers, 1999). Although piezoelectric sensors have capabilities for on-line health monitoring of aeronautical structures, additional investigation is necessary to support the application of the EMI method to civil engineering areas.

In typical applications, piezoelectric elements are embedded into a structure or attached to the surface for local measurements. The EMI method used in the low frequency range is suitable for detecting flaws in the immediate vicinity of the active element. The same set of piezoelectric elements can be utilized for aging monitoring, for damage identification, and for evaluating AE activity of the structure under testing (Guy and Monnier, 2006).

Microelectromechanical Systems (MEMS): Development and Applications.

MEMS, first developed in 1950s, are devices created by silicon wafer fabrication with mechanical transducers or actuators integrally formed with the electronics for information processing (Oppernheim et al, 2000). Applied micromechanics have further developed electromechanical silicon chips to serve as sensors and microstructures (Bryzek, 1996). Due to the ability to transform any energy form into electrical signals, MEMS with integrated circuits (IC) have been developed into an array of microsensors including inertial sensors, pressure sensors, magnetometers and chemical sensors. Microactuators, which actively respond to electrical stimuli, are used as micromirrors, microrelays and micropumps (Judy, 2001). Initial use of the micrometer sized, silicon-based MEMS was limited to aerospace and process control applications but has spread to the automation, healthcare and internet hardware fields.

With wide use outside of the civil engineering infrastructure, the applications of MEMS in diagnosis structural behavior of in service bridges promise that same opportunity (Oppernheim et al 2000). Other applications would include measuring temperature, water and air content, corrosion and strain. Researchers at Carnegie Mellon have developed MEMS including nuclear magnetic resonance sensors on-a-chip for detecting chlorine in concrete. Other applications include the use of “smart rocks” for geo-environmental monitoring to sample water and detect chemical concentrations (Fedder and Mukherjee, 1996). “Smart aggregates” based on MEMS devices have been employed in laboratory specimens with the capability to measure the dynamic response of the concrete in reinforced column configuration. These smart aggregates have demonstrated potential for applications in SHM of concrete structures (Gu et al, 2010).

A structural engineering application of a MEMS system based on an hybrid biaxial strain transducer (BiAST) with high resolution, sampling rate and lower signal noise was developed to monitor the fatigue life of a railroad rail based on strain history (Obadat et al, 2003). Originally developed for measuring strains in aging airframes, each BiAST device has a 1/2 in. (12.7 mm) gage length positioned at approximately 1/10 in. (2.34 mm) over the member substrate, a networking controlling box and cables for communications; software was developed for recording data.

Before field testing, a FEM model of a rail subjected to a moving rail road car loading was developed to identify critical zones were the BiAST sensors would be installed. Field data at the critical sections were collected from a full-scale test track located at the Transportation Technology

Center Inc., Pueblo, Colorado. The obtained strain data were analyzed using fatigue analysis to estimate the fatigue life of the studied rail structure. In general, BiAST was recommended as a tool for detecting the dynamic response of the rail and determine the underlying track condition. One limitation of BiAST prototype was the difficulty of installation on the rail substructures.

A high-performance, planar piezoresistive MEMS accelerometer with capabilities to measure civil structural response was developed by Lynch et al (2003). To validate the performance of this accelerometer, experiments were performed to characterize the sensitivity, bandwidth, and resolution performance of the sensors. This MEMS accelerometer was connected to a wireless sensing unit specially developed for automated SHM for damage detection that rely on local structural response. Both the MEMS accelerometer and the wireless monitoring system were tested on a five degree-of-freedom laboratory test structure. This piezoresistive MEMS accelerometer was compared to a commercially available capacitive MEMS accelerometer. The obtained frequency of the piezoresistive accelerometer revealed greater noise levels than the capacitive accelerometer; nevertheless, the identification of the structural modal properties was possible. The results of this investigation indicated that the manufacturing process of the piezoresistive accelerometer needs to be modified to reduce the noise.

Pakzad et al (2005) developed a wireless MEMS accelerometer sensor board and software for SHM applications of civil structures. The sensor board consisted of a thermometer, one two-axis and one single-axis commercially available accelerometers mounted to register bi-directional vibrations with a total range of +/-2g for earthquake motion and accuracy of tenths for ambient vibration. Software components were developed to collect data with high frequency sampling, time synchronization, and multi-hop networking and reliable transformation of data. As a demonstration for viability, twelve prototype boards were mounted to a tied-arch pedestrian bridge over Interstate Highway 80 near Berkeley, CA. These boards were placed on both sides of the main span, at five different locations spaced every 31.5 ft (9.6 m). Only ambient vibrations were collected to evaluate vertical modal properties. The MEMS system developed in this research was demonstrated to be suitable for SHM applications.

In a work published by Zhao and Xiong (2009), one type of MEMS accelerometer and its data acquisition system were investigated for viability in civil engineering structures. This accelerometer measured up to +/- 0.5 g in its sensing direction at frequencies up to 20 Hz. Two tests were

conducted under laboratory conditions to assess the quality of the acquired dynamic information. The sensor was fixed on a shake table and the collected data were investigated to determine the low-frequency and cross-axis sensitivity ratio. The calibration experiments demonstrated that the MEMS accelerometers can be implemented in civil structures.

Nanoelectromechanical Systems (NEMS): Development and Applications.

At a level even smaller than the microelectromechanical systems lies the NEMS, part of the field of nanotechnology. Defined as the manipulation of atoms, molecules, and materials to form structures on the scale of nanometers ($1x10^{-9}$ m) (Encyclopedia Britannica Online, 2010), these tiny systems can be combined to create a aggregate effect on the macro level. Examples of such technology in use include pressure transmitters that operate under temperatures varying from -148 ^{o}F to 1292 ^{o}F. Another is the use of nanocoatings on fabrics used in outdoor clothing for UV blocking and antibacterial protection. While applied at the nano level, the combined effects of the individual nanostructures provide protection over the system. (Boyes, 2010).

One concept of applying NEMS as sensors revolves around the development of a thin film that acts as a sensing device with high sensitivity. Reliably of this mechanism depends on how the thin films respond to the applied stresses. Research has been developed to model the behavior of the thin films for micro/nano-mechanical testing techniques. The uniaxial tensile test is one method that is adequate for gathering information for elastic and plastic material behavior. The drawback of this test was that when applied to a nano-scale thin film, difficulties resulted at scaled levels of applied force and specimen fabrication and instrumentation. In response, an improved testing device was designed and a new sensor fabrication for cofabrication of a uniaxial tensile sample and force sensor were presented by Haque and Saif (2002). The tensile testing technique applied to this new device indicated that specimen size only affected the yield strength; in contrast, the elastic modulus was not influenced. The improved sensor and testing technique showed that scale of the specimen and applied force still require more research to make the use of micro/nano sensors on macro scale civil structures feasible.

The area of NEMS has demanded more attention due to the potential to fabricate high-sensitivity, low power miniaturized sensing devices based on carbon nanotubes (CNT) (Hierold et al, 2007). Since the 1991 discovery, three methods have been developed to fabricate CNT consisting of arc-discharge, laser ablation and chemical vapor deposition (CVD). Both arc-discharge and laser ablation

involve the condensation of carbon atoms to create entangled nanotubes or nanowires, or “bulk” growth; however, “bulk” growth limits “post-growth” purification, manipulation and assembly of CNTs. The CVD method consists of heating a catalyst material that helps the growth of the single-walled carbon nanotube (SWNT). A nanoscaled force sensor was developed to incorporate the concept of NEMS in a cantilever beam; in this case, MEMS were beams. Suspended SWNT transducers were installed to the cantilever loaded with out-of-plane forces for measuring deflections. The results demonstrated that the transducer response followed expected beam theory. In addition, membrane-based SWNT transducers were installed to the cantilever beam for measuring differential pressures. This investigation confirmed that the developed SWNT transducers can be integrated to MEMS structures. While this laboratory test demonstrated the implementation of SWCT in a sensor application, use on in-service structures will require extensive research and development.

Commercially available SWNTs were utilized to form a composite electrical resistance strain sensor for measuring strains in a macroscale structure. In addition, a multi-walled carbon nanotube (MWNT) was developed and tested as a continuous strain sensor (Kang et al, 2006). The composite SWNT based strain sensors were bonded with a vacuum method to ensure a stiff bond on a cantilever glass beam which was clamped to a table. Measurements of beam end displacements and resistance changes in the sensors demonstrated good agreement with a model based on electromechanical impedance. By increasing the length of the CNT sensor (MWNT), the concept of an artificial neuron was also developed for detecting large strains and cracking for SHM of larger structures. Further research is needed prior to implementation for long term damage detection applications in automation, transportation and civil structures.

One application of CNT fibers in glass FRP (G-FRP) materials was presented by Alexopoulos et al (2010). Conductive CNT fibers were integrated to a non-conductive G-FRP to form sensitive material coupons. Due to the nanoscale, the CNT fibers did not alter the G-FRP mechanical characteristics. Three point bending tests were conducted to monitor the health condition of the “smart material”. Incremental loading and unloading were applied to evaluate the correlation between the mechanical stress of the coupons and the electrical resistance of the CNT fibers. By increasing the load levels, residual resistance responses were obtained in the CNT fiber after removing the load, this was attributed to possible damage of the CNT fiber. Though this “smart material” was developed for monitoring the health of aircraft fuselage, there is potential for use in SHM of civil structures.

2.4. SMART STRUCTURES FOR STRUCTURAL HEALTH MONITORING

Since the late 1980s, the concept of smart or intelligent materials and structures has become more and more present in the minds of engineers with particular interest in the fields of aerospace and civil engineering (Balagueas, 2006). The engineering community has adapted the term smart structures to indicate a certain ability of structures or structural members in performing their design function (Srinivasan and McFarland, 2001). The smartness of the structure indicates the ability of sensing, diagnosing and actuating to perform desired functions (e.g., temperature, strain, pressure measurements, etc.).

Smart structures can be classified as close-loop and open-loop structures. A close-loop smart structure has capabilities to sense a variable, diagnose the condition and extent of possible damage, start an action to address the problem, and store the event for further reference in case the same action has to be implemented. An open-loop smart structure is designed with the ability to enhance its structural integrity only when required, otherwise returns to its original condition (Wadhawan, 2005).

The concept of smart materials/structures (SMS) can be considered as the evolution of man-made objects in which human production have moved from simple to complex. Homogeneous materials with their natural properties have been improved and replaced by developed multi-materials or composite materials that allow constructing new structures with selected properties for specific uses. In the aeronautic field, composite materials have been implemented where SHM system development began.

Further advancement consists of developing materials and structures that adapt to changing conditions. This requires fabricating materials with sensitive, controllable and active qualities; the level of material intelligence depends on possessing one, or two or three qualities. SMS materials are classified into three categories: SMS that exhibit shape control, SMS that exhibit vibration control, and SMS that sense and monitor internal health. According to Balagueas (2006), the lesser SMS are composed of materials and structures that integrate SHM systems, at least in the short term. At this time, the majority of SMS comprise materials or structures with embedded sensors providing sensitive qualities. The next generation of SMS would be materials/structures with self-repairing capabilities and embedded damage-mitigation properties. Examples for damage-mitigation SMS would consist of embedded actuators made of shape memory alloys (SMA) that would induce strains in order to reduce the stresses in regions of strain concentration. The recommended form of the SMA

actuators could be either wires (Yoshida et al, 1996; Choi and Salvia, 1999) or films (Takeda, 2000). In the field of civil engineering, only self-repairing or self-healing concretes have been developed containing hollow adhesive-filled brittle fibers; the fibers break due to cracking and internal adhesive is released to fill the crack (Dry, 1994). A similar method was attempted to repair polymer matrix composites (Dry, 1996; Motoku, 1999).

As stated by Chopra (2002), smart structures can respond to external and internal environmental changes. Smart structures implemented with actuators, sensors, control strategies, and power conditioning electronics can alter the structure mechanical properties (e.g., stiffness, damping, etc.) and/or modify the system respond (e.g., strain, shape, etc). Fiber optics, piezoelectric materials, SMA, electrostrictive materials and magnetostrictive materials, among many others, have been utilized in various sensing applications for civil engineering, especially main load-carrying structures. These sensitive materials can be incorporated on previously constructed members through surface mounting or embedding to members without significantly altering the system mass or structural stiffness.

A smart structure with incorporated fiber optic sensing system was reported by Melle et al (1993) and Measures et al (1995). In Manitoba and Nova Scotia, Canada, an intelligent monitoring evaluation system for collecting static and dynamic field data was introduced by Maalej et al (2002). All structures incorporated innovative materials (prestressed C-FRP tendons, C-FRP bars and polypropylene fibers instead of steel reinforcement) and structural systems that were instrumented with both FOS and electrical resistance strain gage sensors for comparison. This intelligent monitoring system remotely accessed sensor data, analyzed and appraised the performance of the structures.

Smart materials/sensors for the SHM of civil engineering structures applied in laboratory and field studies was critically reviewed by Sun et al (2010). Smart sensing technologies including the applications of fiber optic sensors, piezoelectric sensors, magnetostrictive sensors and self-diagnosing fiber reinforced composites, possess intrinsic capabilities of monitoring various physical or chemical parameters related to the health and therefore, durable service life of structures.

- FOSs for SHM applications in civil engineering (i.e., bridges, hydroelectric projects, and some civil buildings) have been developed for monitoring strains, displacement, vibrations, cracks, corrosion, and chloride ion concentration. Field test demonstrations reported on bridges by

Measures et al (1995), Mufti et al (1997), Bronnimann et al (2000), Furh et al (2000), Tennyson et al (2001) and Lan et al (2008) proved that FBG sensors as smart sensing technology have been found effective. However, the long-term sensing ability of FBG sensors under field conditions due to aging has not been fully established and requires further investigation. FOSs are fragile in some configurations, and the damage is difficult to repair when embedded. The optical connection parts, which connect the embedded optical fiber with the outer data recording system, are also weak elements of the FOS system. One field example using FBG sensors to monitor the structural condition of a critical fracture steel highway bridge has been developed and reported by Doornink (2006), followed by a statistically damage detection approach by Lu (2008).

- Piezoelectric sensors have been used as active sensing technologies in the SHM of civil engineering structures based on electrical impedance and elastic wave methods. The impedance method depends on the self-sensing actuator concept (Ayres et al, 1998; Park et al, 1999; Park et al, 2000; Park et al, 2006; Yang et al, 2008a; Yank et al, 2008b). Wave based approaches can detect larger areas of damage than the impedance-based method and can take advantage of additional information arising from wave propagation to identify damages (Wu et al, 2001; Kawiecki et al, 1998; Saafi and Sayyah, 2001; Sun et al, 2008; Song et al, 2008; Li et al, 2002). However, further studies must be carried out to verify the feasibility of this method to detect various defects in reinforced concrete structures.
- Self-diagnosing fiber reinforced composites are also available as sensors and offer a very simple technology for the SHM of civil engineering structures. One advantage of this type of smart material is the dual purpose of serving as both structural and sensing materials (Chen and Chung, 1995; Sun et al, 1999; Wen and Chung, 2001; Wang et al, 2008; Yang et al, 2008). Laboratory studies have shown that self-diagnosing fiber reinforced composites have the ability to monitor internal strain, damage and temperature. However, the practical applications of this type of smart materials in civil engineering structures are yet to be developed.
- Magnetostrictive sensors can generate different guided wave modes by simply changing the coil or magnet geometry and can be operated wirelessly (Kwun and Bartels, 1998; Khazem et al, 2001; Bouchilloux et al, 2000; Rizzo and Di Scalea, 2006). These sensors can be used as wireless. Guided waves have strong potentials for structural health monitoring because of inherent long distance inspection capability. However, magnetostrictive sensors are only suitable for ferromagnetic materials limiting applicability to steel structures.

2.5. CONCLUDING REMARKS

Over the past century, government and research agencies as well as bridge owners have shown interest in monitoring the structural behavior of both new and existing bridges and the incorporation of new materials and technologies. Though official standards to inspect the structural condition of the bridges were established in 1968, there has always been an interest in understanding and improving the performance of old and new bridges while increasing end user safety. While the NBIS contains a comprehensive bridge data base, this information is not based on quantitative evaluations but rather qualitative inspection which does not readily indicate the structural performance of a given bridge. Structural bridge monitoring and SHM systems (which imply the use of sensors, smart materials/structures, communications, data processing and reporting) have been recognized as important inspection and management tools to base bridge management decisions on qualitative data. The data gathered from SHM systems can aid decision makers in allocating funds in the direction of greatest need and benefit.

The aim of this work is to contribute to the bridge community with new monitoring techniques using existing and new sensing systems in three highway bridge types as well as engineered construction materials, already deployed or to be deployed.

- In a project funded by the Iowa DOT, two basket-handle arch pedestrian bridges located over I-235 were monitored during construction and in service to assess hanger load distribution and minimize crack damage of the pre-cast deck.
- In the Bettendorf Bridge, with the support of the FHWA's IBRC program and the City of Bettendorf, two short-term and one-long term monitoring events of multiple pultruded FRP deck panels supported on prestressed girders were conducted to assess time dependent structural performance parameters.
- A FRP panel temporary bypass bridge was evaluated as a replacement to typical steel temporary bridges. This bridge was instrumented with transducers for measuring deflections and loaded with a static truck at pertinent locations to evaluate its performance.
- As part of the five year Smart Timber Bridge Research Plan supported by the Forest Product Laboratory (FPL), smart timber glulam girders were developed. Prior to the assembling, wood laminates were instrumented with packaged FBG sensors using both custom designed and commercially available packages, assembled and tested for the purpose of developing a SHM system for timber bridges.

2.6. REFERENCES

1. Alampalli, S. (2010). "Special Issue on Bridge Inspection and Evaluation." Journal of Bridge Engineering 2010, ASCE July/August 2010 © ASCE pp. 349-351.

2. Alexopoulos, N. D., Bartholome, C., Poulin, P. and Marioli-Riga, Z. (2010). "Structural Health Monitoring of Glass Fiber Reinforced Composites Using Embedded Carbon Nanotube (CNT) Fibers." Composites Science and Technology (2010). Composites Science and Technology 70 260–271. Science Direct. Web. doi:10.1016/j.compscitech.2009.10.017. Last time accessed: October 2010.

3. American Association of State Highway and Transportation Officials Highway Subcommittee on Bridges and Structures (AASHTO HSCOBS) (2005). "Grand Challenges: A Strategic Plan for Bridge Engineering." http://bridges.transportation.org/Documents/2005strategicplan-websiteversion.pdf. Last time accessed September 2010.

4. Ayres, J. W., Lalande, F., Chaudhry, Z. and Rogers, C. A. (1998). "Qualitative Impedance-Based Health Monitoring of Civil Infrastructures." Smart Materials and Structures, Vol. 7, No. 5, pp. 599-605.

5. Balageas, D., (2006). "Introduction to Structural Health Monitoring." Structural Health Monitoring. Ed. by D. Balageas, C.-P. Fritzen, and A. Guemes. ISTE Ltd. Newport Beach, CA., 490 p.

6. Barbosa, C., Costa, N., Ferreira, L. A., Araujo, L. A., Varum, H, Costa, A., Fernandes, C. and Rodrigues, H. (2008). "Weldable Fibre Bragg Grating Sensors for Steel Bridge Monitoring." Measurement Science and Technology. 19 (2008) 125305, 10 p., © 2008 IOP Publishing Ltd. UK.

7. Bouchilloux, P., Lhermet, N. and Claeyssen, F. (2000). "Electromagnetic Stress Sensor for Bridge Cables and Prestressed Concrete Structures." Journal of Intelligent Material Systems and Structures, Vol. 10, No. 5, pp. 397-401.

8. Boyes, W. (2010). "Nanotechnology for Sensors." Instrumentation Reference Book. Ed. W. Boyes. Fourth Edition. Elsevier, Jordan Hill, Oxford, UK, 905 p.

9. Bronnimann, R., Nellen, P. M and Sennhauser, U. (2000). "Reliability Monitoring of CFRP Structural Elements in Bridges with Fiber Optic Bragg Grating Sensors." Journal of Intelligent Material Systems and Structures, Vol. 10, No. 4, pp. 322-329.

10. Bryzek, J. (1996). "Impact of MEMS Technology on Society." Journal of Sensors and Actuators A 56 (1996) pp. 1-9.

11. Brownjohn, J., Moyo, P., Omenzetter, P and Chakrabotry, S. (2005). "Lessons from Monitoring the Performance of Highway Bridges." Structural Control and Health Monitoring, 2005, V. 12, pp. 227-244. www.interscience.wiley.com, DOI: 10.1002/stc.67.

12. Browhjohn, J. M. W. (2007). "Structural Health Monitoring of Civil Infrastructure." Philosophical Transactions of the Royal Society (2007) 365, pp. 589-622. Doi:10.1098/rsta.2006.1925. Published on line 13 December 2006.

13. Carder, D. (1937). "Observed Vibrations of Bridges." Bulletin of the Seismological Society of America, United States Coast and Geodesic Survey, San Francisco California, Vol. 27 – No. 4, October, 1937, pp. 267-303.

14. Casas, J. R. and Cruz, P. J. S. (2003). "Fiber Optic Sensors for Bridge Monitoring." Journal of Bridge Engineering © ASCE, November/December 2003, Issue 6, pp. 362-373.

15. Chase, S. and Ghasemi, H. (2003). "A Vision for Highway Bridges for the 21st Century." Proceedings of the 4th International Workshop on Structural Health Monitoring, Stanford University, Stanford, CA. Edited by Fu-Kuo Chang, 2003.

16. Chase, S. (2005). "The role of Sensing and Measurement in Achieving FHWA's Strategic Vision for Highway Infrastructure." Sensing Issues in Civil Structural Health Monitoring. Ed. F. Ansari, Springer 2005, pp. 23-32.

17. Chen, P. and Chung, D. D. L. (1995). "Carbon-Fiber-Reinforced Concrete as an Intrinsically Smart Concrete for Damage Assessment during Dynamic Loading." Journal of the American Ceramic Society, Vol. 78, No. 3, pp. 816–818.

18. Choi, Y. K and Salvia, M. (1999). "Processing and Modeling of Adaptive Glass-Epoxy Laminates with Embedded Shape Memory Alloys." Proceedings of the 10th International Conference on Adaptive Structures and Technologies, Paris, France, 1999, Lancaster-Basel, Technomic Publishing Co, Inc., pp. 221-228.

19. Chopra, I. (2002). "Review of State of Art of Smart Structures and Integrated Systems." American Institute of Aeronautics and Astronautics Journal, November 2002, Vol. 40, No. 11, pp. 2145-2187.

20. Doornink, J. D. (2006). "Monitoring the Structural Condition of Fracture Critical Bridges Using Fiber Optic Technology." Ph.D. Dissertation, Iowa State University, Ames, Iowa.

21. Dry, C. (1994). "Timed of Chemicals in Cementitious Material After the Material has Hardened to Repair Cracks, Rebond Fibers, and Increase Flexural Toughening." Fracture Mechanics 25th Vol. ASTM STP 1220, Philadelphia, 1994, pp. 123-127.

22. Dry, C. (1996). "Procedures Developed for Self Repair of Polymer Matrix Composites Materials." Composites Structures, 35, 1996, pp. 263-269.

23. Faber, M. H., Val, D. V. and Stewart, M. G. (2000). "Proof Load Testing for Bridge Assessment and Upgrading." Journal of Engineering and Structures, Elsevier, Vol. 22, (2000), pp. 1677-1689.

24. Farqharson, F. B. (1954). "Aerodynamic Stability of Suspension Bridges with Special Reference to the Tacoma Narrows Bridge." Bulletin No. 116, University of Washington Engineering Experiment Station, Seattle, Washington.

25. Fedder, G. K. and Mukherjee, T. (1996). "Physical Design for Surface-Micromachined MEMS." Proceedings of the 5th ACM/SIGDA Physical Design Work, Reston, VA, USA, April 15-17, 1996, pp. 53-60.

26. Franpogol, D. M., Strauss, A. and Kim, S. (2008). "Bridge Reliability Assessment Based on Monitoring." Journal of Bridge Engineering, ASCE May/June 2010, pp. 312-326.

27. Friedland, I. and Small, E. (2003). "FHWA Bridge Research and Technology Deployment Initiative." Proceedings of the 2003 Mid-Continent Transportation Research Symposium, August 2002, pp. 1-9.

28. Fuhr, P. L., Huston, D. R., Nelson, M., Hu, J., Mowat, E., Spammer, S. and Tamm, W. (2000). "Fiber Optic Sensing of a Bridge in Waterbury, Vermont," Journal of IntelligentMaterial Systems and Structures, vol. 10, no. 4, pp. 293-303.

29. Gangopadhyay, T. K., Majumder, M., Chakraborty, A. K., Dikshit, A. K. and Bahttacharya, D. K. (2009). "Fibre Bragg Grating Strain Sensor and Study of its Packaging material for use in Critical Analysis on Steel Structure." Journal of Sensors and Actuators A 150 (2009), pp. 78-86.

30. Geng, R. S. (2004). "Application of Acoustic Emission for Aviation Industry – Problems and Approaches." Proceedings of the 16th WCNDT 2004 – World Conference on NDT, August 30th to Sep. 3rd, 2004, Montreal, Canada.

31. Ghorbanpoor, A., and Benish, N. (2003). "Non-Destructive Testing of Wisconsin Highway. Bridges." Final Report, Wisconsin Highway Research Program, Project No. 0092-00-15, 102 pp.

32. Guiguirtiu, V. and Rogers, C. (1999). "New Results in the Application of E/M Impedance Method to Machinery Health Monitoring and Failure Prevention." 53rd Meeting of the Society for Machinery Failure Prevention Technology, April 20-22, 1999. Virginia Beach, VA, 9 p.

33. Guy, P. and Monnier, T. (2006). "Structural Health Monitoring with Piezoelectric Sensors." Structural Health Monitoring. Ed. by D. Balageas, C.-P. Fritzen, and A. Guemes. ISTE Ltd. Newport Beach, CA, 490 p.

34. Gu, H. Moslehy, Y., Sanders, D., Song, G. and Mo, Y. L. (2010). "Multi-Functional Smart Aggregate-Based Structural Health Monitoring of Circular Reinforced Concrete Columns Subjected to Seismic Excitation." Earth and Space 2010: Engineering, Science, Construction, and Operation in Challenging Environments. Proceedings of the 12th International Conference on Engineering, Science, Construction and Operation Environments. ASCE Conf. Proc. doi:10.1061/41096(366)272.

35. Hao, J. H., S. Takahashi, Z. H, Cai, J. H., NG, X. F., Yang, Z. H., Chen, C. Lu (2006). "Packaging Effects on Fiber Bragg Grating Sensor Performance." Acta Automatica Sinica, Vol. 32, No. 6, pp. 999-1007.

36. Haque, M. A., and M. Saif, T.A. (2002). "Application of MEMS Force Sensors for in Situ Mechanical Characterization of Nano-scale Thin Films in SEM and TEM." Sensors and

Actuators A Physical Vols. 97-98 (2002), pp. 239-245. Web. doi:10.1016/S0924-4247(01)00861-5. Last time accessed: October 2010.

37. Hierold, C., Jungen, A., Stampfer, C. and Helbling, T. (2007). "Nano Electromechanical Sensors Based on Carbon Nanotubes." Sensors and Actuators A Physical (2007). Science Direct. Elsevier, doi:10.1016/j.sna.2007.02.007, pp, 51-61. Last time accessed: October 2010.

38. Hill, K. O., Fuji, Y., Johnson, D. C. and Kawasaki, B. S. (1978). "Photosensitivity in optical fiber waveguides: Aplication to reflection fabrication." Appl. Physics Lett., Vol. 32, pp. 647-649, 1978.

39. Hill, K. O., Malo, B., Bilodeau, F., Johson, D. C and Albert, J. (1993). "Bragg gratings Fabricated in Monomode Photosentive Optical fiber by UV exposure through a phase mask." Appl. Phys. Letters, Vol. 62, pp. 1035-1037, 1993.

40. Hill, K. O. and Meltz, G. (1997). "Fiber Bragg Gratin, Technology Fundamentals and Overview." Journal of Lightwave Technology, Vol. 15, No. 8, August 1997, pp. 1263-1276.

41. Iowa Deparment of Transportation (DOT) News (2010). "Iowa's Bridge Diagnostic Load Testing Program." Research – Bureau of Research and Technology, Iowa Department of Transportation, Ames, IA, 12 p.

42. Jauregui, D. V. (2001). "A Review of In-Situ Load Testing in the U.S. for Bridge Rating Purposes." Revista Internacional de Desastres Naturales, Accidentes e Infrastructura Civil, 2001, Vol. 1 No. 2, pp. 157-164.

43. Judy, J. W. (2001). "Microelectromechanical Systems (MEMS): Fabrication, Design and Applications." Institute of Physics Publishing, Smart Materials and Structures 10, pp. 1115-1134.

44. Kang, I., Schulz, M. J., Kim, J. H., Shanov, V. and Shi, D. (2006). "A Carbon Nanotube Strain Sensor for Structural Health Monitoring." Smart Materials and Structures. Vol. 15, pp. 737-748. http://iopscience.iop.org/0964-1726/15/3/009/pdf/0964-1726_15_3_009.pdf. Last time accessed October 2010.

45. Kawiecki, G. (1998). "Feasibility of Applying Distributed Piezotransducers to Structural Damage Detection." Journal of Intelligent Material Systems and Structures, Vol. 9, No. 3, pp. 189-197.

46. Khazem, D. A., Kwun, H., Kim, S. Y. and Dynes, C. (2001). "Long-Range Inspection of Suspender Ropes in Suspension Bridges using the Magnetostrictive Sensor Technology." In Proceedings of the 3rd International Workshop on Structural Health Monitoring: The Demands and Challenges, F.-K. Chung, Ed., pp. 384-392, CRC Press, New York, NY, USA.

47. King, G. and Henderson, G. (2007). "Statement of King W. Gee, Associate Administrator for Infrastructure and Gary Henderson, Director, Office of Infrastructure Research and Development Federal Highway Bridge Inspections Before the Committee on Transportation and Infrastructure Subcommittee on Highways and Transit." United States House of

Representatives, October 23, 2007. http://testimony.ost.dot.gov/test/pasttest/07test/gee1.htm. Last time accessed: September 2010.

48. Ko, J. M. and Ni, Y. Q. (2005). "Technology Developments in Structural Health Monitoring of Large-Scale Bridges." Journal of Engineering Structures, Vol. 27 (2005), pp. 1715-1725.

49. Kreuzer, M. (2007). "Strain Measurement with Fiber Bragg Grating Sensors." http://www.hbm.com/fileadmin/mediapool/techarticles/2007/FBGS_StrainMeasurement_en.pdf Accessed in July 2010.

50. Kwun, H. and Bartels, K. A. (1998). "Magnetostrictive Sensor Technology and its Applications." Ultrasonics, Vol. 36, No. 1-5, pp. 171-178.

51. Lan, C., Zhou, Z, Sun, S. and Ou, J. (2008). "FBG Based Intelligent Monitoring System of the Tianjin Yonghe Bridge." Smart Sensor Phenomena, Technology, Networks, and Systems 2008, Vol. 6933, Article 693312 of Proceedings of SPIE, pp. 9, San Diego, California, USA, March 2008.

52. Li, Z., Zhang, D. and Wu, K. (2002). "Cement-Based 0-3 Piezoelectric Composites." Journal of the American Ceramic Society, Vol. 85, No. 2, pp. 305-313.

53. Li, H. N., Li, D. S, and Song, G. B. (2004). "Recent Applications of Fiber Optic Sensors to Health Monitoring in Civil Engineering." Engineering Structures, Vol. 26, Issue 11, September 2004, pp. 1647-1657.

54. Lichtenstein, A. (1993). "The Silver Bridge Collapse Recounted." Journal of Performance of Construction Facilities, ASCE Nov. 1993, Vol. 27, Issue 4, pp. 249-261.

55. Lichtenstein, A. G. and Associates (1998). "Manual for Bridge Rating through Load Testing." Research Results Digest, Number 234, National Cooperative Highway Research Program, 1998, Washington, D.C.

56. Lin, Y. B., Chan, K. C., Chern, J. C. and Wang, L. A. (2005). "Packaging Methods of Fiber-Bragg Grating Sensors in Civil Structure Applications." IEEE Sensors Journal, DOI 10.1109/JSEN.2005.844539.

57. Lu, P. (2008). "A Statistical Based Damage Detection Approach for Highway Bridge Structural Health Monitoring." Ph.D. Dissertation, Iowa State University, Ames, Iowa.

58. Lynch, J. P., Partridge, A., Law, K. H., Kenny, T. W., Kiremidjian, A. S. and Carryer, E. (2003). "Designs of Piezoresistive MEMS-Based Accelerometer for Integration with Wireless Sensing Unit for Structural Monitoring." Journal of Aerospace Engineering, ASCE July 2003, pp. 108-114.

59. Maalej, M., Karasaridis, A., Pantazopoulou, S. and Hatzinakos, D. (2002). "Structural Health Monitoring of Smart Structures." Institute of Physics Publishing, Smart Materials and Structures, Vol. 11, 2002, pp. 581-589.

60. Measures, R. M., Alavie, A. T., Maaskant, R., Ohn, M. Karr, S. and Huang, S. (1995). "A Structurally Integrated Bragg Grating Laser Sensing System for a Carbon Fiber Prestressed Concrete Highway Bridge." Smart Materials and Structures, Vol. 4, No. 1, pp. 20-30.

61. Melle, S. M., Liu, K. and Measures, R. M. (1993). "Practical Fiber-Optic Bragg Grating Strain Gauge System." Applied Optics, July 1993, Vol. 32, No. 19, pp. 3061-3069.

62. Meltz, G., Morey, W. W. and Glenn, W. H. (1989). "Formation of Bragg gratings in optical fiber by a transverse holographic method." Optical Society of America, August 1st 1989, Vol. 14, No. 15, Optic Letters.

63. Mita, A. (1999). "Emerging needs in Japan for Health Monitoring Technologies in Civil and Building Structures." In Proceedings 2nd International. Workshop on Structural Health Monitoring, Stanford University.

64. Moore, M., Phares, B. M., Graybeal, B., Rolander, D. (2001). "Reliability of Visual Inspection for Highway Bridges." Volume I: Final Report. Federal Highway Administration, Report No. FHWARD- 01-020, 486 p.

65. Motoku, M., Valdya, U. K, and Janowski, G. M. (1994). "Parametric Studies on Self Repairing Approaches for Resin Infused Composites Subjected to Low Velocity Impact." Smart Materials and Structures, 8, 1999, pp. 623-638.

66. Moyo, P., Brownjohn, J. M. W., Suresh, R., and Tjin, S. C. (2005). "Development of Fiber Bragg Grating Sensors for Monitoring Civil Infrastructure." Engineering Structures 2005, Vol. 27, pp. 1828-1834.

67. Mufti, A. A., Tadros, G. and Jones, P. R. (1997). "Field Assessment of Fibre-Optic Bragg grating Strain Sensors in the Confederation Bridge." Canadian Journal of Civil Engineering, Vol. 24, No. 6, pp. 963-966.

68. Nanotechnology (2010). Encyclopedia Britannica Online. http://www.britannica.com. Last date accessed: September 2010.

69. National Bridge Inventory (NBI). (2010). "Deficient Bridges by State and Highway System." http://www.fhwa.dot.gov/bridge/deficient.cfm. Last date accessed: March, 2011.

70. Nawy, E., Maher, M., Snitzer, E., Chen, B., Prohaska, J. D. and Latimer, K. (1994). "Fiber Optic Sensors for Strength Evaluation and Early Warning of Impending Failure in Structural Components." The State University of New Jersey Rutgers, College of Engineering, Department of Civil and Environmental Engineering, Founded by the National Science Foundation, March 1994, 210 p.

71. Obadat, M., Lee, H. D., Bhatti, M. A. and Maclean, B. (2003). "Full-Scale Field Evaluation of Microelectromechanical System-Based Biaxial Strain Transducer and Its Application in Fatigue Analysis." Journal of Aerospace Engineering, ASCE July 2003, pp. 100-107.

72. Oppenheim, I. J., Garret, Jr., J. H., and Gabriel, K. J. (2000). "Potential MEMS Applications in Civil Engineering." Proceedings of SPACE 2000, 7th International Conference and Exposition

on Engineering, Construction, Operations and Business in Space, February 27 - March 2, 2000, Albuquerque, New Mexico, pp. 495-501.

73. Pakzad, S. N., Kim, S., Fenves, G. L., Glaser, S. D., Culler, D. E. and Demmel, J. W. (2005). "Multi-Purpose Wireless Accelerometers for Civil Infrastructure Monitoring." In Proceedings of the 5th International Workshop on Structural Health Monitoring (IWSHM 2005), September 2005, 8 p. http://www.cs.berkeley.edu/~binetude/work/IWSHM.pdf. Last date accessed: September, 2010.

74. Park, G., Cudney, H. H., and Inman, D. J. (2000). "Impedance-Based Health Monitoring of Civil Structural Components." Journal of Infrastructure Systems, Vol. 6, No. 4, pp. 153-160.

75. Park, G., Kabeya, K., Cudney, H. H. and Inman, D. J. (1999). "Impedance-Based Structural Health Monitoring for Temperature Varying Applications." JSME International Journal, Series A, Vol. 42, No. 2, pp. 249-258.

76. Park, S., Yun, C.-B., Roh, Y. and Lee, J.-J. (2006). "PZT-Based Active Damage Detection Techniques for Steel Bridge Components." Smart Materials and Structures, Vol. 15, no. 4, pp. 957-966.

77. Parmar, D. S. and Sharp, S. R. (2010). "Short-Term Evaluation of a Bridge Cable using Acoustic Emission Sensors." Final Report VTRC 10-R24, 27 p.

78. Phares, B. M., Wipf, T. J., Klaiber, F. W. and Abu-Hawash, A. (2003). "Bridge Load Rating Using Physical Testing." Proceedings of the 2003 Mid-Continent Transportation Research Symposium, Ames, Iowa, August 2003, 9 p.

79. Piezocryst (2010). "Piezoelectric Sensor." http://www.piezocryst.com/piezoelectric_sensors.php Last time accessed: September 2010.

80. Rizzo, P. and Di Scalea, F. L. (2006). "Wavelet-Based Feature Extraction for Automatic Defect Classification in Strands by Ultrasonic Structural Monitoring." Smart Structures and Systems, Vol. 2, No. 3, pp. 253-274.

81. Ross, R. M. and Matthews, S. L. (1999). "Emerging needs in Japan for Health Monitoring Technologies in Civil and Building Structures." In Proceedings 2nd International. Workshop on Structural Health Monitoring, Stanford University.

82. Saafi, M. and Sayyah, T. (2001). "Health Monitoring of Concrete Structures Strengthened with Advanced Composite Materials Using Piezoelectric Transducers." Composites Part B, vol. 32, No. 4, pp. 333-342.

83. Satori, K., Fukuchi, K., Kurosawa, Y. and Hongo, A. (2001). "Polyimide-Coated Small-Diameter Fiber Sensors for Embedding in Composite." Proceedings SPIE, Vol. 4328, 285 (2001). Newport Beach, CA.

84. Shiotani, T., Aggelis, D. G. and Makishima, O. (2009). "Global Monitoring of Large Concrete Structures using Acoustic Emission and Ultrasonic Techniques: Case Study." Journal of Bridge Engineering, ASCE May/June 2009, pp. 188-192.

85. Song, G. B., Gu, H. C. and Mo, Y.-L. (2008). "Smart Aggregates: Multi-Functional Sensors for Concrete Structures – A Tutorial and a Review." Smart Materials and Structures, Vol. 17, No. 3, Article ID 033001, 2008.

86. Srinivasan, A. V. and McFarland, D. M. (2001). "Smart Structures: Analysis and Design." Cambridge University Press, New York, USA, 231 p.

87. Sun, M. Q., Staszewski, W. J., Swamy, R. N. and Li, Z. Q. (2008). "Application of Low-Profile Piezoceramic Transducers for Health Monitoring of Concrete Structures." NDT and International, Vol. 41, No. 8, pp. 589-595.

88. Sun, M., Li, Z., Mao, Q. and Shen, D. (1999). "A study on Thermal Self-Monitoring of Carbon Fiber Reinforced Concrete." Cement and Concrete Research, Vol. 9, No. 5, pp. 769-771.

89. Sun, M., Staszewski, W. J. and Swamy, R. N. (2010). "Smart Sensing Technologies for Structural Health Monitoring of Civil Engineering Systems." Hindawi Publishing Corporation, Advances in Civil Engineering, Vol. 2010, Art. ID 724962, 13 p.

90. Takeda, N. (2000). "Development of Structural Health Monitoring Systems for Smart Composite Structure Systems." Proceedings of the 11th International Conference on Adaptive Structures and Technologies, Nagoya, Japan, 2000, pp. 269-276.

91. Tennyson, R. C., Mufti, A. A., Rizkalla, S., Tadros, G. and B. Benmokrane, B. (2001). "Structural Health Monitoring of Innovative Bridges in Canada with Fiber Optic Sensors." Journal of Smart Materials and Structures, Vol. 10, No. 2, pp. 560-573.

92. Thompson, K. (2010). "AASHTO-Maintenance of Bridge Design Specifications and Technical Publications." Presentation at the University of Buffalo, New York, April 5th, 2010, 94 p.

93. Udd, E. (1991). "Fiber Optic Sensors, An Introduction for Engineers and Scientists." Edited by E. Udd, John Wiley & Sons, USA, Inc., 1991, 496 p.

94. Vohra, S. T., Johnson, G. A. and Todd, M. D. (1999). "Strain Monitoring During Construction of a Steel Box-Girder Bridge with Array of Fiber Bragg Gratin Sensors." Naval Research Laboratory, NRL/MR/5670-99-8390. Washington, DC 20375-5320, 51 p.

95. Wnuk, V. P., Mendez, A., Fergurson, S. and Graver, T. (2005). "Process for Mounting and Packaging of Fiber Bragg Grating Strain Sensors for use in Harsh Environment Applications." Smart Structures Conference 2005, SPIE paper 5758-5756.

96. Wang, W., Dai, H. and Wu, S. (2008). "Mechanical Behavior and Electrical Property of CFRC-Strengthened RC Beams under Fatigue and Monotonic Loading." Materials Science and Engineering A, Vol. 479, No. 1-2, pp. 191–196.

97. Wadhawan, V. K. (2005) "Smart Structures and Materials." Journal of Science Education - Resonance, Indian Academy of Sciences. November 2005, pp. 27-41

98. Wen, S. and Chung, D. D. L. (2001). "Carbon Fiber-Reinforced Cement as a Strain-Sensing Coating." Cement and Concrete Research, Vol. 31, No. 4, pp. 665-667.

99. Wu, F. and Chang, F. K. (2001). "Diagnosis of Debonding in Steel Reinforced Concrete with Embedded Piezoelectric Elements." In Proceedings of the 3rd International Workshop on Structural Health Monitoring: The Demands and Challenges, F. K. Chang, Ed., pp. 670-679, CRC Press, New York, NY, USA.

100. Yang, C., Wu, Z. and Zhang, Y. (2008). "Structural Health Monitoring of an Existing PC Box Girder Bridge with Distributed HCFRP Sensors in a Destructive Test." Smart Materials and Structures, Vol. 17, No. 3, Article ID 035032, 10 p.

101. Yang, Y., Lim, Y. Y. and Soh, C. K. (2008 a). "Practical Issues Related to the Application of the Electromechanical Impedance Technique in the Structural Health Monitoring of Civil Structures. I. Experiment." Smart Materials and Structures, Vol. 17, No. 3, Article ID 035008, 14 p.

102. Yang, Y., Lim, Y. Y. and Soh, C. K. (2008 b). "Practical Issues Related to the Application of the Electromechanical Impedance Technique in the Structural Health Monitoring of Civil Structures. II. Numerical Verification." Smart Materials and Structures, Vol. 17, No. 3, Article ID 035008, 12 p.

103. Yoshida, H., Funaki, A. and Yano, S. (1996). "On the Response and the Responsive Shape Control of Environmentally Responsive Composite with Embedded Ti-Ni Alloy as Effectors." Proceedings of the Third Internationally Conference on Intelligent Materials, Lyon, France, SPIE Proc. Vol. 2779, 1996, Wilmington (PA), pp. 523-529.

104. Zhao, M. and Xiong, X. (2009). "A New MEMS Accelerometer Applied in Civil Engineering and its Calibration Test." The Ninth International Conference on Electronic Measurement & Instruments ICEMI'2009, pp. 2–122-2–125.

CHAPTER 3. CONSTRUCTION, MONITORING AND EVALUATION OF TWO PEDESTRIAN ARCH BRIDGES WITH PRECAST DECK SYSTEM

A refereed proceeding paper published on conference CD
in *2007 Transportation Research Board 86th Annual Meeting*.

Michal LaViolette, Ursula Deza,
Terry Wipf, Brent Phares, Ahmad Abu-Hawash

3.1. ABSTRACT

This paper presents the rationale for, and results of, structural monitoring of two steel basket-handle arch pedestrian bridges which were constructed in stages to minimize traffic disruptions. These bridges utilize a hanger system consisting of high-strength threaded steel rods to support the precast, post-tensioned concrete deck system. Externally-mounted accelerometers were used to monitor the free vibration of each hanger during all incremental construction stages as well as one year after completion. The acceleration records for each hanger were analyzed using a fast Fourier transform (FFT) to calculate the natural frequency of several modes of vibration. These natural frequencies were then used to estimate the tensile force in each hanger considering both taut-string theory and the flexural stiffness of the steel hanger rod. The results of this work show the value of structural monitoring during construction and indicate that some moderate changes in structural behavior occurred after the bridge entered service.

3.2. BACKGROUND

3.2.1. INTRODUCTION

In the summer of 2003, the Iowa Department of Transportation (Iowa DOT) constructed a 262 ft (80 m) span, basket-handle arch pedestrian bridge over Interstate 235 (I-235) near the Botanical Center in Des Moines, Iowa. This bridge, later named the Edna M. Griffin Memorial Bridge, was the first of three nearly identical bridges to be constructed as part of the reconstruction of I-235.

Interstate 235 is the major transportation corridor through the Des Moines metropolitan area and carries significantly more traffic than any other corridor in the state of Iowa. The Iowa DOT is

currently rebuilding the entire freeway to current design standards, which will improve capacity and greatly reduce the number of traffic accidents. Construction is scheduled for completion in 2007.

As part of this reconstruction, the Iowa DOT and the City of Des Moines wanted to create a set of signature bridges that would provide a "gateway" into the city. Three basket-handle arch pedestrian bridges were designed to provide a dramatic visual entryway into the state capitol (see Figure 3.1). The bridges are the centerpiece of the master aesthetic plan that was developed early in the planning for the I-235 project.

Figure 3.1. Overall View of the 40th Street Pedestrian Bridge Over I-235 – Des Moines, IA

3.2.1. RATIONALE FOR ARCH BRIDGES AND CONSTRUCTION PROCESS

The basket-handle arch spans were designed in response to the Des Moines community's strong pride and association with its arch river bridges as symbolized in the city's graphic logo. A significant advantage to the basket-handle bridge configuration is the ability to span the entire freeway without a central pier, providing an airy, open feeling, while allowing for a secure pedestrian crossing near four different schools.

The steel arch ribs for each bridge were erected in a single overnight closure of the freeway. In order to accelerate the assembly to the greatest extent possible, each set of ribs was pre-assembled into three units that could be erected in place without the use of falsework.

The precast, post-tensioned deck system was selected to allow construction without the need for falsework near the freeway. From a practical standpoint, this type of bridge would greatly limit the amount of interference to traffic on I-235. Deck panels were installed during strictly limited overnight closures of the freeway when installed near the center of the arch. Once a sufficient number of deck panels had been installed to avoid construction interference with open traffic lanes, installation operations were performed during daylight hours.

3.2.2. NEED FOR STRUCTURAL MONITORING

The bridges utilize a precast, post-tensioned concrete deck system and represent the first application of precast, segmental construction on the Iowa highway system. The match-cast concrete deck panels are suspended from the steel arch ribs using 1.42 in. (36 mm) diameter high strength steel rods.

In the months following the construction of the Griffin Bridge, a considerable amount of cracking of the concrete panels was observed at locations near the more-heavily loaded hanger rods. The assessment of hanger loads during construction of the Griffin Bridge was very subjective and consisted only of the contractor and inspection personnel manually “shaking” each hanger to determine relative degrees of tension.

The unusual nature of the bridge structural system, combined with the observed cracking and the upcoming design and construction of two additional basket-handle arch bridges compelled the Iowa DOT to host a post-construction review meeting in February 2004. One of the significant conclusions drawn from this meeting was that a more precise method of determining hanger loads, both during and after construction, of all three bridges was necessary.

The Iowa State University Bridge Engineering Center was contracted to monitor and evaluate the structural performance of the hanger rods on two similar pedestrian bridges which were constructed near 40th and 44th Streets in Des Moines during the summer of 2005. This paper presents results of this study as well as subsequent monitoring which was performed during July 2006.

3.2.3. BRIDGE DESCRIPTION

The arch ribs consist of tubular steel sections which are tapered in both the horizontal and vertical directions from 19.6 in. x 27.6 in. (500 mm x 700 mm) at the crown to 29.5 in. x 49.2 in. (750 mm x 1250 mm) at the base. The arch ribs are inclined at approximately 10 degrees and are connected at the crown by a bolted diaphragm. No other lateral bracing is provided other than a tubular steel strut below the deck level at the 44th Street and Griffin bridges.

The precast concrete deck panels were fabricated using a match-casting system in which the first panel was used as the end form during the casting of the second, or adjacent, panel. During this process, the final shape of the deck profile was precisely replicated by providing a very slight angle change at the joint between adjacent concrete panels. In order to avoid placing undue stress on the concrete panels, they must then be supported at this exact same relative elevation when erected and post-tensioned together in the field.

The hanger system used for the bridges consists of a 1.42 in. (36 mm) diameter high strength rod surrounded by a 2.56 in. (65 mm) diameter High Density Polyethylene (HDPE) pipe sheathing. The annual space surrounding the hanger rod was filled with a cementitious grout prior to delivery to the project site. This pre-grouted system required the contractor to be particularly careful in the way the hangers were handled and erected so as to avoid cracking of the grout material. The hangers were anchored in the arch rib using a standard anchor plate and nut. The hangers passed through a 3.15 in. (80 mm) diameter galvanized trumpet pipe in the deck panels and were anchored using a beveled shim plate in combination with an anchor plate and nut. The contractor was able to rotate this beveled shim plate to accommodate slight irregularities in angular construction.

The support elevations of the concrete panels were controlled by the precise adjustment of the anchor nut located at the bottom of the hanger rod directly beneath the panel. During the construction of the Griffin Bridge, it became evident that, in some cases, the hanger rod anchorage elevation, and therefore the tensile load in that particular hanger, varied considerably from that anticipated by the designers. Some minor cracking of the concrete panels was observed at the panel locations near these more-heavily loaded hanger rods.

In order to eliminate this disparity, the contractor performed a series of small adjustments in the final elevation of the panels during additional overnight closures of I-235. These overnight closures

required considerable expense to the State for traffic control and law enforcement as well as creating inconvenience and potential danger to both the traveling public and the onsite workers.

3.2.4. CONSTRUCTION SEQUENCE

The 40th Street Bridge contains a total of 22 precast concrete panels, while the 44th Street Bridge contains a total of 20 precast concrete panels. The precast panel layout and numbering system for the two bridges are presented in Figure 3.2. It should be noted that the panel layout for the Griffin Bridge was very similar to that used on the 44th Street Bridge.

The panels were segmentally erected and longitudinally post-tensioned using high-strength threaded steel rods meeting the requirements of ASTM A722. In the segmental erection process, the mating faces of adjacent panels were coated with a specialized epoxy adhesive (Unitex Segmental Adhesive) and the panels were then stressed together using a hollow-core jack. The panels are supported by 1.42 in. (36 mm) diameter, high-strength steel bar hangers. The hangers are connected to the arch rib at anchor points located at 13.78 ft (4200 mm) spaces.

The precast panel cross section is not symmetrical about the longitudinal centerline of the bridge. In order to promote bridge deck drainage, the panels were cast such that the eastern side of the panel is considerably heavier than the western side. Due to this unsymmetrical shape, the deck panels, when erected and supported from the hanger rods, and before the deck system was complete, did not hang directly below the longitudinal centerline of the bridge. In fact, these panels were observed to hang as much as 28 in. (711 mm) west of their intended position. The contractor for the 40th Street Bridge used a series of sand-filled barrels as ballast (see Figure 3.3) on the west side of the deck panels, which caused the panels to hang much closer to their intended position relative to the bridge centerline.

The deck construction sequence for each bridge was virtually identical. A brief summary of the sequence is provided below:

- The center pair of panels (1 and 1') were glued and stressed together on the ground prior to being lifted using two cranes (one on each side of the arch ribs).
- The four hanger rods for the center pair of panels (1E, 1W, 1'E and 1'W) were installed and anchored in the arch ribs. The bottom of the hanger rods were held out-of-plumb to match the inclination of the arch ribs.

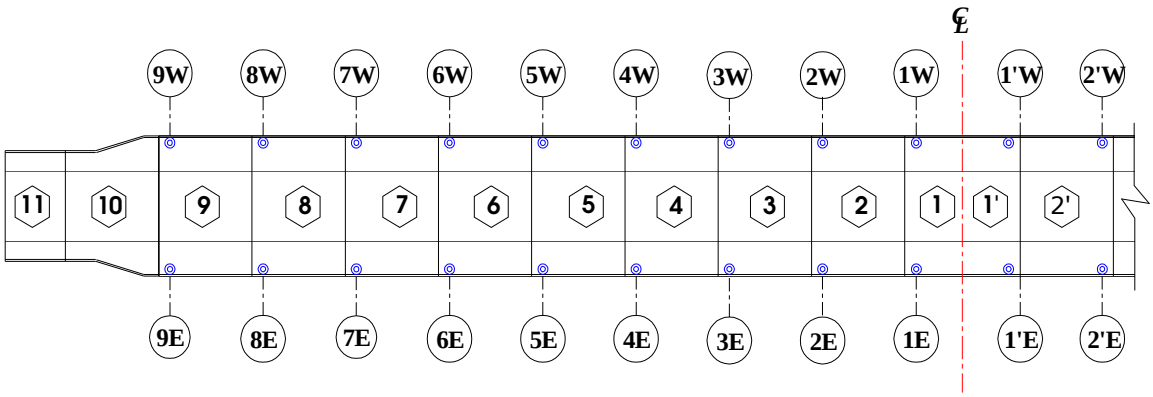

(a) 40th Street Bridge

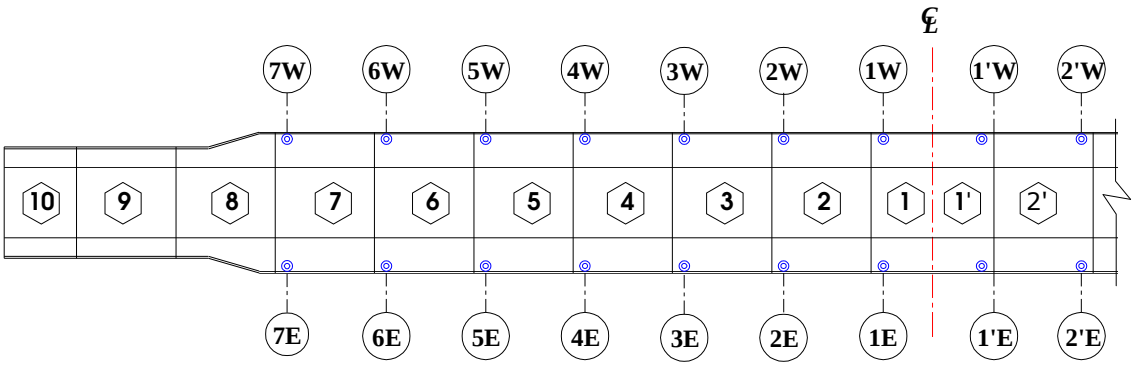

(b) 44th Street Bridge

Figure 3.2. Precast Panel Layout – I-235 Pedestrian Bridges

Figure 3.3. Sand-Filled Barrels Used as Ballast During the Erection of 40th Street Bridge Panels

- The center pair of panels were lifted and held in position just below the bottom of the hanger rods. The panels were carefully lifted as the hanger rods were inserted through the trumpet pipes located near the corner of each panel.
- Surveyed elevations at the leading end of each panel were measured prior to final release of the panels from the cranes.
- Each hanger rod was anchored against the bottom of the panels using a pair of beveled washers and nut (Stage 1).
- Subsequent panels were installed in an alternating sequence (2', 2, 3, 3', 4', 4, etc.) such that the loading on the arch was never more than one panel out of symmetry. Each additional panel added was treated as a separate loading stage for monitoring purposes (e.g., installation of panel 2' = Stage 2, panel 2 = Stage 3, etc.).

At a number of times during the panel erection process, the contractor made intermediate adjustments in the panel support elevations to maintain, to the greatest extent possible, the correct match-cast alignment as well as to roughly equalize the hanger loads. The contractor used a hollow-core jack attached to the bottom of the particular hanger rod to slightly lift panels in question. The anchor nut at the bottom of the panel would then be adjusted as necessary and the jack released to resume normal support on the anchor nut.

During the erection of the deck panels for the 40th Street Bridge, the contractor found that the entire deck was being erected as much as 2 in. (5 mm) higher than the elevation shown in the plans. In order to correct this error, the deck panels were incrementally lowered until the correct elevation was reached. This adjustment operation, as well as all intermediate adjustments, was performed sequentially at alternating hangers so that no panel was out-of-phase from adjacent panels by more than 1/4 in. (6 mm) at any time. It should be noted that on the very shortest hangers, an adjustment in hanger elevation of this amount creates a change in hanger load of nearly 40 kips (178 kN).

3.3. MONITORING AND EVALUATION METHODS

3.3.1. BACKGROUND

The use of vibration monitoring methods for estimating the tension in a bridge stay cable has been used for many years. The typical process is to mount accelerometers on the cables at a convenient location and then use a mechanical shaker is used to provide a reliable means of excitation

of the cable (Irwin, 2005). A similar technique has been used to assess the tension in external post-tensioning rods in both laboratory and field tests (Pessiki and Ozevin, 2006).

In ordinary cable monitoring, such as performed on a suspension or stay cable, the simply taut-string equation is typically used. However, the simple theory may cause unacceptable errors in many applications since the cable sag and bending stiffness are ignored (Ren et al, 2005). Contrary to the process used for strands or wire rope, the vibration monitoring for members such as the referenced hanger rods, must consider both the flexural stiffness as well as the string vibration of the overall system.

3.3.2. INSTRUMENTATION, DATA COLLECTION AND DATA PROCESSING

The test equipment used for the field evaluation consisted of an Optim 3415AC Megadac with laptop PC controller running Test Control Software. The accelerometers were mounted to the hangers approximately 5 ft (1524 mm) above the deck panels using steel clamps and were oriented with their primary axis perpendicular to the centerline of the bridge.

After placing an accelerometer, the initial values were balanced to allow for stabilization of the sensor. The acceleration record for each hanger was collected by manually exciting the hanger using a suddenly applied, horizontal force approximately 4 ft (1219 mm) above deck level. The external force was applied perpendicular to the bridge centerline. Data were collected for a period of approximately 10 sec. from which free vibration records were utilized for data processing. The test was repeated at least two times per hanger to verify the reproducibility of the data. Commercial software was used for processing the free vibration data and to obtain the natural frequencies as illustrated typically in Figure 3.4.

The hanger tensile forces were computed based on vibration methods and cable tension force estimates based on string and beam theory. The following expression (Tedesco et al, 1999) was used and the parameters are defined as:

$$T = \rho A \{ L / (n \pi) [\omega_n - (\beta_n L)^2 (EI / (\rho A L^4))^{1/2}] \}^2 \qquad \textbf{Equation 3.1}$$

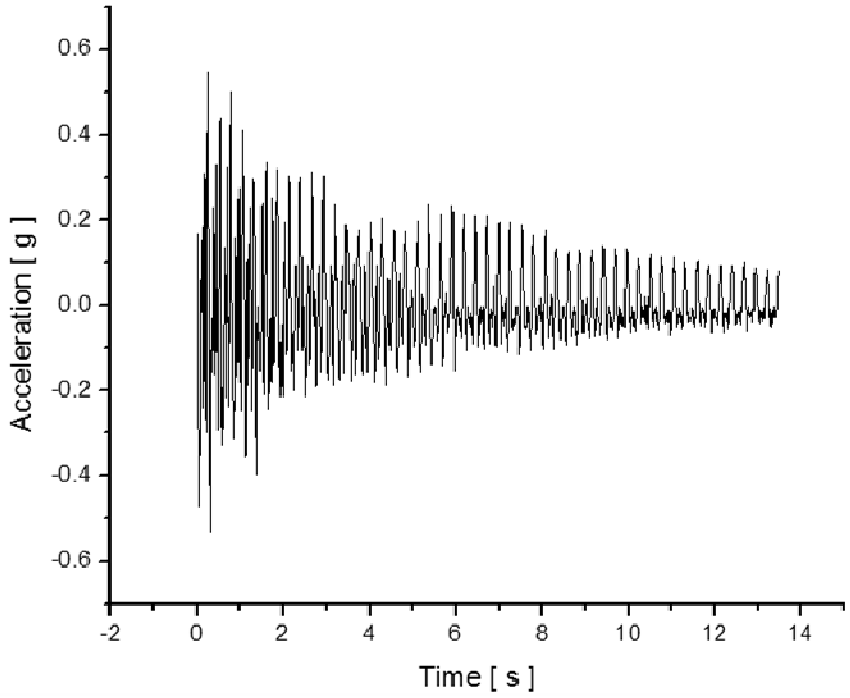

a) Real time vibration record

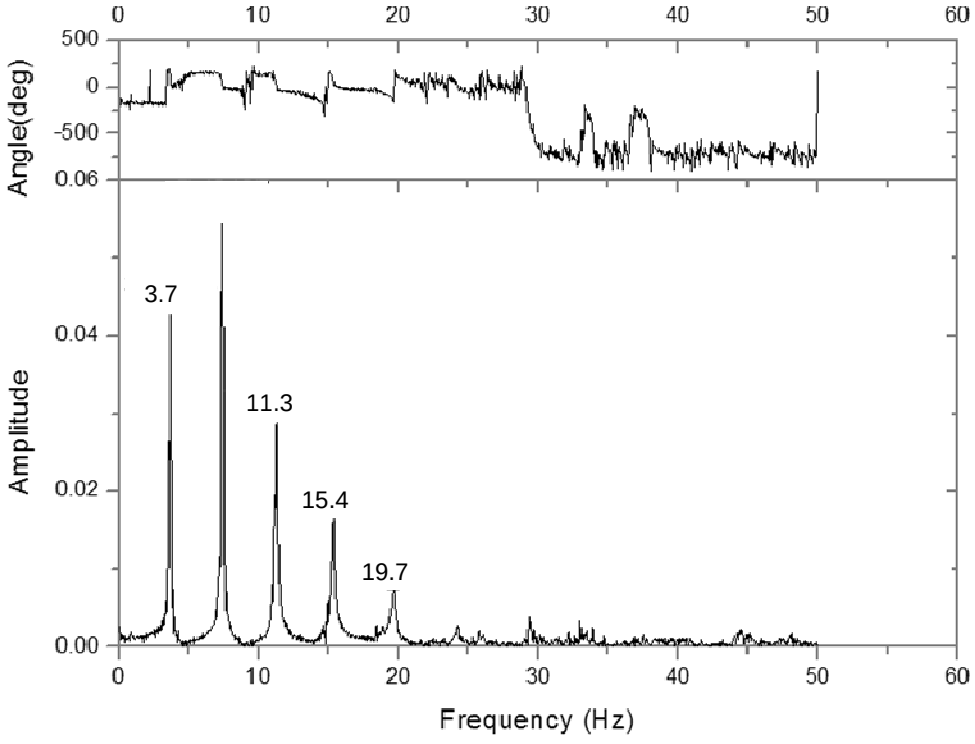

b) FFT Results

Figure 3.4. Measured and Processed Vibration Data for Hanger 2'W of the 40th Street Bridge

Where:

T: Tensile hanger force [kip]

ω_n: Natural frequency obtained from the Fast Fourier Transform (FFP) analysis

$\beta_n L$: Beam frequency constants associated with member end boundary conditions

L: Hanger rod length [ft]

E: Modulus of elasticity of 29,000 ksi for the high-strength steel bar

A: Section of the high-strength steel rod (1.58 in^2)

I: High-strength steel bar inertia, equal to 9.58 x 10^{-6} ft^4

ρ: Density corresponding to the cross section, equal to 23.13 lb-sec^2/ft^4 [concrete + steel]

n: Mode number corresponding to ω_n

The use of Equation 3.1 required some assumptions, partly due to the composite material makeup of the hangers and due to the hanger end support connection details. In particular, that includes the member end support boundary conditions, the effective hanger length, the hanger modulus of elasticity and inertia, etc. The effective flexural stiffness parameter EI of the cross section was computed using only the high strength steel bar properties (i.e., the grout was assumed to be cracked and contribute no flexural stiffness). However, the hanger density was assumed to include both the grout infill plus the steel bar. The length of the hangers was assumed to be the theoretical length between the anchor point in the arch rib and the bottom of the deck panel. For all hanger force computations, the member end support boundary conditions were assumed to be both pinned and fixed against rotation to provide a "bracketed" solution.

3.3.3. 2005 RESULTS: 40TH ST. BRIDGE

40th St. Bridge: Staged Panel Placement. Figure 3.5 presents calculated hanger forces for Construction Stages 1, 2 and 3. The data include force calculation for two member end boundary condition assumptions: 1) complete rotational fixity at both ends (fixed) and 2) no rotational fixity at both ends (pinned). A brief discussion of the data for each stage is described below.

Stage 1. The estimated dead load of the panel (including ballast) was approximately 69.9 kips. The calculated forces for the four hangers was 69.8 kips and 86.4 kips, respectively, for the fixed and the pinned conditions. The four hanger forces were relatively similar and compared closely with the estimated theoretical hanger forces of 17.5 kips (based on equal distribution of dead load to all hangers) (see Figure 3.5 (a)).

Stage 2. The summation of the six hanger forces at the completion of Stage 2 was 126.4 kips and 153.9 kips, respectively, for the fixed and pinned conditions. This compares with the total estimated dead load of the panels of 126.4 kips. Note that the hanger forces in 1'W and 1E were reduced after the second panel was placed, while the other four hanger forces increased in magnitude (Figure 3.5 (b)).

Stage 3. After placement of the Stage 3 deck panel, the estimated dead load was approximately 183.0 kips. In comparison, the calculated forces for the six hangers was 181.4 kips and 217.7 kips, respectively, for the fixed and pinned conditions. It is interesting to note that hanger 2W (one of the newly placed hangers) was very lightly loaded compared to expectations (4.0 kips for the fixed condition). In contrast, hanger 2'E carried 36.7 kips for the fixed condition. There was a considerable non-uniform redistribution of hanger forces throughout the three panels at the end of the Stage 3 construction, with significant hanger force unbalances noted at several panel point pairs (e.g., 1W and 1E, and 2'W and 2'E) (Figure 3.5 (c)).

The hanger force results for the staged construction, as well as the discussion above regarding the sensitivity of the results based on assumptions, suggest that the hanger member end boundary conditions contain some degree of fixity; further, the pinned and fixed conditions likely provide a bounded solution for the actual hanger forces with the results likely closer to the fixed condition. In the interest of simplicity, subsequent data presentation in this paper will include data based upon the assumption of member end boundary condition fixity only unless otherwise stated.

To further validate the magnitude of the hanger forces determined as noted above, strain data were also collected during the staged construction. The data are formally not presented in this paper because of some inconsistencies at several hanger locations due to construction handling issues.

However, a significant amount of data from undamaged sensors validated that the hanger force data tended more toward the assumption of fixed conditions.

It is also noteworthy that during various phases of the panel placement, visual observation of the hanger near the arch connection indicated localized curvature at numerous locations prior to placement of the deck panels, also suggesting some degree of rotational restraint. This particular

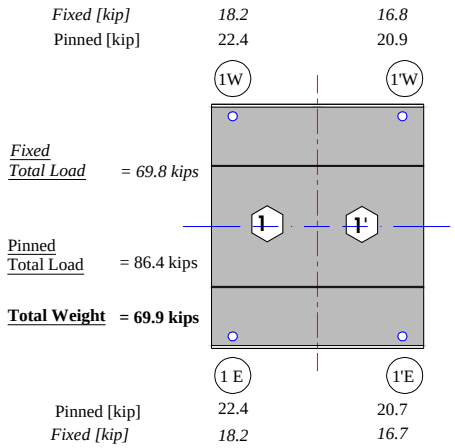

(a) Stage 1

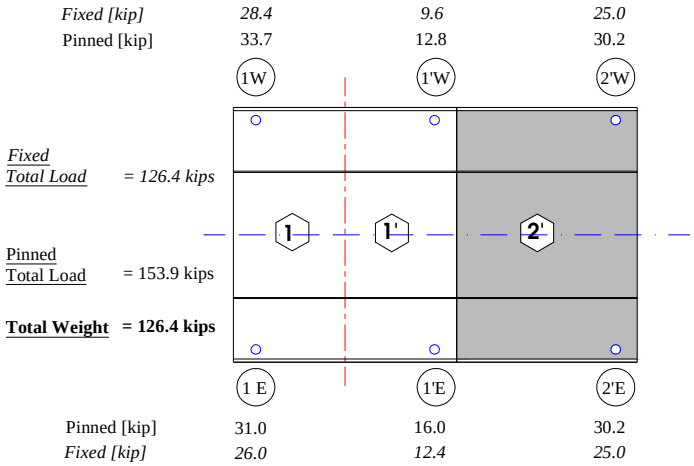

b) Stage 2

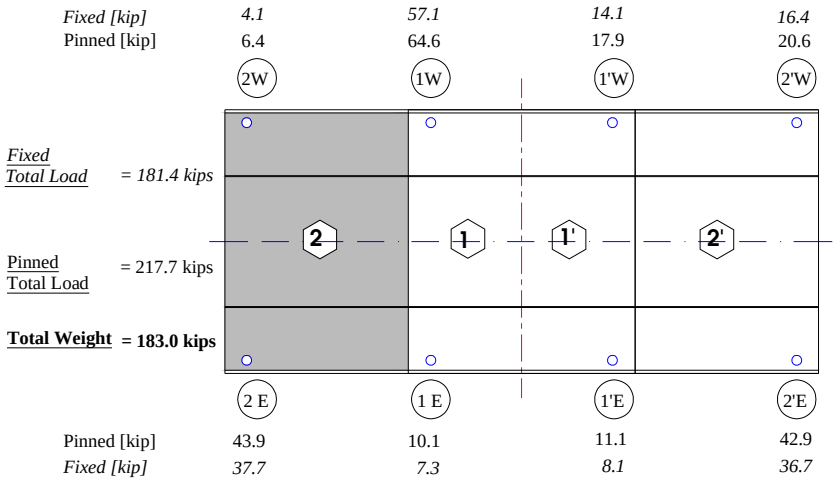

(c) Stage 3

Figure 3.5. Schematic View of Hanger Forces Calculated Using Free Vibration Method

condition was observed at numerous deck panel locations. Subsequent sensitivity calculations of hanger force looking at reasonable ranges of parametric values indicated that the boundary condition assumptions provided the greatest sensitivity.

40th St. Bridge: Preliminary Completion of Panel Placement. Table 3.1 presents the measured hanger forces after preliminary placement of all of the bridge panels (i.e., prior to any hanger force adjustment). Since the four end hangers (two each at the ends of the bridge) were too stiff to effectively measure force with the vibration method, hanger force data for these hangers are not included in Table 3.1. The data shown were collected prior to the placement of the last four end panels (two panels near each abutment). Therefore, the dead load of all of the panels assumed to be supported by the 32 hangers (16 on each arch) was used for comparison.

Based on the assumption above, the estimated deck dead load was approximately 966 kips (this excludes the four end panels, two near each abutment). In comparison, the calculated forces for the hangers (excluding all four end hangers) was 862.4 kips and 1081.1 kips, respectively, for the fixed and pinned conditions.

Other observations noted include the following:

- There was a relative lack of consistency in hanger force values (e.g., 8W, 3W, 1'W, 4'W were extremely low and 1W and 7'W were very high).
- The hanger pairs on the east and west arches tended to be out of balance with each other at many locations (e.g., hangers 5, 1', 3', 4', 5' 7' and 8').
- The total of the hanger forces on the east arch was approximately 7% higher than the forces on the west arch. This is due at least partially to the placement of ballast on the west side of the deck unit to try to balance the unsymmetrical deck weight. In fact, it is possible that this imbalance may have been caused by a slight error in the actual weight or positioning of the ballast barrels (relative to the contractor's calculations).

40th St. Bridge: Final Adjustment of Panel Placement. Table 3.1 also presents the measured hanger forces after the contractors' adjustment of the hangers following completion of the bridge. Observations noted from the table include the following:

- There was relatively good distribution of hanger forces throughout bridge.

- The total summation of hanger forces was reduced by approximately 40 kips. One possible explanation is that the bridge was constructed approximately 1.57 in. high (at the end) to 2.76 in. high (near midspan) and this alignment was corrected by lowering the panel elevations prior to the retesting of the hanger forces. This process might have increased the abutment reactions while decreasing the overall hanger loads.

Figure 3.6 shows a plot of the hanger forces for both of the arches to illustrate the redistribution of the hanger forces after adjustment. The calculated approximate panel dead load values are also shown for comparison. As noted the adjustments eliminated the outliers relative to the design values and improved the overall distribution of the forces.

Table 3.1. 40th Street Bridge: Hanger Forces Before and After Adjustment

Hanger Designation	**Before Adjustment**		**After Adjustment**	
	West Arch [kip]	East Arch [kip]	West Arch [kip]	East Arch [kip]
9	-	-	-	-
8	1.2	0.0	17.7	5.2
7	18.9	12.4	21.9	27.7
6	39.9	54.3	27.5	25.4
5	43.7	13.4	25.8	21.9
4	27.1	40.6	27.4	27.4
3	3.4	3.4	22.5	40.7
2	18.8	33.5	20.9	24.7
1	75.4	50.1	30.7	27.4
1'	3.1	28.5	33	29.6
2'	30.7	30.7	32.2	27.8
3'	54.6	10.5	25.4	19.9
4'	4.4	49.2	23.8	24.6
5'	28.9	2.4	36.4	38.3
6’	24.4	24.4	28.9	31.1
7’	60.8	32.4	23.4	20.4
8'	12.1	28.7	16.8	6.2
9’	-	-	-	-
Total Load	862.1		812.6	
Total Dead Load	996.0		996.0	

Note: “-“ denotes data not considered reliable.

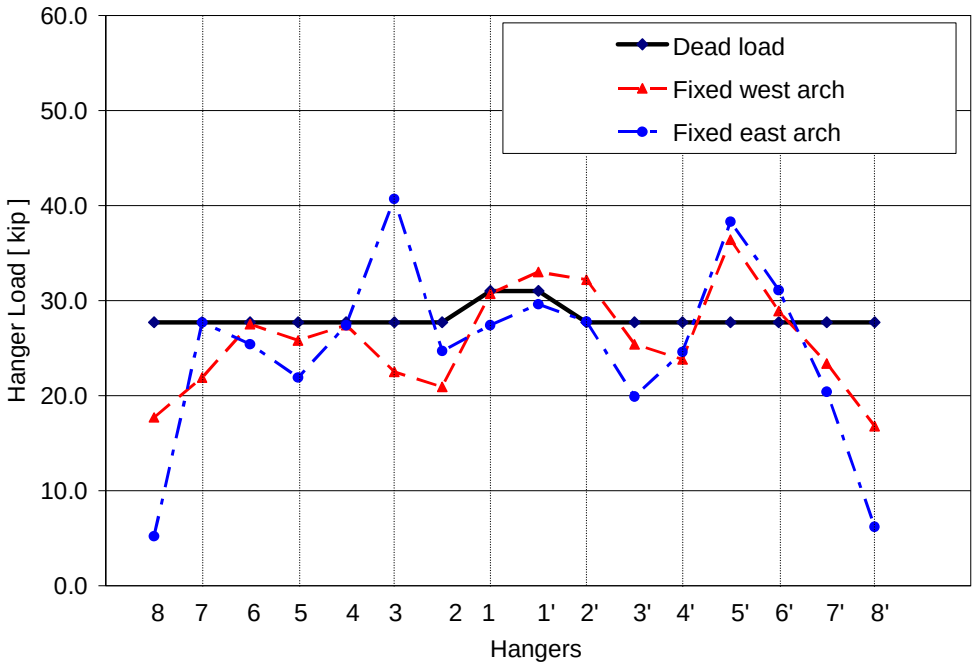

Figure 3.6. Hanger Forces in Both Arches of the 40th Street Bridge After Adjustment

3.3.4. 2005 RESULTS: 44TH ST. BRIDGE

44th St. Bridge: Preliminary Completion of Panel Placement. Table 3.2 shows the hanger forces after initial placement of the deck panels (i.e., prior to any hanger force adjustment). As noted earlier in the paper, this bridge has a strut near each abutment that helps support, along with the abutments, some of the panel dead load in the end span region. Since the four end hangers (two each at the ends of the bridge) were too stiff to effectively measure force with the vibration method, force data for these hangers are not included in the Table 3.2. The dead load of all of the panels assumed to be supported by the 24 hangers (12 on each arch) was used for comparison.

The estimated deck dead load was approximately 742 kips (this excludes the six end panels, three near each abutment). In comparison, the calculated forces for the hangers (excluding all four end hangers) was 605.1 kips and 780.3 kips, respectively, for the fixed and pinned conditions. The following are some additional observations:

- There was a relative lack of consistency in hanger force values (e.g. 4W and 5'W were very low and 5W very high).
- The hanger pairs on the east and west arches tended to be out of balance with each other at many locations.

- The total of the hanger forces on the east arch was approximately 14% higher than the forces on the west arch. It was noted previously that the deck cross section is not symmetrical; it is a deeper section on the east side, which contributes to the unbalanced forces presented. It should be noted that the design plans for both the 40th and 44th Street bridges indicate equal loading on both the east and west arch rib hangers. However, the unsymmetrical cross-section of the deck panels makes this condition unlikely.

Table 3.2. 44th Street Bridge Hanger Forces Before and After Adjustment

Hanger Designation	**Before Adjustment**		**After Adjustment**	
	West Arch [kip]	East Arch [kip]	West Arch [kip]	East Arch [kip]
7	-	-	-	-
6	4.3	34.0	23.7	28.6
5	66.6	10.2	24.3	12.0
4	9.5	11.8	30.0	20.9
3	36.8	18.7	22.2	24.7
2	16.6	42.4	23.4	33.8
1	20.5	39.2	34.0	34.0
1'	39.6	27.9	29.4	23.5
2'	34.9	22.8	24.2	25.6
3'	10.3	17.5	24.7	31.7
4'	22.0	57.1	15.5	37.1
5'	6.6	16.8	16.6	22.6
6'	14.5	24.5	9.1	25.9
7’	-	-	-	-
Total Load	605.1		597.5	
Total Dead Load	742.0		742.0	

Note: “-“ denotes data not considered reliable

44th St. Bridge: Final Adjustment of Panel Placement. Table 3.2 also shows the hanger forces after adjustment of the initial hanger forces following completion of the bridge. Observations noted from the table include the following:

- The distribution of the hanger forces was much more uniform throughout the bridge.
- The total summation of hanger forces reduced by 6 or 7 kips. This may have been caused by the hanger adjustments which slightly lowered the elevation of the deck panels near the end of the bridge, causing the strut between the arch ribs to support additional load through the bearings.

Figure 3.7 shows a plot of the hanger forces for both of the arches to illustrate the redistribution of the hanger forces after adjustment. The calculated approximate panel dead load values for each hanger are also shown for comparison. As noted the adjustments eliminated the outliers relative to the design values and improved the overall distribution of the forces.

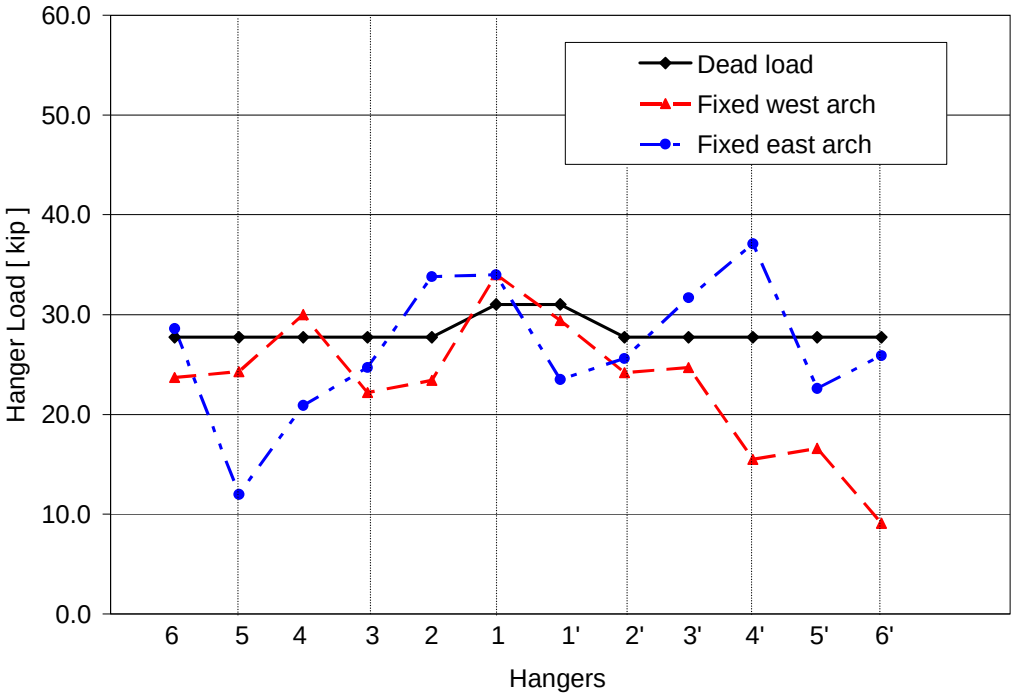

Figure 3.7. Hanger Forces in Both Arches of the 44th Street Bridge After Adjustment

3.3.5. 2006 RESULTS: 40TH ST. BRIDGE AND 44TH ST. BRIDGE

The hangers on both the 40th and 44th Street bridges were monitored approximately 1 year after the initial construction to determine if any significant changes or redistribution in the hanger forces had occurred.

Some force increases were expected due to the increased dead load that was placed after the initial monitoring, primarily due to the addition of a security fences and a deck overlay. The total increase in dead load for the bridges was approximately 96 kips.

Figure 3.8 shows the hanger forces for the 2005 and 2006 monitoring on the 40th St. Bridge (2005 data have already been discussed in the paper). The calculated dead load forces for each hanger for

both years are also shown. Observations noted from comparison of the 2006 data with the 2005 data include the following:

- The total dead load incremented in a minimum of 10% from 2005 to 2006 due to the deck overlay and security fence.
- For the 2006 data only a few hanger forces have exceeded the predicted dead load forces.
- The West Arch forces are more unevenly distributed than are the East Arch forces. Hangers 3W and 2'W changed significantly from 2005.

Figure 3.9 shows the hanger forces for the 2005 and 2006 monitoring on the 44th St. Bridge (2005 data have already been discussed in the paper). The calculated dead load forces for each hanger for both years are also shown. Observations noted from comparison of the 2006 data with the 2005 data include the following:

- The overall distribution of the hanger forces was much more uniform than for the 40th St. Bridge
- There were very moderate changes in the hanger forces during the one year of service.

3.4. CONCLUSIONS

The accelerated construction of the I-235 pedestrian bridges was completed with only minimal interference to the traveling public which satisfied the primary goal of selecting this specialized structure type. The bridges also provide an aesthetically pleasing "gateway" to the city of Des Moines. The following conclusions are based on the study results:

- Deck panel cracking caused by heavily loaded hanger rods was significantly reduced during the construction on the 40th and 44th Street bridges.
- The monitoring of the two bridges during construction provided a means for ensuring that hanger loads could be adjusted to a uniform level at both intermediate and final stages of construction. The key to this was ongoing communication and coordination with the contractor, which should be strongly encouraged for future projects.
- The method of hanger measurement has been validated and should be considered a valuable construction monitoring tool for future projects.
- In the year following construction, the changes in hanger forces on the 44th St. Bridge was more moderate than for the 40th St. Bridge. Significant changes in hanger forces occurred at one pair of hangers on the 40th St. Bridge.

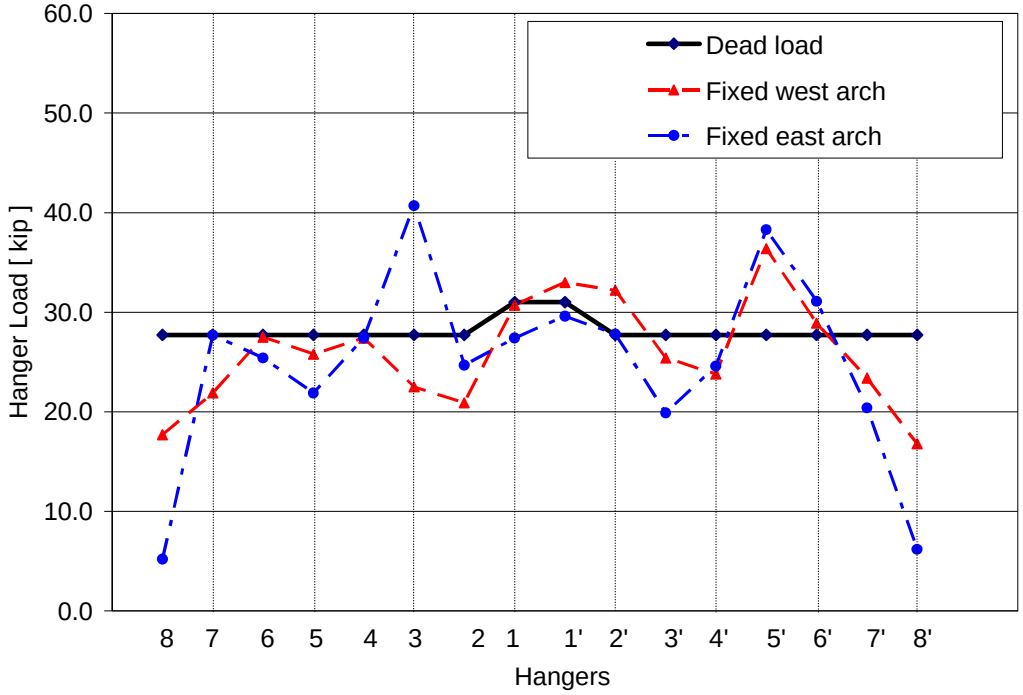

a) 2005 monitoring

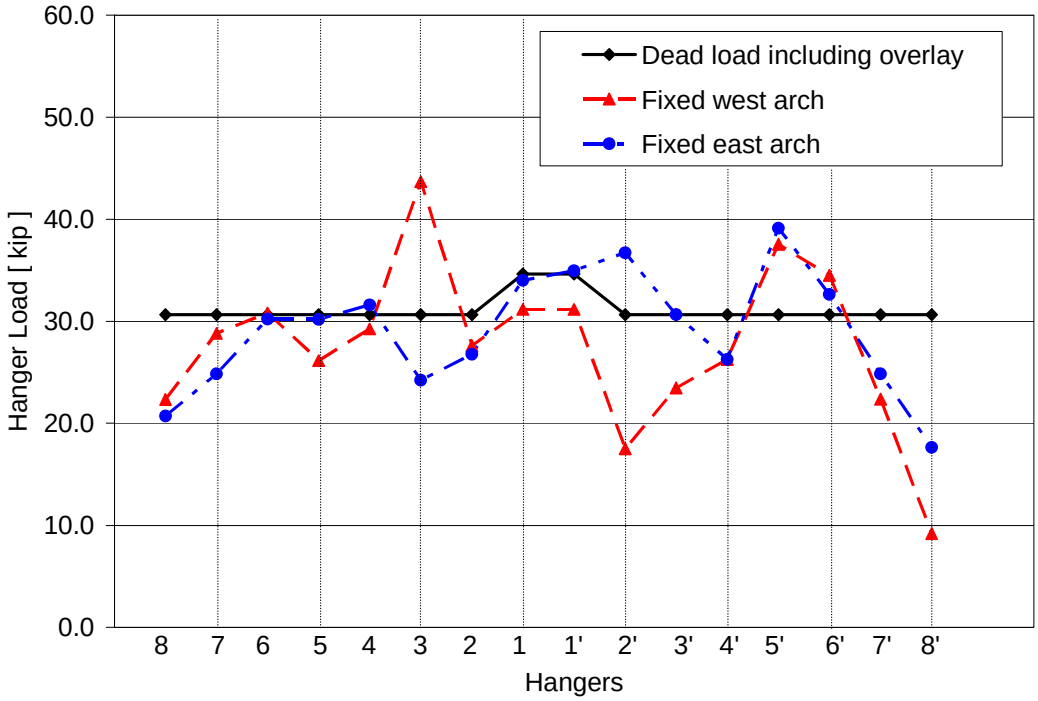

b) 2006 monitoring

Figure 3.8. Hanger Forces in Both Arches of 40th Street Bridge

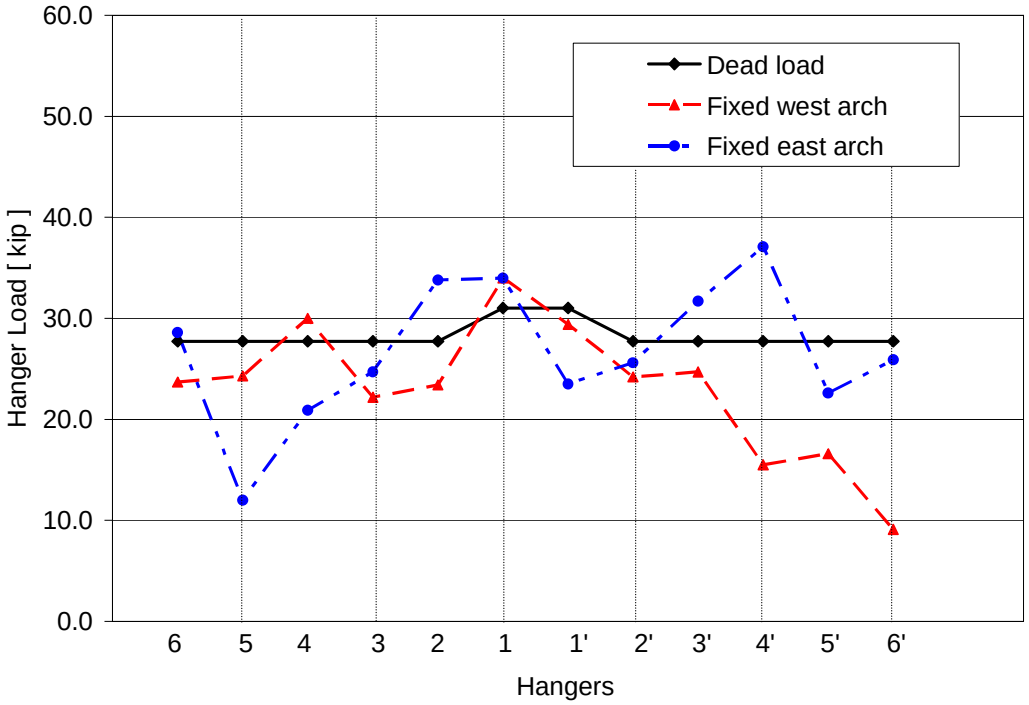

a) 2005 monitoring

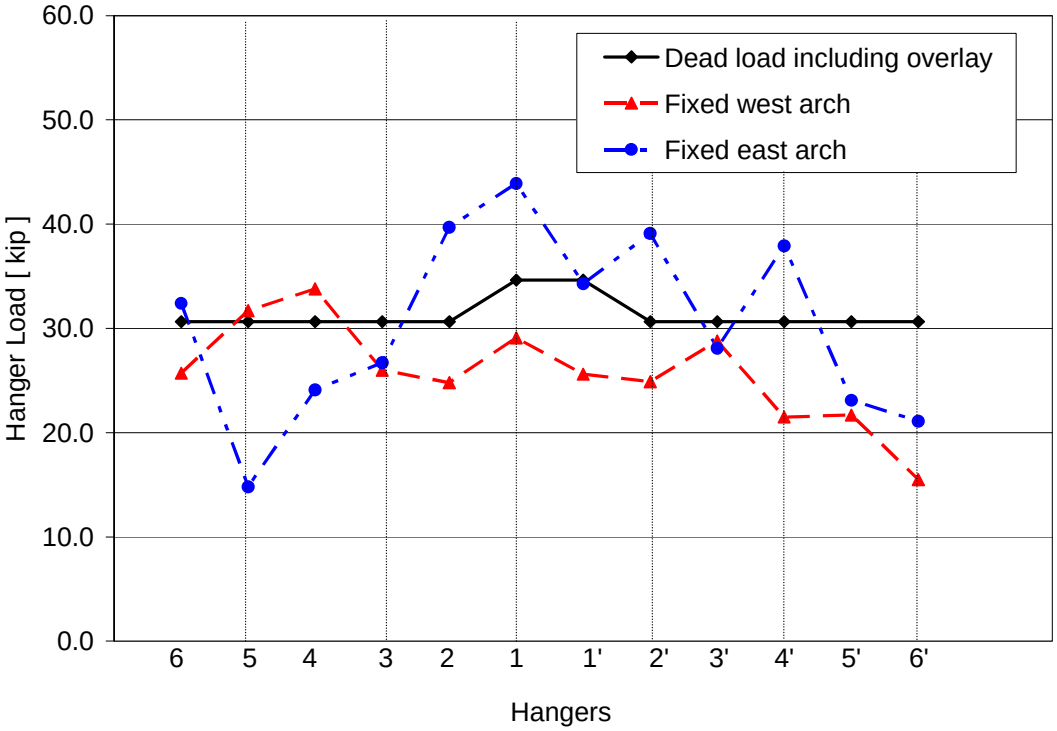

b) 2006 monitoring

Figure 3.9. Hanger forces in both arches of 44th Street Bridge

3.5. ACKNOWLEDGMENTS

The investigation presented in this paper was conducted by the Bridge Engineering Center at Iowa State University through funding provided by the Iowa Department of Transportation (DOT). The authors thank the engineers within the Office of Bridges and Structures at the Iowa DOT for their cooperation and assistance with this project. In addition, special thanks are extended to various ISU students (specifically Justin Doornink) for their help with various aspects of the project, and to Doug Wood, Manager of the Structural Engineering Laboratory, for his guidance and assistance.

3.6. REFERENCES

1. Irwin, P.A., “Field Monitoring of Cable Supported Bridges”, Proceedings of Sixth International Symposium on Cable Dynamics, Charleston, SC, September 19-22, 2005.

2. Pessiki, S. and Ozevin, D., “Evaluation of the Effective Prestress Force in External Post-tensioning Bars ins a Steel Pier Cap”, Proceedings of Structural Faults and Repair 2006, Edinburgh, U.K., June 13-15, 2006.

3. Ren, W.X., Chen, C., and Hu, W., “Empirical formulas to estimate cable tension by cable fundamental frequency”, Structural Engineering and Mechanics, Vol. 20, No. 3 (2005), pp 363-380.

4. Tedesco, J. W., McDougal, W. G. and Ross, C. A. (1999). “Structural Dynamics: Theory and Applications.” Menlo Park, California: Addison Wesley Longman, Inc.

CHAPTER 4. STRUCTURAL FIELD TESTING AND EVALUATION OF TWO DEMONSTRATION FRP DECK BRIDGES: CASE STUDY ON FRP PANEL DECK BRIDGE AND TEMPORARY BYPASS BRIDGE

A refereed proceeding paper published on conference CD
in *2009 Transportation Research Board 88th Annual Meeting*.

Yoon-Si Lee, Travis Hosteng, Ursula Deza, James Nelson,
Terry Wipf, Brent Phares, Doug Wood and F. Wayne Klaiber

4.1. ABSTRACT

In the last decade, the use of fiber reinforced polymer (FRP) composites technology has emerged as an option in structural engineering and has shown its potential for structural applications in bridges. FRP composite materials are appealing in that they are highly resistant to corrosion, have a low weight, and have a high tensile strength. This paper summarizes two projects, funded through the Federal Highway Administration's Innovative Bridge Research and Construction program, that investigate the applicability and effectiveness of using FRP composites in bridge construction: (1) Bettendorf FRP panel deck bridge, the first FRP bridge deck in the US that uses composite action with prestressed concrete girders, and (2) FRP temporary bypass bridge, developed to replace existing steel temporary bridges. The paper presents structural field performance results for each demonstration project and for each bridge provides correlation of the performance with design parameters.

4.2. INTRODUCTION

Fiber Reinforced Polymer (FRP) has gained increasing interest among the bridge engineering community due to its outstanding mechanical characteristics and non-corrosive nature. These unique FRP characteristics eliminate the maintenance problems caused by moisture, salt air, and termites that pose concerns for typical bridges constructed in concrete, steel and wood. In addition, FRP has approximately 10 times higher tensile strength capacity than mild grade steel and its strength is governed by its ability to sustain a load without excessive deformation or failure. It should be noted that for sustained loads, that creep rupture behavior of FRP is less desirable than that for steel. Its

high strength-to-weight ratio is of true benefit since its dead load contribution is minimal and, thereby, allowing a member composed of FRP to support relatively larger live loads.

In the recent past, the use of FRP composites technology has been adopted by many bridge agencies nationwide and has shown its potential for structural applications in bridges (Reising et al, 2004; Stiller et al, 2006). The increased use of composite materials is in large part due to the Federal Highway Administration's (FHWA) Innovative Bridge Research and Construction (IBRC) program, which promotes and reinforces the use of innovative materials, construction techniques, and structures in general. Through support of the IBRC program, the Iowa DOT has initiated numerous projects to investigate the effectiveness and applicability of using FRP composite materials in strengthening, repairing, as well as new construction of bridges. New York State in particular has been active in the implementation and evaluation of FRP bridges, and several reports provide documented construction and structural performance evaluations through load testing (Alampalli et al, 2000; Alampalli et al, 2004). This paper documents one project that evaluates the applicability of FRP decks in bridge construction.

4.3. BETTENDORF FRP PANEL DECK BRIDGE (WIPF ET AL., 2006)

The objective of this study was to evaluate the structural performance of a three span bridge, one span of which was constructed with FRP deck panels, that carries the 53rd Avenue extension over Crow Creek in Bettendorf, Iowa (Figure 4.1). It is the first FRP bridge deck in the US that uses composite action with prestressed concrete girders and, at the time of the construction, was also the widest FRP deck (98 ft – 8 in.). Field monitoring was performed on the subject bridge to assess the performance of the FRP panel deck under actual bridge loading. Instrumentation was placed at important locations to collect displacement and strain data. The testing program consisted of two short-term tests and long-term monitoring of the bridge. The test results are compared, where applicable, with measured conventional-deck field behavior and empirical design assumptions (Wipf et al, 2006).

4.3.1. BRIDGE DESCRIPTION

The bridge is 173 ft-7.5 in. long, 98 ft-8 in. wide and consists of three different deck material combinations that are supported by prestressed concrete (PC) girders. The west and middle span decks were continuously constructed with cast-in-place concrete reinforced with epoxy coated steel and glass Fiber Reinforced Polymer (GFRP) bars, respectively, while the east bridge deck was

constructed with a total of 12 DuraSpan® 766 pultruded FRP panels (thickness equivalent to 7.66 in. as shown in Figure 4.2 (a) and (b)). Two 4-in. deep holes were pre-drilled every 24 in. on the top flange of the C14MS PC girders to hold 3/4-in. u-shape shear stirrups fixed with a two-part epoxy (Figure 4.2 (c)). Between the panels and the girders, two polystyrene supports were attached with adhesive to form the haunch (varying from approximately 1 in. to 2 in. thick). The panels were interconnected by three 6-in. wide FRP splices on the top (Wipf et al, 2006).

(a) Side view

(b) Bottom view

Figure 4.1. Photographs of Bettendorf Bridge

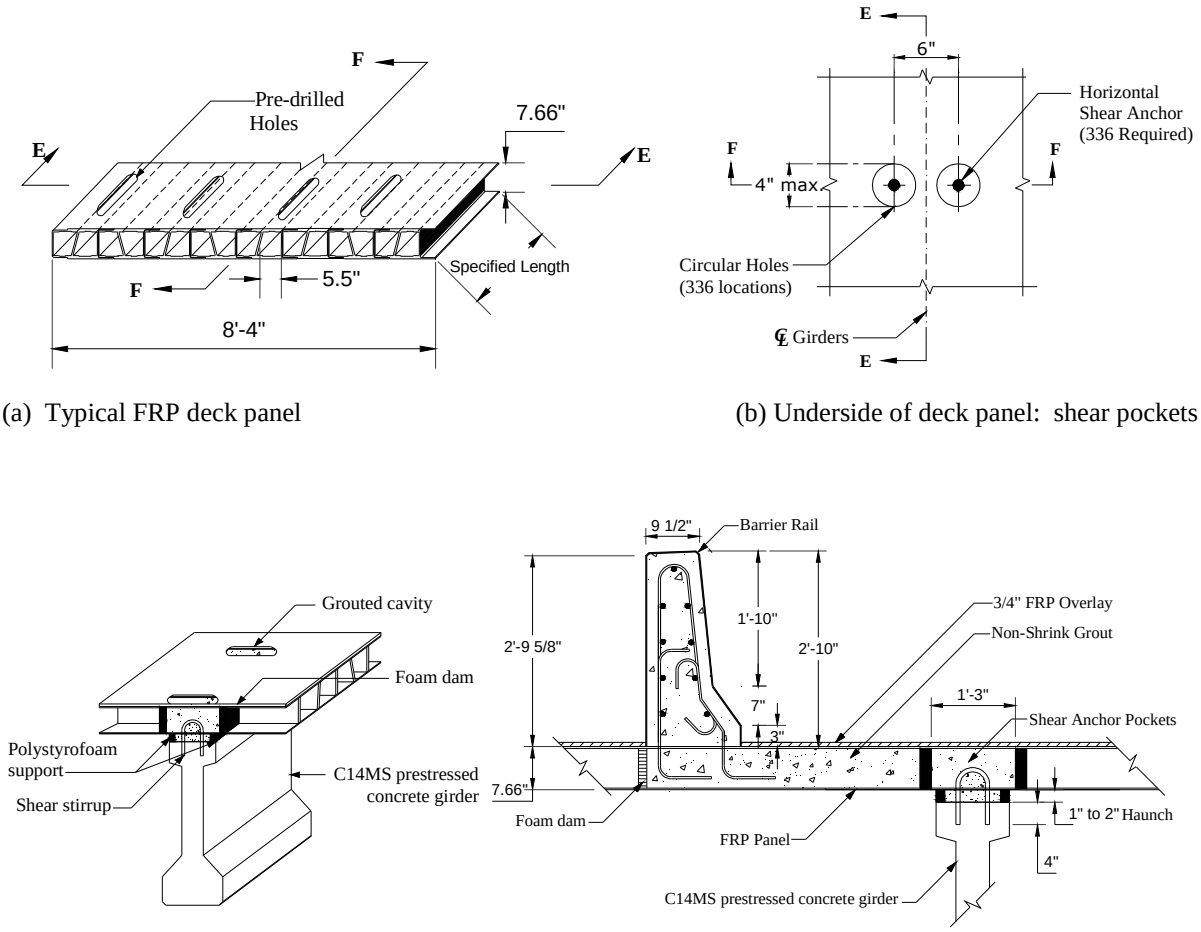

(a) Typical FRP deck panel

(b) Underside of deck panel: shear pockets

(c) FRP deck and girder assembly

(d) Barrier cross section

Figure 4.2. Typical FRP Deck Panel and Prestressed Concrete Girder

The FRP deck holes were filled with non-shrink grout to create composite action. To attach the concrete barrier rail to the FRP deck, stirrups were anchored in the deck with non-shrink grout (Figure 4.2(d)). The barrier railing on the FRP deck span was constructed separately from the rest of the rail system to ensure thermal compatibility. The bridge was opened to traffic in May 2003.

4.3.2. SHORT-TERM MONITORING

The short-term testing consisted of monitoring the bridge behavior under controlled live loading. Strain data were obtained from the top and bottom flange of twelve girders in the FRP-deck span, and six girders in the reinforced concrete (RC) span as well as one FRP panel instrumented with four strain gages (Figure 4.3(a) through (c)). During the testing, the bridge was loaded by driving a

loaded tandem axle dump truck with a total weight of 67.4 kips in 2003 (rear axle of 50.0 kips) and 65.9 kips in 2004 (real axle of 48.9 kips). This truck crossed the bridge at crawl speed in six transverse paths (Figure 4.3 (d) and (e)) which were selected to either produce maximum response levels or represent typical traffic patterns.

By reviewing the recorded strains (Figure 4.4), it was determined that there were no significant changes in strain levels between the two tests that were separated by approximately one year. Note that the results were normalized based on the gross vehicle weight and rear axle differences (1.02) to account for the difference in truck loading between the two tests. In some cases there were slightly lower readings in the second year. Note that the strain data in the FRP-deck span showed noticeable spikes in the top flange data, which can be attributed to the lower stiffness of the FRP composite deck as compared to the concrete deck. In general, based on the data collected, there was no significant loss of stiffness in the FRP-deck span during the two-year monitoring period. As illustrated by the collected data, the FRP-deck span exhibited almost no continuity with the adjacent span, while the RC deck span appeared to be fully continuous with the adjacent span. This may have a significant influence on the moments induced in each span (i.e., this infers that the positive region moments of the FRP-deck span will not be reduced due to continuity as would the RC deck span in the positive region moments). When comparing both spans, it is observed that the girder strains were larger in the FRP-deck span than in the RC-deck span. The higher strain levels in the FRP span are primarily attributed to the much lower stiffness of the composite FRP deck/girder section (the approximate cross section EI values, respectively, for the FRP span and the RC span are $EI_{\text{FRP-PC girder}} = 581$, 139,000 kip-in^2 and $EI_{\text{RC-PC girder}} = 1{,}362{,}300{,}000$ kip-in^2).

The load distribution coefficients (LDCs) were calculated using the measured bottom flange girder strains. As expected, the most critical loading condition occurred when the truck was driven close to the barrier. The resulting maximum LDC in the FRP-deck span was 47% in 2003, and 43% in 2004 (Figure 4.5 (a)). For the same loading, the LDC in the RC deck span was 43% in 2003, and 41% in 2004. The obtained data indicated that the RC-deck span was more effective in laterally distributing the loading than the FRP-deck span. The AASHTO Standard Specification (AASHTO, 1996) provides distribution factors (LDFs) in terms of truck percentage while the AASHTO LRFD Specifications (AASHTO LRFD, 2005) defines the LDFs to be calculated based on the mechanical and materialistic properties of the composite section. In the absence of code specifications for FRP panel decks, it should be noted that the design was strength based. Figure 4.5 (b) presents the LDCs

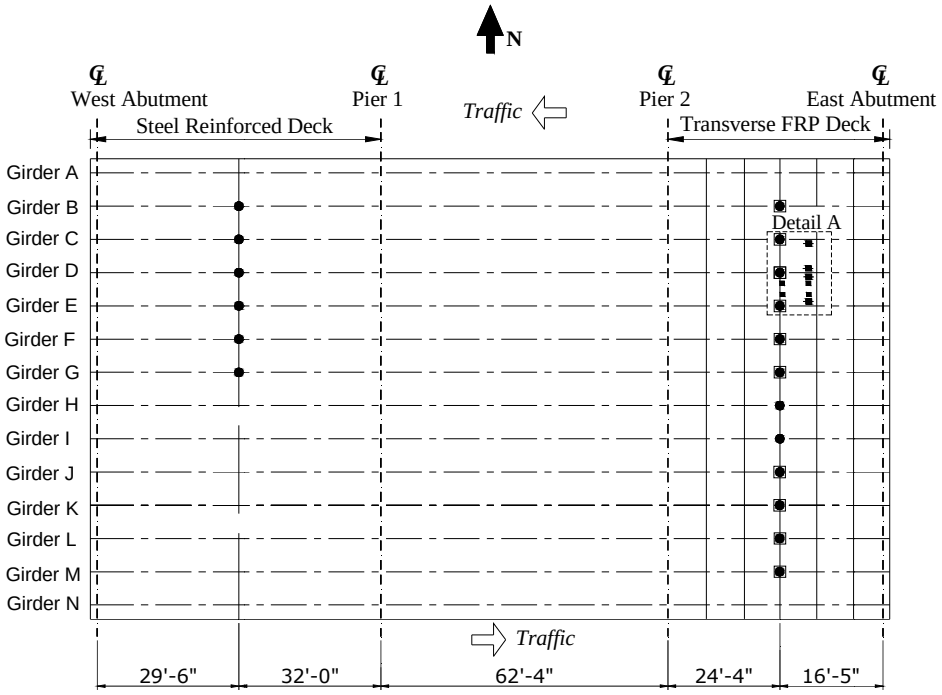

(a) Overall instrumentation layout

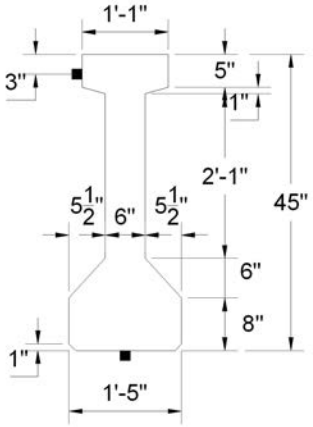

(b) Girder strain gage location

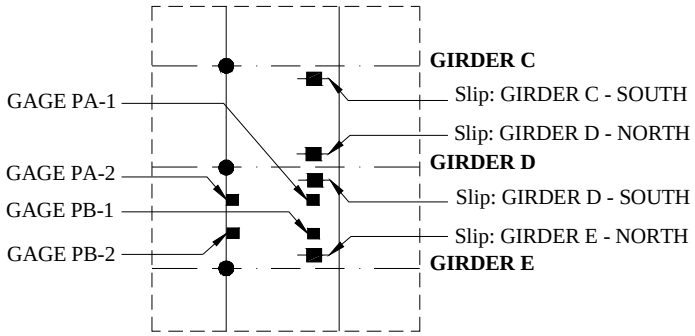

(c) Detail A: FRP strain gages and slip gages location

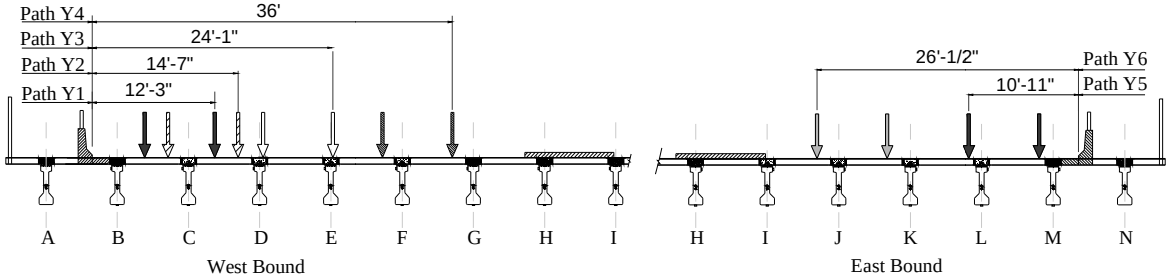

(d) Truck path Y1 through Y4 – West bound (e) Truck path Y5 and Y6 – East bound

Figure 4.3. Overall Instrumentation and Load Truck Location Details

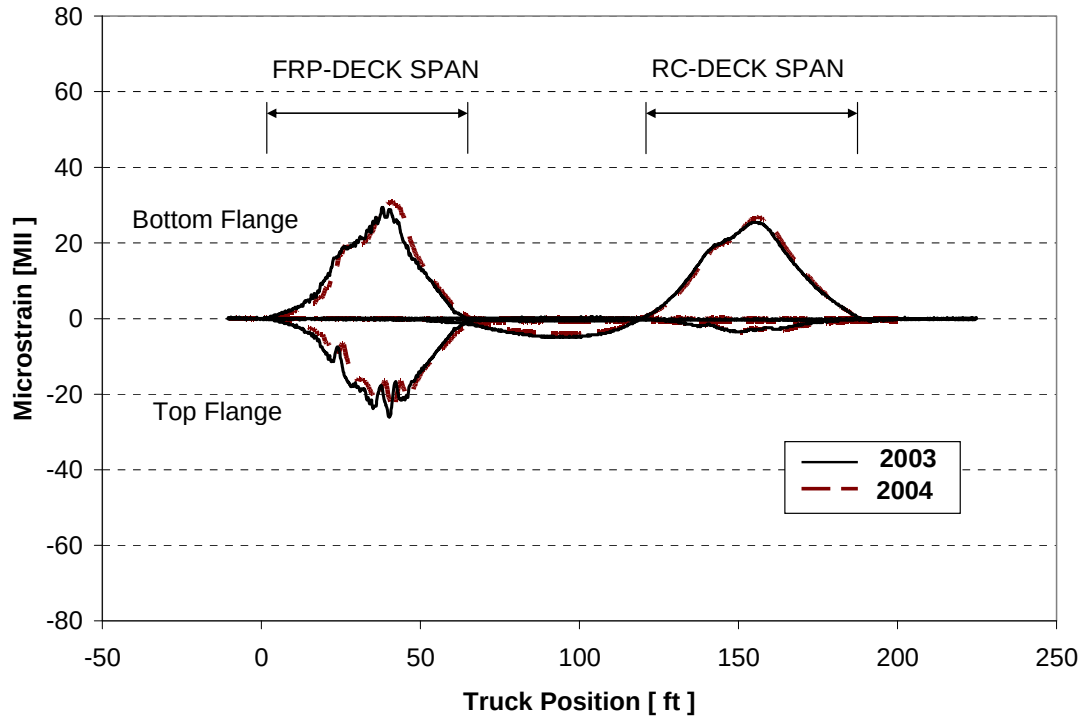

(a) Girder B

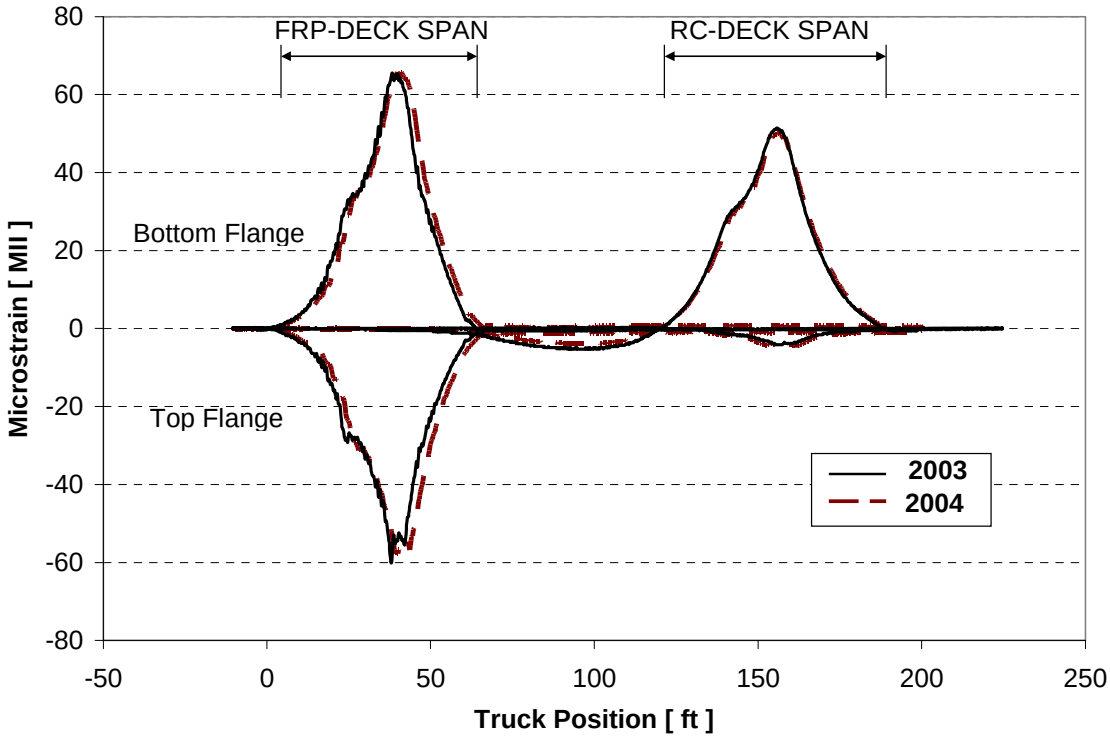

(b) Girder C

Figure 4.4. Strain Response Comparison Near Mid Span – Path Y1

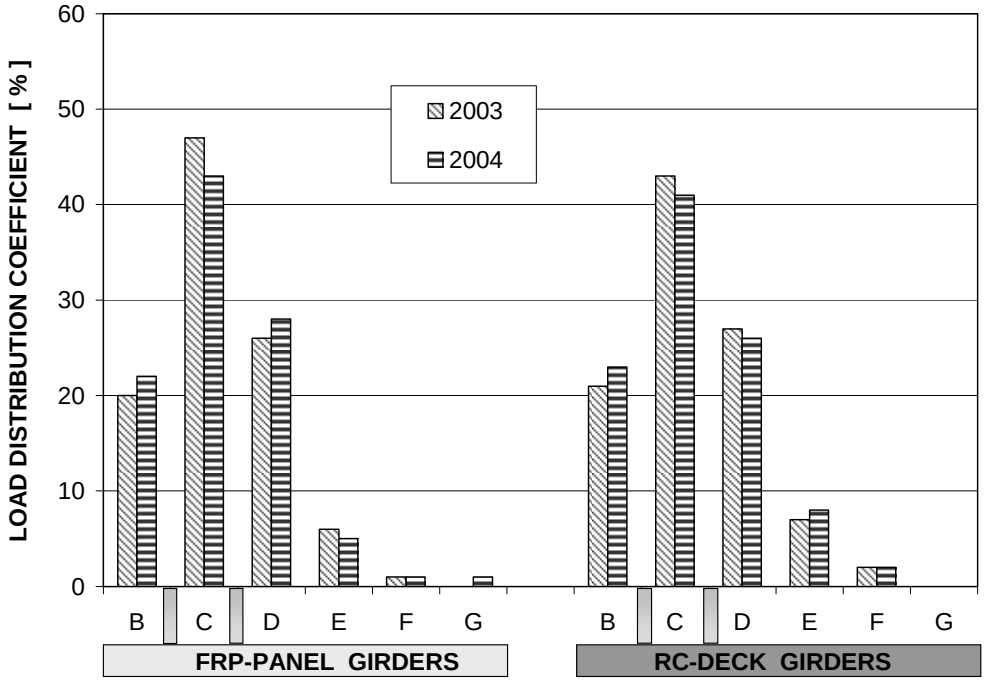

(a) Comparison of FRP and RC deck – Path Y1

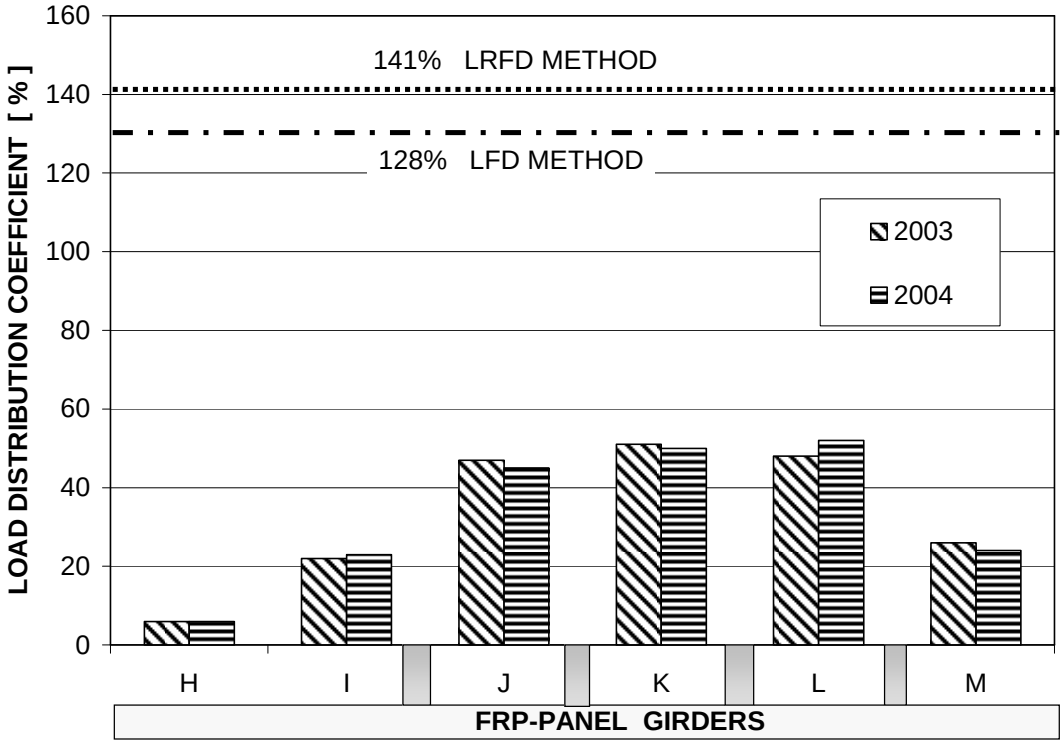

(b) LDCs superposition – Path Y5 and Y6

Figure 4.5. Load Distribution Coefficient Comparison

for two lanes computed by superimposing multiple passes of the test truck. The LDC per girder was calculated as a percentage of the superposition of bottom strains and assuming the linear elastic response of the bridge superstructure. As can be seen, the test LDCs were below the AASHTO values and no significant change was observed during the two-year monitoring period.

In order to evaluate the deck-to-girder connectivity, the neutral axis of the composite section was computed based on the gage locations and field collected strain data and compared with theoretical calculations of the neutral axis location (provided by the designer), assuming full composite action. The results indicated that the central girders were resisting a notable level of torsional forces that were neglected in the original design. Figure 4.6 presents the results of the neutral axis location for Path Y1 measured from the bottom flange over the most heavily loaded girders. In general, it appears that the neutral axis locations did not significantly change over time and that the central girders may not have achieved full composite action with the FRP deck panels. While the composite actions for the Girders B and C appear to be likely achieved, the measured neutral axis location for Girder D was below the non-composite action (19.5 in.). This can likely be attributed to a weak shear connection and the possibility of torsion effects of the truck loading typically ignored during design. Despite these findings, the measured strain levels were below the design values, thereby, giving assurance that the torsional effects and partial composite action may not be significantly impacting the strength of the prestressed girders.

4.3.3. FINDINGS

The following conclusions and observations are drawn from the field monitoring, analysis and field inspection:

- The FRP panels appear to behave elastically.
- The PC girder strains levels remained similar over the test period. Variations in strain over time indicate that there had been no decline in flexural stiffness.
- The LDCs from field tests were less than the AASHTO Specification (Standard and LRFD) LDC values and indicated no significant change from 2003 to 2004.
- In general, it was observed that some intermediate girders may not have fully attained composite action with the FRP deck. However, the strain levels measured were below the design strains.
- After one year of service, there were signs of deck overlay cracking in the transverse direction to the traffic, but the cracking had no effect on the structural performance of the bridge. The cracks

aligned with the edges of the FRP tube components that comprise the panels. Maintenance to the overlay was performed by the bridge owner.

- No damage to the girders was observed.

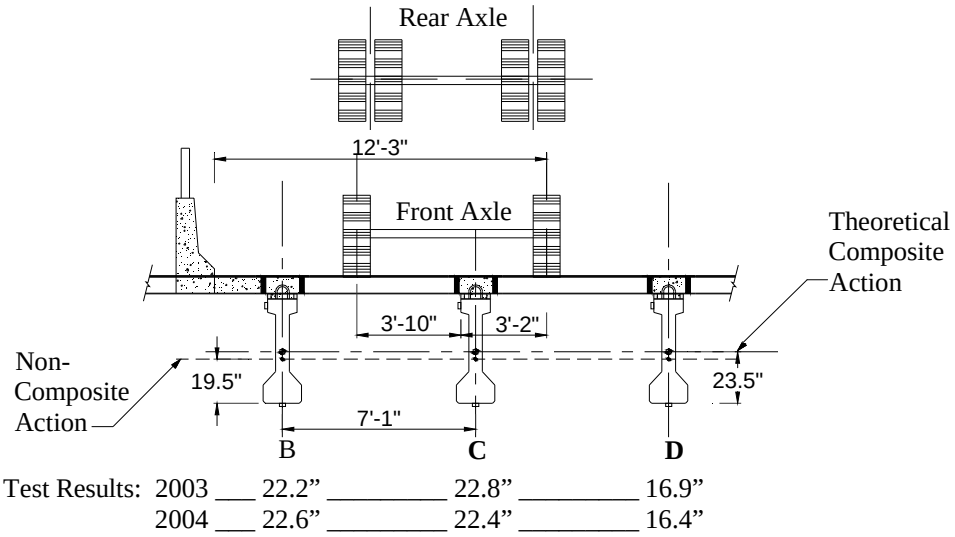

Figure 4.6. Neutral Axis of FRP Deck Span – Path Y1

4.4. IOWA DOT FRP TEMPORARY BYPASS BRIDGE (WIPF EL AL., 2007)

Due to the deteriorating condition of existing steel temporary bridges (Figure 4.7(a)), the Iowa DOT initiated a research project to determine if a FRP deck bridge could be a suitable replacement for the steel temporary bridges. The replacement system is approximately 35 percent lighter than the steel alternative, potentially easier to transport, and the few components that may deteriorate are readily replaceable. This new FRP deck bridge for temporary bypass applications consists of two 39 ft-10 in. by 13 ft-6 ½ in. deck panels, measuring approximately 3 ft in thickness, that are spliced with steel plates along the centerline of the roadway to form a bridge that spans 39 ft-0 in. with a roadway width of 24 ft-0 in. (from face of one barrier rail to that of opposite side barrier rail) for two 12 ft-0 in. traffic lanes (Figure 4.7(b)). Brief summaries of the design, fabrication and evaluation of the FRP deck bridge for temporary bypass applications are followed.

4.4.1. DESIGN

The design of the FRP deck bridge was a proprietary design by Hardcore Composites that was verified by HNTB Corporation. The design was based on an allowable stress analysis and elastic

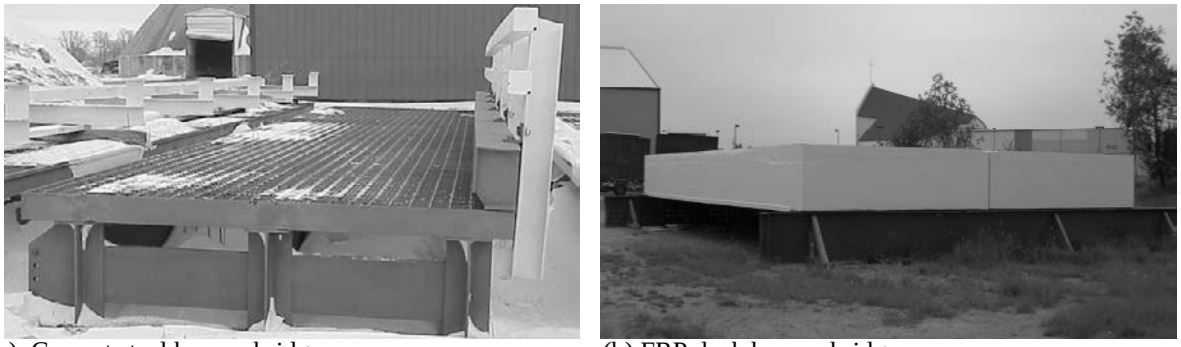

(a) Current steel bypass bridge (b) FRP deck bypass bridge

Figure 4.7. Steel and FRP Deck Temporary Bypass Bridges

deflection limits. Final design calculations were completed by Hardcore Composites, and checked by engineers at the Iowa DOT and Iowa State University. The FRP deck bridge is assumed to behave on a quasi-isotropic basis for calculating moments and shears due to dead load and live load. Design load stresses due to live load were based on the AASHTO HS20 loading. The Factor of Safety (FS) used for the allowable stress was FS=5 in accordance with the current recommended practices from the FHWA (O'Connor, 2007). The railing connection is designed to satisfy Test Level Two (TL-2) requirements. Deflection limits were per the AASHTO Standard Specification L/800 allowable deflection criteria. The assumed clear span was 39 ft-0 in. leading to a 0.59 in. deflection limit. Deflection calculations were based on an AASHTO H20 loading that yielded a deflection of 0.473 in. satisfying the allowable deflection criteria. The bridge traffic barrier rail is designed for Test Level Two (TL-2) in accordance with NCHRP Report 350 "Recommended Procedures for the Safety Performance Evaluation of Highway Features" (Ross et al., 1993). According to ASHTO LRFD Bridge Design Specifications (AASHTO, 2006) is generally acceptable for work zones and most local and collector roads with favorable site conditions as well as where a small number of heavy vehicles is expected and posted speeds are reduced.

4.4.2. FABRICATION AND CONSTRUCTION

Each panel is composed of seven layers, called plies, of QM6408 FRP fabric on the bottom and top and 3 plies on each vertical side. These layers of FRP are what provide the resistance to bending stresses in the structure. The core of each panel is composed of 600 8 in. x 16 in. x 36 in. foam 'bottles' individually wrapped with one ply of TV3400 FRP fabric, and as a whole provide the shear resistance for the structure. Once all the bottles are installed and wrapped with FRP plies, vinyl ester resin was infused into the structure through a process called Vacuum Assisted Resin Transfer Molding (VARTM). Presented in Figure 4.8 are various stages of fabrication of the FRP panels.

Prior to the delivery, the FRP deck panels were painted for protection of the FRP material from ultraviolet (UV) degradation and the top of the deck was coated with the epoxy and aggregate wearing surface. When the bridge traffic barrier rail is not attached both panels can be shipped on a flatbed trailer as an oversized legal load (Figure 4.9(a)). The panels are lifted off the trailer using a small crane as shown in Figure 4.9(b). At calculated locations, eight foam bottles in each panel were replaced with bottles outfitted with the lifting hardware that consists of an anchored steel plate with a threaded hole to accept bolt-on D-rings.

The FRP Deck panels were set on the temporary abutments that are comprised of wide flange steel beams to allow for the installation of the steel splice plates and testing of the panels. Splicing the two FRP deck sections together was accomplished by using a series of steel plates with rods welded to them. The connection was then completed by bolting bottom splice plates to the rods. Once the splice plates are installed, the riding surface is complete for traffic, which was followed by installing the bridge traffic barrier railing. The wearing surface of the deck panels consists of a 3/8 in. layer of abrasive epoxy covering the entire deck surface except the areas occupied by connection plates. The barrier rail is bolted through the deck in a similar fashion as the splice plates (Figure 4.9(c) and (d)). The only difference is that the rods are threaded at both ends and secured with nuts instead of welding. Note that the temporary detour bridge can be transported with or without the bridge traffic barrier railing installed. The signed speed for the temporary detour will be 35 mph.

4.4.1. TESTING AND EVALUATION

A load testing was performed in November, 2005 using a fully loaded Iowa DOT tandem axle truck with axle weights of 11.9 kip, 16.1 kip and 16.3 kip spaced at 17 ft-6 in. and 4 ft-6 in. The two segments of the bridge were joined together with the center splice plates prior to loading. The truck was statically placed on the structure in three load positions and, in all cases, was positioned longitudinally, facing north, to induce the maximum moment in the bridge. Figure 4.10 illustrates the transverse load positioning of the truck (LC1, LC2 and LC3) and test data collection instrumentation.

Figure 4.11 illustrate the transverse distribution of strain at mid-span for a single lane loaded and two lanes loaded, respectively. The two lanes loaded case was approximated by superposition of LC 1 and 3. As shown, it is evident that the distribution of strain is relatively symmetric about the longitudinal centerline of the bridge, which suggests adequate load transfer from panel to panel by the steel connection plates. Generally, the flexural strain measured in the steel connection plates were

smaller in magnitude than those in the FRP, possibly the result of slip occurring between the connection plate and the panels as well as other factors.

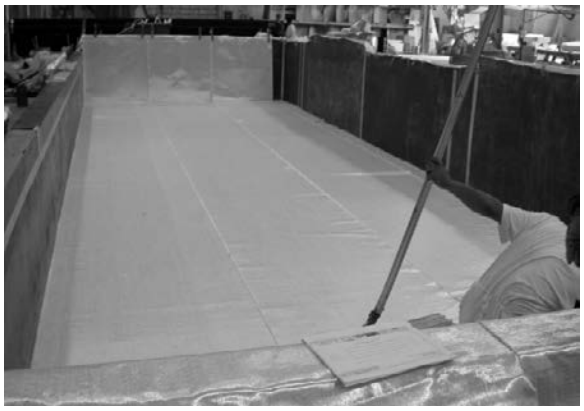

(a) Installation of bottom FRP plies

(b) Bottles

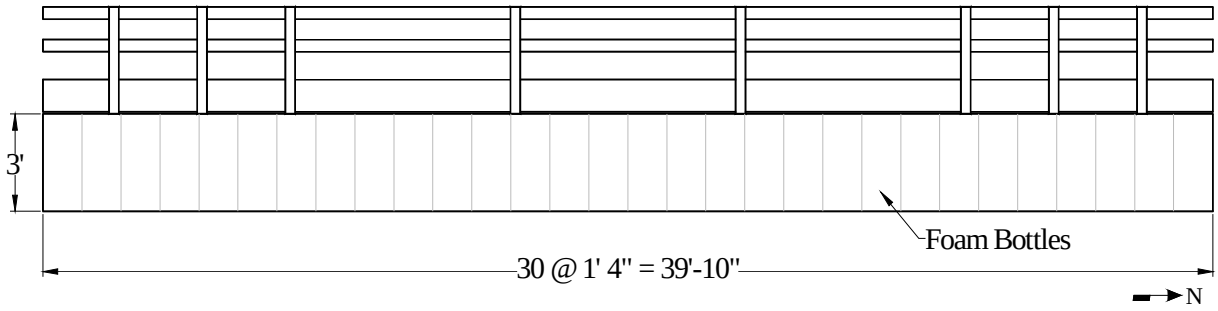

(c) Elevation view of panel

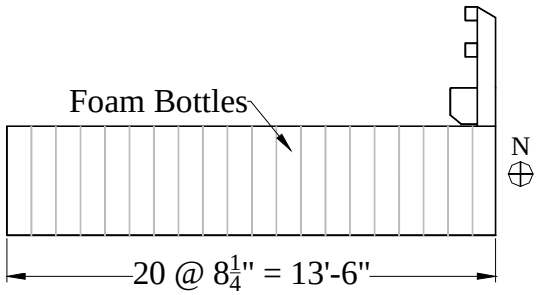

(d) End view of panel

Figure 4.8. Installation of Bottom FRP Piles and FRP Wrapped Foam Bottles

(a) FRP deck panel delivery

(b) FRP deck panel lifting

(c) Barrier rail connection

(d) Barrier rail installed

Figure 4.9. Temporary FRP Bridge Delivery and Installed Traffic Barrier Rail

The truck positioning induces a maximum moment of 292 ft-kip in the simple span bridge occurring under the middle axle. The maximum moment and the maximum measured deflection induced by the truck positioning was 292 ft-kip and 0.34 in., respectively. The design deflection limit is L/800 or 0.59 in. for an H20 loading. An H20 loading induces a calculated maximum moment of 336 ft-kip and a calculated maximum deflection of 0.47 inches. The ratio of applied test load maximum moment to calculated H20 maximum moment is 87%, which correlated reasonably with the ratio of applied test load maximum deflection to the calculated H20 deflection of 72%. Strain data also correlated reasonably well with the expected strains. For example, the average mid-span strain for load case LC2 was 117 microstrain. The calculated mid-span strain from the test truck was 132 microstrain. Therefore the average measured mid-span strain was within 13% of the anticipated

mid-span strain. One potential source of the discrepancy is that the steel splice plate was not taken into account in the calculated mid-span microstrain which has the effect of reducing the strain in the FRP as some of the load is carried by the steel plates. Maximum strain recorded in the steel plate for load case LC2 was 8 microstrain.

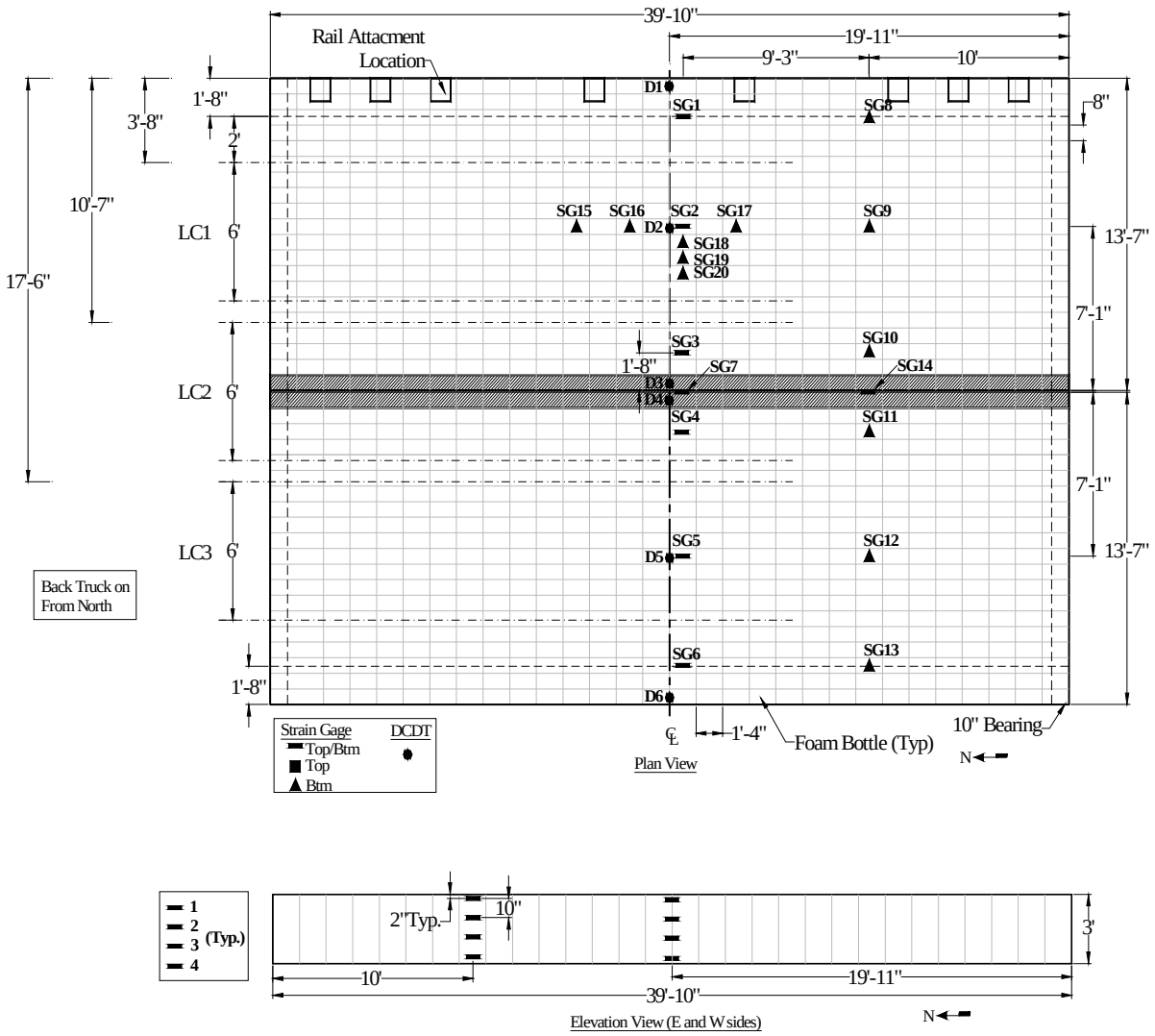

Figure 4.10. Instrumentation and Truck Positioning

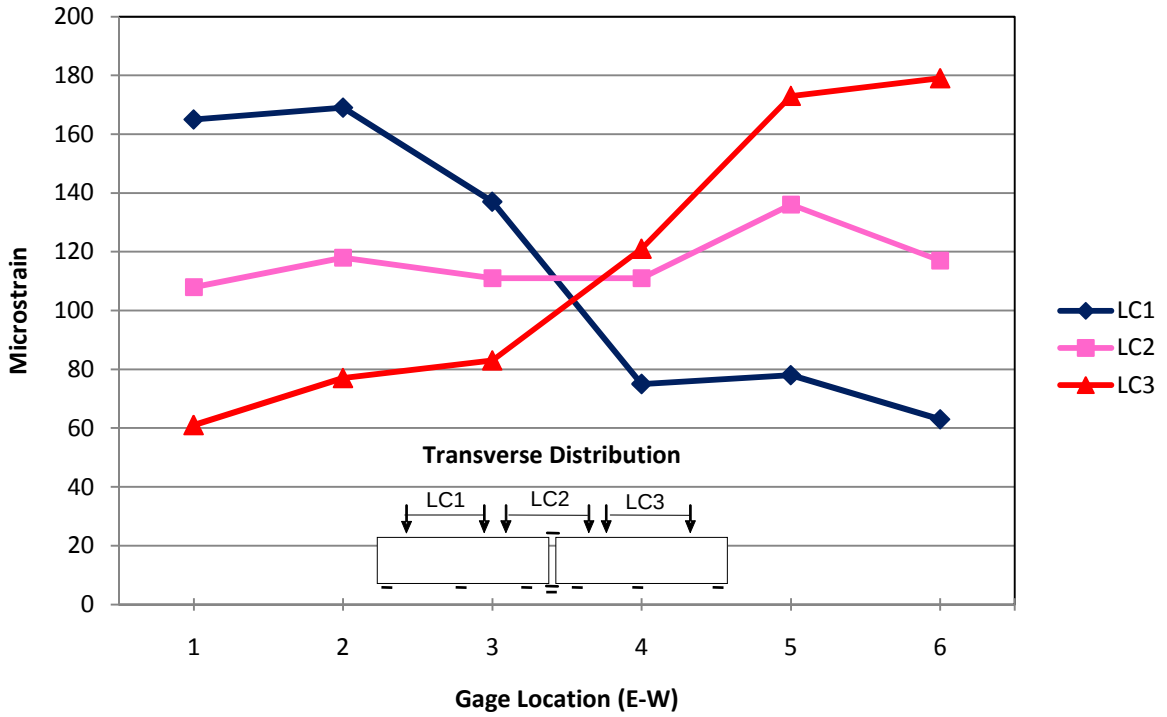

(a) Single lane loaded

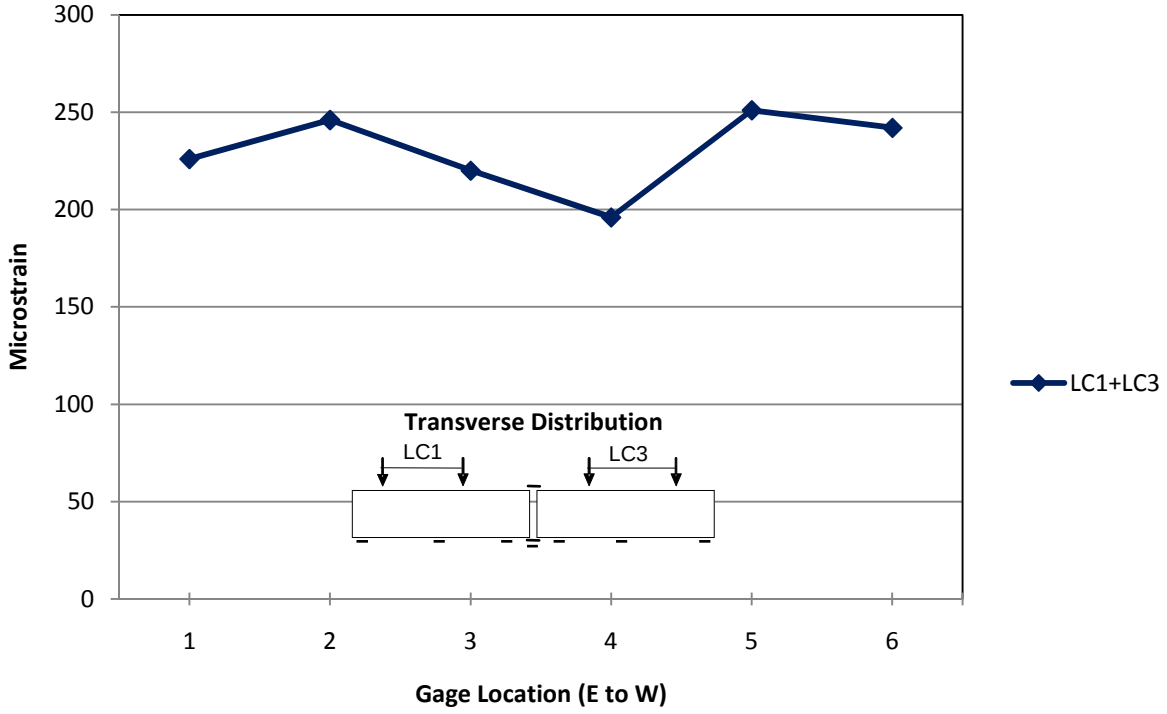

(b) Two lanes loaded

Figure 4.11. Transverse Load Distribution at Mid Span

4.4.1. FIELD IMPLEMENTATION

In the spring of 2007, the FRP temporary bypass bridge was installed (see Figure 4.12(a)) on a construction project in NE Iowa to allow traffic to flow around a mainline bridge structure that was being replaced. The temporary bridge would have an approximate ADT of 1,000 to 2,000. Timber abutments and backwalls were constructed as specified in the plan documents. However, after placement of the bridge panels it was found that maintaining the specified gap between the abutment backwall and the end of the panels was difficult given the flexibility of the backwall and the pressure from the compacted back fill. After placement of the backfill and the approach roadway sections, the backwalls were found to be partially in contact with the end of the bridge panels raising concern that this could possibly cause premature deterioration of the edge of the panels. Traffic was allowed across the structure and the panel ends were periodically monitored for any signs of wear or damage.

Not long after traffic was allowed on the bridge, Iowa DOT inspectors noticed that the transverse edge at the end of one of the panels was showing signs of damage (see Figure 4.12(b)). Investigation of the area found that the elevation of the top of the backwall was approximately 1 in. lower than the elevation of the top of the panel, which caused the leading edge of the panel to be exposed to the full force of oncoming traffic loads. Due to construction time constraints and the need to keep traffic maintained, steel plates were used to span from the approach roadway section to the bridge deck across the abutment joint in an attempt to stop the progression of the deck deterioration (see Figure 4.12(a)). In addition, the traffic was reduced from two lanes to one lane.

Shortly after the steel plates were installed, inspection found that the top layer of FRP and the wearing surface had debonded on one of the deck panels over approximately half of the panel surface area (the other panel showed no signs of delamination or deterioration otherwise). In addition, it appeared that water and debris had entered through holes in the top layer of FRP near the lifting lug locations and was resulting in the deterioration of the foam bottles that comprised the core of the panels. It is noteworthy that a load test using strain measurements at the mid-span of the bridge was implemented on the delaminated bridge to assess structural condition. The test results showed that the measured midspan tensile strains were similar to those measured prior to the bridge installation. Even though the tests results indicated no reduction in overall bridge stiffness and adequate lateral load distribution, the bridge was removed from service. The bridge is currently being stored on DOT property on temporary abutments and is being maintained and routinely inspected. After a thorough

inspection and evaluation of the damage has been performed, a follow-up load test is likely to evaluate any strength degradation.

4.4.2. FINDINGS

The initial structural performance of the FRP bridge was satisfactory based on a load test conducted prior to installation. The performance of the bridge was what was expected where the design control is primarily an issue of deflection limitations rather than strength limitations.

(a) Installed FRP Bridge

(b) Deterioration at end of deck panel

Figure 4.12. Photographs of Temporary Bypass Bridge Installation and Subsequent Deterioration

fabricated was $136 per square foot. The total superstructure cost includes the bridge traffic barrier rail, splice plates and neoprene bearing. The unit cost without the bridge traffic barrier rail or neoprene bearing is $121 per square foot. Cost to fabricate new steel temporary detour bridges spans is estimated at $81,000 per span including the traffic railing for a total superstructure unit cost of $75 per square foot.

The delamination of the deck surface at the end of the bridge was 1) likely initially due to vehicle impact from the vertical positioning of the deck at the abutments combined with a lack of edge protection on the deck and 2) subsequently caused by moisture that infiltrated the deck from the surface openings at the end.

4.5. OVERALL GENERAL CONCLUSIONS

Based upon structural testing and evaluation, both the FRP panel deck bridge and the FRP detour bridge performed satisfactorily. In both bridges some serviceability issues were observed in the field. Specifically for: 1) the FRP panel deck bridge some degree of delamination/debonding after the first year was observed; however, this initial material deterioration did not significantly affect the structural response, and 2) the FRP detour bridge end details at the bridge approach allowed initiation of deck edge damage from tire impact.

4.6. ACKNOWLEDGMENTS

This investigation was conducted by the Bridge Engineering Center at Iowa State University. The authors wish to acknowledge to the Federal Highway Administration, the Iowa Department of Transportation, Highway Division and the Iowa Highway Research Board for the funding to sponsor this research project. Also, they would like to thank the staff of the Bettendorf Public Works Department, especially Public Works Director Wally Mook, for all the assistance provided during this work.

4.7. REFERENCES

1. Reising, R. M. W., B. M. Shahrooz, V. J. Hunt, A. R. Newman and A. J. Helmicki. 2004. *Performance comparison on four fiber-reinforced polymer deck panels.* Journal of Composite Structures 2004; 8(3), pp. 265–274.

2. Stiller, W. B., J. Gergely, and R. Rochelle. 2006. *Testing, Analysis, and Evaluation of a GFRP Deck on Steels Girders.* Journal of Bridge Engineering © ASCE. July/August 2006. pp. 394–400.
3. Alampalli, S, J. O'Connor, and A. P. Yannotti. , *Design, Fabrication, Construction, and Testing of an FRP Superstructure*, Special Report 134, Transportation Research and Development Bureau, New York State Department of Transportation, December 2000.

4. Alampalli, S, G. Schongar, and H. Greenberg, *In-Service Performance of an FRP Superstruture*, Special Report 141, Transportation Rese arch and Development Bureau, New York State Department of Transportation, March 2004.

5. Wipf, T. J., B. M. Phares, F. W. Klaiber, and U. Deza, *Evaluation of the Bettendorf Bridge, Iowa*, Final Report, Center for Transportation Research and Education, July 2006. http://www.ctre.iastate.edu/research/reports.cfm

6. AASHTO. *Standard Specifications for Highway Bridges, Sixteenth Edition*. Washington, DC. American Association of State Highway and Transportation Officials. 1996.

7. AASHTO LRFD. *LRFD Bridge Design Specifications*. Washington, DC. American Association of State Highway and Transportation Officials.

8. Wipf, T. J., B. M. Phares, D. L. Wood and J. S. Nelson, Testing and Evaluation of the Iowa DOT FRP Temporary Bypass Bridge, Final Report, Center for Transportation Research and Education, March 2008. http://www.ctre.iastate.edu/research/reports.cfm

9. O'Connor, J. FRP Decks and Superstructures: Current Practice. US Department of Transportation, Federal Highway Administration, March 2007 http://www.fhwa.dot.gov/bridge/frp/deckprac.cfm

10. Ross, H. E., D. L. Sicking, R.A. Zimmer, and J.D. Michie. NCHRP Report 350: Recommended Procedures for the Safety Performance and Evaluation of Highway Features. TRB, National Research Council, Washington, DC. 1993.

11. AASHTO. 2006. LRFD Bridge Design Specifications with Interim Revisions. 3rd Edition. American Association of State Highway and Transportation Officials, Washington, DC.

CHAPTER 5. DEVELOPMENT OF A SMART TIMBER BRIDGE — A 5-YEAR RESEARCH PLAN

A refereed report accepted for publication and currently in editing by the
United States Department of Agriculture – Forest Product Laboratory, 2010

Brent Phares, Ursula Deza, Terry Wipf, James Wacker

5.1. ABSTRACT

This peer-reviewed report outlines a 5-year research plan for the development of a structural health monitoring system for timber bridges. A series of proposed studies are included which identify and evaluate various sensing technologies for measurement of structural adequacy and/or deterioration parameters. The overall goal is to develop a turnkey system to analyze, monitor, and report on the performance and condition of timber bridges. The introduction of structural health monitoring technologies for timber bridges should result in improved safety, longer service life, and improved load ratings.

5.2. BACKGROUND

The critical deterioration of bridges nationwide has initiated the search for new methods to rehabilitate, repair, manage, and construct bridges. In this context, smart structures have recently emerged as a new technology to help improve future management. This approach can be thought of as a potential replacement for, or complementary to, on-site inspections currently specified by the National Bridge Inspection Program. In general, research on smart structures involves materials, structural mechanics, electronics, signal processing, communication, and control (ISIS, 2001; Bruhwiler, 2003). In practice, a smart structure would typically incorporate the use of sensors, data reduction techniques, and remote systems that allow for monitoring of the structure (Maalej et al, 2002; Muthumani et al, 2003; Koh et al, 2003). With these elements, the smart structure is able to monitor the in situ behavior of the structure, to assess its performance under service loads, to detect damage and deterioration, and to determine its current condition (Udd et al, 2000; Li et al, 2004).

To date, fiber optic sensors (FOSs) have been used in concrete and steel structures (Merzbacher et al, 1996; Doornink et al, 2005; Kim et al, 2004; Ansari, 2005; Sumant et al, 2005). Fiber Bragg

gratings (FBGs), a type of diffraction grating of an optical fiber that filters out particular wavelengths of light, have many advantages over other FOS types. Besides being absolute, linear in response, interrupt immune, and readily multiplexed, these sensors have the ability to be both embedded and surface mounted. In laboratory and field tests, good agreement with foil strain gages has been demonstrated in both steel and concrete structures.

In recent research efforts involving existing steel and concrete bridges, health monitoring systems have been applied with the purpose of detecting early damage and deterioration and prolonging service life. Health monitoring systems have also been applied in newly constructed bridges with the goal of reducing the total life maintenance cost and improving bridge management (Koh et al, 2003). The purpose of using structural health monitoring (SHM) systems is to provide real-time monitoring of various structural and serviceability changes through measurement metrics such as strain, temperature, among others. In the case of bridge structures, the data provided by these sensors are usually transmitted to remote data acquisition centers. Thus, an active structural control based on the collected information is possible.

In the past, timber bridge evaluation and maintenance efforts have principally focused on the internal integrity of timber components and improving day-to-day performance (Ritter, 1992; FPL, 1990; Kainz et al, 2001). The goal of the research plan that is the subject of this report is to develop a smart timber bridge that improves the long-term performance, maintenance, and management of timber bridges through the development of smart timber bridge concepts (Wipt et al, 2005). The development of the smart timber bridge will utilize current and new sensors, health monitoring technologies, and bridge management approaches that will be integrated in one turn-key SHM system. Thus, the work described herein is to develop a system to analyze, monitor, and report on the performance and condition of the most commonly constructed timber bridge. This work will be accomplished over a 5-year period.

5.3. CONCEPTUAL SMART TIMBER BRIDGE

5.3.1. THE CONCEPTUAL STRUCTURAL SYSTEM

Not surprisingly, the material used in the smart timber bridge will be glued-laminated timber (glulam) members (Ritter, 1992; FPL, 1990; Russell, 1997). In contrast to the variable range of solid wood, glulam is an engineered wood product that provides distinct advantages over solid-sawn

timber. Glulam consists of (2-in. nominal) lumber laminations that are bonded together on their wide faces with structural adhesive. Fundamentally, glulam members can be manufactured from any softwood or hardwood lumber. In the United States, glulam has been applied successfully in buildings and bridges since the 1930s.

The superstructure of the conceptual bridge is composed of a series of transverse glulam deck panels supported on beams. In general, these superstructures can span 20 to 80 ft. Based on the Standard Plans for Timber Bridge Superstructures (Wacker and Smith, USDA 2001), the baseline smart timber bridge considered during development will be a simply supported 60-ft-long span with a 24-ft roadway width with zero skew supported on concrete abutments.

The baseline superstructure system consists of three primary components: seven girders spaced at 44 in., four sets of diaphragms spaced at 18 ft, and bearings. The girders will be assumed to be Southern Pine 24F-V3 designed for a HS25-44 truck loading. The resulting girder cross section is 8-1/2 in. wide and 45-3/8 in. deep (Figure 5.1). The diaphragms are 5-3/8-in.-thick, 37-3/8-in.-deep, and 35-1/2-in.-long glulam sections with the same denomination as the deck panels and beams (Southern Pine combination 48), and placed perpendicular to the girders. The diaphragms are attached to the girders with 7/8-in.-diameter tie rods that extend through the diaphragms at the third glue line from the top and bottom of the diaphragm. The bearing connections for the glulam beams are fixed to prevent longitudinal movement. The bearing shoe consists of two 4 by 8 by 1/2 in. steel angles that connect the beams to the substructure (concrete backwall) with 3/4-in.-diameter anchor bolts and to the glulam beams with 3/4-in.-diameter through bolts. And a 3/4-in.-thick bearing pad made of elastomeric rubber will also be assumed.

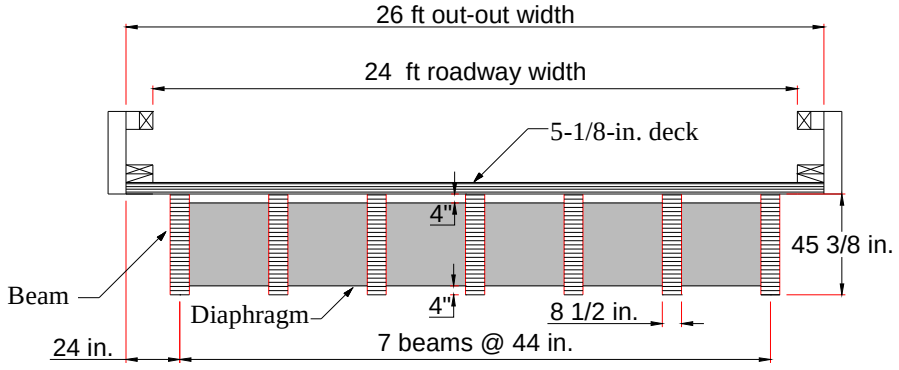

Figure 5.1. Beam Configuration and Size – 24-ft Roadway Width

The baseline bridge deck consists of transverse glulam deck panels with vertical laminations. The glulam deck panels are 5-1/8-in. thick. All standard interior and end panels are 4-ft wide (Figure 5.2). The panels are attached to the beams with 5/8-in.-diameter dome head bolts and cast aluminum alloy deck brackets. The deck brackets are connected to the glulam beam sides in 3/4-in. by 8-in. slots. For the interior panels, two brackets per beam side are connected to the deck panel with bolts placed 6 in. from the panel edge and spaced at 2 ft and not coincident with the other side. In the end panels, the brackets are connected to the deck panel with bolts placed 6 in. from the panel edges.

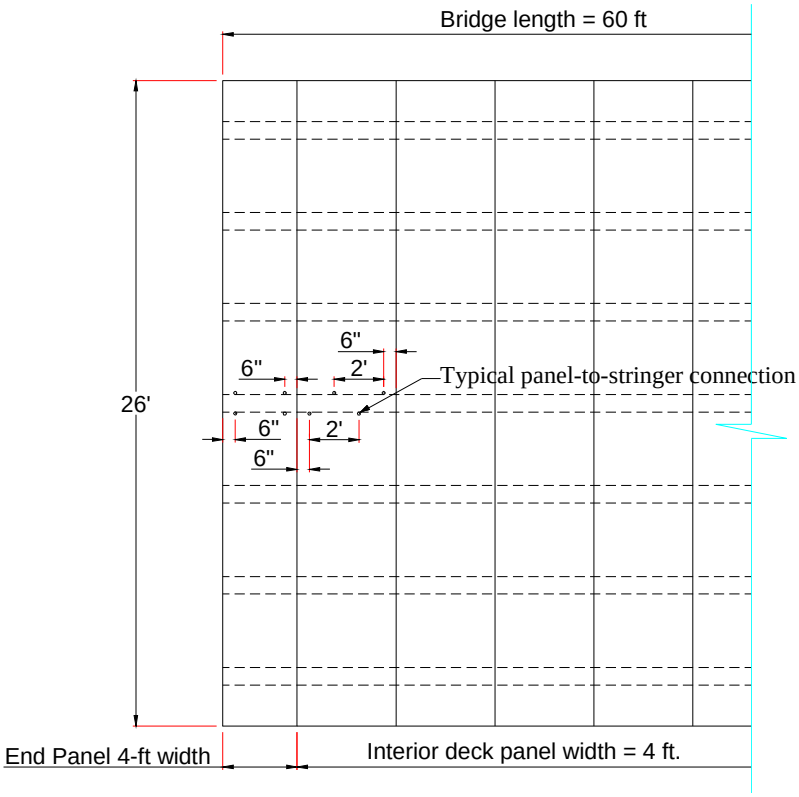

Figure 5.2. Deck Panel Layout for Unskewed 60-ft Long Bridge

5.3.1. MEASUREMENT ATTRIBUTES OF THE SMART TIMBER BRIDGE

Development of the smart timber bridge focuses first on understanding bridge-specific behaviors and deterioration modes (Ritter, 1990; FPL; 1999; NFPA, 2005) and then designing an instrumentation and data processing plan that allows extraction of the needed information. Assessment of structural adequacy and deterioration of a structure is key to the success of a smart

timber bridge. The needed variables thought to define the attributes of the smart timber bridge constructed with glued laminates are described below.

5.3.1.1. STRUCTURAL ADEQUACY

Structural behavior attributes, which are related to the load side of structural capacity, will be evaluated with respect to three engineering metrics: lateral load distribution, dynamic load allowance, and fatigue life usage (Hosteng, 2004; Le et al, 1998; Ansell, 2003; Clorius, 2000; Davids et al, 2005). Lateral load distribution obtained from the live loads is an important parameter that indicates how loads are being resisted by the structure and may be an indicator of changes in stiffness and possible deterioration of the bridge over time. Also, quantification of the dynamic load allowance will give a similar indicator. Finally, fatigue life usage (which can be used in bridge management and in other ways) of critical members (e.g., girder-to-deck and girder-to-bearing connections) will be assessed through stress cycle counting.

Another structural adequacy requirement is serviceability of the structure, which focuses on ensuring functionality and appearance of the structure. In the smart timber bridge, live load deflection, or measurements related to deflection (e.g., strain) will be monitored to investigate functionality and changes in stiffness of the bridge superstructure. Somewhat related, a technique to assess configuration and loading of vehicles will be obtained from measurement responses. Evaluation of all assessed parameters, in the light of the actual response of the structure, would provide information about usage of the structure and could be used to predict remaining service life of the smart timber bridge.

Structural damage is an equally important characteristic of timber bridges. The SHM system would need to assess changes in stiffness resulting from factors such as delamination, vehicular collision, and other sources. This will most likely be accomplished through statistical evaluation of the above parameters.

5.3.1.2. DETERIORATION

When properly engineered throughout the design, fabrication, and installation process, wood is a durable bridge material (Ritter, 1990; FPL; 1999; NFPA, 2005). However, over extended periods under service, wood may decay due to exposure to biologics and other deleterious environment

factors. To preserve the utility of the bridge and to ensure the safety of road users, the smart timber bridge will need to assess the condition of the structure by measuring factors that are associated with decay and deterioration. Moisture content, corrosion, and ultraviolet light degradation are the primary metrics to be monitored by the smart timber bridge. Proactive maintenance measures triggered by monitoring these metrics may prevent future problems related to performance and integrity of the structure.

Moisture has a detrimental influence on the service life of many structures, especially in wood, causing several deterioration processes. In the presence of water, the microstructure of wood swells until the fiber saturation point, which can make the cellulose more accessible to fungal enzymes, thereby enhancing the rate of decay. The repeated wetting and drying or continuous exposure to moisture can result in leaching of toxic heartwood extractives and some preservatives, reducing the resistance to decay (Ritter 1992). Currently, early assessment of moisture content and resulting preventive maintenance have proven to effectively control and prevent decay in timber bridges. Thus, moisture content monitoring will aid in the development of an active management program.

Ultraviolet light is a source of deterioration often found in timber bridges. Ultraviolet light chemically degrades the lignin near the wood surface of members such as deck edges, exterior girders and barriers. Continued removal of the damaged wood eventually reduces the member dimensions, affecting both stiffness and strength parameters. Wood lignin degradation will be detected by FOSs in exposed smart timber bridge members.

Finally, wood degradation due to metal corrosion will be assessed. Corrosion in timber bridges is an extreme case of bridge deterioration. Marine environments and deicing of roadways may cause deterioration in exposed bolts and other steel components such as diaphragms, and truss ties. Early detection of corrosion in exposed bolted connections, steel trusses and diaphragms will be monitored by detecting ferric in susceptible areas.

5.3.2. THE ANTICIPATED SENSOR TYPES TO BE USED

In the light of their attractive attributes, the sensors of choice for the smart-timber bridge are likely to be FOSs. In particular, FOS based on FBG technology, which can measure different parameters such as strain, temperature, pressure, vibrations, acceleration, and potentially other metrics (Swart et al, 2001; Wiese et al, 1999; Yeo et al, 2006; Furh et al, 1998; Maalej et al, 2002),

will be the primary focus of investigation. In a properly designed FBG sensor, a change in the desired parameter will induce a change in the wavelength measured by the sensor. In comparison with electrical sensors, FBG sensors are free from electromagnetic interference and time-related drift typically encountered with electrical sensors. FBG sensors are lightweight and small and can be embedded and integrated in virtually any structure (Kuang et al, 2001; Measures et al, 1995; Ritdumrongkul et al, 2003). Also, only a limited number of lead wires are needed to transmit data obtained from a large number of FBG sensors.

5.3.3. COMMUNICATION AND REPORTING

After the raw data are collected and cleansed, they are ready for processing, storage, and interpretation (ISIS, 2001; Bruhwiler, 2003). Data collected during continuous monitoring activities of the smart timber bridge will need to be processed before being stored. The developed performance algorithm would not only cleanse but process the obtained data (e.g., strain, temperature, moisture content, deflection, delamination, truck loads, ultraviolet light exposure, and corrosion). Following interpretation, a simple report would be developed by the smart timber bridge. The behavior of the superstructure would be summarized in the report which would integrate all responses related to attributes of the smart timber bridge described in this section and report on overall bridge condition. This report would also serve as an alert to early damage or deterioration. This information would need to be translated into a clear language that the owner can interpret for prompt evaluation and programming of routine maintenance and/or rehabilitation of the bridge.

5.4. PROBLEM STATEMENTS

Problem statements are required to achieve the overall objectives are summarized in Table 5.1. Detailed project descriptions for each problem statement are also provided in the following sections.

5.4.1. DEVELOPMENT OF FBG SENSORS TO DETECT MOISTURE CONTENT IN TIMBER

Background: Moisture plays an important role in determining the life of wood and is known to cause several deterioration processes (Ritter, 1992). Moisture can both reduce the decay resistance of wood and cause severe degradation of material properties. Also, moisture can accelerate fatigue life usage in compression members. Currently, several techniques to evaluate moisture are used during regular inspections. This practice has demonstrated that detection of moisture content and associated preventive maintenance of timber bridges can effectively control and prevent decay in timber bridges.

Table 5.1. Problem Statements Required for Achieving the Development of the Smart Timber Bridge

Phase	Project Focus	Est. Cost	Total Cost
Research Plan	Develop 5-Year Plan for Smart Glulam Bridge		Completed
Development of Reliable Sensors for Timber Bridge Performance Monitoring	1. Embedding sensors during manufacture of glulam bridge components	$93,000*	
	2. Attaching sensors to existing sawn lumber and glulam bridges	$250,000	
	3. Develop new sensors for measuring in-situ moisture contents	$200,000	
	4. Develop new sensors for detecting ferric ions caused by metal fastener corrosion	$200,000	
	5. Develop new sensors for detecting lignin loss caused by UV degradation	$250,000	$900,000
Development of an Efficient Structural Health Monitoring System [A]	1. Data processing techniques for structural adequacy parameters	$125,000	
	2. Data processing techniques for detecting systemic changes in stiffness	$125,000	
	3. Data processing for determining truck loading characteristics	$175,000	
	4. Bridge management software development	$100,000	$525,000
Field Demonstration [B]	Construct a new "smart glulam bridge" with embedded sensors and 1-year data collection	$250,000	$125,000
		Total →	$1,550,000

Note. - A – This phase can be performed concurrently after sensor development is complete;
B – Field demonstration does not include the costs for design, construction, or installation of a new bridge;
**-- This study is currently in-progress.*

Objectives: To develop a FBG sensor that can reliably measure moisture content in timber over a range of 10% to approximately 30%.

Task 1: Develop FBG sensors capable of detecting moisture content in timber members. Recent studies have demonstrated that fiber-optic-based humidity sensors can measure moisture absorption in concrete by using FBG sensors with a moisture-sensitive polymer, indicating their potential use in timber members. The developed sensors should have accuracy levels similar to currently used technologies and should be able to be embedded within timber members.

Task 2: Test FBG sensors under various moisture and ambient temperature conditions including wetting and drying cycles. Small and full scale glulam members are to be fabricated and instrumented with the developed FBG moisture sensor. The specimens should be exposed to accelerated environmental conditions and the FBG moisture sensor readings compared with traditional moisture content probe readings.

Task 3: Develop a final report that summarizes the work related to sensor development and laboratory tests. This report will include details on the FBG sensor materials and specifications for future installation.

Duration: Estimated project time is 18 months.

Cost: Estimated project cost is $125,000.

5.4.2. DEVELOPMENT OF TECHNIQUES FOR RETROFITTING SENSORS TO EXISTING SAWN LUMBER AND GLULAM BRIDGE COMPONENTS

Background: A sizeable inventory of timber highway bridges is currently in service. Gathering better data about their condition and performance through SHM techniques will improve management decisions regarding maintenance and repairs. This smart bridge approach will significantly extend the service life of many timber highway bridges, thereby conserving bridge replacement funds.

Objective: Develop techniques for embedding and attaching FBG sensors to existing sawn lumber or glulam bridge members of in-service structures.

Task 1: Evaluate surface conditions of treated and weathered bridge components for bondability bondability issues. This information will be needed to determine what degree of surface preparation will be required for adequate bonding. Several studies have investigated surface condition for bonding FRP reinforcements to structural wood, and near-infrared spectroscopy has been used for this purpose.

Task 2: Develop surface preparation protocols for bonding of FBG sensors to weathered bridge members treated with oil-borne preservatives. This information will be essential to achieving quality bonds in the field.

Task 3: Evaluate existing and new adhesive technologies for their potential to provide adequate and durable bonds to treated timber bridge components. Select candidate adhesives for bonding FBG sensors for further evaluations.

Task 4: Evaluate the performance of attached sensors within compression, tension, and bending members. Prepare scaled-sized bridge members for laboratory tests under simultaneous loading and

environmental conditions. Where possible, compare new sensor data against benchmark data collected with conventional instrumentation. Select the sensor and adhesive technique with best overall performance.

Task 5: Evaluate sensor and adhesive performance in full scale laboratory specimens under static and cyclic load testing. Where possible, compare new sensor data against benchmark data collected with conventional instrumentation.

Task 6: Prepare a final report that will document recommended practices for attaching FBG sensors to existing sawn lumber and/or glulam members in field bridges.

Duration: Estimated project time is 24 months.

Cost: Estimated project cost is $250,000.

5.4.3. DEVELOPMENT OF FBG SENSORS TO DETECT FERRIC IONS

Background: Wood degradation due to metal corrosion is a type of timber bridge deterioration that is often observed in marine environments. A similar effect can also result from the application of deicing chemicals to a bridge roadway. In the presence of moisture, fasteners made of iron corrode and release ferric ions, which deteriorate wood cell walls. This occurs because acidity at the anode causes cellulose hydrolysis, which decreases wood strength.

Objective: To develop a FBG sensor that indirectly measures corrosion activity by detecting the presence of ferric ions.

Task 1: Develop FBG sensors that detect ferric ions released from bolts and other metal fasteners. A limited amount of documented research indicates that multi-parameter FBG sensors are capable of indirectly measuring steel reinforcement corrosion in reinforced concrete roadways and bridges by detecting changes in chemical composition or simply changes in material color. Such a sensor is to be developed; it is desirable that the developed sensor be able to detect both corrosion initiation and growth rate.

Task 2: Test FBG ferric ion sensors in typical saline environments, including marine water and in the presence of chloride-based deicing chemical. Testing of the developed sensor should be

conducted on small scale specimens with a variety of fastener types. When possible, comparisons with electromechanical methods will be made.

Task 3: Prepare a final report that summarizes the FBG sensor development and testing. This report will include details on the FBG sensor materials and specifications for future installation.

Duration: Estimated project time is 18 months.

Cost: Estimated project cost is $200,000.

5.4.4. DEVELOPMENT OF SENSORS TO DETECT DEGRADATION IN WOOD LIGNIN

Background: Chemical degradation of wood lignin can be caused by ultraviolet sunlight exposure. This deterioration typically affects the surface and, over time, results in a reduction in member physical dimensions, which in turn reduces the associated member strength and stiffness. This deterioration becomes critical when the continued removal of material reduces the member capacity below the required demand or compromises the protective outer layer of preservative-treated material.

Objectives: To detect wood deterioration associated with ultraviolet light exposure, FBG sensors will be developed to detect the initial loss of wood lignin.

Task 1: Develop FBG sensors that detect the breakdown of wood lignin associated with ultraviolet light exposure. The developed sensor could be either surface mounted or embedded. In either case, it is desirable to detect the initiation of the breakdown and, if possible, to determine the rate of deterioration.

Task 2: Evaluate the performance of the developed FBG sensors under controlled ultraviolet light. The amount of exposure should be varied to simulate varying degrees of exposure and should be used to study the sensitivity of the sensor to deterioration. When possible, correlations to conventional detection techniques are to be made.

Task 3: Develop a final report that documents the sensor development and laboratory testing. The final report will detail the sensor materials and specifications.

Duration: Estimated project time is 18 months

Cost: Estimated project cost is $250,000.

5.4.5. EVALUATION OF TECHNIQUES FOR EMBEDDING AND ATTACHING FBG SENSORS TO TIMBER MEMBERS

Background: FBG sensors have been embedded and attached to structural materials such as steel and reinforced concrete with proven success. These deployed systems are currently working under harsh climatic conditions and are reporting on the health condition of highway bridges around the world. However, no such applications exist for timber members.

Objectives: To measure the desired physical attributes of the smart timber bridge, techniques for embedding and attaching FBG sensors to timber members need to be developed and evaluated under static, cyclic, and sustained loads.

Task 1: Collect information on available structural adhesives for adhering FBG sensor to timber members. Existing and emerging adhesives for glulam are to be investigated. The most promising adhesives for attaching and embedding FOS sensors to timber will be selected for further evaluation.

Task 2: Develop potential techniques (e.g., packaging, configurations, etc.) for embedding and attaching FBG sensors to timber members. These techniques need to include designs for sensors that require structural adhesion as well as those sensors that need to be isolated from the structural behavior.

Task 3: Evaluate the performance of attached and embedded sensors within tension members under static loads. Prepare and test small scale glulam specimens with various adhesives and attachment methods. Select adhesive types that show the best agreement with conventional instrumentation.

Task 4: Evaluate the performance of embedded and attached sensors within tension members under cyclic loads. Prepare small scale glulam specimens with candidate adhesives and packaging. Determine the fatigue life of the adhesive and compare responses with conventional instrumentation.

Task 5: Evaluate adhesive responses under sustained tensile load and temperature variations. Prepare small scale glulam specimens and test them under different sustained loads with temperature

and humidity variations. Analyze failure modes, effect of the applied variables, and bond-slip behavior based on the effects of adhesive thickness and protective coating materials.

Task 6: Select the embedment and attachment methods with best performance.

Task 7: Evaluate sensor and adhesive performance in full scale laboratory specimens under static and cyclic loads. Where possible, make comparisons under both static and cyclic loads with conventional instrumentation.

Task 8: Prepare a final report that will document the developed techniques for embedding and attaching FBG sensors to timber members.

Duration: Estimated project time is 24 months.

Cost: Actual project cost was $93,000, as this study is funded and currently in progress.

5.4.6. Development of Data Processing Techniques for Determining Structural Adequacy Parameters

Background: Lateral load distribution between girders and dynamic load allowance, as defined in current bridge standards, are engineering metrics that indicate how loads are resisted by bridge superstructures. Processing techniques and associated instrumentation are needed to extract this information. In addition, fatigue life usage, when combined with other information (e.g., moisture content, etc.), gives a bridge owner a sense of how much usage a bridge has seen.

Objective: The objective of this work is to develop data processing techniques to determine lateral load distribution, dynamic load allowance, and fatigue life usage.

Task 1: Identify FBG strain sensor locations in the conceptual smart timber bridge that are needed for determining structural adequacy parameters. Identify alternative sensors location in other possible positions.

Task 2: Review currently developed data processing techniques for determining structural adequacy (e.g., fatigue life usage in real time). Select tools that may be implemented to the data processing techniques.

Task 3: Collect data from a selected highway timber bridge subjected under ambient traffics load for a period of time to be used in the beta testing of data processing techniques for evaluating structural adequacy. These data should be collected using conventional instrumentation.

Task 4: Develop data processing techniques for determining lateral load distribution characteristics in real time. These techniques should identify vehicle position such that the lateral load distribution factors may be "normalized." The developed techniques should be tested with the data collected in Task 3.

Task 5: Develop data processing techniques for determining dynamic load allowance characteristics in real time. The developed techniques should be tested with the data collected in Task 3.

Task 6: Develop data processing techniques for determining fatigue life usage in real time. The developed techniques should be tested with the data collected in Task 3.

Task 7: Prepare a final report summarizing the data processing techniques for lateral load distribution, dynamic load allowance, and fatigue life usage.

Duration: Estimated project time is 12 months.

Cost: Estimated project cost is $125,000.

5.4.7. DEVELOPMENT OF DATA PROCESS TECHNIQUES FOR DETERMINING CHANGES IN STRUCTURAL STIFFNESS

Background: In general, changes in structural stiffness imply that a change in member properties has occurred. Techniques for identifying both instantaneous and gradual changes in stiffness are needed.

Objectives: Develop techniques for assessing changes in structural stiffness through statistical evaluation of measured physical properties.

Task 1: Investigate statistical evaluation methods for evaluating changes in large and diverse population measurements. Select statistical evaluation methods most suitable for processing data of this type for the purpose of identifying statistical differences over short and long periods of time.

Task 2: Modify collected data from a highway timber bridge subjected to ambient traffics load to generate synthetic changes in structural stiffness. These modifications should include both gradual and significant variations in lateral load distribution and dynamic allowance characteristics.

Task 3: Develop techniques for evaluating gradual and significant changes in stiffness through statistical evaluation of lateral load distribution and dynamic allowance. It is desired that the technique will both identify and quantify the level of structural stiffness change. Beta test the developed techniques using the synthetic data obtained in Task 2.

Task 4: Develop data processing techniques and required instrumentation for detecting vehicle collisions. The data processing techniques and needed instrumentation should be capable of detecting collision both on and below the bridge. Validate the technique with analytical modeling.

Task 5: Prepare a final report with the developed data processing techniques for stiffness degradation. This report will document the defined damage levels in each case and the beta test results.

Duration: Estimated project time is 12 months.

Cost: Estimated project cost is $125,000.

5.4.8. DEVELOPMENT OF DATA PROCESSING TECHNIQUES TO DETERMINE VEHICLE CHARACTERISTICS

Background: Bridges are designed to carry truck traffic, and it is desirable to know the number, geometry and weight of the passing trucks. By determining vehicle characteristics, it will be possible to better predict usage and induced damage or deterioration.

Objective: Develop a data processing technique for determining vehicle characteristics such as vehicle weight, configuration, and speed.

Task 1: Review previous work for determining vehicle characteristics. Select tools that could be possibly integrated into other data processing technique development.

Task 2: Develop initial conceptual tools to determine vehicle characteristics and an associated instrumentation scheme.

Task 3: With the developed instrumentation scheme developed in Task 2 in mind, collect response data from a typical timber bridge using conventional instrumentation.

Task 4: Using the data collected in Task 3 and the techniques develop in Task 2, determine the effectiveness of various tools at predicting vehicle characteristics. If required, refine the developed tools to improve overall performance.

Task 5: Prepare a final report that documents the development and resulting data processing tools.

Duration: Estimated project time is 18 months

Cost: Estimated project cost is $175,000.

5.4.9. DEVELOPMENT OF SMART TIMBER BRIDGE SOFTWARE APPLICATION

Background: Any effective Structural Health Monitoring System must integrate data from many sources and evaluate it in a simple, turn-key application. Such a software application is needed for the smart timber bridge.

Objectives: Develop a software application to collect, reduce, extract, analyze and report on the health condition of the smart bridge by using collected data and data processing techniques that evaluate and translate obtained responses in clear formats.

Task 1: Develop software to collect data obtained from FBG sensors. In this task, detection of possible data cross over will be conducted and revised. Also, this software will verify sensor performance and collected data consistency.

Task 2: Develop tools to cleanse the collected data from noise and undesired data record characteristics.

Task 3: Develop tools to preprocess the obtained data by extracting data related to loading events and discarding other insignificant data. Selected data will be saved in compressed form so that they may be retrieved and used for near-real time analysis.

Task 4: Develop an application that analyzes the stored data. This analysis should include converting measured wavelengths to engineering parameters. The software should integrate all applications and procedures developed under separate work. The software should develop condition

reports on a daily, weekly, monthly, and yearly basis that are clear and understandable to bridge owners.

Task 5: Prepare a final report that documents the developed software application.

Duration: Estimated project time is 1 year.

Cost: Estimated project cost is $100,000.

5.4.10. DEMONSTRATION OF THE SMART TIMBER BRIDGE

Background: Work conducted separately has resulted in the development of several new sensors types for measuring engineering parameters such as moisture content, degradation due to corrosion and ultraviolet exposure, and others. Further other work has led to the development of data processing techniques for evaluating collected behavior data in real time.

Objectives: Demonstrate all the developed components of the smart timber bridge in a field application.

Task 1: Prepare detailed construction plans and specifications for the assembly of the smart timber bridge members and installation of FBG sensors. Also, design the data acquisition system including sensor positions, cabling routes, storage cabinets, etc.

Task 2: Working with selected construction contractors, equipment manufacturers, and timber fabricators fabricate and construct the smart timber bridge.

Task 3: Test the SHM system under ambient traffic loading. Verify the performance of all sensors and calculations with known loads. Where possible, validate the performance of sensors and algorithms with other sensors and tests.

Task 4: Monitor the smart timber bridge and the monitoring system for 1 year. Complete any needed revisions to the system.

Task 5: Prepare a final report that documents the performance of the smart timber bridge. The report should include detailed construction specifications for future smart timber bridges.

Duration: Estimated project time is 12 months.

Cost: Estimated project cost is $125,000 plus bridge costs.

5.5. REFERENCES

1. Ansari, F. (2005). "Fiber-Optic Health Monitoring of Civil Structures Using Long Gage and Acoustic sensors." Chicago, IL: University of Illinois. Smart Mat. Struct. 14 (2005), pp. S1-S8. http://iopscience.iop.org/0964-1726/14/3/001/pdf/sms5_3_001.pdf. Last accessed in August, 2010.

2. Ansell, M. (2003). "Fatigue of Wood and Wood Panel Products." In: Fatigue en Composites. United Kingdom: University of Bath, pp. 339- 360.

3. Bruhwiler, E. (2003). "Conceptual Design of a Monitoring System." In: Wu; Abe, eds. Proceedings, Structural Health Monitoring and Intelligent Infrastructure (SHMII). MCS-CONF-2007-048. Tokyo, Japan. November 13–15. Vol. CD-Rom, Num. 2003.

4. Clorius, C., Pedersen, M., Hoffmeyer, P., and Damkilde, L. (2000). "Compressive Fatigue in Wood." Germany: Springer–Berlin/Heidelberg. Wood Science and Technology. 34(1), pp. 21-37.

5. Davids, W., Dagher, H., Richie, M., and Sanchez, O. (2005). "Fatigue of Glulam Beams with Fiber-Reinforced Polymer Tension Reinforcing." Forest Products Journal, Forest Products Society, 55 (1), pp. 93-101.

6. Doornink, J., Phares, B., Zhou, Z., Ou, J., Graver, T. and Xu, Z. (2005). "Fiber Bragg Grating Sensing for Structural Health Monitoring of Civil Structures." In: International symposium on advances and trends in fiber optics and applications. October 11–14, 2004. China, pp. 4. http://www.micronoptics.com/uploads/library/documents/FBGsensingSHMcivil.pdf. Last time accessed in August 2010.
7. Forest Product Laboratory (FPL). (1999). "Wood Handbook - Wood as an Engineering Material." Gen. Tech. Rep. FPL–GTR–113. Madison, WI: U.S. Department of Agriculture, Forest Service, Forest Products Laboratory, pp. 463.

8. Fuhr, P. and Houston, D. (1998). "Corrosion Detection in Reinforced Concrete Roadways and Bridges Via Embedded Fiber Optic Sensors." Smart Materials and Structures. 7: pp. 217–228.

9. Hosteng, T. (2004). "Live Load Deflection Criteria for Glue-Laminated Timber Bridges." M.S. thesis. Ames, IA: Iowa State University. pp. 300.

10. Intelligent Sensing for Innovative Structures (ISIS) Canada. (2001). "Guidelines for Structural Health. Monitoring – Design Manual No. 2." University of Manitoba, Winnipeg, Manitoba 2001, pp. 127.

11. Kainz, J., Wacker, J., Ritter, M. and Bishop, S. (2001). "Field Performance of Timber Bridges—Humphrey Stress-Laminated T-Beam Bridge." Res. Pap. FPL–RP–597. Madison, WI: U.S. Department of Agriculture, Forest Service, Forest Products Laboratory, pp. 16.

12. Kim, N. and Cho, N. (2004). "Estimating Deflection of a Simple Beam Model Using Fiber Optic Bragg Grating Sensors." Journal of Sound and Vibration. 305(3): pp. 534-542.

13. Koh, H., Choo, J., Kim, S. and Kim, C. (2003). "Recent Application and Development of Structural Health Monitoring Systems and Intelligent Structures in Korea." In: Wu; Abe, eds. Proceedings, Structural Health Monitoring and Intelligent Infrastructure (SHMII). November 13–15. Tokyo, Japan.

14. Kuang, K., Kenny, R., Whelan, M., Cantwell, W. and Chalker, P. (2001). "Residual Strain Measurement and Impact Response of Optical Fibre Bragg Grating Sensors in Fibre Metal Laminates." Institute of Physics Publishing, Smart Materials and Structures. 10: pp. 338–246.

15. LaViolette, M., Vis, J., Phares, B., Wipf, T., Hagan, T. and Murphy, J. (2005). "Remote Security Monitoring of Historic Covered Bridges." Ames, IA: Iowa State University, Bridge Engineering Center—CTRE. pp. 55.

16. Le, X., Kainz, J., Peterson, M.L. and Landisic, E.N. (1998). "Smart Timber Bridges For In-Situ Evaluation." Madison, WI: U.S. Department of Agriculture, Forest Service, Forest Products, pp. 8. http://www.fpl.fs.fed.us/documnts/pdf1998/le98a.pdf. Last date accessed in August 2010.

17. Li, H., N., Li, D. S, and Song, G. B. (2004). "Recent Applications of Fiber Optic Sensors to Health Monitoring in Civil Engineering." Engineering Structures 2004, Vol. 26, pp. 1647-1657.

18. Maalej, M., Ahmed, S., Kuang, K. and Paramasivam, P. (2004). "Fiber Optic Sensing for Monitoring Corrosion-Induced Damage." Structural Health Monitoring and Intelligent Infrastructure (SHMII). 3(2): pp. 165–176.

19. Maalej, M., Karasaridis, A., Pantazopoulou, S. and Hatzinakos, D. (2002). "Structural Health Monitoring of Smart Structures." Institute of Physics Publishing, Smart Materials and Structures. 11(4): pp. 581–589.

20. Measures, M., Alavie, A., Maaskant, R., Ohn, M., Karr, S. and Huang, S. (1995). "A Structurally Integrated Bragg Grating Laser Sensing System for a Carbon Fiber Prestressed Concrete Highway Bridge." Institute of Physics Publishing, Smart Materials and Structures. 4: pp. 20–30.

21. Merzbacher, C., Kersey, A. and Friebele, E. (1996). "Fiber Optic Sensors in Concrete Structures: a Review." Institute of Physics Publishing, Smart Materials and Structures. 5: pp. 96–208.

22. Muragishi, O., Nihei, K., Kobayashi, T., Ohgaki, K., Kawaguchi, Y. and Umeda, A. (2003). "Remaining Life Evaluation by Fatigue Detecting Sensor." Structural Health Monitoring and Intelligent Infrastructure (SHMII). IIW. Doc XIII-2018-04.

23. Muthumani, K. and Sreekala, R. (2003). "Structural Application of Smart Materials." In: Smart Materials. Edited by Mel Shwartz. CRC Press 2009, pp. 4-1 – 4-4. http://www.crcnetbase.com/doi/pdfplus/10.1201/9781420043730.ch4. Last time accessed in August 2010.

24. NFPA. (2005). "National Design Specification: Wood Construction - Structural Lumber, Glue Laminated Timber, Timber Piling, Fastenings." Washington, DC: National Forest Products Association, pp. 1000.

25. Phares, B., Wipf, T., Greimann L.F. and Lee, Y.S. (2005). "Health Monitoring of Bridge Structures and Components Using Smart Structure Technology. Ames, IA: Iowa State University, Bridge Engineering Center—CTRE. pp. 57. http://www.intrans.iastate.edu/reports/health_monitor_wi_vol1.pdf. Last date accessed August 2010.

26. Ritdumrongkul, S., Abe, M. and Fujino, Y. (2003). "Experimental Study on Health Monitoring of Bolted Joints using Piezoceramic and Laser Doppler Vibrometers. In: Wu, A., ed. Structural Health Monitoring and Intelligent Infrastructure (SHMII), pp. 825-830.

27. Ritter, M.A. (1992). "Timber Bridges: Design, Construction, Inspection and Maintenance." EM 7700–8. Washington, DC: U.S. Department of Agriculture, Forest Service. (Approved for reprinting, August 1992), pp, 970.

28. Russel, C. (1997). "Glued-Laminated Timber." In: Engineered Wood Product. Smulki, E. Editor. pp 340.

29. Sumant, P. and Maiti, S. (2006). "Crack Detection in a Beam Using PZT Sensors." Smart Mat. Struct. 5, pp. 695-703. http://iopscience.iop.org/0964-1726/15/3/004/pdf/sms6_3_004.pdf. Last date accessed August 2010.

30. Swart, P.L., Naude, R. and Lacquet, B.M. (2001). "Determining the Moisture Content in Concrete with Fibre Optic Mach-Zehnder Interferometer: a Feasibility Study." Institute of Physics Publishing, Measurement Science and Technology. 12(2001): pp. 927–931.

31. Tsuda, H., Toyama, N., Urabe, K. and Takatsubo, J. (2004). "Impact Damage Detection in CFRP Using Fiber Bragg Gratings." Institute of Physics Publishing, Smart Materials and Structures. 13(4): pp. 719–724.

32. Tsutsui, H., Kawamata, A., Sanda, T. and Takeda, N. (2004). "Detection of Impact Damage of Stiffened Composite Panels Using Embedded Small-Diameter Optical Fibers." Institute of Physics Publishing, Smart Materials and Structures. 13(6): pp. 1284-1290.

33. Udd, E., Schulz, W. and Seim, J. (1998). "Advanced Fiber Optic Sensors Capable of Multiparameter Sensing." In: SPIE Proceedings. Gresham, OR: Blue Road Research. Vol. 3489, pp. 66.

34. Udd, E., Seim, J., Schulz, W. and McMahon, R. (2000). "Monitoring Trucks, Cars, and Joggers on the Horsetail Falls Bridge Using Fiber Optics Granting Strain Sensors." SPIE Proceedings, Vol. 4185, pp.872.

35. Wacker, J.P. and Smith, M.S. (2001). "Standard Plans for Timber Bridge Superstructures." Gen. Tech. Rep. FPL–GTR–125. Madison, WI: U.S. Department of Agriculture, Forest Service, Forest Product Laboratory, pp. 53.

36. Wiese, S., Kowalsky, W., Wichern, J. and Grahn, W. (1999). "Fiberoptical Sensors for On-Line Monitoring of Moisture in Concrete Structures." In: Chang, F.K., ed. Structural Health Monitoring and Intelligent Infrastructure (SHMII), pp. 643-650.

37. Wipf, T. and Phares, B. (2005). "A 5-year Research Plan for the Development of A Smart Glue-Laminated Timber Bridge." Ames, IA: Iowa State University, Bridge Engineering Center—CTRE, pp. 2. http://www.fpl.fs.fed.us/documnts/rips/fplrip-eml-004-glued-laminated-timber-bridge.pdf. Last date accessed August 2010.

38. Yeo, T.L., Eckstein, D., McKinley, B., Boswell, L.F., Sun, T. and Grattan, K.T.V. (2006). "Demonstration of a Fibre-Optic Sensing Technique for the Measurement of Moisture Absorption in Concrete. Institute of Physics Publishing, Smart Materials and Structures. 15(2006): pp. N40-N-45.

CHAPTER 6. EVALUATION OF TECHNIQUES FOR EMBEDDING AND ATTACHING FBG SENSORS TO GLULAM BRIDGE MEMBERS

A refereed report in preparation for the
United States Department of Agriculture – Forest Product Laboratory, 2010

Ursula Deza, Brent Phares, Terry Wipf

6.1. INTRODUCTION

6.1.1. BACKGROUND

The deterioration of bridge structures has created vigorous interest in the development of new techniques for bridge construction, reparation, rehabilitation, and monitoring. In the case of timber bridges, traditional condition assessments have been determinated by visual inspections of the structure's members with maintenance decisions being based upon the gathered information. To improve this situation, the development of an innovative timber bridge structure with the capability to monitor long-term performance parameters through the implementation of fiber optic strain gages was cooperatively developed (Phares et al, 2007).

A smart structure would typically incorporate structural materials, sensors, data reduction techniques and remote systems that allow for the monitoring of the structure. With these elements, the smart structure is able to monitor the in-situ behavior of the structure, to assess performance under service loads, detect damage/deterioration, and determine the current condition (ISIS, 2001). In this context, a conceptual smart timber bridge was developed with the purpose of improving the long-term performance, maintenance, and management of timber bridges. Four concepts were established to develop the smart timber bridge comprising of:

- Selection of the bridge structural materials
- Identification of the measured performance metrics (attributes)
- Selection/development of the sensor types
- Communication/processing and reporting.

Stress rated glued laminated timber members were selected as the material for the smart timber bridge. Specifically, the superstructure of the conceptual bridge, composed of a series of transverse

glulam deck panels supported on longitudinal glulam beams, was the focus of the smart timber bridge development.

By identifying the bridge-specific behaviors and deterioration modes, the assessment of the smart timber bridge condition will be conducted through the evaluation of the structural adequacy and decay/deterioration. Structural adequacy of the bridge will be determined by measuring flexural strains. In addition, the decay/deterioration of the timber structure, specifically due to moisture, metal corrosion and ultraviolet light will be evaluated through the application of sensors housed in non-structural packages.

The overall health condition of the smart timber bridge will be monitored using commercially available, as well as new sensors. In the work described here sensors based upon Fiber Bragg Grating (FBG) technology were used. Besides being linear and absolute in response, electrical interrupt immune and readily multiplexed, these FBG sensors have the ability to be both embedded and surface mounted. In previous laboratory as well as field tests, good agreement between FBG strain sensors and conventional strain sensors was demonstrated for both steel and concrete structures (Merzbacher et al, 1996;Childers et al, 2001; Tahir et al, 2005; Rao et al, 2006). In recent research on steel bridge structures conducted by the Bridge Engineering Center, FBG sensors demonstrated 99% agreement with foil strain sensors (Doornink, 2006). These FBG strain sensors will be used to measure the structural response of the timber bridge. In addition, sensors to detect moisture content, ferric ions and degradation of wood lignin will be integrated to detect the decay/deterioration.

In addition, as a part of the health monitoring technologies and bridge management approaches, a communication/reporting system will be developed. This system will be comprised of a data acquisition system, development of data processing techniques and software applications to interpret and report on the results of the data obtained during monitoring activities. The behavior of the superstructure will be summarized by integrating all the responses related to the attributes of the smart timber bridge and be addressed to the bridge owner in a clear report. With this information, the owner can review and program routine maintenance and/or rehabilitation of the bridge. Also, this system will serve as an immediate alert to early damage catastrophic event.

In this investigation, the development of techniques for embedding and attaching FBG sensors to glulam timber members for detecting either structural or non-structural attributes of the timber

members was conducted. Using the proposed smart timber bridge concepts, members were constructed at the laboratory level with engineered glulam and commercially available FBG strain sensors. Although FBG strain sensors have been utilized in steel and reinforced concrete bridges with proven success, this is the first known application of embedded and attached FBG sensors in timber members for measuring structural and non-structural metrics in a structural health monitoring system.

This research is divided in two parts; the first focused on the development of new sets of structural and non-structural packages to protect the FBG sensors for detecting strains in glulam members. The second part focused on the development of attaching and embedding techniques for installing these FBG sensor packages in glulam members. In the laboratory, the developed external and internal FBG sensor packages were bonded to typical wood laminates. Small scale glulam specimens were constructed using the instrumented laminates. The specimens were tested under multiple loading cases and temperature variations to investigate the elastic and/or viscoelastic behavior of the sensor packages. After processing the data and analyzing the results, the most promising structural and non-structural FBG sensor packages and attachment techniques were selected to be implemented in a full-scale glulam bridge girder. This girder and its load/strain response were evaluated in the laboratory.

6.1.2. OBJECTIVE AND SCOPE

The main objective of this research work is the development of techniques for embedding and attaching sensors to glulam timber members for detecting either structural or non-structural attributes of the timber members. This consisted of the development of various structural and non-structural sensor packages and the selection of appropriate adhesives. Further, techniques for embedding and attaching the sensors were developed. To evaluate the responsiveness of the sensor packages, laboratory testing was conducted under variable laboratory and temperature conditions. The most promising sensor packages were selected and installed in a full-scale glulam girder which was, again, tested in the laboratory.

6.1.3. LITERATURE REVIEW

The literature review briefly summarized here was conducted and focused on providing information on previous investigations related to the installation and application of FBG sensors civil engineering structures. At this time no fiber optic sensors have yet to be embedded in or attached to glued laminated timber bridges members.

6.1.3.1. GENERAL OVERVIEW OF FIBER OPTIC SENSORS

Currently available and on-going research in fiber optic sensors (FOSs) is based on the advances in laser technologies and in low-loss optical fiber in the 1960s (Grattan and Sun, 2000) and the expansion of telecommunication optical fiber networks in the early 1980s (Meggitt, 2008). Recently, extensive research to develop FOSs with multi- and single-mode techniques has been the focus of many investigations. Typically, a fiber optic consists of the fiber core, cladding and jacket. Under environmental conditions, fiber optics experience geometrical and optical changes (i.e., size, shape, refractive index, mode conversion) while still reliably transmitting light. As a result, fiber optics can be used as sensors to measure external environmental parameters (Li et al, 2004). Environmental FOSs have typically been desirable where electronic and electrical sensors simply do not perform reliably. In Figure 6.33(a), a synopsis of FOSs and their associated measurement parameters is presented, grouped according to the most common methods of evaluation: extrinsic and intrinsic methods (Udd, 1991). An extrinsic FOS or hybrid FOS consists of carrying-light input and output fibers and a black box; the latter element interprets the FOS to an environmental change. An intrinsic FOS or all-fiber FOS reacts upon environmental actions and converts these actions into a modulation of the light beam passing through it (Nolan et al, 1991). Additionally in Figure 6.33(b), interferometric FOSs and their corresponding parameters are presented as reference. FOSs have found niche applications in various fields including medicine, chemical products, aerospace, concrete structures, electrical power industry, etc.

In civil engineering applications, FOSs have been used during the last two decades to monitor the structural health of steel and concrete bridges by providing structural response measurements (e.g., stress, displacements, capacity, etc.) and environmental condition parameters (e.g., wind speed, temperature, etc.). Three groups of FOSs for structural health monitoring were presented by Li et al (2004). These sensors are classified by their sensing ranges including local, quasi-distributed and distributed capabilities (see Table 6.1). Local FOSs can detect optical phase changes at specific, discrete locations within structures. Distributed FOSs are recommended for large structures where every portion of the fiber is a sensor. Due to their weak resolution and detectable signal, these FOSs have limited applications, which include the evaluation of fracture losses or local damages in a structures. Similarly, a quasi-distributed FOS measures strains along the determined sensor length.

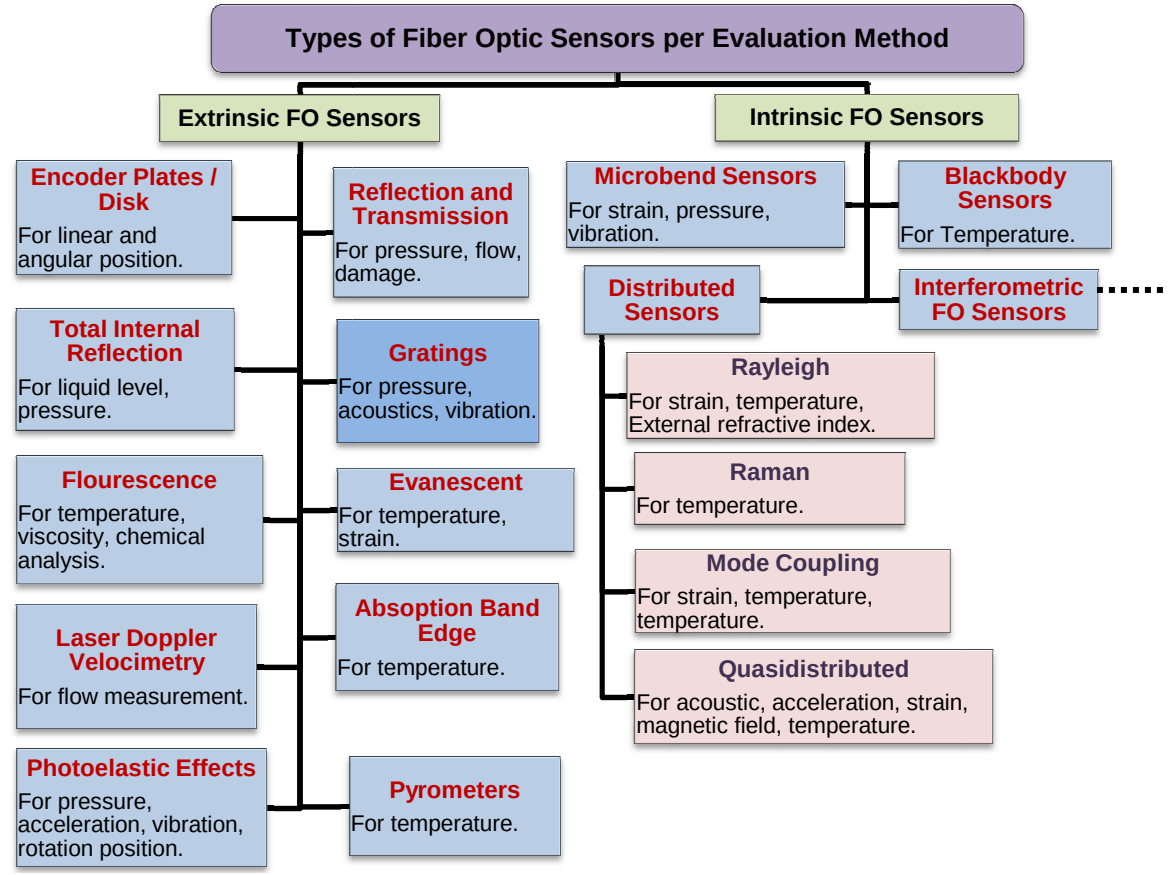

(a) Extrinsic and Intrinsic Fiber Optic Sensors

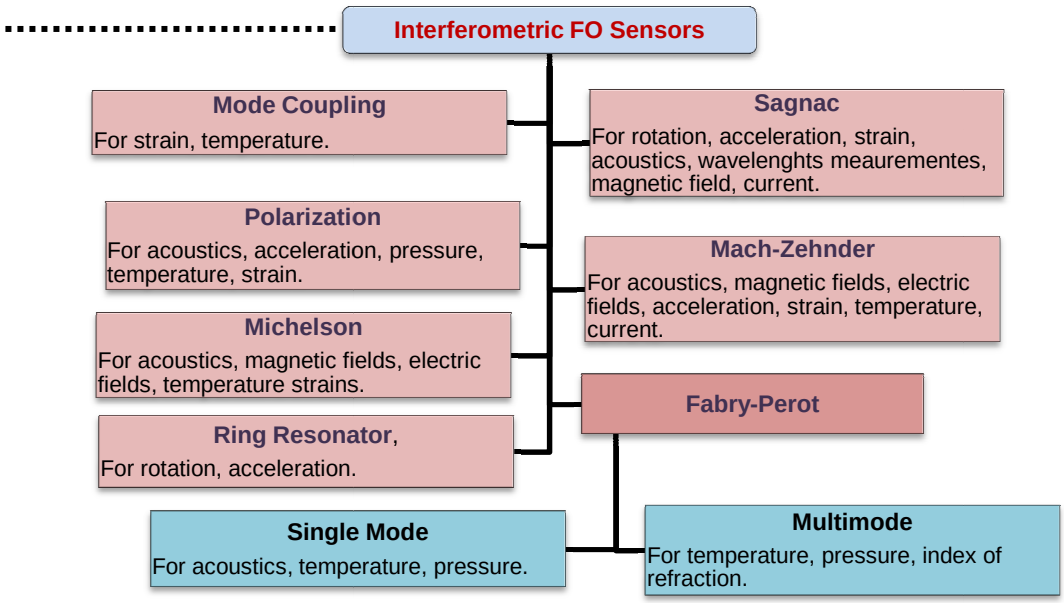

(b) Interferometric Fiber Optic Sensors

Figure 6.1. Chart of the Types of Fiber Optic Sensors (Udd, 1991)

Table 6.1. Fiber Optic Sensors for Civil Structural Health Monitoring (Li et al, 2004)

Sensing Type	Sensors	Measurements	Linear Response	Intrinsic/ Extrinsic
Local	Fabry-Perot	Strain, also configured to measure displacement, pressure, temperature	Yes	Both
	Long Gage Sensor	Displacement	Yes	Intrinsic
Quasi-distributed	Fiber Bragg Grating (FBG)	Strain, also configured to measure displacement, acceleration, pressure, temperature, relative fissure and inclination, corrosion, etc.	Yes	Intrinsic
Distributed	Raman / Rayleigh (OTDR)	Temperature / strain	No	Intrinsic
	Brillouin (BOTDR)	Temperature / strain	No	Intrinsic

6.1.3.2. CHARACTERISTICS OF THE FIBER BRAGG GRATING AS OPTICAL SENSORS

A Fiber Bragg grating (FBG) is defined as a periodic perturbation of the refractive index along an optical fiber length (grating length). The FBG is formed by exposure of the core to an intense optical interference (Hill and Metlz, 1997). The writing techniques of the grating have evolved from the internal laser writing (Hill et al, 1978) and transverse holographic methods (Metlz et al, 1989) to the phase mask method (Hill, 1993). The optical fibers consist of a small inner core and an outer core of glass (cladding). A coating of polyimide, or acrylate or ORMOCER (organic modulated ceramic) is applied to protect the fiber from water and hydrogen which can cause cracking (Kreuzer, 2007). To write the fiber into the core, the process includes dismantling the coat and writing the Bragg grating in a single mode. The fiber is thoroughly recoated to prevent the breakup of the fiber at lower strain levels.

In general, a FBG sensor is characterized by its high sensitivity and performance when compared to the other types of sensors (i.e., foil strain gages, strain transducers). FBG sensors have long life cycles, are corrosion resistant (made from silica) and withstand high tensile loading (up to 5% elongation) (Li et al, 2004). In addition, FBG sensors are passive (dielectric), immune to electromagnetic interference, light weight, small, have high-temperature performance, large bandwidth, high sensitivity, easy to be installed and optically multiplexed (Udd, 1991). When local strains or temperature variations alter the grating period, shifted wavelengths are measured by interrogators with resolutions and short-term stability of +/-1 pm. Currently, FBG sensors systems for measuring strains and temperatures interrogate over 512 sensors.

The durability of the FBGs depends on not only the quality of the manufacturing processes but also on the system usage. In the telecommunication industry, the system usage has been established and the associated failure mechanisms have been determined and modeled using standard accelerated aging tests for a 25-year usage pattern. However, in the health monitoring systems, the FBG sensors are applied in different environmental conditions for various measuring tasks (Lefebvre et al, 2006). Consequently, the failure mechanisms vary from application to application; therefore, the prediction of the life cycle of the FBG sensors cannot be estimated through characterization tests. After installing the FBG sensors in/on structural members, environmental conditions are expected to generate micro-crack growth and thermo-dynamic decay generating mechanisms of failure. To ensure the long term reliability of the FBG sensors, the life expectancy of the FBG components must be established. Although FBG sensors have been installed in various civil structures including bridges, buildings, piles, pipelines, tunnels and dams (Merzbacher et al, 1999; Li et al, 2004), the oldest reported and still operative fiber optic sensors were embedded in polymer matrix composites in 1982 at the NASA Langley Research Center. Fifteen years later, the FBG sensors were examined to study the possible degradation of the material in the vicinity of the embedded fiber elements (Claus et al, 1998). The main conclusions of the study were that all fiber optic sensors indicated to be operative after being interrogated, sensor leads have not be sheared off after 15 years of use, and the composite specimen had no sign of degradation. Issues faced then and still present today were the cross sensitivities of the wavelengths due to the number of FBG sensors interrogated and the interconnection problem of the sensors which implied the ingress/egress of the FBG leads and connectors at the host structures.

Though bare FBG sensors have demonstrated to be compatible with different infrastructures; due to their inherent fragility, FBG sensors are not suitable to be directly installed in structures (Moyo et al, 2005). FBG sensors when properly packaged can be operative under severe conditions imposed by construction environments and service. In the following sections, packaging techniques utilized in laboratory and field demonstrations for long-term monitoring are presented.

6.1.3.3. PACKAGING DEVELOPMENT

In the last two decades, FBG sensors have been installed in concrete (i.e., on steel and FRP reinforcement), on steel girders and other civil structural members with relative success (Vohra et al, 1999, Tennyson et 2001, Casas et al, 2003, Li et al, 2004). Though FBG sensors made from bare fiber are easy to be embeddable, when improperly handled during and after fabrication, FBG sensors

can be easily damaged. As a means to minimize damage and extend the FBG sensor life, either recoating the bare fiber or providing a protective packaging is desirable. In addition, it is desired that both bare fiber materials (i.e., polyamide or acrylate coating) and package epoxies last as long as the bridge service life (Lin et al, 2005).

In health monitoring systems developed in Japan, FBG sensors for damage detection embedded in FRP composite was studied by Satori et al (Satori et al, 2001). In this study, FBG sensors were fabricated in small optical fibers with cladding diameter of 40 μm and coated with polyimide. These sensors were heat treated at 300^{o} C (572^{o} F). After the high temperature treatment, the retained mechanical strength and reflectivity were verified. From the temperature and tensile test results, the coated and packaged FBG sensors were recommended to be implemented in health monitoring systems for sensing strains or temperatures.

One study on recoating and steel-tube packaging FBG sensors for civil engineering applications was conducted by Lin et al (Lin et al, 2005). Three techniques for packaging bare FBG sensors, which included nickel recoating, quartz glue and steel tube with 1- and 2-mm wall thickness, were prepared and evaluated. The bonding effect was studied in each FBG sensor, with or without packaging, to understand the strain transmission between the sensor and its host material member (specimen). The experimental results were compared to the finite element model (FEM) results verifying that the bare FBG sensors attached with different adhesive thicknesses (i.e., 2 to 100 μm) and various modulus of elasticity values (i.e., 5 to 100 GPa) did not interfere in the strain transmission rate.

Hao et al investigated the effects of packaging materials on the FBG sensors performance (Hao et al, 2006). Theoretical and experimental optical fiber constants such as thermo-optic and photo-elastic constants were investigated for two embedding materials (backing materials). Polymethyl methacrylate (PMMA) and carbon fiber reinforced composite (C-FRC) were selected for their high tensile strength and lower thermal expansion coefficients. In the laboratory, temperature and strain sensitivities of bare FBGs were measured as 10.9 pm/ ^{o}C and 1.1 pm/με, respectively. With respect to the PMMA, the FBG sensor was embedded into a small groove and fixed to the PMMA plate with hard epoxy resin. A variant of this packaging technique was the application of second layer of PMMA plate to form a sandwich structure. When subjected to heat, the temperature sensitivity of both packaged FBG sensors was at least nine times larger than the bare sensor. The experimental thermal expansion coefficients of the packages were on the order of the theoretical PMMA value

compared to the glass fiber. For the C-FRC, two unidirectional layer configurations were selected; bare FBG sensors were embedded into layers orientated at 0^o and 90^o with respect to the longitudinal direction of the FBG sensors. After testing, it was found that the 0^o C-FRP packaged FBG sensor had temperature sensitivity similar to the bare FBG sensor (i.e., C-FRP thermal expansion coefficient of $-1 \times 10^{-7} / {}^o C$). For the 90^o C C-FRC packaged FBG sensor, the resulting thermal expansion coefficient was on the order of the 90^o C-FRP package value as expected (i.e., five times larger than the bare sensor value).

FBG sensors were developed and deployed on reinforced concrete highway bridges to measure dynamic strain, static strain and temperature by the research program involving the School of Civil and Structural Engineering and School of Electrical and Electronic Engineering at Nanyang Technological University in Singapore (Moyo et al, 2005). Three sensor packages were developed to evaluate temperature, strain and temperature compensated strains. For the temperature sensor, a 35 mm (1.4 in.) long tube was used to protect the FBG sensor from external stress and increase the temperature sensing range with a coefficient of 25 pm/ ${}^o C$. The strain sensor package consisted of layers of 50-mm (2-in.) carbon composite material. The third FBG strain sensor was composed of two bare FBG sensors, one protected by a steel tube while the other embedded into carbon composite layers, similar to the previous developed sensors. Both sensors were inserted into a custom designed dumbbell in which the temperature FBG sensor was set lose and the strain FBG sensor was bonded to the inner surface of the dumbbell. Tensile, bending and dynamic loading tests as well as temperature tests were performed on steel reinforcement and in reinforced concrete beams to evaluate dynamic and static strain levels as well as the associate temperature per sensor type. Both FBG strain sensors and electrical resistance gages were installed for comparison. The FBG sensors that were protected during casting and isolated from pressure effects survived. From the test results, the surviving sensors were found to operate after construction and to provide accurate strain and temperature measurements. These sensors were recommended for being used in long term structural health monitoring besides short term load tests, vibration and seismic response.

Wnuk et al reported on bonding agents and methods for surface mounting FBG strain and temperature sensors to be used in harsh environments (Wnuk et al, 2005). Two FBG sensors were bonded with ceramic fillers and epoxy binder which were applied with a brush technique. Two other sensors were bonded with a material which consisted of a fiberglass pad bonded with a polymeric compound. Two FBG sensors were manufactured using a pure aluminum oxide sprayed coating; this

technique was used for strain gages exposed to temperatures over 1200 ^{o}C and did not exhibit creep or shrinkage as did the polymeric based adhesive. All materials were bonded onto a metal shim substrate, Hastalloy X super-alloy. The packaged FBG sensors with ceramic and fiberglass were spot-welded onto a steel beam and strain and temperature tests were performed. The results indicated that the FBG sensors displayed large residual strains due to the bonding agents and the spot-welding.

A weldable strain and temperature FBG sensor was developed for structural health monitoring of steel bridges in Portugal (Barbosa et al, 2008). The bare FBG sensor was embedded in a capillarity stainless steel tube and bonded with a thermal curing epoxy. The steel tube was laser welded to a 45 x 15 x 0.3 mm stainless steel base which was spot welded to the steel structure. The ingress/egress fibers were protected with a standard 990 μm buffer. To protect the weldable FBG sensor, a protective stainless steel cap was prepared and welded to the structure. The input/output fibers were also protected by a 3-mm PVC tube containing an internal stainless steel coil. The packaged temperature sensor was protected with a steel cap which was spot welded to the structure. Both weldable strain and temperature sensors were laboratory calibrated. The strain sensors proved to be stable and reliable under cyclic loading.

Two packages were developed for strain measurement using bare FBG strain sensors and composite materials (Gangopadhyay et al, 2009). One bare FBG sensor was packaged with a two part epoxy resins mixed in the molar ratio of 4:1 at room temperature. The other sensor was package with glass FRP material. Only the two-resin packaged FBG sensor was subjected to laboratory tests. The packaged sensor was installed on a steel cantilever beam and compared to mechanical strain gages and bare FBG sensors verifying the strain results. A study of the packaging material was conducted to evaluate the characteristics of the epoxy resin sheet. X-ray diffraction profile, thermo gravimetric analysis, differential analysis and scanning electron microscope (SEM) for epoxy polymer resin were performed to confirm the packaging performance. From the experiments, it was recommended to use a thin layer of adhesive, a high modulus coating material and a sufficient embedment length.

6.1.3.4. USE OF STRAIN SENSORS IN WOOD MEMBERS

Electrical resistance strain gages were used in the 1940's by the U. S. Forest Product Laboratory for determination of strains in wood and wood-base materials and for the determination of stress distribution patterns in wood structures. Methods for measuring the elastic properties (Doyle et al,

1946) and the shear moduli in wood (Kuenzi et al, 1942) using these gages have shown to be more accurate than the mechanical strain gages, in which the measurement of the gage lengths induced errors. Radcliffe reported on the use of electric resistance strain gages on wood for the determination of the elastic constants for wood considered as an orthotropic material (Radcliffe, 1955). In this investigation, a method for determining the moduli of rigidity from compression tests at the angle of the grain was introduced. In addition, methods for correcting errors were developed for when more exact values were required.

Later, Youngquist reported on the performance of bonded wire strain gages (Youngquist, 1957). The purpose of that report was to outline the methods used at the Forest Product Laboratory for bonding these gages to wood, to indicate certain limitations on the gage usage, to present some comparative strain data obtained with bonded strain gages and other types of strain gages commonly used with wood, and to report the results of some limited special tests of these strain gages. In addition, a method for mounting bonded wire strain gages and recommended precautions for obtaining reliable data were also presented. These tests confirm the fact that a deviation from straight grain in a wood specimen may significantly affect the measured modulus of elasticity of the piece. Special emphasis on the proper orientation of the gages with respect to the desired elastic property to be measured was recommended to reduce error.

In 1985, glued laminated timber bridges composed of 48-in. stringerless deck panels connected by stiffeners were studied by Iowa State University. An analytical study was conducted to develop the design criteria for the live load distribution, later approved for submission into the AASHTO Bridge Specification (Sanders et al, 1985). However, to understand the behavior of this timber bridge type, a full-scale timber bridge was tested in the laboratory (Funke Jr., 1986). Strain gages were placed on the panels and one of the stiffener beams to measure strains; deflections were also measured at midspan. Several experimental bridge parameters as the elastic properties of the panels and stiffener beams were experimentally determined. In addition, an analytical model was refined to predict the behavior of the bridge components to the experimental behavior. Experimental test results were found to be comparable to the finite element models. However, the load distribution criteria were shown to be conservative.

The long term performance of FPR reinforced glulam girders in a HS-25 highway bridge constructed over the Clallam River, near Sekiu, Washington, was monitored under in-service

conditions (Tingley et al, 1996). General purpose strain gages were internally installed on the wood and on the FRP reinforcement of one internal and two internal girders. These strain gages had 1-in. effective gage lengths with 120 ohm resistance at 75^{o} F and could to operate between -100^{o} F and 350^{o} F. From the study, strain gage data were evaluated using a Fourier analysis. The most relevant recommendation was the addition of control strain gages which are only subjected to thermal changes.

6.2. SMALL SCALE SPECIMEN CONSTRUCTION AND EXPERIMENTAL TESTING PROTOCOLS

This chapter documents the materials utilized and the techniques developed for embedding and attaching Fiber Optic Sensors (FOSs) with structural and non-structural packages to glulam members. Specifically, construction details for the small scale specimens and the test protocols used to evaluate the response of the packages are presented. FBG sensors are free from electromagnetic interference and have no drift commonly found with resistance strain gages. FBG sensors are lightweight with diameters ranging from 145 to 165 μm (manufacture's specifications). In addition, FBG sensors can likely quantify multiple behaviors.

FBG sensors are constructed from bare lengths of fiber optic cable and can be easily damaged during and after installation (Lin et al, 2005). To avoid damage which would render the gages inoperable, techniques for packaging FBG sensors for both structural and non-structural purposes are needed. The FBG structural package conceptually consists of a backing material and the bare FBG strain sensor bonded together. The resulting system could be attached to an exposed wood surface or embedded between the laminates of glulam members to measure the response of the member to external forces. In this work, five new package types were developed and assembled. The fundamental technique consists of the surface preparation of the backing material and the application of a structural adhesive to bond the FBG sensor to the backing material that was developed by the BEC (Doornink, 2006). In addition to the five developed FBG structural packages, one commercially available C-FRP package developed for surface mountable FBG strain sensors was also evaluated. All FBG structural packages were bonded to constructed three-laminate glulam specimens with structural adhesives.

The FBG non-structural package conceptually consists of a backing material and an adhesive/adhesive tape that protects and isolates the FBG sensor from load induced behaviors. The

FBG non-structural package was bonded to an external surface of the wood laminate (in a recess) with the purpose of protecting and isolating the housed FBG sensor.

The experimental testing program consisted of bending tests on fourteen small scale glulam specimens. Each of nine specimens were instrumented with four FBG structural packages, two embedded between the wood laminates and the other two attached to the external flexural surface of the glulam specimens. The remaining five specimens had two FBG sensors that were protected with non-structural packages.

The nine specimens instrumented with structural FBG sensor packages were tested in bending with variable load durations, variable rates of loading, pseudo cyclic loadings and variable temperatures. In most cases, the tests were repeated twice to corroborate the test results. By examining the measurements, the most promising package configurations were selected for further evaluation.

6.2.1. FIBER OPTIC SENSORS

In general, FOSs are materially inert adding extended longevity to data collection system making them an attractive choice for use in structures undergoing degradation. FOSs are electromagnetic/radio frequency (EM/RF) interference free, and have non electrical conductive elements that can be utilized in hazardous environments. The sensors used in this work are able to measure strains ranges of 5000 με through reflected wavelength shifts. The measured responses can travel distances up to 50 miles with minimal signal resolution loss allowing numerous FBG sensors to be connected in series without signal decay.

Commercially available fiber optic strain sensors, used in other research at the Bridge Engineering Center (BEC) at Iowa State University (Doornink, 2006; Wipf et al, 2007), were utilized in this work. Currently, FBG sensors are manufactured with different material packages for a variety of external and internal applications for conventional structural materials, specifically steel and concrete. Both commercially manufactured surface mountable and bare FBG strain sensors (with custom package designs) were selected for this investigation.

The selected commercially available surface mountable FBG strain sensors are written onto a single mode polyimide fiber coated with polyimide coating. This FBG sensor is embedded into a

package that consists of carbon fiber reinforced polymer (C-FRP) material and bonded together with epoxy. The dimensions of the C-FRP package are 8 x 3/4 x 5/128 in. The manufactured surface mountable FBG strain sensors are ready to be attached to structural members (Figure 6.2). Because of the small thickness (5/128 in.), this FBG sensor can be embedded between wood laminates.

The bare FBG strain sensors used in the custom structural sensor packages are written on to a polyamide fiber that has a protective polyimide layer over the grating (Figure 6.3). A disadvantage with bare FBG strain sensors is the fragile nature which is why sensor packaging is required.

In this work, a total of thirty bare FBG sensors protected with custom-made structural packages and six commercially manufactured surface mountable FBG sensors were utilized. All sensors possessed center wavelengths between 1520 and 1570 nm with bandwidths at -3 dB between 0.1 to 0.3 nm. Each sensor was manufactured with two, 3-foot leads and FC/APC (fiber channel/angle polished connectors) connectors on both ends.

The non-structural package sensors consisted of FBGs written on a compatible single mode fiber (SMF28-Compatible) coated with polyimide over the bare fiber (Figure 6.4). Each of these sensors was manufactured with two 3-foot leads and two FC/APC connectors. The FBG wavelengths ranged from 1520 to 1570 nm and were verified for operability before and after packaging.

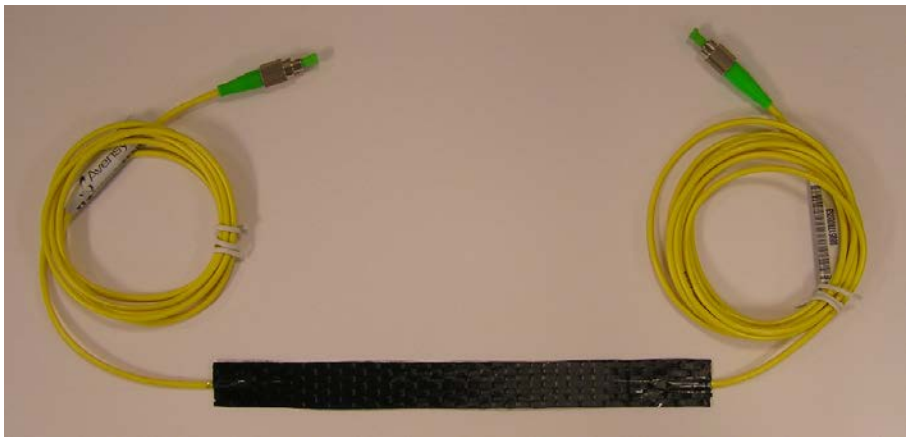

Figure 6.2. Surface Mountable FBG Sensor: Strain Sense ™ – Avensys ™: C-FRP Package and Two Leads with FC/APC Connectors (Doornink, 2006)

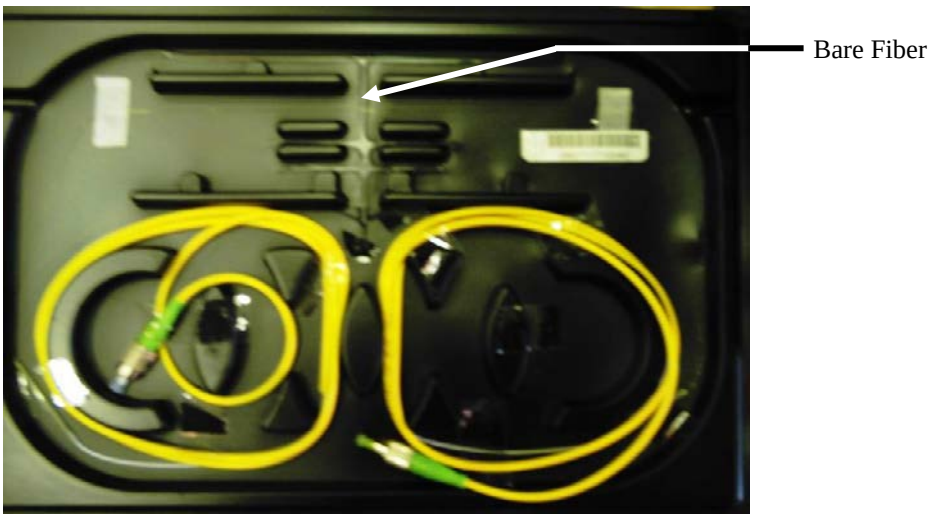

Figure 6.3. Bare FBG sensor: Polyimide Fiber FBG ™ Avensys ™ - Bare Fiber and Two Leads with FC/APC Connectors

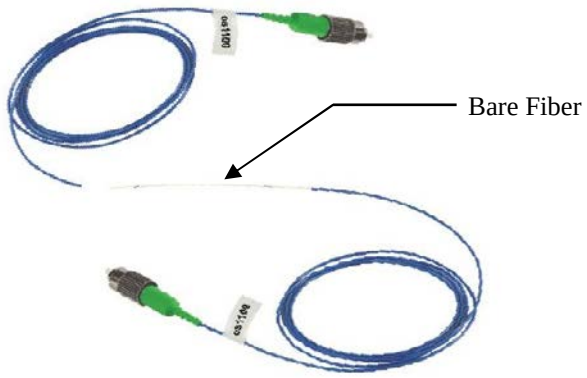

Figure 6.4. Bare FBG Sensors: Os1100 series FBG sensor with polyimide coat – Micron Optics ™: Bare Fiber and Two Leads with FC/APC Connectors

Both bare sensor types can be directly mounted on the structure to be used as conventional strain or temperature sensors. Alternatively, these sensors can be packaged to provide protection during handling, installation and use in diverse structural materials. In this investigation, packages were developed to protect the FBG sensor against potential damage during handling and installation into the specimens.

6.2.2. PACKAGE TYPES

In this section, the configurations of the structural and non-structural packages are presented. In addition to protecting the bare FBG sensors, one group of packages was developed to transmit the

flexural strain in the specimen to the FBG sensor (structural packages), while the other group isolated the FBG sensor from strains (non-structural packages). Five structural packages were designed and constructed using two types of backing materials selected based upon their general material properties. These packages were prepared to be either externally attached or embedded into the small scale glulam specimens. For the non-structural packages, two backing materials were selected based upon their potential for isolating the sensors from structural strains.

6.2.2.1. STRUCTURAL PACKAGE

The configuration of the structural packages must protect the fragile bare FBG strain sensor during handling and installation and while also providing mechanical connectivity between the FBG sensor and the glulam specimen. Initial design of the structural packages was based on a previously mentioned study completed by the BEC. These previously developed structural packages consisted of a bare acrylate coated FBG sensor bonded to a 0.005-in. thick stainless steel shim with a structural adhesive. This 1 5/8 in. long and 5/8 in. wide package, developed and tested by the BEC (Doornink, 2006), was surface welded to steel coupons and tested under static and cyclic tensile loadings. The obtained results confirmed the accuracy of the structural package when compared to electrical resistance (foil) strain gages. In the same study, commercially available surface mountable FBG sensors with C-FRP backing material were also evaluated as an additional reference. Strain results from the tensile tests indicated that the surface mountable FBG sensors were comparable in precision and accuracy to the foil strain sensors.

In this research, the timber materials and packages to be bonded differed in texture, porosity, stiffness and moisture content. The designed FBG structural packages (to be either attached or embedded between the laminates) must be capable of transmitting the flexural strains to the sensors. The selection of the package backing material was based on the preceding work, available materials, and anticipated shear stresses between the member material and the sensor substrate. In addition to the commercially manufactured C-FRP package, four designed structural packages constructed from 0.005 in. thick stainless steel shims were evaluated. A fifth designed package 0.0021-in. diameter aluminum mesh sheet was evaluated. In Table 6.3, the nomenclature assigned to each backing material and the FBG sensor type is presented. In addition, the various geometric configurations and backing materials are shown in Figure 6.5.

Table 6.2. Backing Material for FBG Structural Packages

Designation	Backing Material	Sensor Type
C-FRP	Manufactured Carbon Fiber Reinforced Polymer and epoxy (0.04 in. thick)	Surface Mountable FBG Sensor
RS-SS	Rectangular shape – stainless steel shim (0.005 in. thick)	Bare FBG Sensor
CS-SS	C Shape – stainless steel shim (0.005 in. thick)	Bare FBG Sensor
IS-SS	I Shape – stainless steel shim (0.005 in. thick)	Bare FBG Sensor
72H-SS	72 Holes – stainless steel shim (0.005 in. thick)	Bare FBG Sensor
AM-SS	Aluminum mesh sheet (0.004 in. thick) and stainless steel shim (0.005 in. thick)	Bare FBG Sensor

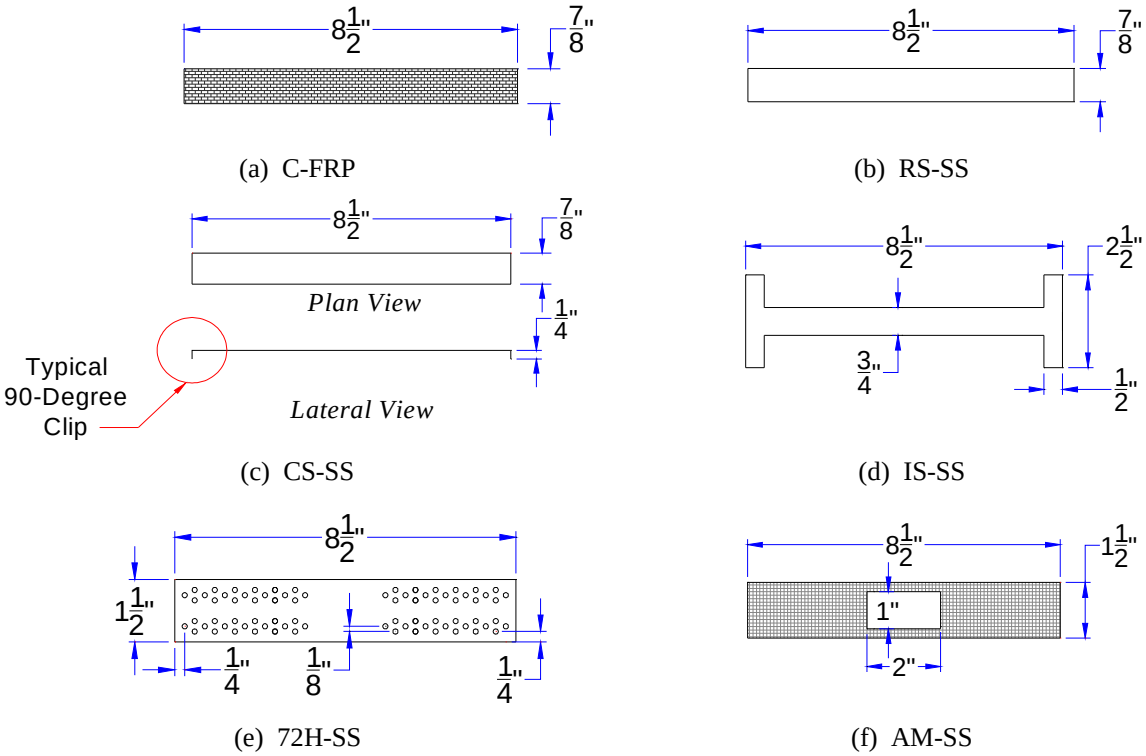

Figure 6.5. Structural Packages: Backing Material Geometry

The geometry and dimensions of the structural packages were developed to resist the shear stresses and to allow for the redistribution of localized strain irregularities between the package and the wood laminates. Specifically, the dimensions were designed to resist at least an average shear stress of 1700 psi.

The RS-SS package backing material was shaped in an 8 1/2 x 7/8 in. rectangle similar to the commercially available C-FRP package. In comparison to the 0.04-in. thickness of the C-FRP

package, the stainless steel shim has an approximately one-two hundredth-inch thickness (0.005 in.). The CS-SS package had the same rectangular shape as the preceding packages but included two 90-degree clips that were intended to mechanically anchor the shim at both ends (C shape, Figure 6.5(c)). This package in addition to being bonded was also anchored by inserting the clips into 1/4-in. deep grooves in the wood laminate. The IS-SS package is another variation of the localized anchorage concept. This package was shaped in the form of an "I" to concentrate the bonding area near the ends.

Another investigated means to improve the interlock between the package and the wood laminates was to introduce holes into the backing material thereby creating shear dowels of adhesive. The 72H-SS package was prepared with 72 evenly distributed 1/8-in.-diameter holes over an area of 8 1/2 x 1 1/2 in. In a similar way, the AM-SS package was developed with two backing materials. The on-center stainless shim provided a smooth bonding area for the bare FBG sensor while the external aluminum mesh increased the mechanical interlock factor by exposing a larger surface area to which to bond.

6.2.2.2. NON-STRUCTURAL PACKAGE

The non-structural packages were developed to isolate the strain response of the member from the FBG sensors. The isolation of these sensors will be important as efforts are put towards the development of decay/deterioration detection sensors.

Three pairs of non-structural packages were constructed using aluminum foil and two others with stainless steel shims as shown in Figure 6.6(a). In all cases, the FBG sensors were not attached to these backing materials. The non-structural packages only served to protect and isolate the sensors in a 1/4-in. deep recess area (Figure 6.6 (b)).

6.2.3. ADHESIVE

The selection of potential adhesives was based on the wood and package substrate properties, fixture time, curing time, viscosity during application, and long term performance. The selected adhesives for structural and non-structural purposes are capable of bonding non-porous to porous materials. For the structural packages, the selected structural adhesives were required to resist at least a minimum shear stress of 1700 psi. For the non-structural packages, adhesives and double coated adhesive tapes were selected for their short fixture time and low viscosity.

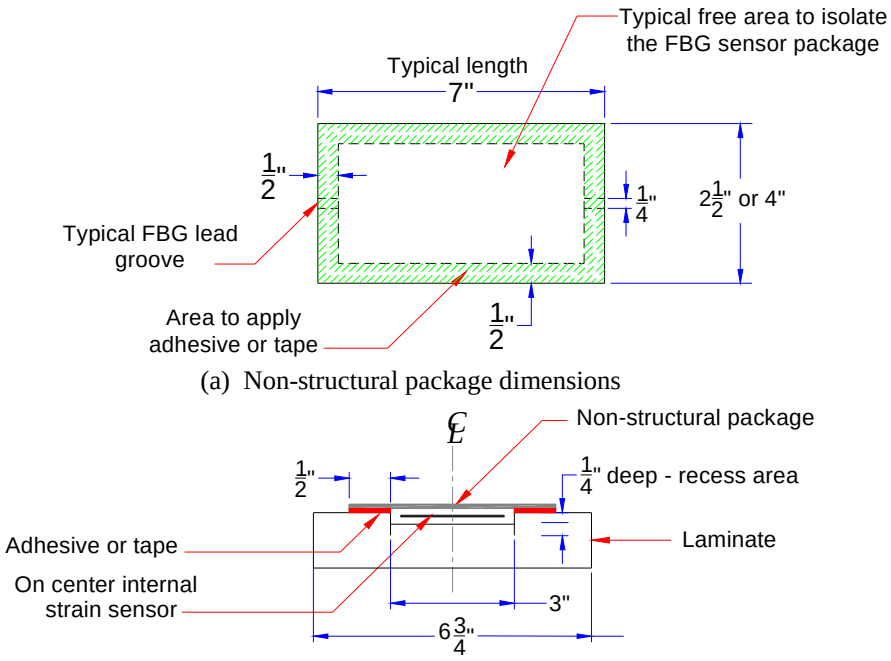

(a) Non-structural package dimensions

(b) Non-structural package location

Figure 6.6. Non-Structural Package: Geometry and Location

6.2.3.1. STRUCTURAL PACKAGE

No records of adhesive used for attaching packaged FBG sensors to timber bridge members were found in any technical literature. The selection of adhesives to bond the structural packages to wood laminates was based on the theoretical stress calculations for a typical 60-foot bridge glulam stringer with an expected moisture content of 16%. For the structural packages, adhesives with shear strength greater than 1700 psi, corresponding to the maximum flexural stress of a HS 20-44 truck at service level, were selected.

Among the various structural adhesive types that include two-part epoxy, one-part polyurethane and one-part cyanoacrylate adhesives, only cyanoacrylate adhesives have been proven to bond various material substrates (e.g., metals, plastics, rubber and wood to each other). Cyanoacrylate adhesives are one-part, rapid set adhesives that are available in a variety of viscosities (ranging from liquids to gels) with operating temperatures between -65^{o}F and 180^{o}F. These adhesive fixture times vary from 15 seconds to 6 minutes. Typically, this adhesive type cures in 24 hours at room temperature conditions. The estimated lap shear tensile strength for cyanoacrylate adhesive is approximately 3000 psi for steel materials (ASTM D1002, 2005).

Based upon published manufacturer's properties, Loctite 454™ Prism ®, 426™ Prism ® and 4212™ Prism ® (here after Loctite 454, Loctite 426 and Loctite 4212 respectively) were selected for evaluation. In Table 6.3, the data provided by the manufacturer are presented (Henkel ®, 2005). In all cases, the adhesives were cured for at least 48 hours. Note that manufacturer recommended cure times are at least 50% less than that used in this work.

Table 6.3. Adhesive for Bonding FBG Structural Packages

Denomination	Color	Gap Fill	Viscosity	Fixture Time	Tensile Shear Strength	Temperature Range
		[in.]	[cP]	[sec]	[psi]	[^{o}F]
454 ™ Prism ®	Clear	0.010	Gel	30	3,200	-65 to 180
426 ™ Prism ®	Black	0.010	Gel	15	3,000	-65 to 210
4212 ™ Prism ®	Black	0.008	11,000	360	3,900	-65 to 250

In addition, the adhesive used to bond the backing material and the bare FBG strain sensor was Loctite 410, a cyanoacrylate adhesive type utilized in a similar application (Doornink et al, 2005). Based upon the data provided by Loctite ™, the Loctite 410 adhesive has a tensile shear strength of 3,200 psi for steel materials, a fixture time of 90 seconds for a gap of 0.008 in. and a temperature operation range from -65^{o} F to 225^{o} F.

6.2.3.2. NON-STRUCTURAL PACKAGE

Two adhesives and two adhesive tapes were for their ability to attaching the non-structural package. The selected adhesives had low viscosities and short fixture times to prevent the adhesives from flowing into the recess area. Adhesive tapes with double coat were selected because of the direct application with a uniform pressure between the material package and the wood laminate.

Loctite 454 ™ Prism ® and 3M Rite-Lok ™ – PR54 ® adhesives were selected for their capability to bond porous and non-porous substrates and for their short fixture time. In addition, 3M Rite-Lok ™ – PR54® with a viscosity of 20,000 cP (centi Poises) (3M™ Technical Sheet, 2009) was evaluated. In Table 6.4, the published material properties of both adhesives are summarized.

Additionally, 3M™ VHB™ – 5915 and 3M™ Double Coated Tape with Adhesive 350 – 9500PC adhesive tapes were evaluated. These tapes provide interior and exterior bonding capabilities thereby replacing liquid adhesives. The 3M™ VHB™ – 5915 tape is a viscoelastic acrylic foam that bonds to both porous and non-porous materials. According to the manufacturer's information, the adhesive

reaches 100% of the bond strength after 72 hours at room temperature (3M™ VHB ™, 2010). The Double Coated with Adhesive 350 – 9500PC structural tape is a thin clear polyester film covered on both sides with a medium-firm acrylic adhesive 350 – 9500PC 3M™. The recommended temperatures for tape application are between 70° F to 100° F. As reported by the manufacturer, both tapes have a static shear strength of approximately 4.4 lbs/in^2 in accordance to Standard Test Methods for Shear Adhesion of Pressure-Sensitive Tapes (ASTM D 3654/D 3654 M-06, 2006).

Table 6.4. Adhesive for Bonding Non-Structural Package

Denomination	Color	Gap Fill	Viscosity	Fixture Time	Tensile Shear Strength	Temperature Range
		[in.]	[cP]	[sec]	[psi]	[°F]
Loctite 454 Prism™	Clear	0.010	Gel	5 – 30	3,200	-65 to 180
3M Rite-Lok™ PR54®	Clear	0.020	20,000	3 – 60	4,600	-65 to 180

6.2.4. INSTALLATION TECHNIQUES FOR PACKAGES

Techniques developed for embedding and attaching packages to timber members are presented in this section. These techniques include preparation of the wood laminates, packaging of the FBG strain sensors and the application of the adhesives.

6.2.4.1. STRUCTURAL PACKAGE

Prior to assembling the small scale glulam specimens, the internal laminates were instrumented with FBG structural packages. After assembling the specimens, both exterior flexural surfaces were then instrumented with FBG sensor. In Figure 6.7, the layout of the four FBG sensor package locations in a typical specimen is presented. In each specimen, two types of structural packages were utilized.

6.2.4.1.1. **Embedding Technique**

In each specimen, two internal laminate surfaces were instrumented with FBG structural packages using the technique described below. This technique consisted of laminate preparation, backing material preparation and sensor package installation.

6.2.4.1.1.1. Internal Laminate Preparation

Douglas-Fir wood laminates were utilized in the construction of the small scale glulam specimens. The 27 individual wood laminates were surfaced by the manufacturer to a nominal cross

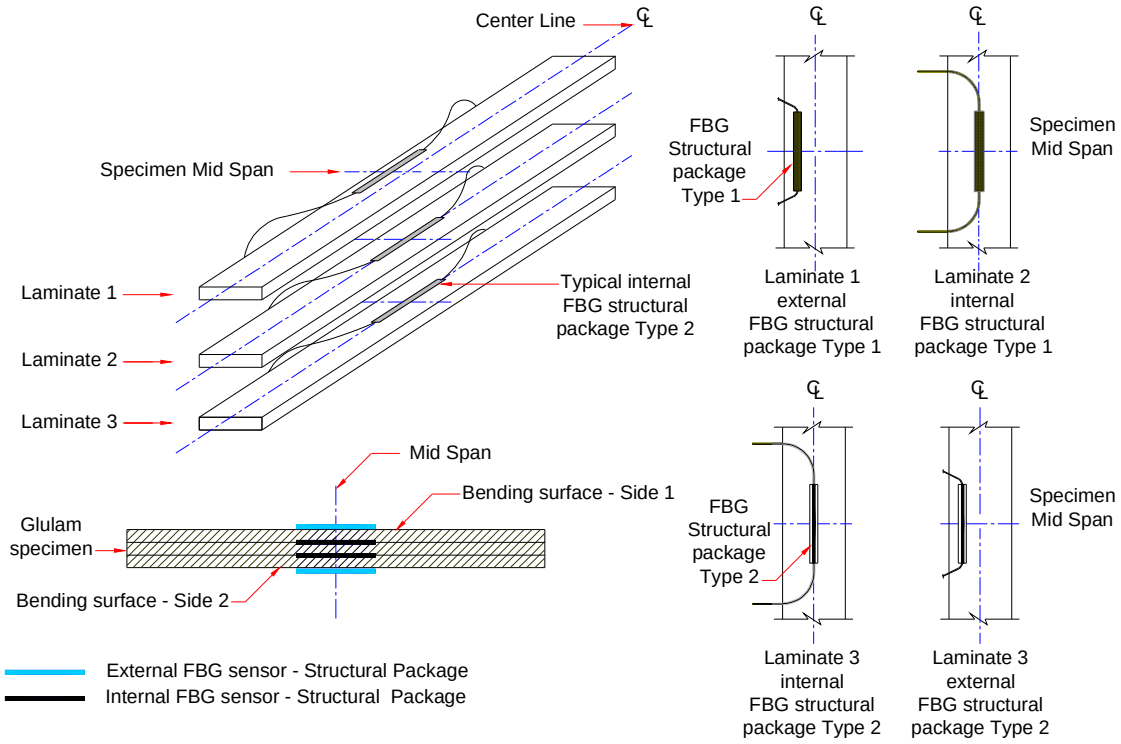

Figure 6.7. Structural Package: External and Internal FBG Sensor Location

section of 6 3/4-in. x 1 3/8-in. and a total length of 44 in. These laminates were grouped into nine specimens according to their general dimensions and absence of knots in the anticipated sensor package area at mid span. Each of the eighteen interior laminate surfaces was prepared to receive one FBG structural package.

The preparation of the internal laminates consisted of the routing of the recess areas to house either the FBG sensor package and/or the leads. Prior to routing, the position of the package backing material and leads were traced on the selected internal laminate face. Using a router and different straight router bits, a recess area was cut in the wood laminate following the patterns shown in Figure 6.8.

For the stainless steel shim backing materials, no recess area was required because of the minimal thickness (0.005 in.); only the leads were housed in a 1/8-in.-deep curved groove. In the C shape stainless shim (CS-SS) backing material, two additional straight cuts 1/4 in. deep and 7/8 in. long located 8 1/2 in. apart were formed to house the 90-degree clips (see Figure 6.8 (a)). In three of the

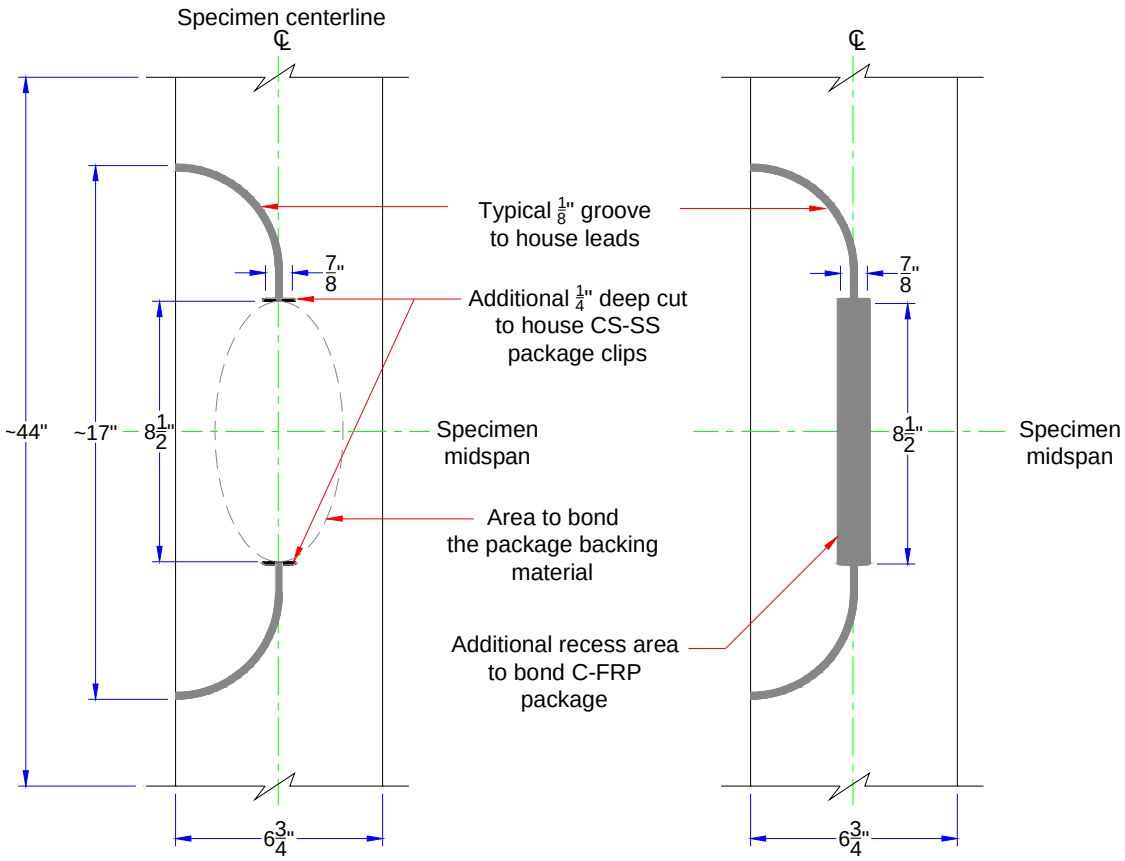

(a) Recessed area for structural package with bare FBG sensor

(b) Recessed area for surface mounted FBG sensor package

Figure 6.8. Structural Package: Internal Laminate Preparation

wood laminates, an additional recess area of 8 1/2 x 7/8 in. and approximately 0.03-in. deep was cut to receive the C-FRP surface mountable FBG sensor package (see Figure 6.8 (b)).

6.2.4.1.1.2. Backing Material Preparation

Five backing material designs (Section 6.2.2.1), were fabricated to the previously discussed pattern and dimensions (see Figure 6.5). The CS-SS packages were mechanically bent to obtain the 1/4-in.-long 90-degree clips and the 72H-SS packages were drilled with a 1/8-in. diameter bit to create the indicated holes pattern. All backing material substrates were cleaned with an antistatic wipe wetted with 99.9% alcohol to remove contaminants. Backing materials were installed to provide a consistent mounting surface for the bare FBG strain sensors.

6.2.4.1.1.3. Embedded FBG Structural Package Installation

The procedure for bonding the FBG structural packages basically consisted of the installation of

the backing materials and bare FBG strain sensors. The scheme of the embedding technique is presented in Figure 6.9 and the procedure is described as follows:

- After routing grooves for the leads and prior to sensor installation, the wood laminates were cleaned with a brush to eliminate wood debris (Figure 6.9 (a)).
- The backing material was bonded with the adhesive to the wood substrate (Figure 6.9 (b)). The adhesive was uniformly spread over the clean wood substrate with a putty knife at the outlined sensor location. Immediately after, the selected backing material was placed on the adhesive and bonded to the wood by applying uniform pressure by hand for the recommended fixture time. For the AM-SS backing materials, the stainless steel shim was bonded to aluminum mesh right after the completed the fixture time. After initial set (less than a minute), the packages were undisturbed for approximately 48 hours to ensure full adhesive curing.
- After curing, preparations were undertaken to mount the bare FBG sensor to the installed backing materials. Three layers of tape were bonded to the backing strip to make a straight narrow groove. The tape layers were located on top of the shim at both sides of the center line to form a "reservoir" for the adhesive and to create a 1/4-in. wide uniform layer (Figure 6.9 (c)).
- A 320-grade sand paper was used to further smooth the exposed area of the stainless steel shim (Figure 6.9 (d)). The purpose was to provide a consistent surface that was a slightly roughened to facilitate proper adhesion.
- The adhesive for the bare FBG sensor was poured into the groove formed by the tape layers (Figure 6.9 (e)).
- Immediately, the bare FBG sensor was lightly wiped with an antistatic wipe wetted with 99.9% grade alcohol to clean the surface (Figure 6.9 (f)).
- By manually gripping the fiber leads at both ends, the FBG sensor was fully submerged into the adhesive groove (Figure 6.9 (g)); the bare FBG sensor was aligned over the center line of the laminate and held in place for at least one minute during initial set of adhesive.
- To ensure the FBG remained in the desired location, both fiber ends were taped into place until completing the full curing time.
- After the allotted curing time, the three tape layers were carefully removed.
- The bare fiber optic strand and/or leads were directly inserted in the corresponding curved recess area (Figure 6.9 (h)).

This procedure was performed to embed fifteen FBG structural packages. In the CS-SS packages, additional adhesive was applied over the 90-degre clips and into the 1/4-in. deep recess

area. In all cases, an additional load of 2 lbs was placed on top of the bonded backing material maintain a uniform pressure during the curing time. After completing the sensor installation, measurements were taken to ensure that the FBG sensors were operative.

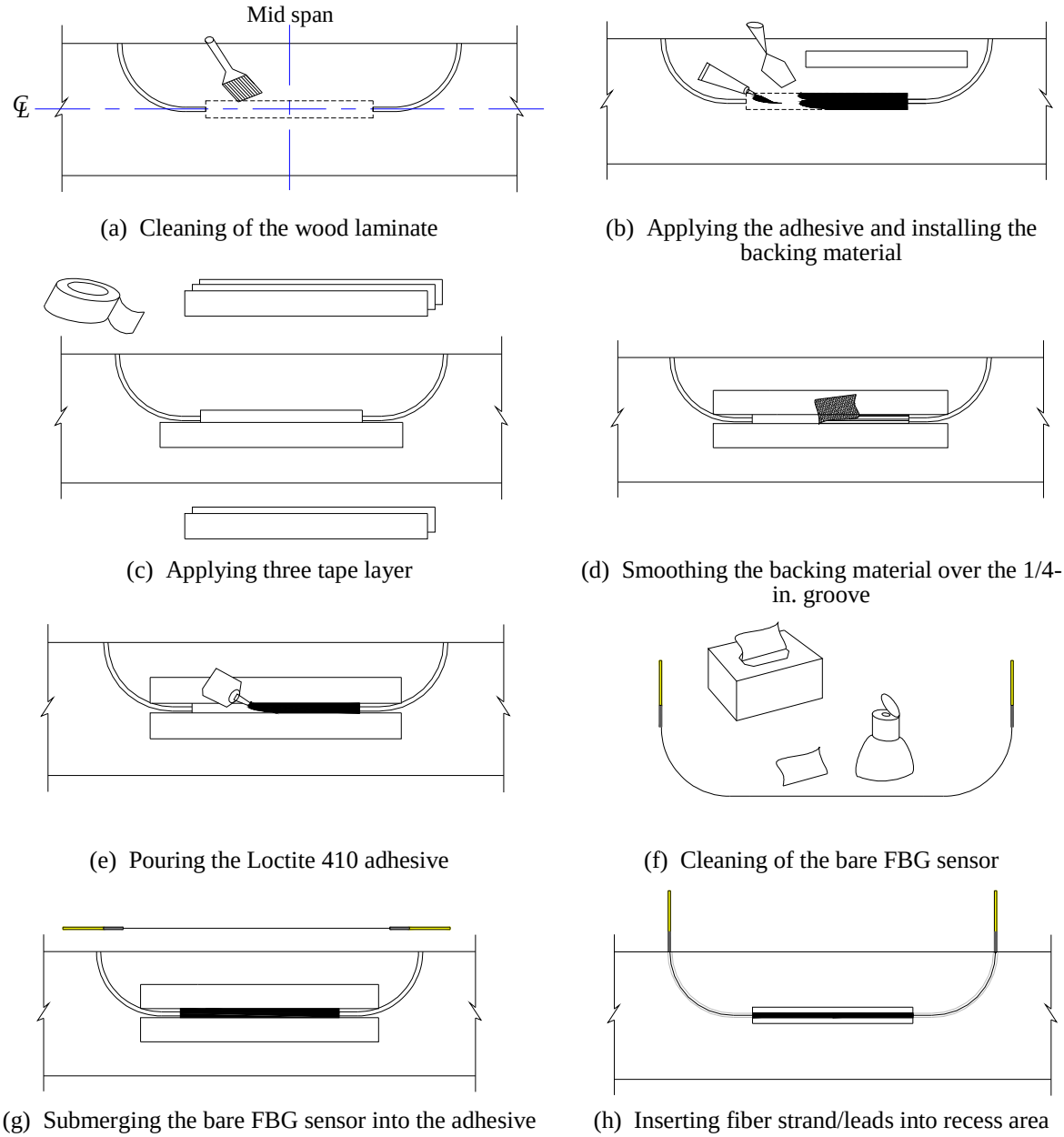

(a) Cleaning of the wood laminate

(b) Applying the adhesive and installing the backing material

(c) Applying three tape layer

(d) Smoothing the backing material over the 1/4-in. groove

(e) Pouring the Loctite 410 adhesive

(f) Cleaning of the bare FBG sensor

(g) Submerging the bare FBG sensor into the adhesive

(h) Inserting fiber strand/leads into recess area

Figure 6.9. Structural Package: Embedding Technique of the Bare FBG Sensor with Structural Package

In the case of the commercially available surface mounted C-FRP package, the installation comprised of:

- Cleaning of the wood laminate recess area with a brush to eliminate debris (similar to Figure 6.9 (a)).
- Applying the adhesive over the package recess area (see Figure 6.10 (a)).
- Cleaning the C-FRP package with an antistatic wipe wetted with 99% grade alcohol, similar to the procedure described in Figure 6.9 (f).
- Bonding the C-FRP FBG sensor package and insertion of the leads in the recess areas once (Figure 6.10 (b)).

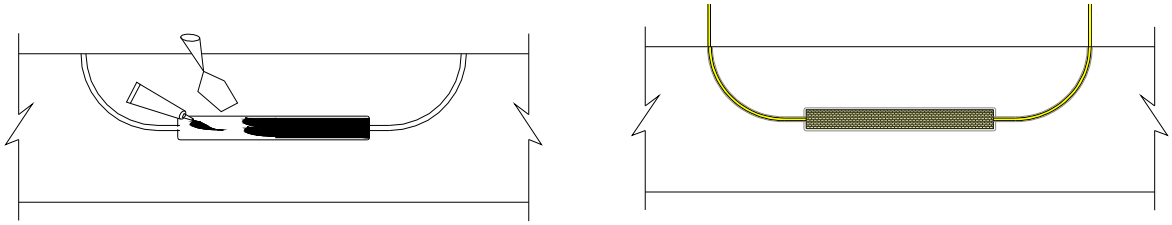

(a) Adhesive application

(b) Bonding the structural package and inserting the leads into the recess area

Figure 6.10. Structural Package: Embedding Technique of the Manufactured C-FRP Structural Package

An additional weight of 2 lbs was placed on top of the bonded C-FRP package to apply a uniform pressure throughout the curing process. This internal FBG structural package installation was less complex than the previously described custom packages since the manufactured FBG sensor included the backing material (C-FRP).

To illustrate the attachment process, the installation of the RS-SS package is presented in Figure 6.11 (a). As shown, the wood laminate has two grooves free from debris to house the FBG leads and one of the three layers of tape to form the 1/4-in. groove to host the bare FBG strain sensor in place. In Figure 6.11 (b), the CS-SS Loctite 426 package is fully installed and ready to be assembled to the glulam specimen.

The eighteen internal FBG structural packages were installed using combinations of the five developed package backing materials, bare FBG strain sensors and one commercially manufactured surface mountable FBG strain sensor with C-FRP package; all sensors were attached by applying either Loctite 454, 426 or 4212 adhesives. Eighteen internal laminates were instrumented using the embedding technique. The structural packages and the respective adhesive are summarized in Table 6.5.

(a) Bonded backing material and tape to host the FBG sensor

(b) Installed internal CS-SS Loctite 426 package

Figure 6.11. Structural Package: Laboratory Installation of the FBG Structural Package

Table 6.5. Type of Internal FBG Structural Packages

Specimen	Adhesive	Backing Material	Internal Side 1	Internal Side 2
1	Loctite 454 ™ Prism ®	C-FPR and RS-SS	C-FRP Loctite 454	RS-SS Loctite 454
2		CS-SS and IS-SS	IS-SS Loctite 454	IS-SS Loctite 454
3		72H-SS and AM-SS	72H-SS Loctite 454	AM-SS Loctite 454
4	Loctite 426 ™ Prism ®	C-FPR and RS-SS	C-FRP Loctite 426	RS-SS Loctite 426
5		CS-SS and IS-SS	CS-SS Loctite 426	IS-SS Loctite 426
6		72H-SS and AM-SS	72H-SS Loctite 426	AM-SS Loctite 426
7	Loctite 4212 ™ Prism ®	CFPR and RS-SS	C-FRP Loctite 4212	RS-SS Loctite 426
8		CS-SS and IS-SS	CS-SS Loctite 4212	IS-SS Loctite 4212
9		72H-SS and AM-SS	72H-SS Loctite 4212	AM-SS Loctite 4212

6.2.4.1.2. **Attaching Technique**

After assembling the nine small scale glulam specimens, FBG structural packages were attached to the external surfaces. The laminate preparation consisted of cleaning the external surface of the specimen and outlining the package backing material position. At mid span, the backing material was placed at 1 1/2 in. offset measured from the package center to the laminate edge, as shown in Figure 6.12. For the IS-SS packages, the distance was 1 3/4 in. to accommodate the wide I Shape ends. The external FBG sensor packages were attached with a technique that utilized the same material

preparation and installation methodology as the embedded FBG sensor packages. The attaching technique consisted of:

- Outlining the backing material location.
- Cleaning the exterior wood surface prior to sensor installation with a brush.
- Bonding the package backing material to the wood substrates and curing for approximately 48 hours.
- Bonding two lines of three tape layers separated by 1/4 in. to form a straight narrow groove.
- Surface preparation of the backing material with a 320-grade sand paper and cleaning with a brush.
- Pouring the Loctite 410 adhesive into the 1/4-in. groove (see Figure 6.12).
- Cleaning the bare FBG sensor with an antistatic wipe wetted with 99.9% grade alcohol.
- Submerging the bare FBG sensor into the bottom of the adhesive groove resting on the shim over the center line of the laminate.
- Straightening and immobilizing of the FBG sensor with tape at both ends.
- After curing for approximately 48 hours, removing the three tape layers with caution.

All external FBG structural packages were installed off center of the laminate, while alternative strain sensors, foil strain gages and strain transducers, were positioned on center (see Figure 6.13). According to the ASTM 198-05a provisions (ASTM 198-05a, 2005), proven sensors are to be placed on center to investigate the mechanical properties of the glulam members.

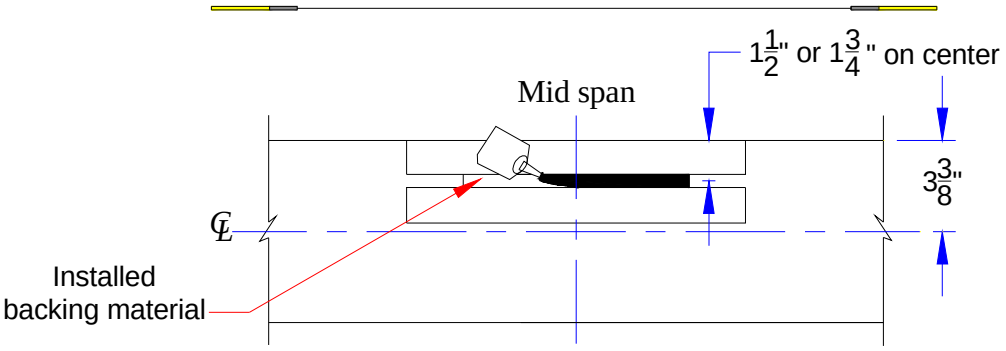

Figure 6.12. Structural Package: Attaching Technique – Package Backing Material, Immobilizing Tape and Adhesive application

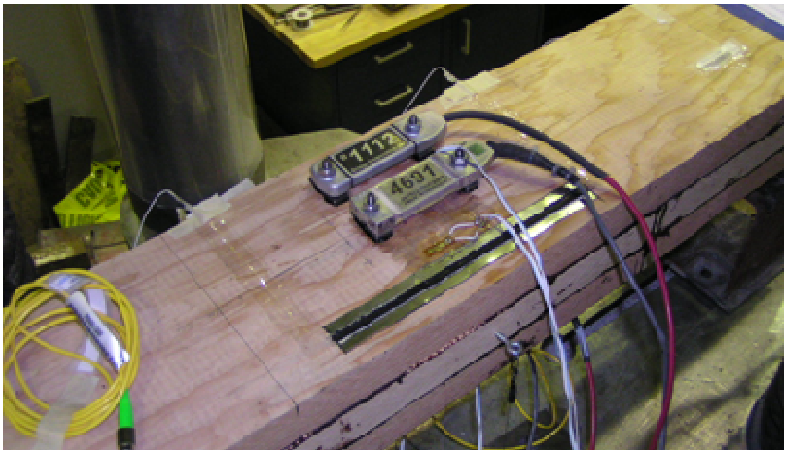

Figure 6.13. Installed External FBG Sensor with Structural Package (CS-SS Loctite 454), Foil Strain Gages and Strain Transducers

6.2.4.1. NON-STRUCTURAL PACKAGE

Two non-structural packages were installed in the internal laminates of five small scale specimens to isolate the FBG sensors from strain effects and protect them from damage during handling and assemblage of the specimens (see Figure 6.14).

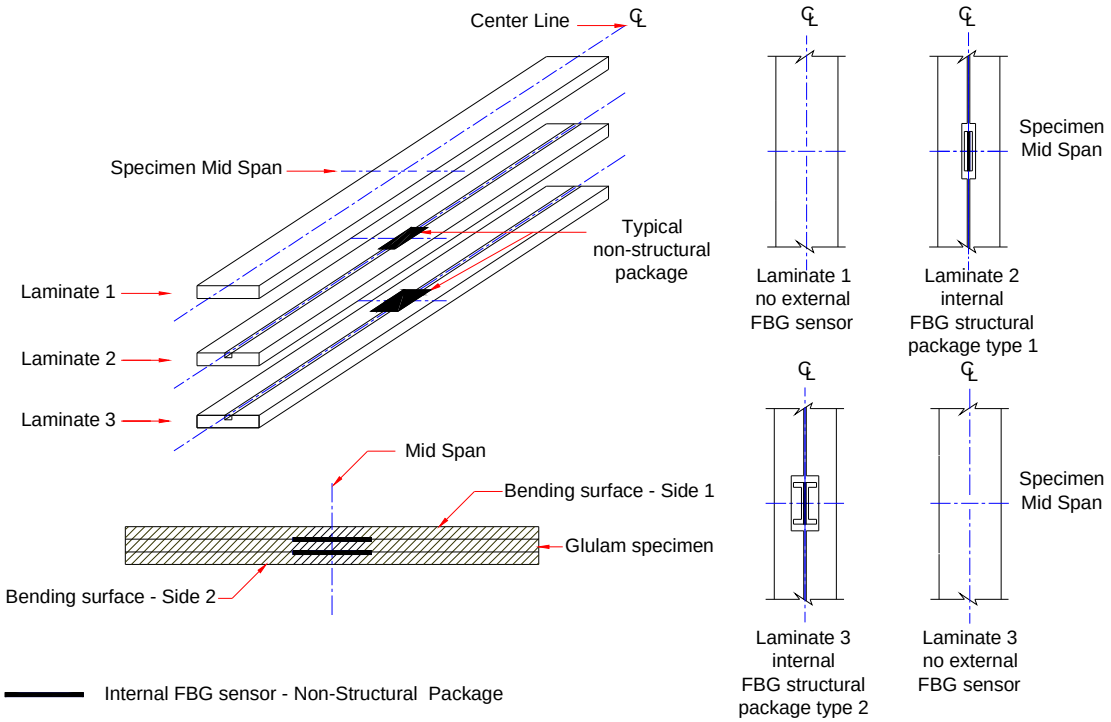

Figure 6.14. Non-Structural Package: Internal FBG sensors and Package Location

6.2.4.1.1. **Embedding Technique**

The embedding technique of the non-structural packages consisted of the laminate preparation, backing material preparation and installation of the non-structural package.

6.2.4.1.1.1. Internal Laminate Preparation

Fifteen individual Douglas-Fir laminates were selected to assemble five small scale specimens with nominal dimensions of 6 3/4 x 4 1/8 x 44 in. The location of the non-structural package and the FBG sensor leads were outlined on the internal laminate as shown in Figure 6.15. A recess area was routed in the surface of Laminates 2 and 3 with a constant depth of 1/4 in. to house FBG sensors. In Laminate 2, the recess area at mid span was 6 x 1 1/2 in., while in Laminate 3 the recess area was 6 x 3 in. Additionally, both laminates were routed to form a groove with a 1/4 x 1/4 in. shape along the longitudinal direction of the laminate to house the FBG leads. In all cases, the recess areas were at least 1/2 in. wider and 1 1/2 in. longer than the corresponding FBG structural package dimensions with the purpose of isolating the FBG sensor and adjacent leads from the adhesive.

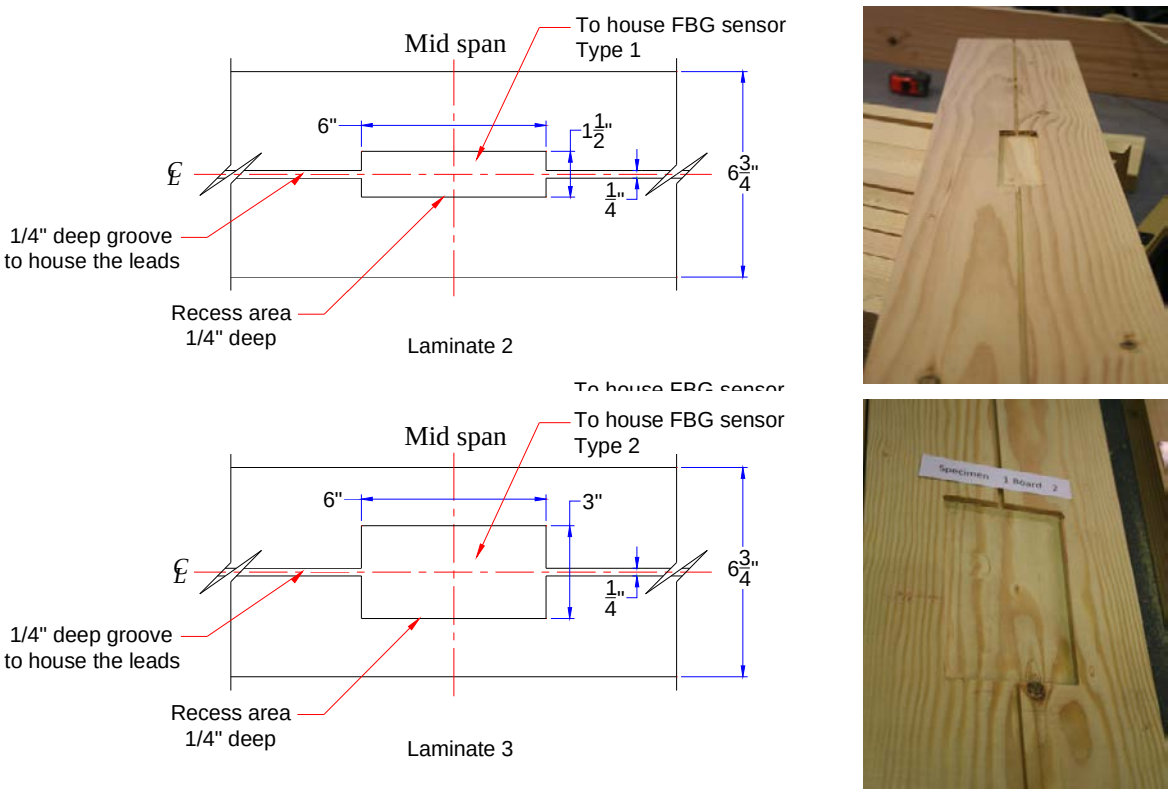

Figure 6.15. Non-Structural Package: Location and Dimensions of the Recess Area to House the FBG Sensors

6.2.4.1.1.1. Backing Material Preparation

Pairs of package backing materials shown in Section 6.2.2.2 were manually cut (see Figure 6.6). Three pairs were prepared from aluminum foil and two others from stainless steel shim material. Both the stainless steel shim and the aluminum foil were sanded and cleaned with an antistatic wipe wetted with 99% alcohol.

6.2.4.1.1.2. Embedded Non-Structural Package Installation

Prior to installing the non-structural packages, ten FBG strain sensors were protected with two types of structural packages (Figure 6.5 (c) and (d)). These packages were constructed using part of technique developed in Section 0 that comprised of the backing material preparation and the bonding of the FBG sensor. CS-SS and IS-SS package backing materials were prepared with a total length of 4 1/2 in. (see Figure 6.16). The resulting FBG structural packages were not bonded to the wood members.

The non-structural package installation was performed as follows:

- The specimen laminates were brushed to eliminate any wood debris.
- The FBG sensor for non-structural purpose was placed over the recessed area on center with a 1/2 in. gap (Figure 6.16). The 1/2-in. long leads nearby the FBG sensor package were set loose into the recess area to avoid any contact with the non-structural adhesive that could cause axial strains due to bending. The other portion of the leads were inserted into the 1/4 in. groove and protected from external damage with a commercially available silicone. Wavelength readings were taken to verify that the FBG sensors were operative.

(a) Laminate 2: CS-SS structural package with cotton fiber

(b) Laminate 3: IS-SS structural package with cotton fabric

Figure 6.16. Non-structural package: Installation of the packages FBG sensors

- The selected adhesive or adhesive tape was applied outside the recessed area over a width of 1/2 in. After placing the package, a uniform hand pressure was applied during the recommended fixture time for the adhesive. For the adhesive tape, a 1-pound roller was utilized to add an approximate 15 psi pressure on the package. In Figure 6.17 and Figure 6.18, the application of the adhesive and adhesive tape as well as the installed non-structural packages are shown.

All non-structural packages were cured for approximately 72 hours before assembling the wood laminates. In Table 6.6, the non-structural package materials per specimen are indicated.

(a) Adhesive application (b) Steel shim bonded with adhesive

Figure 6.17. Non structural package: Adhesive Application and Package Backing Material Installation

(a) Tape application (b) Aluminum foil package bonded with tape

Figure 6.18. Non Structural Package: Adhesive Tape Application and Package Backing Material Installation

Table 6.6. Type of Non-Structural Package per Specimen

Specimen	Backing material	Adhesive/Adhesive Tape
NS1	Aluminum foil	3M VHB Tape
NS2	Stainless Steel shim	Rite-Lok 3M Eng. Instant Adhesive
NS3	Aluminum foil	Loctite 454 Prism™
NS4	Stainless Steel shim	3M VHB Tape
NS5	Aluminum foil	3M Double coated tape with Adhesive 350 – 9500PC

6.2.5. ASSEMBLY OF THE SMALL SCALE GLULAM SPECIMENS

After the internal laminate instrumentation, the small scale glulam specimens were assembled in the laboratory. The following is the description of the assembly of specimens.

6.2.5.1. SPECIMENS WITH STRUCTURAL PACKAGES

The individual laminates were bonded together with Cascophen LT-5210, a conventional phenol-resorcinol resin for timber laminating mixed with the Cascoset FM-6210 hardener (Hexion, 2010). The hardener was dissolved in water in a weight proportion of 2 to 1, and the resulting mix was proportioned to the resin in a weight ratio of 1 to 2.2 and mixed until a uniform mixture was obtained. The adhesive was immediately applied over the wood laminate substrate with a paintbrush and the instrumented laminate was then placed on top (see Figure 6.19). This process was repeated to complete three laminates per specimen. The assembly of the specimens was conducted in two groups; the first group comprised of Specimens 1 through 6 and the second group included Specimens 7 through 9.

Figure 6.19. Assembly of the Glulam Specimens: Adhesive Application to Wood Laminates

According to the manufacturer's specifications, a pressure of 100 psi between laminates must be sustained for at least 24 hours with a constant room temperature of 70^{o}F. This clamping pressure was attained by using a steel frame consisting of two 1 7/8-in. diameter 150-ksi bars and a steel girder, and two hydraulic jacks (see Figure 6.20 (a)). The recently bonded specimens were placed under the steel frame, covered with 1-in. thick plate for improving the load distribution and clamped with a total load of 30 kips (Figure 6.20 (b)).

(a) Steel frame with hydraulic jacks

(b) Pressing of the glued laminates

Figure 6.20. Assembly of the Glulam Specimens: Laboratory Equipment

FBG sensor measurements were taken during the curing process and after the assembly of the specimens. In the first group, Specimens 1 through 6 had operative FBG sensors throughout the curing process. Of the two connectors, wavelength readings were detected by at least one connector. After releasing the load, additional readings were taken; with the results indicating that Specimen 2 lost one embedded FBG sensor constructed with IS-SS package and bonded with Loctite 454 adhesive. Although the leads were attached to the sensor, internal damage may have occurred to the bare fiber optic strands. After assembling the second group, Specimens 7 through 9, one internal FBG strain sensor with C-FRP package, located at Specimen 7, was operative. A visual inspection of the specimens showed that the fiber leads were apparently intact and internal damage in the bare fiber optic strand may have occurred. After assembling the glulam specimens, twelve of the original eighteen embedded FBG strain sensors were operative.

6.2.5.2. SPECIMENS WITH NON-STRUCTURAL PACKAGES

After curing the non-structural packages installations, the laminates were grouped to form Specimens 1 through 5. The laminates were bonded with the established wet-adhesive, Cascophen LT-5210 mixed with the Cascoset FM-6210 hardener, applying the same procedure as described in the previous Section 6.2.5.1 (Hexion, 2010). Wooden dowels were inserted into the predrilled holes to align the laminates (see Figure 6.21). The relative humidity and temperature in the laboratory were approximately 50% and 71^{o} F, respectively.

Figure 6.21. Assembly of the Glulam Specimens with Non-Structural Packages: Insertion of the Wooden Dowels

Prior to the bonding of the laminates, one steel frame for applying the clamping force was constructed in the laboratory with the same characteristics described in the preceding section. After placing the specimens under the steel frame covered with a 1-in. thick plate, a total load of 30 kips was applied to generate a constant pressure of approximately 100 psi over an area of 6 3/4 x 44 in. The glulam specimens were cured for 48 hours. The FBG wavelength readings taken during and after assembling the small scale glulam specimens indicated that all sensors were operative.

6.2.6. SMALL SCALE SPECIMENS: MECHANICAL PROPERTIES

Prior to testing, the mechanical properties of the small scale glulam specimens were assessed by visually grading the laminates utilizing known standards (AITC 117, 2004) and utilizing the specifications (AASHTO, 2006). With the estimated mechanical properties, the response of the specimens to applied load was estimated. All specimens were assembled utilizing softwood Douglas Fir laminates.

6.2.6.1. STRUCTURAL PACKAGES

Before assembling the nine fabricated small-scale glulam beam specimens instrumented with structural FBG sensor package, each laminate was visually graded according to the provisions established in the Annex C of the Standard Specifications for Structural Glued Laminated Timber of Softwood Species (AITC 117, 2004). As stipulated in the Annex C, graded Douglas Fir laminates ranged from L1 to L3. With these references, the bending design values for structural glued

laminates contained in Tables 1 and 2 of Chapter 8 of the AASHTO specifications (AASHTO 2006) were selected. Upper and lower moduli of elasticity (MOEs) for flexure of 2000 and 1500 ksi respectively were selected. These flexural MOEs corresponded to the grading limits of L1 and L3.

With a total load of 2500 lbs applied in the elastic range of the specimens, the theoretical strains and deflections were calculated based upon common mechanics of materials equations for the third-point loading that would be performed. The external flexural strain values were expected to range from +/-522 με to +/-392 με, for moduli of elasticity of 1500 ksi and 2000 ksi, respectively. For the internal laminates, the estimated flexural strains ranged from +/-174 με to +/-130 με. Theoretical displacements at mid span were estimated to be between 0.035 in. and 0.026 in., respectively.

6.2.6.2. NON-STRUCTURAL PACKAGES

Similarly to the previous section, theoretical strains were estimated based on the assumed material properties, established in the preceding section, and the reduced cross section of the specimens with non-structural packages. With two recess areas of 1 1/2 in. x 1/4 in. and 3 in. x 1/4 in. at mid span, the cross section decreased from 27.8 in^2 to 26.7 in^2. The moment of inertia decreased to 38.9 in^4, 98% of the gross section (39.5 in^4). The theoretical external flexural strains were estimated to be between +/-530 με and +/-398 με, for moduli of elasticity of 1500 ksi and 2000 ksi, respectively. For the internal laminates, the calculated theoretical flexural strains were +/-177 με and +/-133 με, respectively. These theoretical strains were compared to the attached strain transducers and internal FBG sensors to assess the effectiveness of the non-structural packages.

6.2.7. STATUS OF SPECIMENS

For the nine specimens with structural FBG sensor packages, twelve internal FBG sensors were functioning after assembling the specimens. All external FBG sensors were operative after installation; however, two external FBG sensors were damaged when readying the specimens for testing. The status of each FBG sensor per specimen before starting the testing program is summarized in Table 6.7.

In addition, the moisture content of the specimens was obtained using a two-prong resistance type moisture meter. The moisture content measurements were taken on both sides (i.e., side 1 and side 2) at three locations on each side (i.e., 1 ft from both ends and at mid span) and ranged from 7% to 10%.

These values are lower than would normally be found in field bridge applications (e.g., 16% in bridge superstructures).

Table 6.7. FBG Structural Packages – Status of the FBG Sensors

Specimen	Adhesive	External Side 1		Internal Side 1		Internal Side 2		External Side 2	
		Package	Status	Package	Status	Package	Status	Package	Status
1	Loctite 454	CFPR	O	CFPR	O	RS-SS	O	RS-SS	O
2		CS-SS	O	CS-SS	O	IS-SS	X	IS-SS	O
3		72H-SS	O	72H-SS	O	AM-SS	O	AM-SS	X
4	Loctite 426	CFPR	O	CFPR	O	RS-SS	O	RS-SS	O
5		CS-SS	O	CS-SS	O	IS-SS	O	IS-SS	O
6		72H-SS	O	72H-SS	O	AM-SS	O	AM-SS	X
7	Loctite 4212	CFPR	O	CFPR	O	RS-SS	X	RS-SS	O
8		CS-SS	O	CS-SS	X	IS-SS	X	IS-SS	O
9		72H-SS	O	72H-SS	X	AM-SS	X	AM-SS	O

Note.- "O" denotes that the FBG sensor is operative
"X" denotes that the FBG sensor is inoperative.

After the assembling of the five specimens with FBG non-structural packages, all ten FBG sensors were operative. The moisture content ranged from 10% to 11%.

6.2.8. TESTING PROGRAM

The following is a description of the testing program followed to evaluate the techniques for embedding and attaching FBG sensors. All specimens were tested in bending by third-point loading.

The specimens with FBG structural packages were tested under variable time of loading, loading rate and temperature conditions. The assessment of the different adhesive/package combinations was completed by analyzing the strain response with respect to time, and with respect to each other. The specimens were tested with the purpose of evaluating:

- The strain response during loading and unloading as compared to the estimated theoretical strain values.
- The strain response by comparing the obtained FBG strain data to electrical resistance strain gages (foil strain sensors) and BDI strain transducers (strain transducers).
- FBG strain data when subject to a sustained load at laboratory temperature conditions.
- The behavior of the FBG packages and adhesives under "fast" loads, followed by a sustained load under laboratory temperature conditions.
- Mechanical energy dissipation in the FBG packages through cyclic loading at laboratory temperature conditions.

- FBG package response at elevated temperatures when subjected to a sustained load.
- FBG package response at suppressed temperatures when subjected to a sustained load.

The five specimens with non-structural packages were, again, tested under three-point bending with the purpose of investigating the efficiency of the developed techniques for packages to isolate the sensors from mechanical strains.

6.2.8.1. TEST SETUP

Loading of the small scale glulam specimens was by third-point loading thereby creating a region with uniform bending moment and zero shear. As shown in Figure 6.22, two steel beams were placed 36 in. apart from center to center establishing the support conditions. The two roller supports were constructed with 2-in. diameter bars and 1/4-in. thick plates; another 1/4-in. thick plate was placed diametrically opposite to only allow rotation. The two pin supports were constructed by placing a free 2-in. diameter bar between two 1/4-in. thick plates allowing for both horizontal displacement and rotation. The glulam specimen was placed over one set of pin and roller supports with an effective span length of 36 in. The second set of supports was placed on the top surface of the specimen collocated 12 in. apart, coinciding with the mid span. To equally distribute the load from the universal testing machine head, a 1-in. thick steel plate was symmetrically placed on top the upper pin and roller assembly.

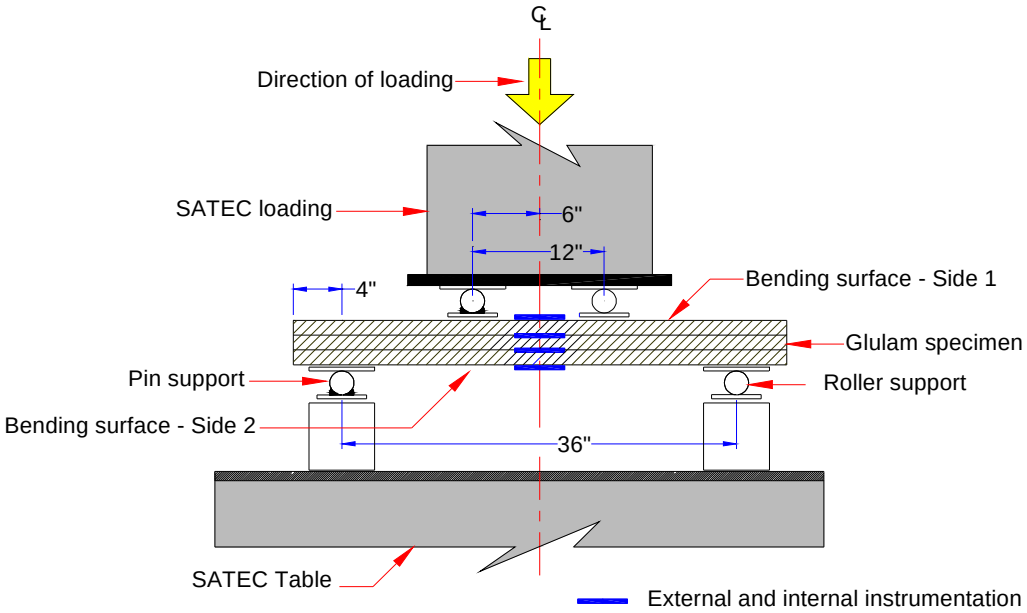

Figure 6.22. Typical Bending Test Configuration

6.2.8.1. STRUCTURAL PACKAGE TESTING PROGRAM

This section describes the test protocols followed to evaluate the structural performance of the FBG structural packages. In general the test protocols were adapted from the ASTM 198 05a standards (ASTM 198-05a, 2005).

6.2.8.1.1. **Sensors and Testing Equipment**

For the small scale specimens, additional sensors were installed to provide sensor performance verification data. The additional sensors consisted of BDI strain transducers (strain transducers), electrical resistance strain gages (foil strain sensors) and direct current displacement transducers (DCDTs).

BDI (Bridge Diagnostic, Inc.) strain transducers (hereafter strain transducers) are a full-wheatstone bridge sensors consisting of four active 350 Ohm foil gages, with 4-wire hookups that can be interfaced with standard data acquisition systems. The strain transducers have been used on steel, concrete and timber bridges with proven success in short term monitoring tests. These strains transducers have an effective gage length of 3 in. and recordable strain levels over 1000 $\mu\varepsilon$. These sensors were bonded to the wood surface using Loctite 410 ^{TM}-Prism ® and Loctite-7452 accelerator based upon previous experience with these sensors.

Electrical resistance strain gages (hereafter foil strain gages) have been utilized in the evaluation of the material properties of wood laminates and composite wood laminates with proven success (Sliker, 1972; Piao et al, 2004). With this background, general purpose foil strain gages with a gage length of 0.39 in. were utilized. These foil strain gages were externally bonded to the timber members using the manufacturer's recommended adhesive (cyanoacrylate type).

The foil strain gages and strain transducers were attached parallel to the longitudinal direction of the specimen. These sensors were positioned on both external bending surfaces of the specimens to measure bending strains for comparison to the FBG sensors. Note that for the FBG sensors, the effective gage length was smaller than the other strain sensors (i.e., 0.39 in.); in all cases all sensors were approximately aligned on with their mid-lengths at the same cross-section. In addition, deflection transducers were attached at mid span of the specimen to record vertical displacements. Additionally, thermocouples were attached to the specimens for any test lasting longer than a minute. All sensors were monitored with appropriate data acquisition hardware. All tests were conducted in a hydraulic universal testing machine.

The nine small scale glulam specimens were instrumented with two foil strain gages; each one was located on the intersection of the center line and the mid span of the specimen, parallel to the FBG sensor packages. Also parallel to these sensors, two strain transducers were positioned "over" the foil strain sensor with a second placed off center, 1 1/2 in. from the edge on both external bending surfaces (see Figure 6.23). Specimens 1, 4 and 7 had an additional pair of foil sensors located next to the FBG sensor packages, also at mid span (see Figure 6.24). Finally, two deflection transducers were attached at mid height of the glulam beam to record the vertical displacements at mid span.

Figure 6.23. Specimens with Structural Packages: FBG Sensor, Foil Strain Gage and Strain Transducers

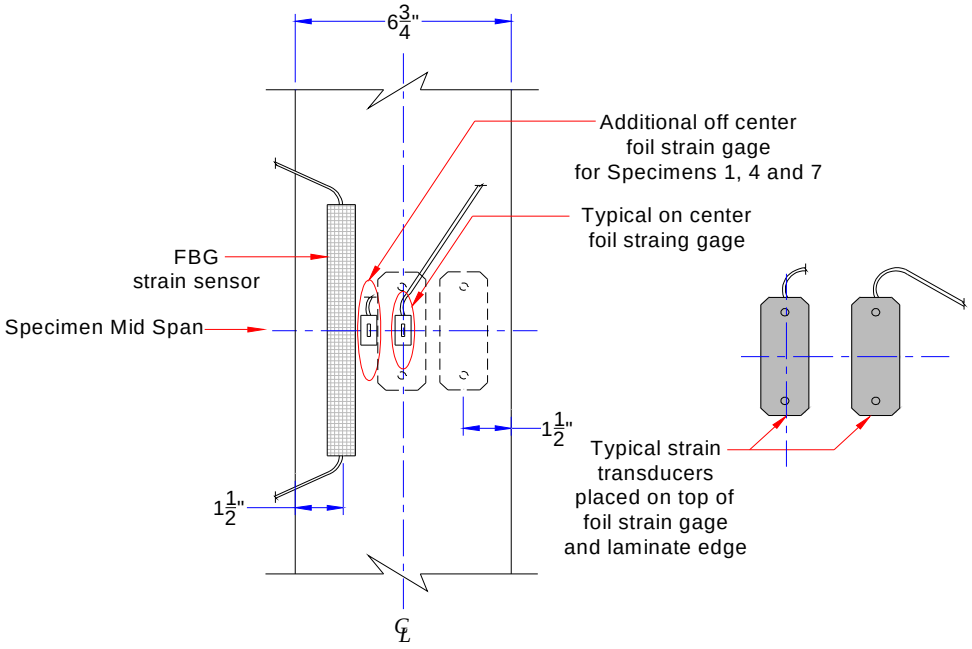

Figure 6.24. Specimens with Structural Packages: Scheme of External Instrumentation at Mid Span

6.2.8.1.2. **Test Protocols**

Initially, the nine specimens were tested in bending to investigate the basic elastic behavior as compare to conventional strain sensors. In Figure 6.25, a typical specimen is shown. Three additional series of bending tests applying the same third-point loading method were performed by modifying the period of sustained load and loading rate. In one case, a total load of 2500 lbs was sustained for 24 hours to observe potential creep or temperature influence on the structural package. To observe any rate of loading (i.e., shear lag), tests were performed by applying the load at three different rates. Two pseudo cyclic tests were also conducted to observe if any dissipation of mechanical energy had occurred in the specimen packages. Two additional test series were performed on the specimens by maintaining a constant load for 24 hours with at variable temperatures to evaluate the FBG sensor behavior at expected service temperatures.

6.2.8.1.2.1. Bending Test

The bending test was performed to establish the flexural behavior in the elastic range, observe the FBG structural package performance during the loading and unloading process, and compare the response to the foil strain gages and strain transducers. The specimens were first loaded on one

Figure 6.25. Small Scale Glulam Specimen with Structural Package and Test Setup

bending surface (Side 1, as seen in Figure 6.22). For the bending tests, the rate of loading was approximately 1000 lbs/min until a total load of 2500 lbs was applied. This load was sustained for approximately 30 seconds and then instantaneously removed. The FBG data sampling rate was approximately 5 Hertz; while for the other strain sensors, the sampling rate was 1 Hertz. The

specimens were turned over to the other bending surface (hereafter Side 2) and tested in the same manner to verify the symmetry of the specimens.

6.2.8.1.2.2. Sustained Loading Test

Using the same test frame configuration and instrumentation as in the bending test, a 24-hour sustained load was applied to each of the nine specimens to assess the time and temperature dependent strain response and potential creep effects in the adhesive. Because of the duration of the test and sensitivity of the temperature fluctuations, additional thermocouples were attached on the top and bottom of the specimen adjacent to the external FBG sensors. After synchronizing all sensors, data were collected at a rate of 1 sample/min during the load ramp up and until completing the test.

After reaching the maximum load of 2500 lbs with a loading rate of approximately 1250 lbs/min, the load was sustained for 24 hours under uncontrolled laboratory temperature conditions. After 24 hours the load was released and FBG sensor strain data were recorded for another 15 minutes to observe any residual strains. All nine specimens were first tested with Side 1 in compression. To complete the assessment of the sustained loading, additional tests were performed three months later applying the load to Side 2. Only seven operative specimens were tested following the same test protocol. In Specimen 6, the bare fiber strand adjacent to the packages broke during handling and both external FBG sensors were not able to be reconnected. Specimen 2 was tested on Side 1; this specimen failed under an accidental overloading when completing one set of the fast loading test.

6.2.8.1.2.3. Accelerated Loading Test

The goal with conducting this test was to evaluate the viscoelastic behavior of the adhesives utilized to bond the structural packages to the glulam members using different rate of loadings. The viscoelastic behavior was evaluated through the strains during the process of loading (effective stiffness) and unloading (residual strains) of the specimens.

After placing each specimen in the test fixture, the 2500-lb load was applied with loading rates of 2500 lbs/min, 5000 lbs/min and 2,500 lbs/sec. The latter loading rate was performed twice to observe the reproducibility of the test. Each test was conducted at 30 minute intervals to allow for the full recovery of the strain energy. The sampling rate for the 2500-lbs/min and 5000-lbs/min rate of loading tests was 1 Hertz for all sensors; while for the 2,500-lbs/sec rate of loading, the sampling rate was 30 Hertz. Immediately after reaching the maximum load of 2500 lbs, this load was sustained for

approximately 20 minutes and then removed. After removing the load, data were recorded for other 3 minutes to observe any residual strains.

Eight specimens were operative during the accelerated loading tests. These tests were performed on both external bending surfaces. After completing one of the accelerated loading tests, Specimens 2 and 7 were accidentally overloaded causing debonding of the external fiber optic sensors with the subsequent failure of one. Specimen 2 failed at approximately 2500 με, seven times higher than the bending strain at 2500 lbs. In this specimen, the 5000-lbs/min and 2,500-lbs/min loading tests were not performed on Side 2. In the case of Specimen 7, no visible damage was observed after an accidental overloading. The strain levels at the time of debonding were approximately 1200 με on the tension side, at least 4 times larger than the bending test strain. The C-FRP package located on the tension side debonded without damaging the FBG sensor. This sensor package was reattached with the same adhesive, Loctite 4212, and techniques as described in the previous section and then tested for operativeness. After testing this specimen and comparing to the initial behavior, the obtained strain results were deemed satisfactory. After completing the accelerated loading tests, only seven specimens were operatives.

6.2.8.1.2.4. Pseudo Cyclic Loading Test

The goal with this test was to observe the viscoelastic behavior of the adhesive utilized to bond the FBG structural packages to the glulam specimens through any sign of strain phase lag, if present, upon loading and after the removal of the applied load.

Using the same test frame configuration for the bending test, each specimen was loaded with a total load of 2500 lbs. Two pseudo cyclic loading tests were performed with rates of loading of 1250 lbs/min and 5000 lbs/min, and unloaded at the same rate. Each test was run for 10 cycles with data sampling rates of 10 Hertz. Each specimen was reloaded only after 30 minutes allowing for strain recovery. The pseudo cyclic loading was performed on eight specimens on Side 1. After the failure of Specimen 2, the pseudo cyclic test protocol was performed on the seven operative specimens turned over to Side 2.

6.2.8.1.2.5. Heat and Sustained Loading Test

Before starting this test, the moisture content per specimen was reassessed in all specimens. Using the same two-prong resistance moisture meter, no electrical response was obtained in the

specimens. The lower scale of the moisture meter was 6%, indicating a drier condition of the specimens than at the beginning of the test program. The moisture content decreased in an interval of six months from the initial moisture content (between 7 % and 10%) to less than 6%. With lower moisture content, the strength and stiffness of wood specimens is expected to relatively increase (Ritter, 1992).

The purpose of this test was to observe the effect of high temperatures on the viscoelastic behavior of adhesive attaching the FBG sensor packages. A total of seven operative small-scale specimens were tested under sustained load with temperatures that ranged from laboratory condition to approximately 120^{o}F. The small-scale specimens were subjected to higher temperatures than a bridge would potentially experience in summer. To heat the specimen, a heat box was constructed to completely enclose the specimen. The box consisted of two sets of rigid board (blue board) insulation walls sealed with insulation silicone, and aluminum foil tape. Additionally, one layer of aluminum foil was attached to the interior of the walls to prevent overheating and burning of the insulation board. The box was designed to fit inside the testing machine frame and to host the specimen and the heat source. The heat source comprised of four 100-watt bulbs distributed inside the box surrounding the specimen (see Figure 6.26).

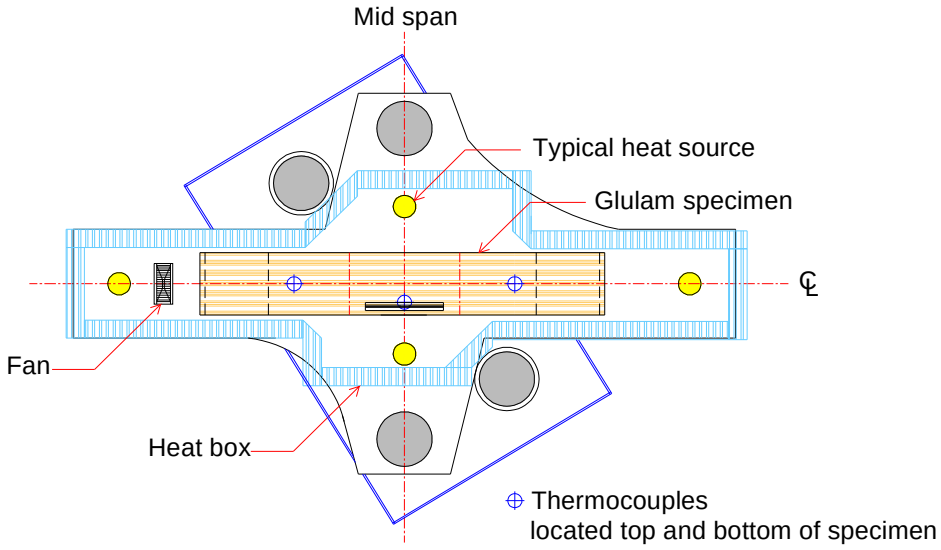

Figure 6.26. Heat and Sustained Loading Test: Test Setup and Instrumentation

Strain data were collected from the FBG sensors, foil strain gages and DCDTs throughout the heat test. In this case, the strain transducers were disconnected and removed due to the potential for heat damage. In addition to the two original thermocouples, four additional thermocouples were

placed at each end of the beam, two on top and two on the bottom to observe the heat distribution along the specimen. After placing the specimen in the bending frame, verifying the sensors operability, the same protocol for the sustained loading test was utilized. Each specimen was loaded with a maximum load of 2500 lbs and a loading rate of 1250 lbs/ min. In the entire test, strain, temperature and load data were collected with a sampling rate data of 1 Hertz. The data were collected for approximately 20 minutes at ambient temperature to observe the initial behavior. After this initial period, the specimen was enclosed in the heat box. The heat source then was connected for 24 hours (see Figure 6.27). Additional strain and temperature data were collected for at least four hours after the heat source removal to observe the recovery of the specimens while cooling.

During the test of Specimen 1, Side 1, some overheating occurred after five hours. The FBG sensor reached 173^{o}F on the tension side (RS-SS package bonded with 454-Loctite adhesive); which is near the maximum recommended operating temperature of the adhesive (180^{o}F). At this point, the lids were partially opened to reduce the temperature. Although the temperature decreased, a sustained temperature of approximately 163^{o}F was still present. To moderate the internal temperature, a small fan was installed to distribute the heat and the heat box lids were partially open to release the excess of heat (see Figure 6.28). This change in the methodology of testing provided sustained temperatures between 110^{o}F and 120^{o}F on average and was repeated as part of the test protocol for the remaining tests.

Figure 6.27. Heat and Sustained Loading Test: Assembling of the Heat Box

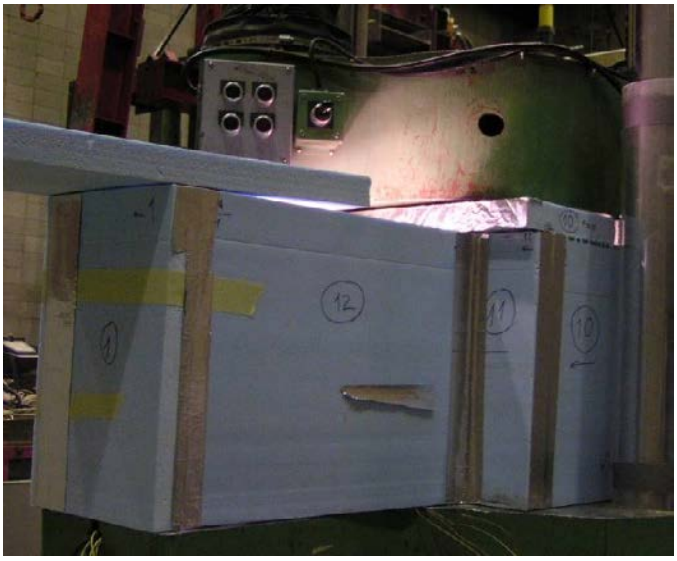

Figure 6.28. Heat and Sustained Loading Test: Regulating the Internal Temperature

6.2.8.1.2.1. Cold and Sustained Loading Test

The remaining seven operational small-scale glulam specimens were tested in cold temperatures to evaluate the response of the adhesives. A cold box was constructed to reduce the temperatures to approximately 0^{o}F. The cold box contained the core of the instrumented specimen between the supports of the bending frame of the third-point loading test setup (see Figure 6.29). Only operational FBG sensors and foil strain gages were utilized to collect strain data. Strain transducers were not installed because of the potential for damage. To record the temperatures, the specimens were externally instrumented with six thermocouples placed in the same locations as those using during the heat and sustained loading test. Typically, two thermocouples were located in the vicinity of external FBG sensors on top and bottom of the glulam specimen, while four others were placed at approximately 12 in. from the center of the specimen.

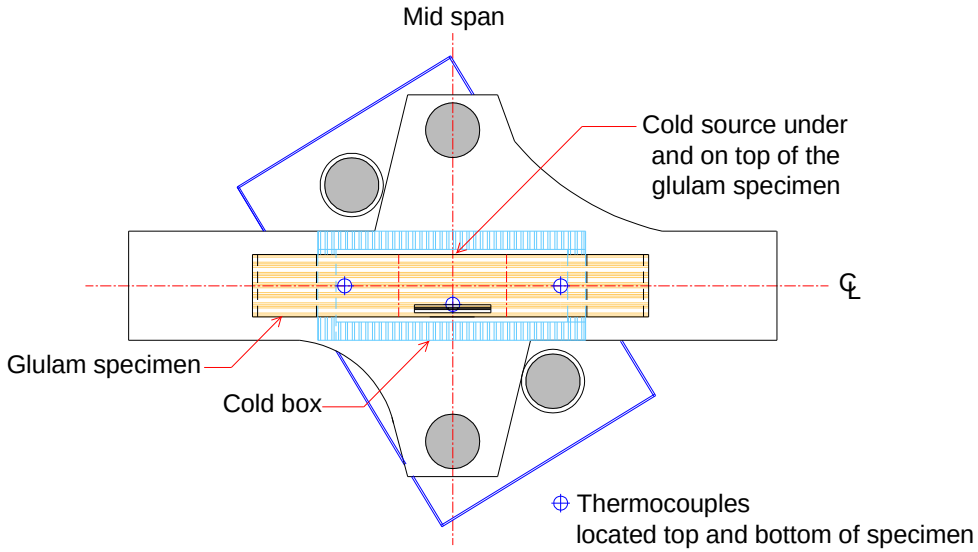

Figure 6.29. Cold and Sustained Loading Test: Test Setup and Instrumentation

Prior to the test, the instrumented glulam specimen was positioned on top of the supports located outside the cold box (Figure 6.30). Initial laboratory temperature and zero strain levels were recorded for two minutes with a sampling rate of 1 Hertz. Following initial data collection, dry ice pellets were deposited on the top and the bottom of the specimen while strain and temperature data were recorded. Immediately after, the universal test machine was prepared for testing. After closing the cold box (Figure 6.31), the test machine was calibrated to zero. The cooler box lids and universal test machine head were additionally taped to confine the cold temperature. Each specimen was loaded at a loading rate of 1250 lbs/min until reaching the maximum load of 2500 lbs. This load was sustained for 24 hours. After completing the load testing, the specimen was released and allowed to warm for approximately two hours with the assistance of a fan. Additional strain and temperature data were obtained during this process to observe the response of the package during warming. The specimens were tested on both bending surfaces, on Side 1and later on Side 2 to complete the study.

Figure 6.30. Cold and Sustained Loading Test: Placing the Specimen in the Cold Box

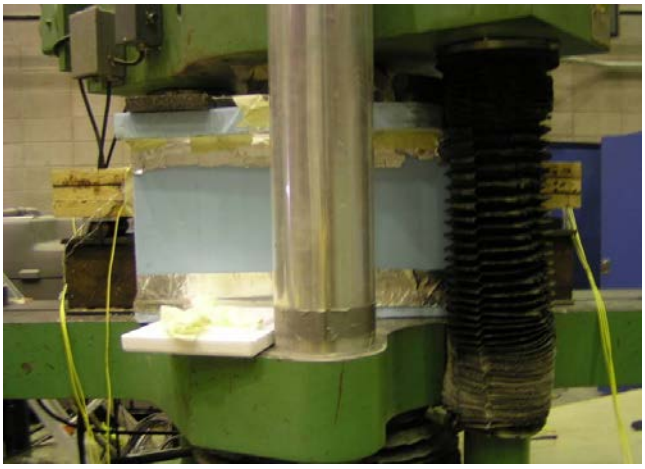

Figure 6.31. Cold and Sustained Loading Test: Assembling the Cold Box

6.2.8.2. NON-STRUCTURAL PACKAGE TEST PROGRAM

In this section, the test protocols adapted from the ASTM 198-05a standards were utilized to evaluate the non-structural packages installed in five small scaled glulam specimens.

6.2.8.2.1. **Sensors and Test Equipment**

Two strain transducers were bonded with Loctite 410 adhesive and Loctite-7452 accelerator. Each strain transducer was placed at mid span on the specimen's external bending surface. FBG

sensors, strain transducers and load cells were monitored with the data acquisition hardware used in other phases of this work.

6.2.8.2.2. **Test Protocol**

Only one bending test protocol was applied to each specimen to measure the mechanical strains in the FBG sensors.

6.2.8.2.2.1. Modified Bending Test

The purpose of this test was to investigate the effectiveness of the non-structural package techniques by measuring the mechanical strains in the FBG sensors (zero strain would indicate perfect isolation). The five specimens were tested in bending using the same third-point loading method with a total load of 2500 lbs under ambient laboratory temperatures. All specimens were placed on the test fixture described in the previous section 6.2.8.1 (see Figure 6.22). The sampling rate for FBG strain sensors, strain transducers and load cell data were set to 10 Hertz. After synchronizing the instruments, the load was applied with a loading rate of 500 lbs/min; this slower loading rate was applied with the purpose of avoiding vibration of the partially restrained FBG strain sensors. The 2500-lbs load was sustained for five minutes, and then removed with an unloading rate of 500 lbs/min. Each specimen was loaded twice to verify reproducibility of the results. Each loading test was performed within intervals of 30 min allowing the strain recovery.

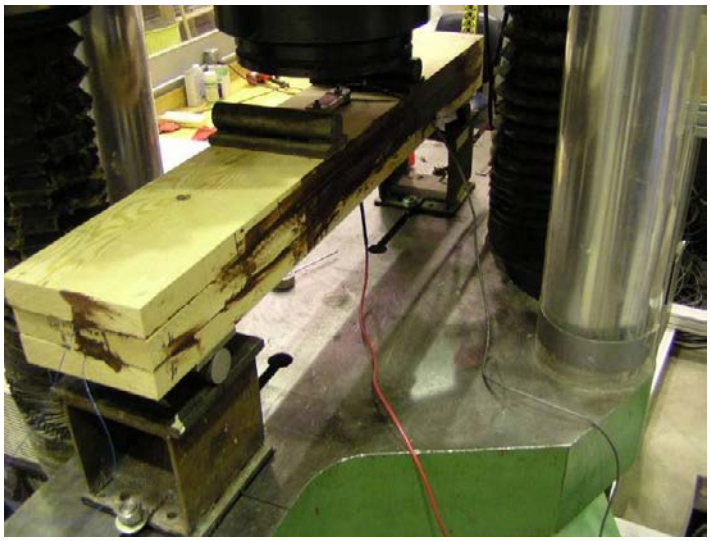

Figure 6.32. Modified Bending Test: Specimens with Non-Structural Package

6.3. EXPERIMENTAL RESULTS OF THE SMALL SCALE SPECIMENS

This section presents the analyses of the test results for the fourteen small scale glulam specimens described in the preceding section.

Nine specimens instrumented with structural FBG sensor packages were tested in bending to verify their consistency by evaluating their initial conditions, by comparison to theoretical strains and by comparison to data gathered with foil strain gages and strain transducers. The strain data were collected for variable load duration and temperature conditions (Section **6.2.8.1**). The objective of these tests was to evaluate both the elastic and viscous-like behavior of the structural packages. The following flow chart summarized the steps taken in the subsequent sections to evaluate the structural FBG sensor packages (see Figure 6.33 and Figure 6.34).

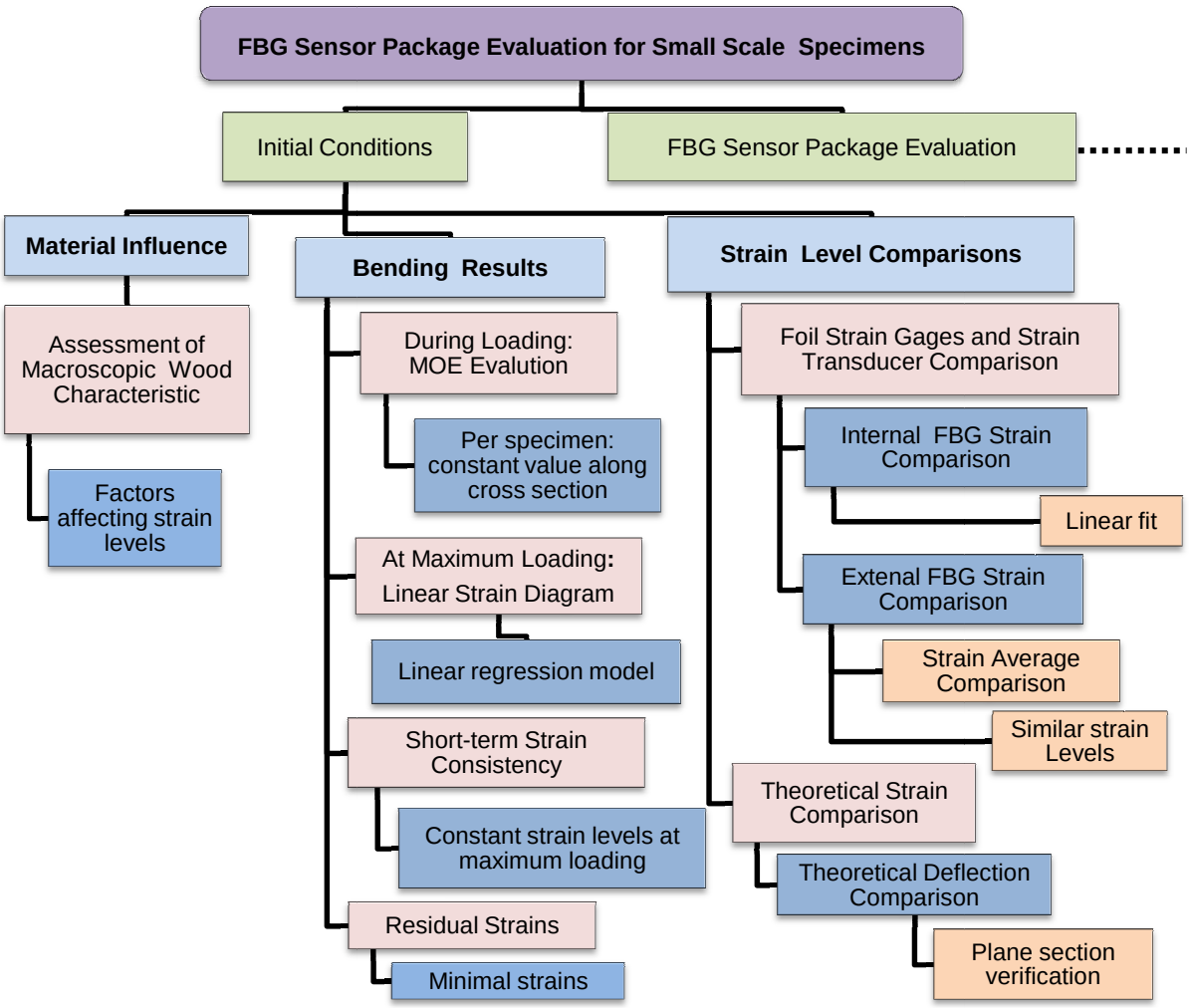

Figure 6.33. Chart of the Evaluation of the Structural FBG Sensor Package

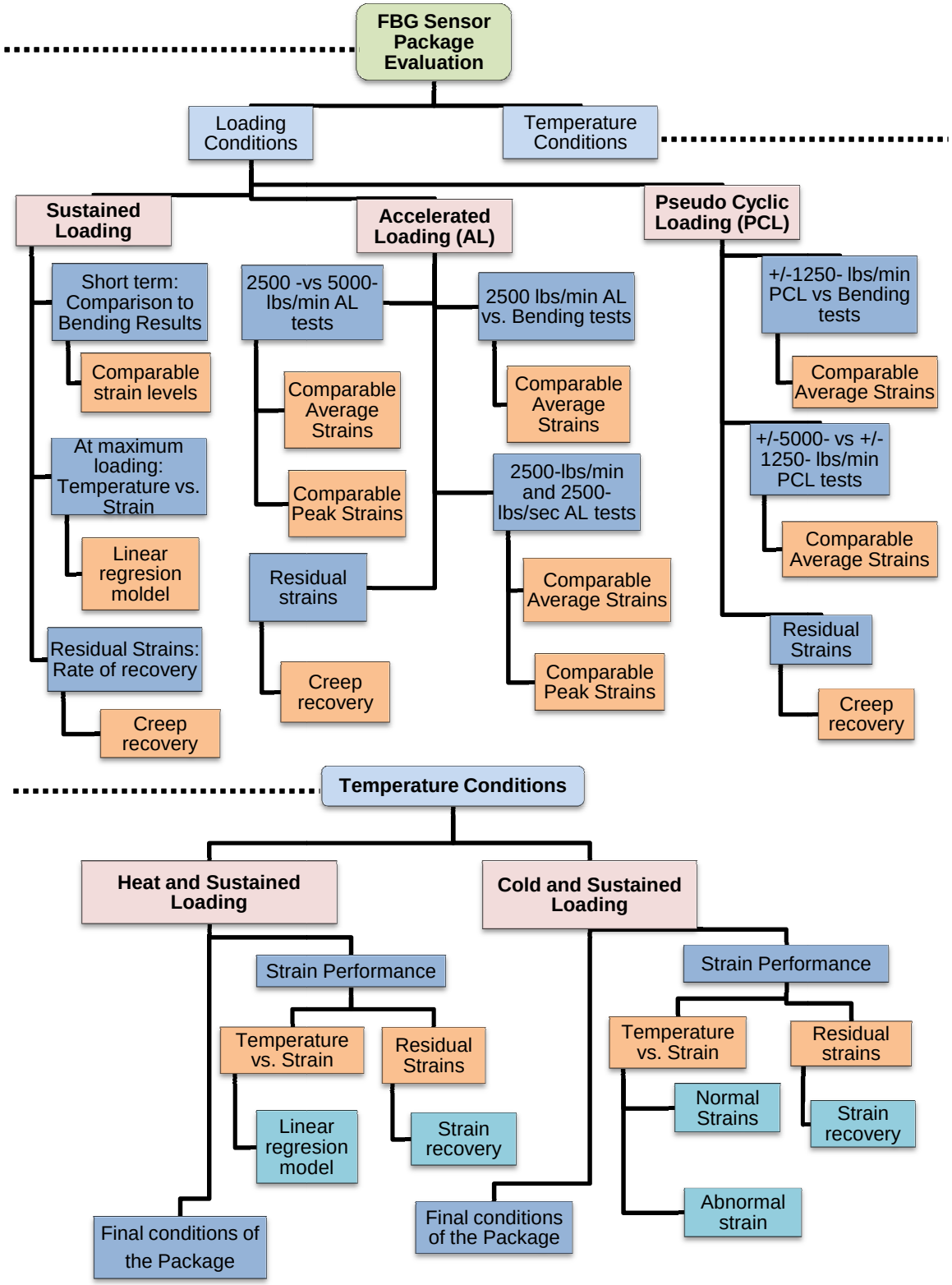

Figure 6.34. Chart of the Evaluation of the Structural FBG Sensor Package (Continuation)

Five specimens instrumented with non-structural FBG sensor packages were also tested under bending loads (Section 6.2.8.2). The main objective of this testing was to evaluate the effectiveness of the non-structural packages in isolating the FBG sensors from mechanical strain response for potential use in measuring environmental effects within the member.

6.3.1. Assessment of Macroscopic Wood Characteristics in the Small Specimens

Prior to evaluating the test results, all specimens were visually inspected to later explain and/or justify the experimental strain levels. Note that this was limited to the exposed Side 1 and 2 surfaces. So defects on the middle lam are not reflected here. Only Specimens 1, 3, 5 and 9 are presented from Figure 6.35 through Figure 6.38. The following macroscopic wood characteristics were observed on the external bending surfaces (i.e., Side 1 or Side 2), and were grouped as follows:

- The presence of knots was observed on two specimens:
  - In Figure 6.35 (a), a 1 1/2-in. intergrown knot was located near the strain transducers at Specimen 1, Side 1.
  - In Figure 6.38 (a), a small encased knot was located at Specimen 9, Side 2, far from the sensors locations.
- Slope of grain patterns, defined as the deviation of the wood fiber orientation with respect to the longitudinal direction of the specimen:
  - In Figure 6.35 (b), abrupt change in the fiber orientation classified as grain deviations were observed in Specimen 1, Side 2.
  - In Figure 6.37 (a), diagonal grains deviating from the longitudinal specimen direction were observed in Specimen 5.
  - Straight grains, where the fiber orientation mainly followed the longitudinal direction of the specimen, were observed at regions of Specimen 2, Specimen 9, Side 2 near the FBG sensor (see Figure 6.38 (b)).

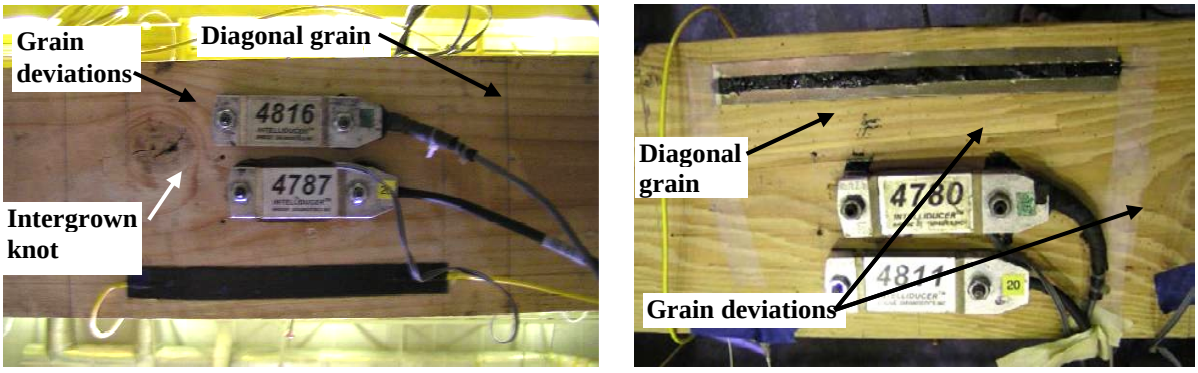

(a) Side 1 – C-FRP Loctite 454 package (b) Side 2 – RS-SS Loctite 454 Package

Figure 6.35. Specimen 1: Bending Surfaces Side 1 and 2

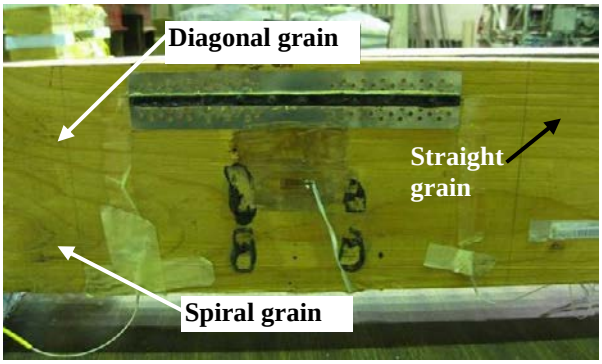

(a) Side 1 – 72H-SS Loctite 454 package

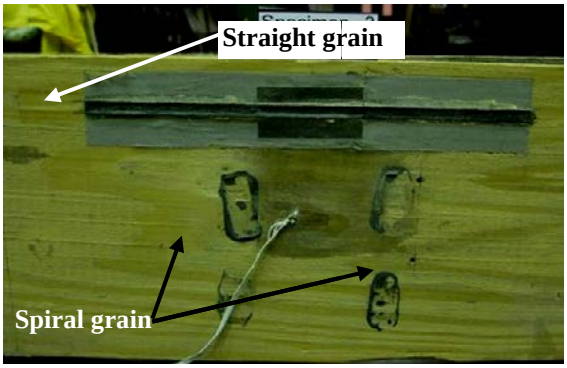

(b) Side 2 –AM-SS Loctite 454 Package

Figure 6.36. Specimen 3: Bending Surfaces Side 1 and 2

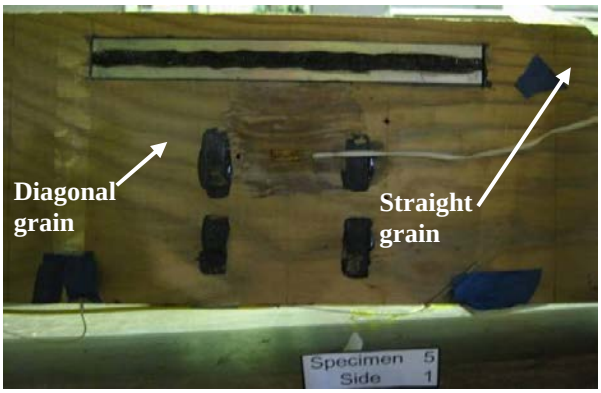

(a) Side 1 – CS-SS Loctite 426 package

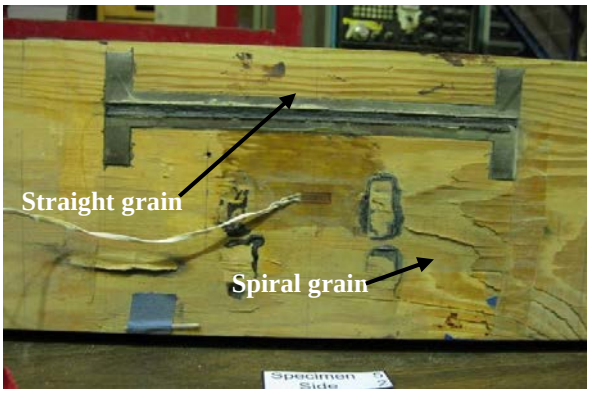

(b) Side 2 – IS-SS Loctite 426 Package

Figure 6.37. Specimen 5: Bending Surfaces Side 1 and 2

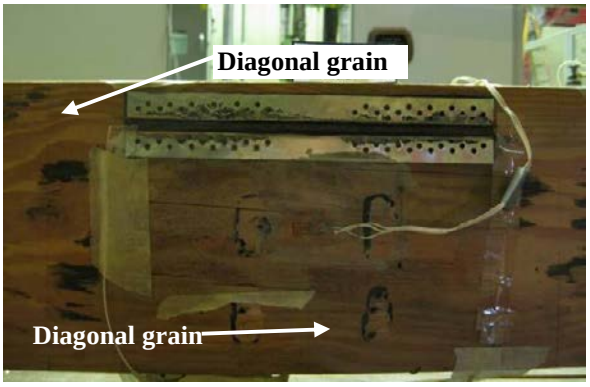

(a) Side 1 – 72H-SS Loctite 4212 package

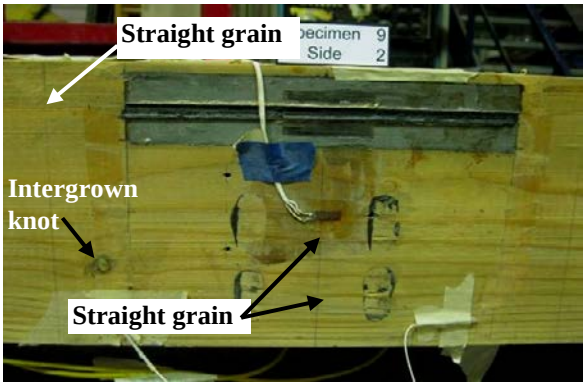

(b) Side 2 –AM-SS Loctite 4212 Package

Figure 6.38. Specimen 9: Bending Surfaces Side 1 and 2

Regarding the instrumentation, the three sensor types were installed at determined locations with arbitrary macroscopic wood characteristics. In general, the foil strain gages with a 0.39-in. long gage were located at the straight grains parallel to the longitudinal direction of the specimens. For the strain transducers, the 3-in. effective gage was located either at regions with straight grain (Figure 6.38 (b)) or where the slope of grain changed in orientation, which represented a reduction in the stress levels (see Figure 6.35 (b)). The FBG sensor were observed to be located at regions were the slope of grain was either straight (Figure 6.37 (b)) or the combination of both straight and diagonal grains (Figure 6.37 (a)).

6.3.2. STRUCTURAL FBG SENSOR PACKAGES

The experimental results of the nine structural package specimens are presented in two parts. The first part is comprised of the evaluation of the FBG sensors under bending loads with the purpose of establishing the initial flexural behavior. The second part presents the FBG strains obtained from additional bending tests varying the duration of the loading, the rate of loading, and the temperature conditions to assess the viscoelastic behavior of the adhesive.

6.3.2.1. FBG SENSOR EVALUATION UNDER BENDING TEST

The specimens were tested using the bending test protocol explained in Section 6.2.8.1.2.1.

6.3.2.2. BENDING TEST RESULTS

The nine specimens were subjected to third point bending with a maximum load of 2500 lbs. The load was applied to each bending surface (Side 1 and Side 2) to evaluate the compressive and tensile response of each sensor. In Figure 6.39, a typical response of the FBG sensors with respect to the applied load versus time are presented.

The following were calculated and/or identified from experimental:

- The relationship between strain and stress at mid span.
- The neutral axis location (assuming that plane sections remain plane).
- The dispersion of the strain data during the application of a sustained load for 30 seconds.
- The occurrence of any residual strain after removing the load.

The results are presented per Side 1 and Side 2 Loading.

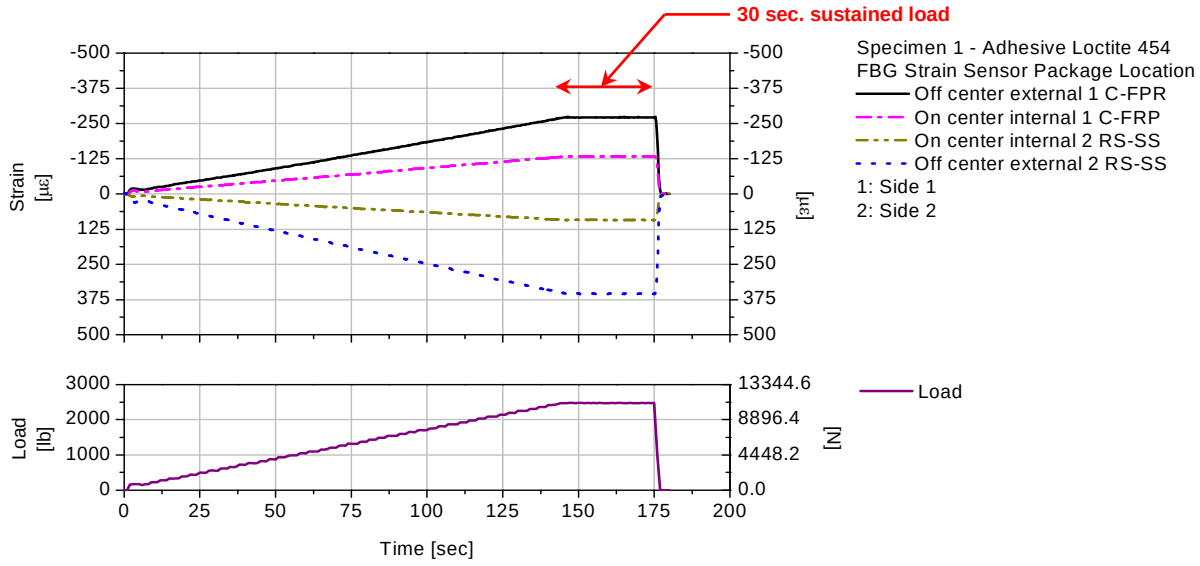

Figure 6.39. Representative Bending Test Results upon Loading

Stress-Strain Behavior. The experimental strains and theoretically calculated stresses from the applied load were compared to a linear regression model. To quantify the fit, a coefficient of determination (R^2 coefficient) was calculated as the squared correlation between the experimental data and the predicted values.

As stipulated in the ASTM standards (ASTM 198-05a, 2005), the apparent MOE is recommended to be calculated using the experimental deflection data and beam theory. In the small specimen tests, the deflection data were not sufficient to estimate this standard MOE value. However, an equivalent experimental modulus of elasticity (MOE) was calculated using the external FBG sensor strains where the flexural behavior was predominant. The average MOE (Avg. MOE) was defined as the average slope between stress and strain data. In addition, the standard deviation (Std. Dev.) was calculated.

In Figure 6.40, examples of the strain-stress results are presented for two external FBG sensor types on Specimen 1. For the FBG 1 sensor, the Avg. MOE was 3034 ksi (+/-136); this relatively large value may have been cause by the presence of an intergrown knot in the vicinity of the sensor (see Figure 6.35 (a)). For the FBG 2 sensor, the Avg. MOE value was 2170 ksi (+/-61) (see Figure 6.35 (b)). When comparing the experimental data to the predicted values using the linear regression, the R^2 coefficients were above 0.998.

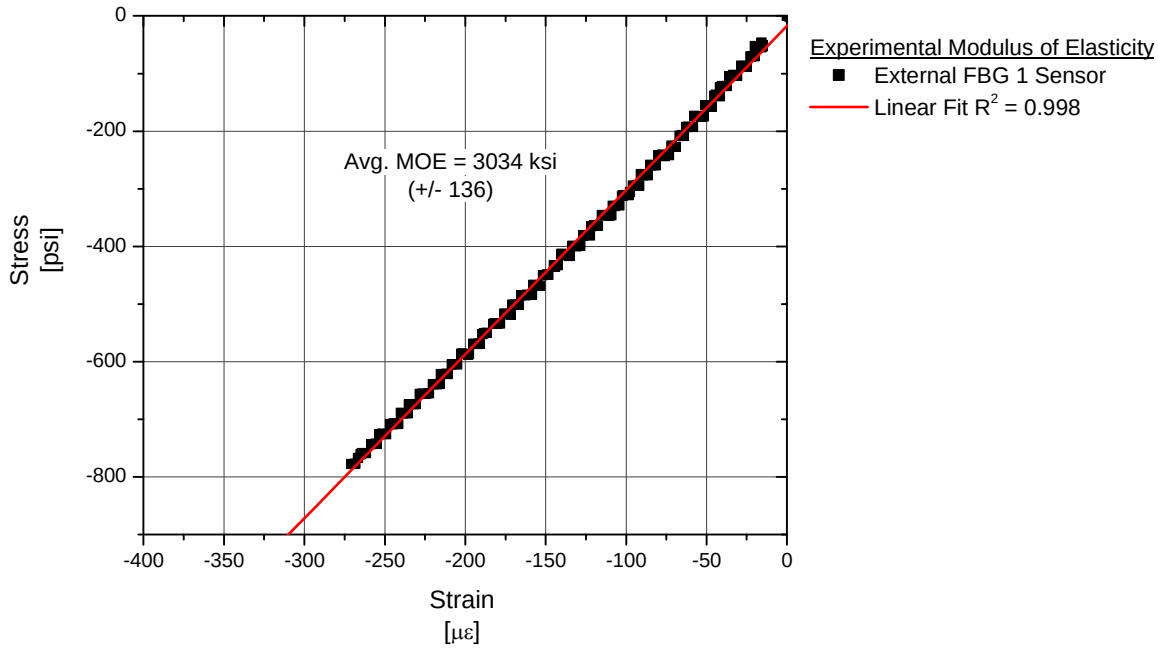

(a) External FBG 1 Sensor

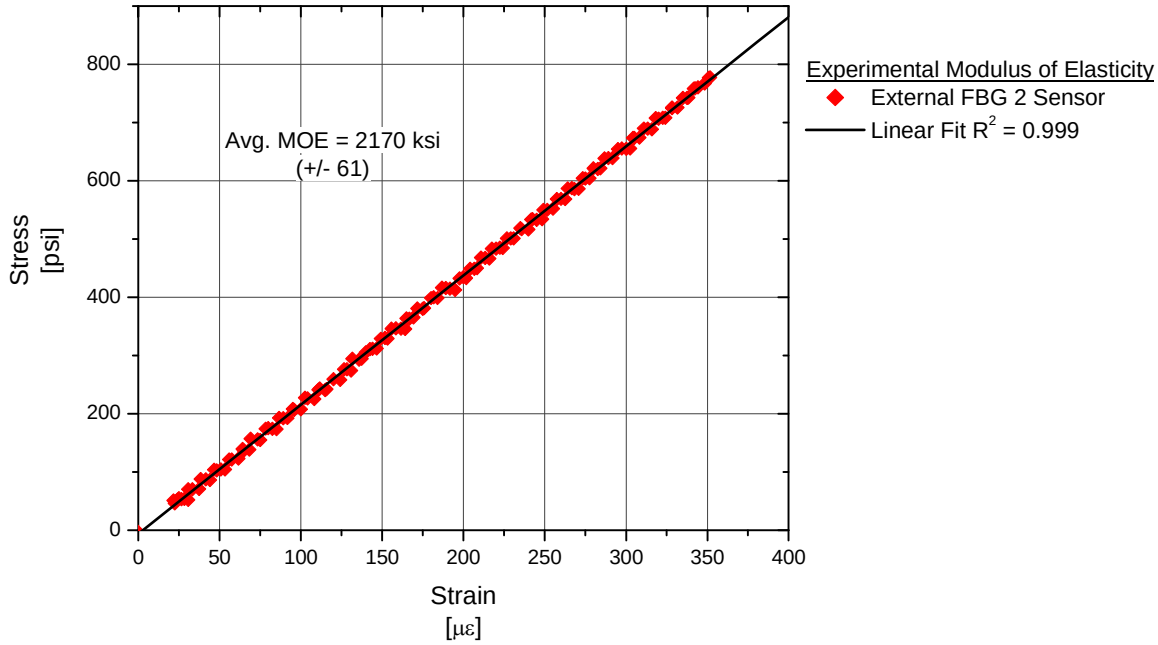

(b) External FBG 2 Sensor

Figure 6.40. Bending Test: Stress-Strain Behavior for Specimens 1, Side 1 and Side 2 Loadings

In Table 6.8, the experimental Avg. MOE and standard deviation (Std. Dev.) values are presented for all operative sensors. For the external FBG sensors, the tensile Avg. MOEs were consistently lower than the compressive values, with exception of the external FBG 1 sensor at Specimen 9. In

general, the Std. Dev. values were between 2% and 9% of the Avg. MOEs indicating a low dispersion. In the linear regression model evaluation, the R^2 coefficients for all sensors were between 0.998 and 0.999, indicating that experimental strains and calculated stresses were linearly related.

The calculated MOEs were compared to the theoretical MOEs for a glulam member with up to three laminates; as noted in Section 6.2.6, the theoretical lower and upper MOE values were 1500 ksi and 2000 ksi, respectively. From the MOE evaluation, Specimens 3 and 4 had Avg. MOEs within the theoretical values (see Table 6.8). For other specimens, the Avg. MOEs varied between 1803 ksi (Specimen 3) and 3384 ksi (Specimen 7).

From the MOE evaluation, the experimental strains at the depth of the cross section were relatively dissimilar and consequently asymmetrical with respect to the center of gravity of each specimen. In this context, more study was needed and is described in the subsequent section.

Table 6.8. Bending Test: Summary of Average Modulus of Elasticity and Standard Deviation

Specimen	Side Loading	External FBG 1		External FBG 2	
		Avg. MOE [ksi]	Std. Dev. [ksi]	Avg. MOE [ksi]	Std. Dev. [ksi]
1	1	(3034)	136	2170	61
	2	2410	59	(2467)	58
2	1	(2332)	99	1884	67
	2	2130	83	(1958)	70
3	1	(2042)	46	---	---
	2	*1803*	*113*	---	---
4	1	(1970)	99	1672	58
	2	1815	72	(1888)	80
5	1	(2654)	104	2090	70
	2	2200	88	(2190)	78
6	1	(2679)	181	---	---
	2	2159	40	---	---
7	1	(2954)	208	2631	212
	2	2676	164	*(3384)*	*184*
8	1	(2101)	191	2173	169
	2	1913	97	(2256)	116
9	1	(2469)	126	2197	118
	2	2608	93	(2732)	97

Note. - ( ) corresponds to the compressive Avg. MOE.
"---" indicates an inoperative FBG sensor.

Maximum Loading – Experimental Strain versus Linear Regression Model Comparison. To assess if the sensor readings indicated plane cross-sections remained plane, the internal and external flexural FBG strains presented in Table 6.9 were compared at approximately 2500 lbs. The FBG strains at maximum loading per Side 1 and Side 2 loading were compared for the purpose of:

- Obtaining the range of the flexural strain per sensor.
- Investigating the linear strain relationship with R^2 coefficients.
- Evaluating the position of the neutral axis.

Table 6.9. Bending Test: Maximum External FBG Strain Results per Structural Package

Specimen	Side Loading	External FBG 1 [με]	Internal FBG 1 [με]	Internal FBG 2 [με]	External FBG 2 [με]
1	1	-272	-133	92	355
	2	322	133	-87	-320
2	1	-345	---	156	423
	2	370	---	-136	-398
3	1	-386	-171	132	---
	2	413	168	-137	---
4	1	-396	-140	143	451
	2	427	121	-149	-422
5	1	-305	-171	82	380
	2	344	165	-84	-351
6	1	-310	-129	86	---
	2	358	124	-89	---
7	1	-260	-109	---	283
	2	282	113	---	-235
8	1	-392	---	---	369
	2	412	---	---	-357
9	1	-312	---	---	349
	2	300	---	---	-293

Note. - "---" indicates an inoperative FBG sensor.

Using a linear regression method, the external and internal strain levels per specimen and per Side 1 and Side 2 loadings were correlated to investigate the strain relationship and position of the neutral axis. Typical linear strain models for Specimens 1, 4 and 7 with four operative FBG sensor packages are plotted in Figure 6.41. With three operative sensors, the typical linear model for Specimens 2, 3, 6 and 7 are shown in Figure 6.42. Specimens 8 and 9 had only two operative FBG sensors.

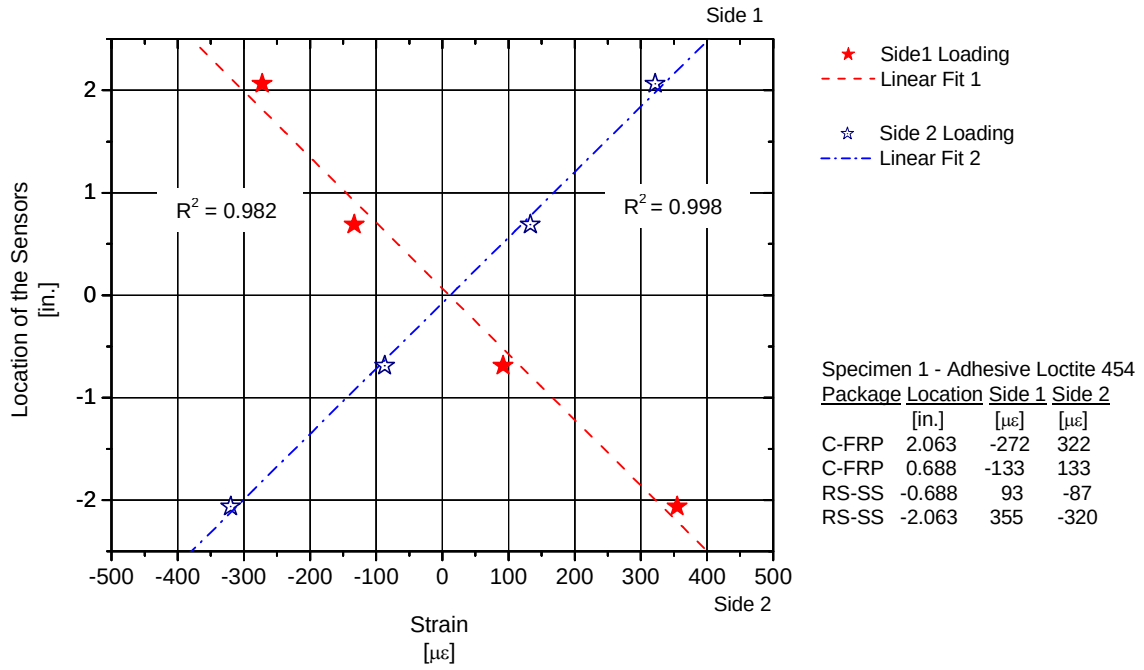

Figure 6.41. Bending Test: Specimen 1, Side 1 and Side 2 Loading – Maximum FBG Strains

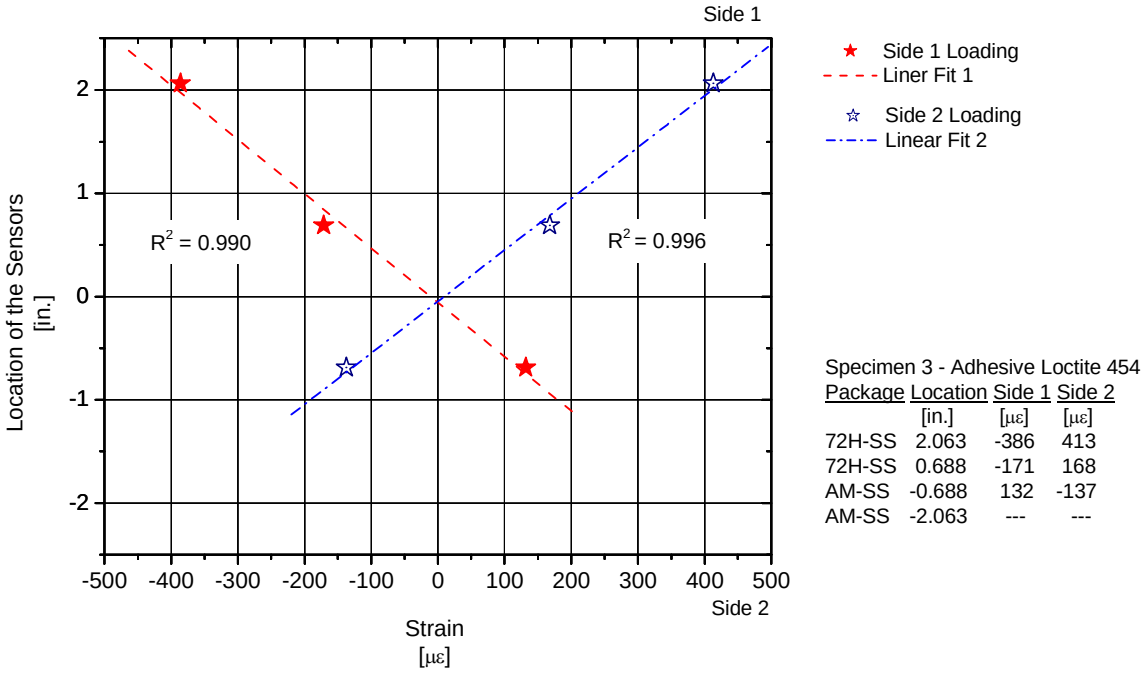

Figure 6.42. Bending Test: Specimen 3, Side 1 and 2 Loading – Maximum FBG Strains

Independently of the number of operative FBG sensors and their locations, the following general observations were made:

- For Specimens 1 through 7, the R^2 coefficients ranged from 0.974 to 0.999 which indicated that the measured strains are approximately contained within plane sections. The relative error in predicting a linear strain response for specimens with three of four operative sensors indicated that the sensor error may be independent of the strain magnitude.
- In all cases, the neutral axis was located between 0.10 in. and 0.22 in. from the center of gravity of the specimen cross section.

Short-Term Sustained Load. To evaluate the repeatability of the strain readings, the specimens were subjected to a short-term sustained load for approximately 30 seconds (see Figure 6.39). During testing, the temperature was assumed constant and the strains due temperature variations were neglected. Examples of the responses are presented in Table 6.10 and Table 6.11 for Specimens 1 and 4. In these tables, the maximum strains, the average strains and associated standard deviations are given.

In general, the differences between the maximum strains and the average strains were negligible. The associated standard deviations were similarly also negligible. In this 30 seconds short term loading, the repeatability of the strain levels indicates that the adhesives were behaving with negligible viscoelastic influences.

Residual Strain. After removing the load, residual strains were assessed to determine the behavior of the adhesive. Examples of residual strains are shown in Table 6.10 and Table 6.11. In general, the residual strains at the end of the data collection varied from 0.0 to 8.3 με. (e.g., Specimen 4).

Table 6.10. Bending Test: Specimen 1 – Short Term Loading Analysis and Residual Strains

Response	Side 1 Loading – Sensors				Side 2 Loading – Sensors			
	External FBG 1	Internal FBG 1	Internal FBG 2	External FBG 2	Internal FBG 1	Internal FBG 1	External FBG 2	Internal FBG 2
	[με]	[με]	[με]	[με]	[με]	[με]	[με]	[με]
Max. Strain	-271.7	-133.3	92.8	355.0	321.7	133.3	-86.7	-320.3
Avg. Strain	-271.6	-132.8	92.5	354.8	321.5	132.7	-86.1	-320.0
Std. Dev.	0.5	0.8	0.5	0.8	0.5	0.4	0.4	0.4
Residual Strain	0.0	0.0	0.0	5.0	-0.8	1.7	-1.7	-2.5

Table 6.11. Bending Test: Specimen 4 – Short Term Loading Analysis and Residual Strains

Response	Side 1 Loading – Sensors				Side 2 Loading – Sensors			
	External FBG 1	Internal FBG 1	Internal FBG 2	External FBG 2	Internal FBG 1	Internal FBG 1	External FBG 2	Internal FBG 2
	[με]	[με]	[με]	[με]	[με]	[με]	[με]	[με]
Max. Strain	-395.8	-140.0	142.5	450.8	427.5	120.8	-149.2	-421.7
Avg. Strain	-394.1	-139.4	142.9	450.5	426.7	120.2	-149.0	-420.9
Std. Dev.	0.5	0.4	0.7	0.6	0.6	0.6	0.4	0.8
Residual Strain	0.0	-1.7	-1.7	5.8	2.5	1.7	-1.7	-8.3

In the second part of the FBG sensor evaluation, the structural FBG sensor packages were subjected to 24-hour sustained loading to investigate the long term viscoelastic behavior.

STRAIN COMPARISONS. In the following sections, the maximum FBG strains were compared to the theoretical strains and the measured strains from foil strain gages and strain transducers. In addition, the experimental deflections were compared to the theoretical values to corroborate the specimens' strain levels.

Theoretical Strain Comparison. In Section 6.2.6.1, theoretical strains were calculated at the sensor locations using the modulus of elasticity values as tabulated in the AASHTO specifications (AASHTO, 2006). The upper and lower bound of the theoretical external strains are +/-522 με and +/-392 με and the theoretical internal strains are +/-174 με and +/-130 με, for moduli of elasticity of 1500 ksi and 2000 ksi, respectively.

External FBG Strains. In Figure 6.43, the maximum external strains for FBG 1 and FBG 2 sensors per specimen are presented. In the same plot, the theoretical upper bound (+/-522 με) and lower bound (+/-392 με) strains are shown for comparison.

From the plot, the following observations were made:

- All external FBG strains were lower than the upper bound strain of +/-522 με. The maximum strain was 451 με, corresponding to the Specimen 4, external FBG 2 sensor.
- The external FBG strains were observed to vary in the vicinity of the lower bound theoretical value of +/-392 με. For Specimens 2, 3 4 and 8, the strain levels were in the range of +/-15%.

- With respect to the theoretical lower bound strain of +/-392 με, the measured strains for Specimens 1, 5, 6, 7 and 9 were smaller. The lowest experimental strains were found in Specimen 7, between 235με and 283με.

Internal FBG Strains. In Figure 6.44, the maximum internal strains for Specimens 1 through 7 are shown. In the same graph, the theoretical upper and lower bound strains of 174 με and 130 με were plotted for comparison. From the plot, the following observations were made:

- The internal FBG strains were lower than the upper bound strain of +/-174 με. For Specimens 3 and 5, FBG 1 sensors, the strain levels were between 165 and 171 με.
- The FBG 2 strains at Specimens 1, 5 and 6 were consistently lower, ranging from +/-82 με to +/-92 με.
- The rest of internal FBG sensors were contained within the vicinity of the theoretical lower bound strain of +/-130 με. Strain values were in the range of +/-16% of the lower bound strain.

For all FBG sensors, the experimental strain values were smaller than the theoretical strains based on the assumed moduli of elasticity values.

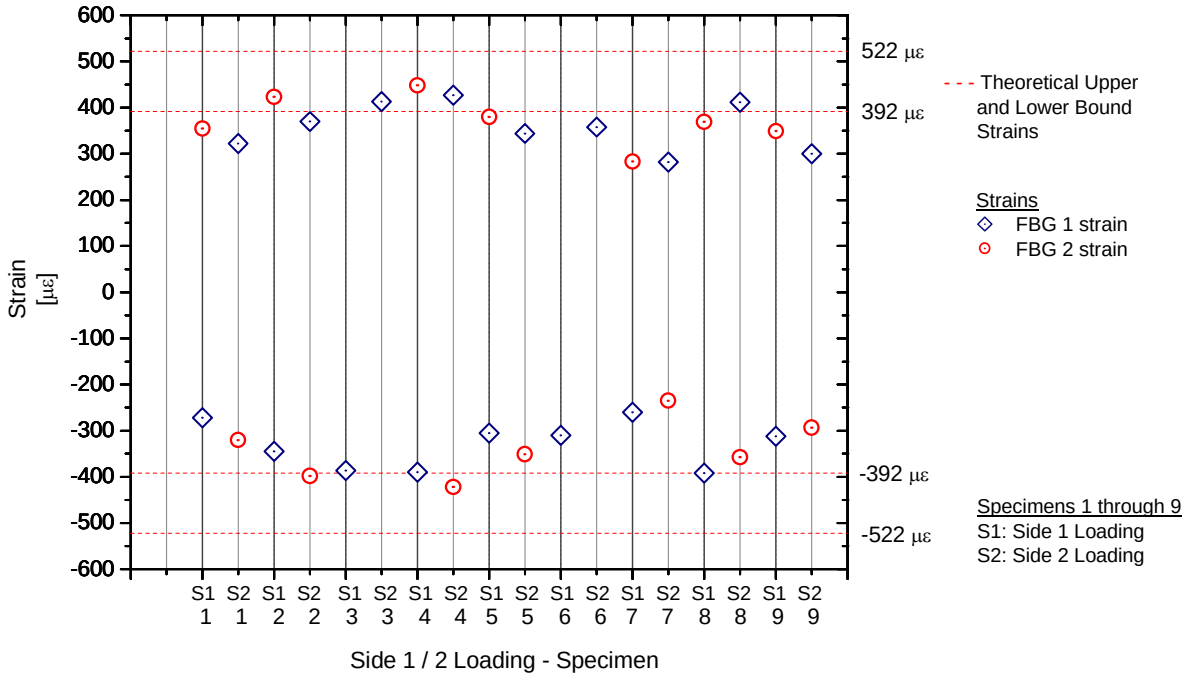

Figure 6.43. Bending Test: Comparison of Theoretical and Experimental External FBG Strains

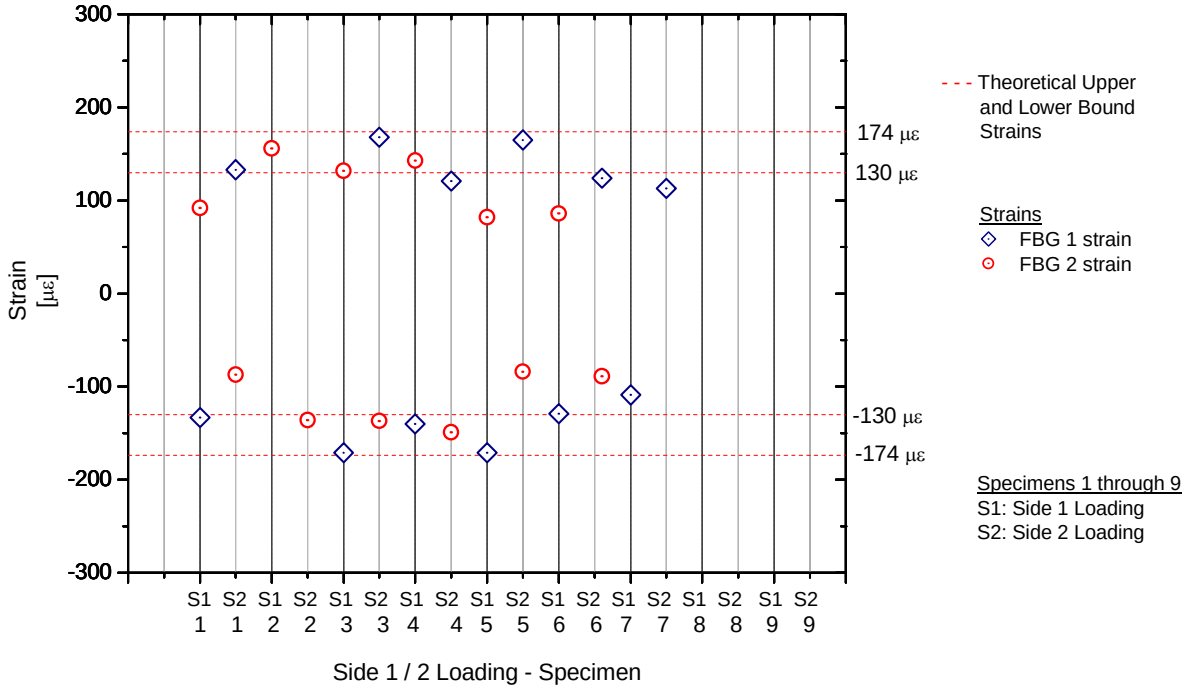

Figure 6.44. Bending Test: Comparison of Theoretical and Experimental Internal FBG Strains

Theoretical Deflection Comparison. The vertical deflections at the maximum load measured at the specimen mid span are plotted in Figure 6.45. In the same plot, the theoretical upper and lower bound deflections of 0.035 in. and 0.026 in. correspond to deflections estimated using a modulus of elasticity of 1500 ksi and 2000 ksi, respectively.

From the theoretical strain comparisons presented earlier, the measured strains were smaller than the theoretical upper values; in contrast, the specimen deflections were approximately equal or higher than the theoretical upper limit of 0.035 in. When comparing the experimental strains and deflection levels, similar variabilities were observed.

The experimental strains and deflections were non-dimensionalized using the theoretical values and compared. Theoretical strains and deflections were calculated for various load and MOE values using the third point loading beam relations and the specimen geometry. The relationship between non dimensional strains and deflections was evaluated using a linear regression model. The linear fit, R^2 coefficients were determined.

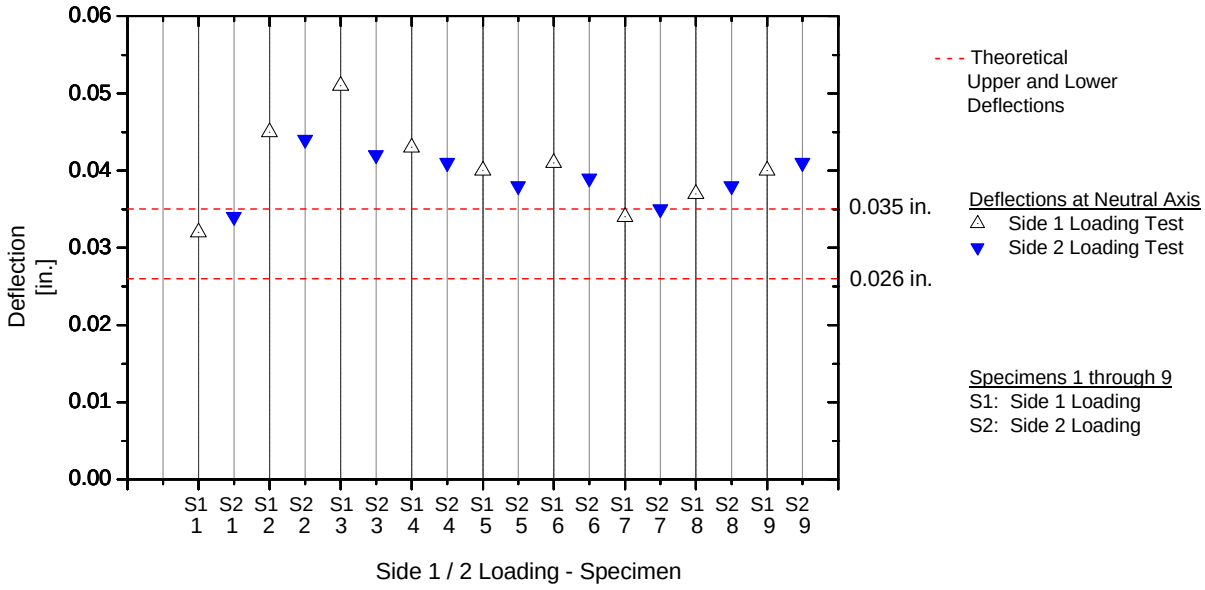

Figure 6.45. Bending Test: Comparison of Maximum Theoretical vs. Experimental Deflection at Mid Span for Specimens 1 through 9, Side 1 and 2 Loadings

Examples of the non-dimensional strain-deflection plots for external pair of FBG sensor packages are presented in Figure 6.46 and Figure 6.47. As indicated in the figures, approximate linear relationships were observed between the non-dimensional strains and deflections for both the external FBG sensors. For all specimens, the non dimensional strain-deflection curves had R^2 coefficients that varied from 0.972 to 0.997.

Foil Strain Gages and Strain Transducer Comparison. Recall that the small scale glulam specimens were instrumented with foil strain gages and strain transducers (Section **6.2.8.1.1**); in this section, these values are compared to the FBG strain values. In Figure 6.48, a typical response of the sensor strain levels and the applied load are plotted against time.

To investigate that the FBG sensors provided reliable readings, the following comparisons were made:

- The FBG sensor flexural strains were compared to flexural strains for the foil strain gages and strain transducers at the maximum load.
- Each FBG sensor strain was compared to the average strain calculated as the arithmetic mean of all sensor results. Standard deviations were determined to evaluate the response between the FBG sensor response and average strain for all sensors.

External Sensors Strain Comparison. In Figure 6.49 though Figure 6.52, the theoretical upper and lower bound strains (i.e., 522 με and 392 με, respectively), FBG sensors, foil strain gages and strain transducers for compressive and tensile strains are presented for Specimens 1, 3, 5 and 9.

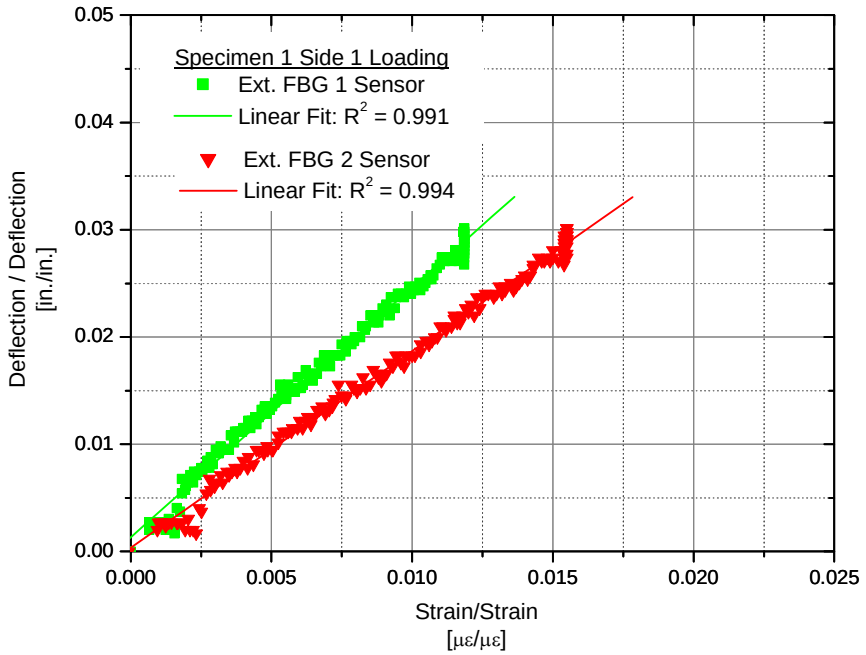

Figure 6.46. Bending Test: Non-Dimensional Strain-Deflection Curves – Specimen 1, Side 1 Loading

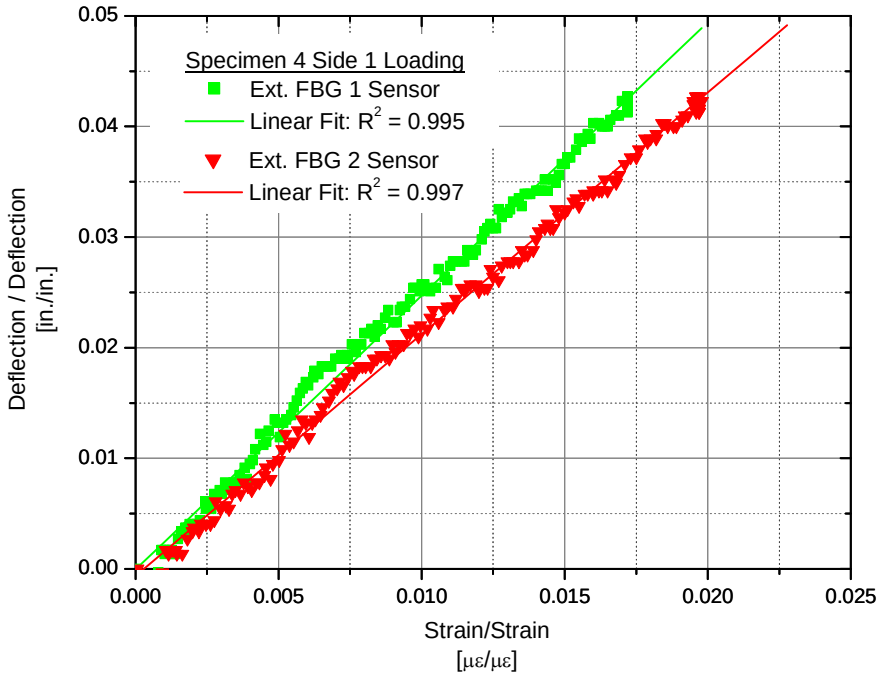

Figure 6.47. Bending Test: Non-Dimensional Strain-Deflection Curves – Specimen 4, Side 1 Loading

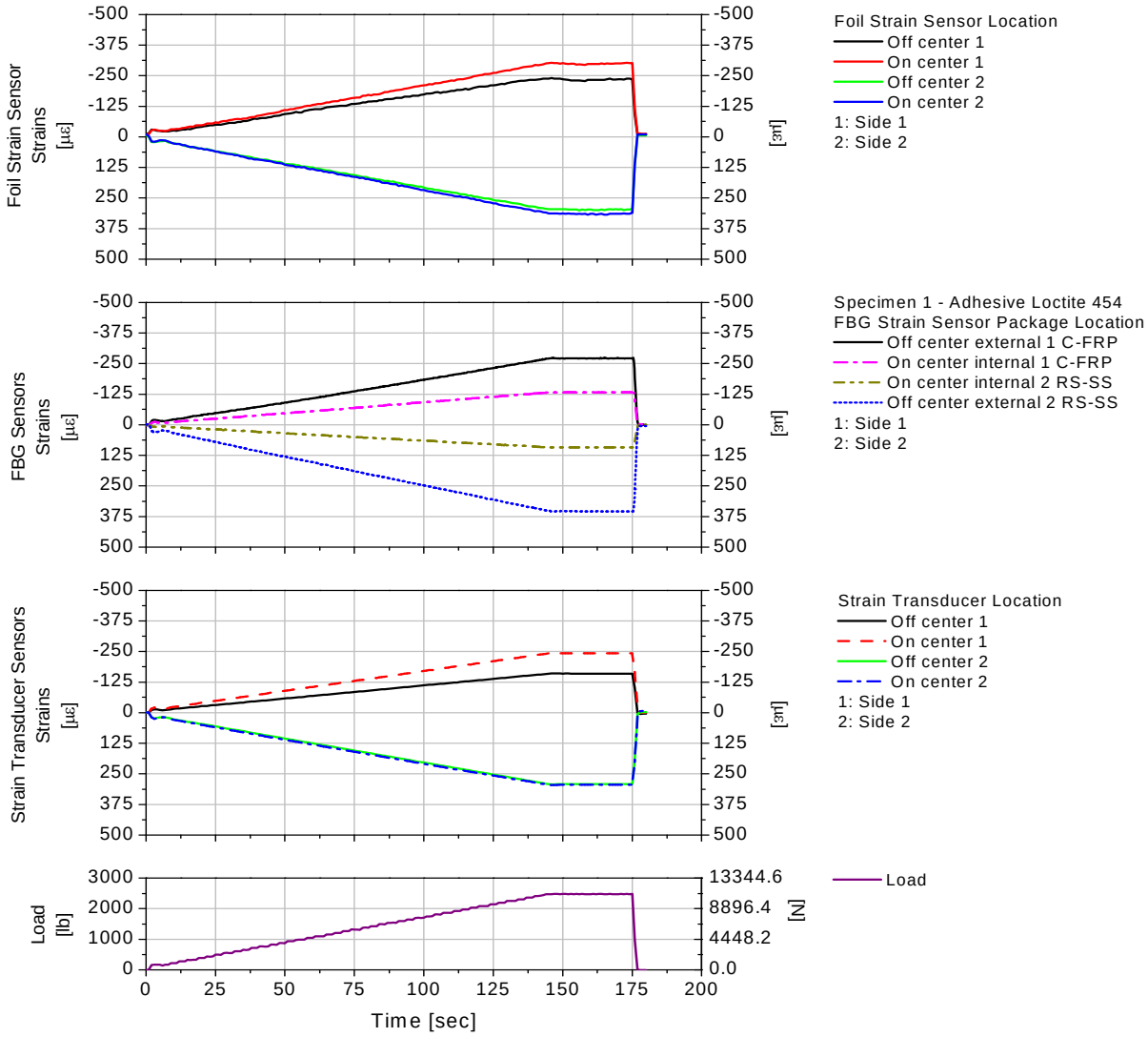

Figure 6.48: Bending Test: Representative Strain History and Load for Three Sensor Types

When comparing data between the FBG sensors and the other sensor types, the following was observed:

- For Specimens 1 and 5, all strains were lower than theoretical values (see Figure 6.49 and Figure 6.51).
- In Specimen 1, Side 1 Loading, the FBG 1 strains differed by approximately 30 με with respect to the both foil strain gages and the on center strain transducer values. However, the differences between the FBG strains and the off center strain transducer values were at least 100 με. In the Side 2 Loading, similar strain differences were observed (see Figure 6.49).
- In Specimen 3, (see Figure 6.50), aside from the fact that the FBG 2 sensor was inoperative,

noticeable strain differences were observed in the other sensor types. The on center sensors' response differed by at least 200 με.

- In Specimens 2 through 8, the FBG sensors were up to 14% different to the other sensor responses (e.g., Figure 6.51).
- In Specimen 9 (Figure 6.52), both FBG sensor strains were smaller than the other sensor types. In the FBG 2 sensors, strain differences were up to 143 με.

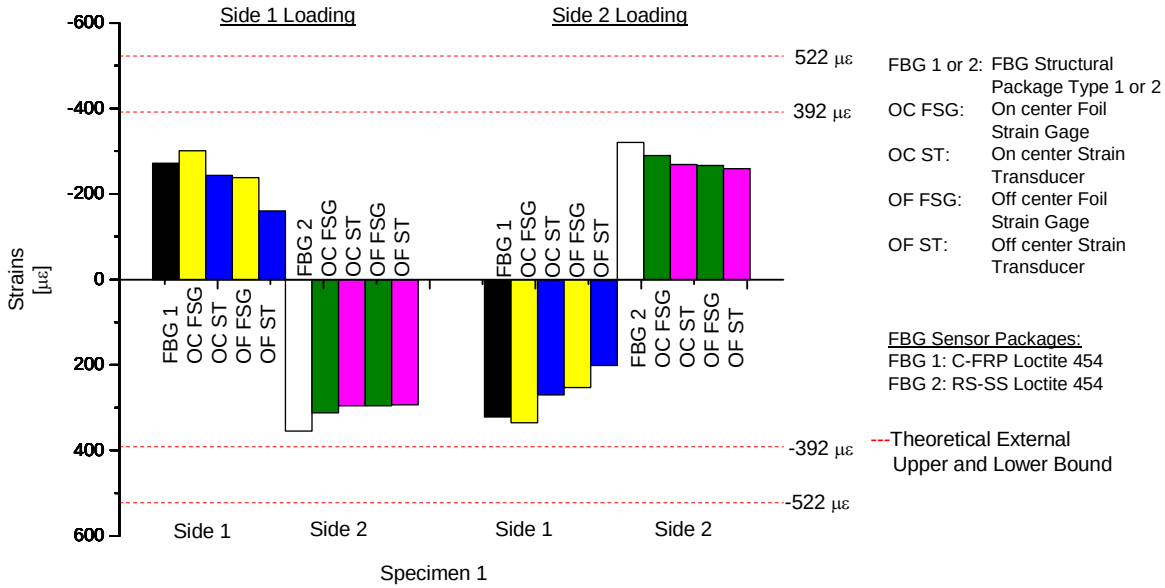

Figure 6.49. Bending Test: Specimen 1 – Experimental External Strains vs. Theoretical Strains

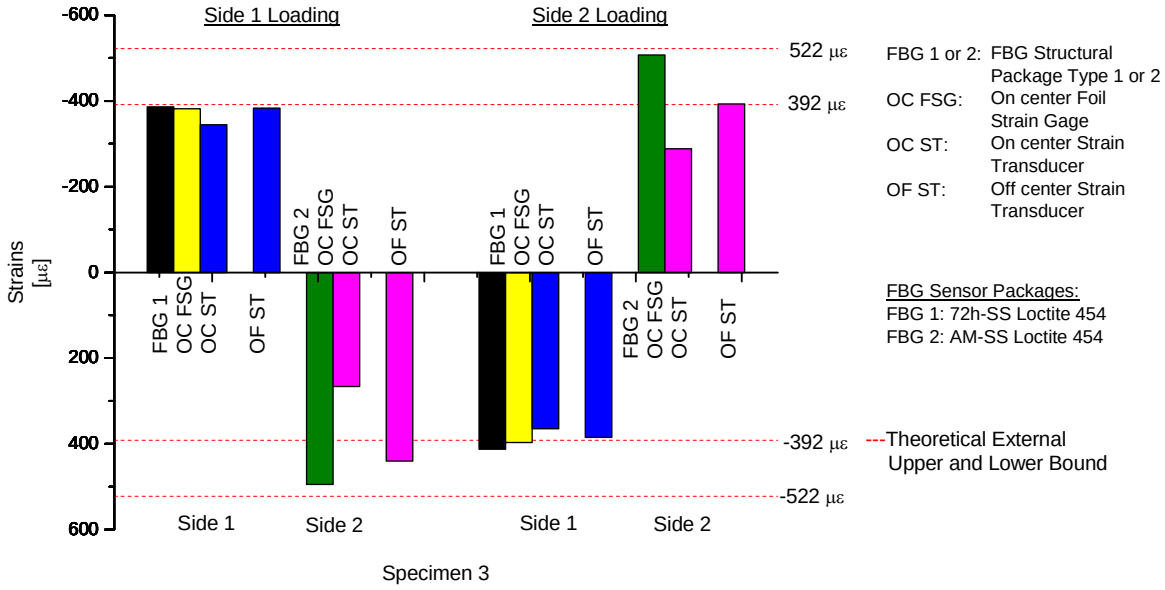

Figure 6.50. Bending Test: Specimen 3 – Experimental External Strains vs. Theoretical Strains

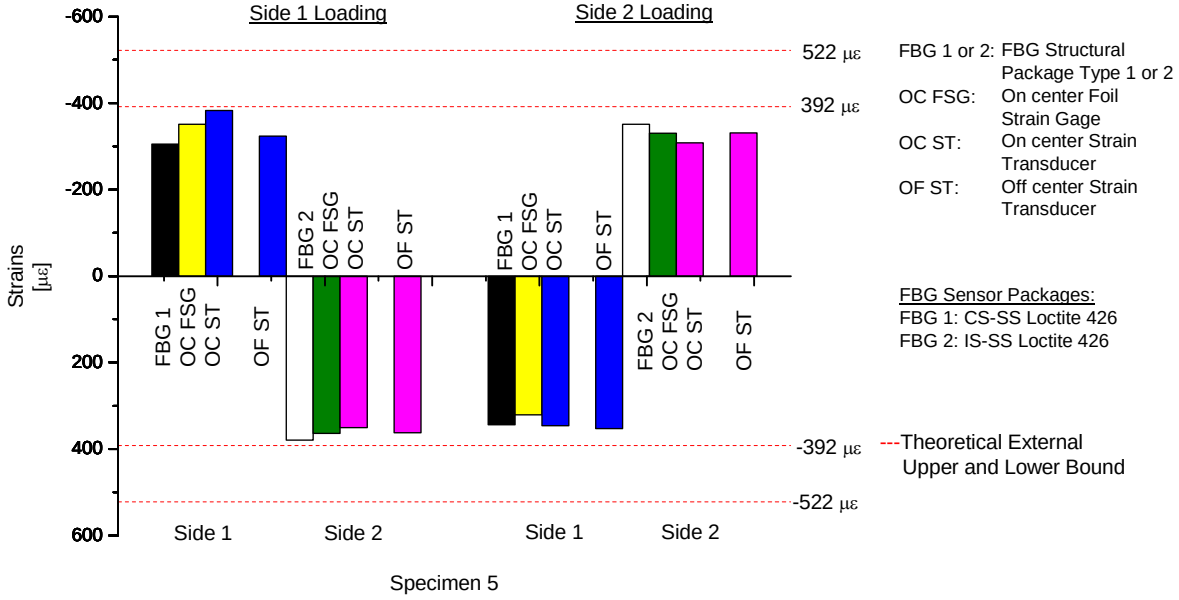

Specimen 5

Figure 6.51. Bending Test: Specimen 5 – Experimental External Strains vs. Theoretical Strains

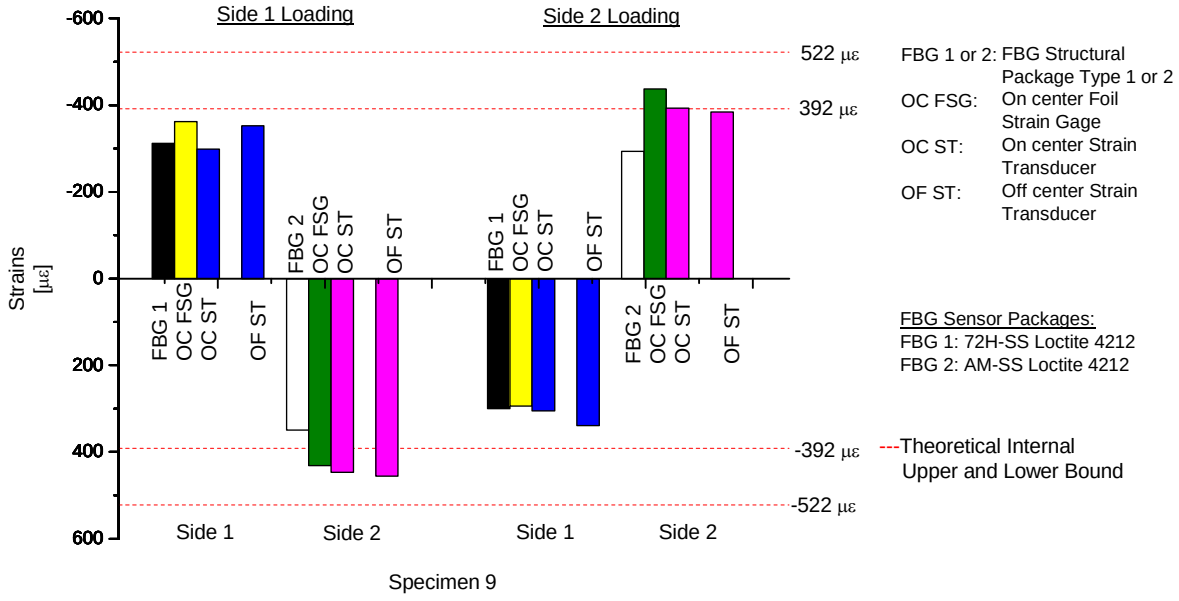

Specimen 9

Figure 6.52. Bending Test: Specimen 9 – Experimental External Strains vs. Theoretical Strains

For all specimens, the strain data for the foil strain gages and strain transducers were lower than the theoretical upper bound strain (i.e., +/-522 με). Comparison of all sensor types indicated that the strain data for the FBG sensors were of the order of magnitude as the other sensors, which indicated

the reliability of the FBG strain data. Note that, as previously explained in section 3.1, the influence of the wood surface irregularities may have altered the strain levels in all sensors.

External Average Strain Comparison. Average strains and associated standard deviations were calculated over all external sensor results to estimate the strain level only at each bending surface, Side 1 and Side 2. The FBG sensor strains were compared to the average strain for all sensors to quantify the strain differences.

As observed in Table 6.12, higher differences were observed among the Specimen 1, FBG 1 and FBG 2 sensors and Specimen 9, FBG 2 sensor strain values and their respective average strains (e.g., between 12% and 22%). In Specimens 1 and 9, FBG 2 sensors, both flexural strains exceeded the standard deviations of the average strains by at least 14 με.

In Specimens 2 through 8, the differences between FBG sensor strains and average strains varied from 0% to 11%. Most FBG sensors' strains were contained within their respective standard deviation of the average strains. Few other FBG sensor strains exceeded this interval by 1 με to 7 με, which can be considered minimal.

With the exception of the Specimen 1 and Specimen 9, the FBG strains varied in the range of the standard variations in most cases. Strain differences were assumed to be at least partially influenced by the inherent wood mechanical properties and/or the localized wood surface irregularities, and/or material properties of the FBG sensor packages.

Internal FBG Strain Comparison. The internal FBG strains were compared to external strain for foil strain gages, strain transducers and external FBG sensors using a linear regression model to assess if the strains were contained in a plane section. The internal strains (predicted internal strains) were calculated at the FBG sensor locations and compared to the experimental internal strain values. Experimental and predicted internal strains with their respective R^2 coefficients are given in Table 6.13. With the exception of the noted FBG sensors at Specimens 1, 3 and 5 (see Table 6.13), the strains differences between the experimental FBG strains and the predicted internal values were between 3% and 19%. Examples of the strain comparison plots for Specimen 1 and Specimen 3 are shown in Figure 6.53 and Figure 6.54, respectively.

Table 6.12. Bending Test: External FBG Sensor vs. Average Strain

Specimen	Loading Side	FBG 1 Sensor			FBG 2 Sensor		
		FBG Strain	Avg. Strain (Std. Dev.)	Difference	FBG Strain	Avg. Strain (Std. Dev.)	Difference
		[με]	[με]	%	[με]	[με]	%
1	*1*	*-272*	*-243 (53)*	*12%*	*355*	*311 (26)*	*14%*
	2	*322*	*276 (54)*	*17%*	*-320*	*-281 (25)*	*14%*
2	1	-345	-358 (9)	-4%	423	399 (27)	6%
	2	370	391 (21)	-5%	-398	-397 (30)	0%
3	1	-386	-374 (20)	3%	---	400 (119)	---
	2	413	390 (20)	6%	---	-396 (110)	---
4	1	-396	-389 (23)	2%	451	436 (25)	3%
	2	427	405 (21)	6%	-422	-415 (37)	2%
5	1	-305	-341 (34)	-10%	380	364 (12)	4%
	2	344	341 (14)	1%	-351	-330 (18)	6%
6	1	-310	-339 (22)	-8%	---	304 (2)	---
	2	358	359 (10)	0%	---	-289 (19)	---
7	1	-260	-260 (18)	0%	283	255 (27)	11%
	2	282	277 (19)	2%	-235	-247 (27)	-5%
8	1	-392	-379 (12)	3%	369	359 (34)	3%
	2	412	405 (16)	2%	-357	-365 (27)	-2%
9	1	-312	-331 (31)	-6%	*349*	*421 (49)*	*-17%*
	2	300	310 (20)	-3%	*-293*	*-377 (60)*	*-22%*

Note. - Avg. Strain: average strain, Std. Dev.: standard deviation, "---": data not available.

Table 6.13. Bending Test Results: Internal FBG Strains vs. Predicted Strains using Linear Regression Calculation (Associated R^2)

Specimen	Loading Side	FBG 1 Sensor			FBG 2 Sensor			R^2
		Internal Strain	Predicted Strain	Percent Diff.	Internal Strain	Predicted Strain	Percent Diff.	
		[με]	[με]		[με]	[με]		
1	1	*-133*	*-69*	*48%*	*92*	*120*	*30%*	0.976
	2	*133*	*96*	*28%*	-87	-93	7%	0.981
2	1	---	-92	---	156	158	1%	0.998
	2	---	127	---	-136	-135	1%	0.997
3	1	*-171*	*-124*	*27%*	132	141	7%	0.971
	2	*168*	*133*	*21%*	-137	-135	1%	0.976
4	1	-140	-117	16%	143	158	10%	0.997
	2	121	129	7%	-149	-144	3%	0.996
5	1	*-171*	*-117*	*32%*	*82*	*119*	*45%*	0.991
	2	*165*	*124*	*25%*	-84	-100	19%	0.996
6	1	-129	-124	4%	86	89	3%	0.998
	2	86	89	3%	-89	-77	13%	0.998
7	1	-109	-90	17%	---	83	---	0.993
	2	113	103	9%	---	-72	---	0.997

Note. - Percent Diff.: percent difference, "---": data not available.

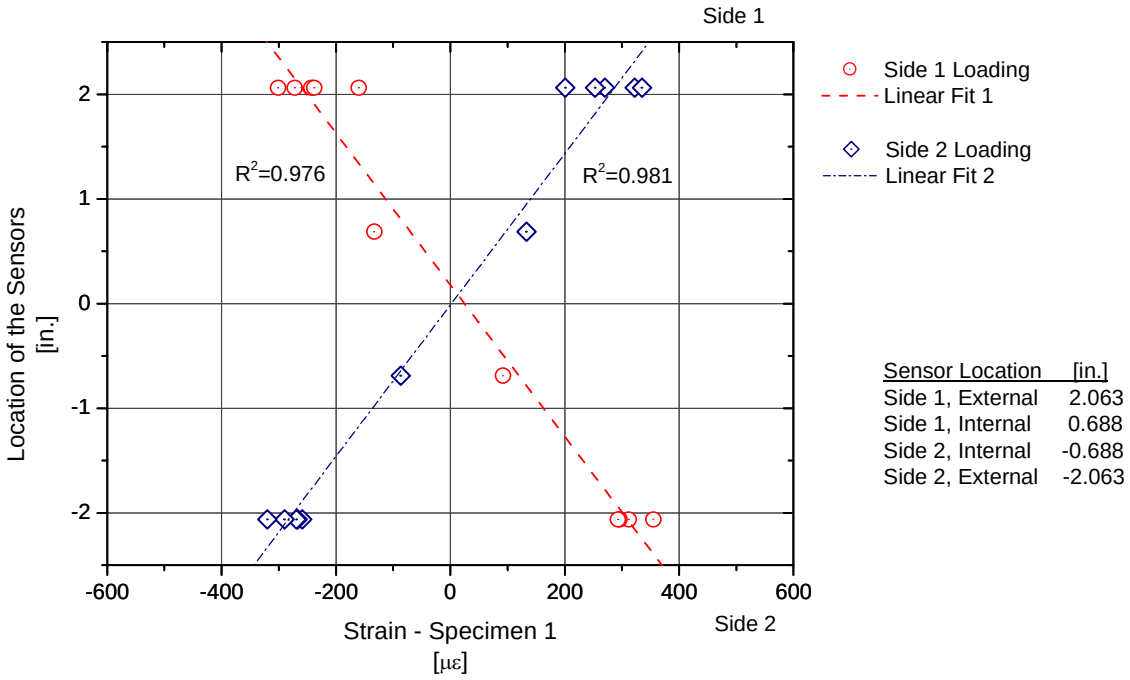

Figure 6.53. Bending Test: Specimen 1 – Strains along the Cross Section at the Maximum Loading

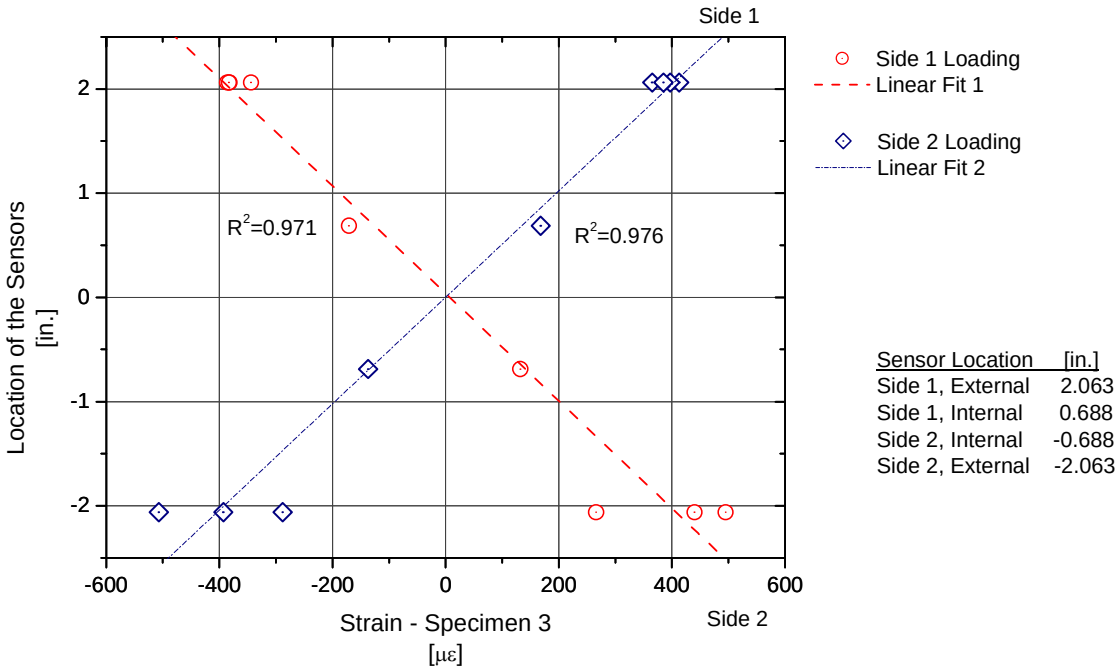

Figure 6.54. Bending Test: Specimen 3 – Strains along the Cross Section at the Maximum Loading

In general, the strain levels were well correlated (i.e., R^2 larger than 0.95). The R^2 coefficients varied from 0.971 (Specimen 3) to 0.998 (Specimen 6) indicating that flexural strains can be

approximated to a plane section. In addition, linear regression calculations were also obtained only for the external strain sensors; the R^2 coefficients were between 0.991 and 0.999. The relative error in predicting the linear strain response for specimens with various external and internal sensors indicated that the sensor error may be independent of the strain magnitude.

6.3.3. INFLUENCE OF MACROSCOPIC WOOD CHARACTERISTICS IN THE EXPERIMENTAL STRAINS

In the light of the strain results, the macroscopic wood characteristics observed in all specimens had influenced the local strain levels. The presence of a knot in Specimen 1, Side 1, demonstrated that wood strains levels were reduced throughout the obtained lower strain levels in the adjacent sensors. In the other specimens, the sensors located at spiral grain had the lowest strain levels while the sensors at the straight grain had relatively high strain levels (i.e., sensors at Specimen 1, Side 2). In Specimen 9, the low FBG 2 strains were not associated to the straight grain orientation. In this FBG sensor with AM-SS Loctite 4212 package, a weak bonding line between both material packages (i.e., aluminum mesh and stainless steel sheet) was suspected.

Overall, despite the efforts to select the top quality uniform wood laminates (i.e., clear straight-grain wood without reducing strength characteristics) on the regions of the sensors' locations, the presence of macroscopic wood characteristics as the slope of grain and knots affected the external and internal FBG sensors' results. In the global behavior of the specimen, the FBG sensors' strains along the cross section were approximately contained in a plane section indicating that the beam theory is present. However, deflection readings were larger than the predicted theoretical values and were only proved to have similar variabilities strain values. In the local behavior of the FBG sensors was affected by the variations in the structure and/or properties of the wood laminates resulting from inherent wood growth characteristics. From the previous evaluation, the FBG sensors have demonstrated to perform in the ranges established by the beam theory and other proven sensors with an acceptable performance. More tests were conducted under different rate of loadings and temperature conditions to prove the effectiveness of the structural FBG sensor packages.

6.3.3.1. FBG STRAIN SENSOR PACKAGE EVALUATION UNDER VARIABLE LOADING AND TEMPERATURE CONDITIONS

The strain performance of the FBG sensors with structural packages was evaluated considering the influence of load duration and temperature variations as established in the bending test methods

described in Section 6.2.8. The specimens were tested with a total load of 2500 lbs as follows:

- Sustained loading tests were performed over 24 hours at uncontrolled laboratory temperatures, with variable increasing and decreasing temperatures.
- Variable load rates of 2500 lbs/min, 5000 lbs/min and 2500 lbs/sec were applied.
- Cyclic rates of loading and unloading of +/-5000 lbs/min and +/-1250 lbs/min.

The main objective of this task was to select the structural FBG sensor package or packages for implementation in a full scale glulam specimen.

6.3.3.1.1. **Sustained Loading Test**

The objective of this test was to evaluate the viscoelastic behavior of the FBG structural packages subjected to 24-hour sustained loading and uncontrolled ambient laboratory temperature. The structural FBG sensor packages' strains were analyzed as follows:

- Comparison of the short term sustained loading strains with the previous bending test results.
- Establishment of a relationship between FBG strains and temperature variations.
- Measurement of residual strains (short term creep deformation), to investigate the viscoelastic behavior of the FBG structural packages (short term creep recovery).

In Figure 6.55, the strain history response of the external and internal FBG sensors for Specimen 1 is shown with the load and laboratory temperature. In Table 6.14, initial peak, final and residual strains are summarized for Specimen 1, Side 1 Loading. After removing the load for three minutes, the residual strains varied from 1.6 με to 14.2 με.

For all specimens, the strain changes were observed to vary with temperature fluctuations. Residual strains also occurred in all eight specimens. At the end of the testing program, the specimens were visually inspected; no sign of deterioration was observed in the packages.

Short Term Strain Comparison. In the initial 15 minutes of the sustained loading (see Figure 6.55), the strains for all specimens were averaged for comparison to the bending test results. The laboratory temperature variations during the 15-min loading were minimal (i.e., +/-0.2 ^{o}F), and strain variations were minimal. The calculated strain dispersions were in the range of +/-1 με, indicating that the strain readings were stable. In this context, the average strains for the bending tests and sustained loading tests were compared. In Figure 6.56, the average strain comparisons are presented for Specimens 1, 4 and 7. Prior to testing, FBG sensor leads for Specimen 6 were damaged during

handling. After the sustained loading test, Side 1 Loading, Specimen 2 was damaged when placed on the testing fixture; however, the FBG sensors were still operative.

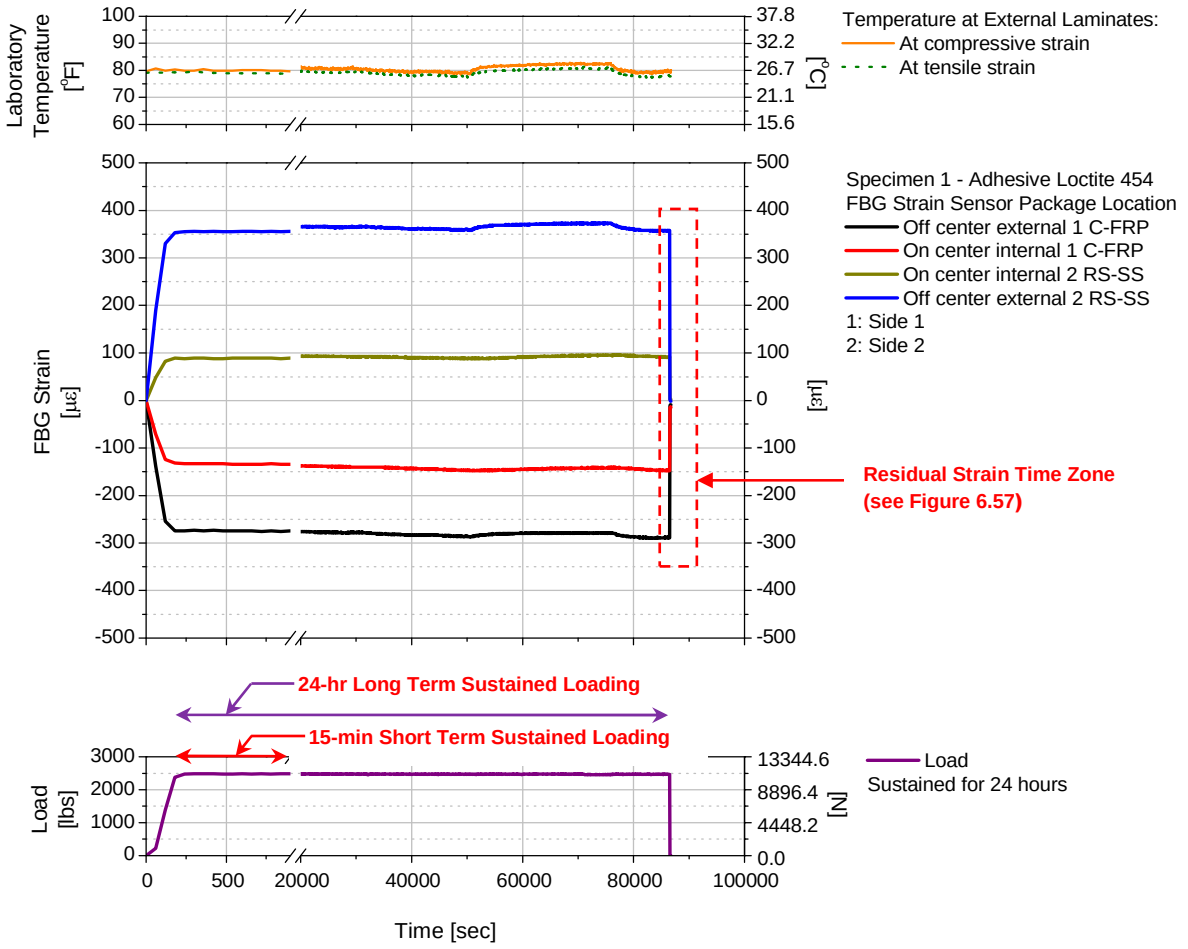

Figure 6.55. Sustained Loading Test: Typical FBG Strains, Temperature and Load vs. Time Responses

Table 6.14. Sustained Loading Test: Summary of the FBG Sensor Strains for Specimen 1, Side 1

Response	Side 1		Side 2		Load	Temperature	
	External [με]	Internal [με]	Internal [με]	External [με]	[lbs]	Side 1 [°F]	Side 2 [°F]
Initial peak	-274.2	-131.7	89.2	353.3	2475.8	79.1	79.9
24-hr loading	-289.2	-147.5	92.5	358.3	2471.9	79.6	77.7
Residual strains	-9.2	-14.2	2.5	-1.6	---	---	---

Based on the average strain comparison, the following observations were made:

- For both Side 1 and Side 2 loading results, the differences between the average strains for the bending and sustained loading tests were between 2 με and 18 με.

- When comparing to the bending test average strains, low sustained loading average strains were observed in four operative sensors for Specimen 1, Side 2 Loading. The low strain levels could be possibly explained by either the weakening of the structural package bonding line or errors in the data collection system. Further investigation of Specimen 1 was necessary to evaluate the FBG sensors readings and conditions after the 24-hour loading.

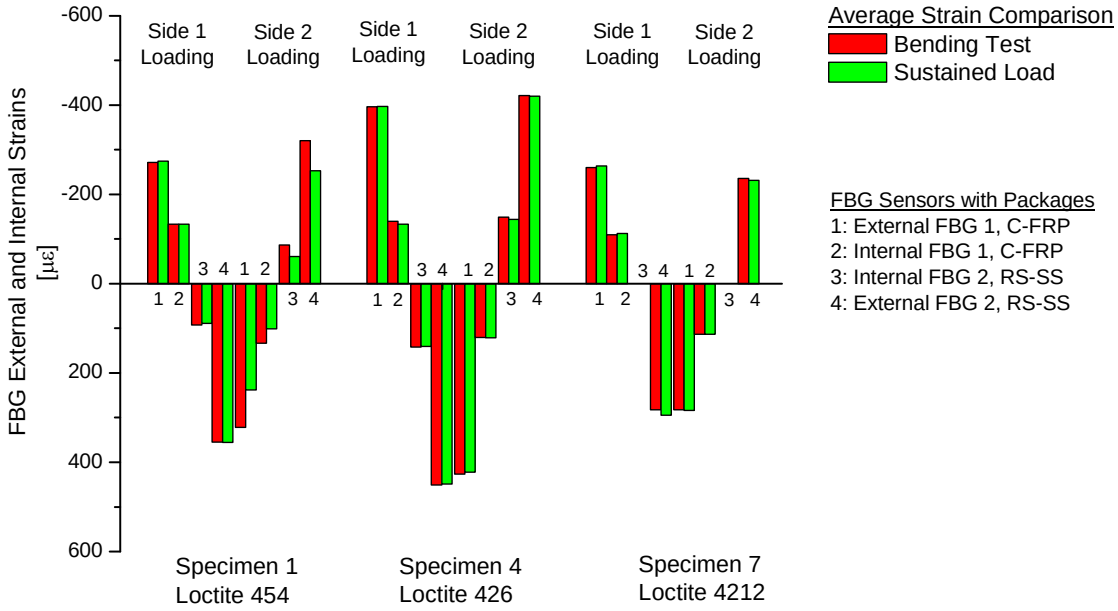

Figure 6.56. Comparison of Initial Strains Between Bending Load Test vs. Sustained Loading Test for Specimens 1, 4 and 7

Strain and Temperature Relationship. The FBG strains from sustained loading varied with the temperature fluctuations over the 24-hour loading period (see Figure 6.55). In this context, the external strain data were compared to temperature variations for 24 hours to determine the strain-temperature relationship.

Prior to the strain-temperature evaluation, thermal coefficients of the specimens and sensor packages were examined. Wood with moisture contents between 8% and 20% (i.e., moisture contents for specimens varied from 8% to 11%) and package materials (i.e., C-FRP, stainless shim and adhesive) will have negligible temperature effect on the package response. However, the only material that could be significantly affected by temperature variations is the bare FBG sensor. The gage factor temperature for a bare FBG strain sensor is approximately 10 pm/^{o}C, while the gage factor due to strains is proportional to 1.2 pm/με.

A linear regression calculation was made for each set of strain and temperature data. R^2 coefficients were obtained for the Sides 1 and 2 loadings for the external FBG sensor strains and the corresponding temperature data. In Table 6.15, R^2 coefficients and associated standard deviations for the temperature data are presented per package. The calculated R^2 coefficients varied from 0.000 to 0.975 (i.e., in Specimen 4 and Specimen 5 respectively).

Table 6.15. Sustained Loading Test: Linear Regression between Strains and Temperatures

Specimen	Structural Package	R^2 Coefficient Side 1 Loading		Temp. Std. Dev. [°F]	R^2 Coefficient Side 2 Loading		Temp. Std. Dev. [°F]
1	C-FPP – Loctite 454	0.791	(C)	1.1	0.421	(T)	0.4
	RS-SS – Loctite 454	0.237	(T)	0.9	0.429	(C)	0.3
4	C-FPP – Loctite 426	*0.000*	*(C)*	*2.1*	*0.951*	*(T)*	*1.6*
	RS-SS – Loctite 426	0.879	(T)	2.0	0.331	(C)	1.4
7	C-FPP – Loctite 4212	0.171	(C)	1.2	0.804	(T)	1.5
	RS-SS – Loctite 4212	0.722	(T)	1.1	0.890	(C)	2.0
2	IS-SS – Loctite 454	0.697	(C)	0.8	---	---	---
	CS-SS – Loctite 454	0.356	(T)	0.9	---	---	---
5	CS-SS – Loctite 426	0.669	(C)	0.7	0.708	(T)	1.4
	IS-SS – Loctite 426	0.255	(T)	0.8	0.975	(C)	1.6
8	CS-SS – Loctite 4212	0.697	(C)	0.5	0.935	(T)	4.0
	IS-SS – Loctite 4212	0.274	(T)	0.6	0.961	(C)	3.6
3	72H-SS – Loctite 454	0.311	(C)	0.9	0.671	(T)	1.9
	AM-SS – Loctite 454	---	---	1.1	---	---	2.6
6	72H-SS – Loctite 426	0.772	(C)	2.8	---	---	---
	AM-SS – Loctite 426	---	---	3.7	---	---	---
9	72H-SS – Loctite 4212	0.562	(C)	0.6	0.858	(T)	1.2
	AM-SS – Loctite 4212	0.251	(T)	0.8	0.439	(C)	1.0

Note. - Temp: temperature, Std. Dev.: standard deviation.
"---" indicates an inoperative FBG sensor.

In general, R^2 coefficients above 0.95 indicated a well correlation between strain and temperature (e.g., Side 2 Loading responses of Specimens 4, 5, and 8). In contrast, low R^2 coefficients (less than 0.95) indicated that the strain levels were partially affected by temperature variations. Other factor that influenced in the strain response was possibly attributed to the viscoelastic behavior of the package material components under the sustained loading. For a 24-hour loading, the only material that could have been affected by the loading was the adhesive that bonded the structural FBG sensor packages to the glulam specimens.

Residual Strain Evaluation. From the close up of Figure 6.55, "Residual Strain Time Zone", the typical strain levels before and after removing the load are shown in Figure 6.57 (a) for Specimen 1, Side 1 Loading. As observed in Figure 6.57 (b), the residual strain levels gradually decreased over three minutes. As noted in Table 6.14, the residual strains levels at the end of the collected data were between 1.6 με and 14.2 με.

Wood exhibits viscoelastic behavior when subjected to time-dependent loads (i.e., for short term and load term, deformations are not immediately recovered after the removal of the load). However, the residual deformations should disappear over a period of time after the unloading (Ritter, 1992). Similar to wood, the structural adhesives bonding the packages to glulam specimen are viscoelastic materials. However, after a 24-hour loading, wood was expected to behave elastically and consequently not to deform. After the sustained load removal, residual strains existed for all sensor packages and were attributed to the viscoelastic behavior of the adhesive.

One way to measure the viscoelastic strain recovery was through the rate of recovery, defined as the residual strain reduction per unit of time. For each FBG sensor, the residual strains were collected for periods between 3 and 15 minutes. During this time, the temperature fluctuations were negligible (i.e., 0.2^{o}F). The positive rates of recovery were defined as the strain decrease over time; in contrast, negative values were interpreted as the "no strain recovery" of the adhesive. In Table 6.16, the calculated strain rate of recovery and the final residual strains at the end of the data recording are given for Specimens 1, 3 and 7. For Specimen 1, Side 2 Loading, the residual strains were between 15.0 με and 59.2 με. In addition, the rates of recovery were negative in all cases. The larger residual strain levels could be possibly explained by either the structural package bonding line weakening or data collection errors.

To examine the recovery of the FBG sensor packages, rates of recovery were compared after both Side 1 and 2 Loadings. For most specimens, the positive rates of recovery associated with small strain levels demonstrated the creep recovery (see Table 6.16, Specimen 9, FBG 1 sensor). However, other package adhesives had residual strains with negative rate of recovery (see Table 6.16, Specimen 1, FBG 2 sensor). However, other package adhesives had residual strains with negative rate of recovery (see Table 6.16, Specimen 1, FBG 2 sensor). In Figure 6.58, the residual strain history for two operative FBG sensors at Specimen 9 is presented. After the Side 1 and Side 2

Loadings, one of FBG sensor packages (external 72H-SS Loctite 4212) showed residual strain levels that decreased to 4.2 με over 10 minutes.

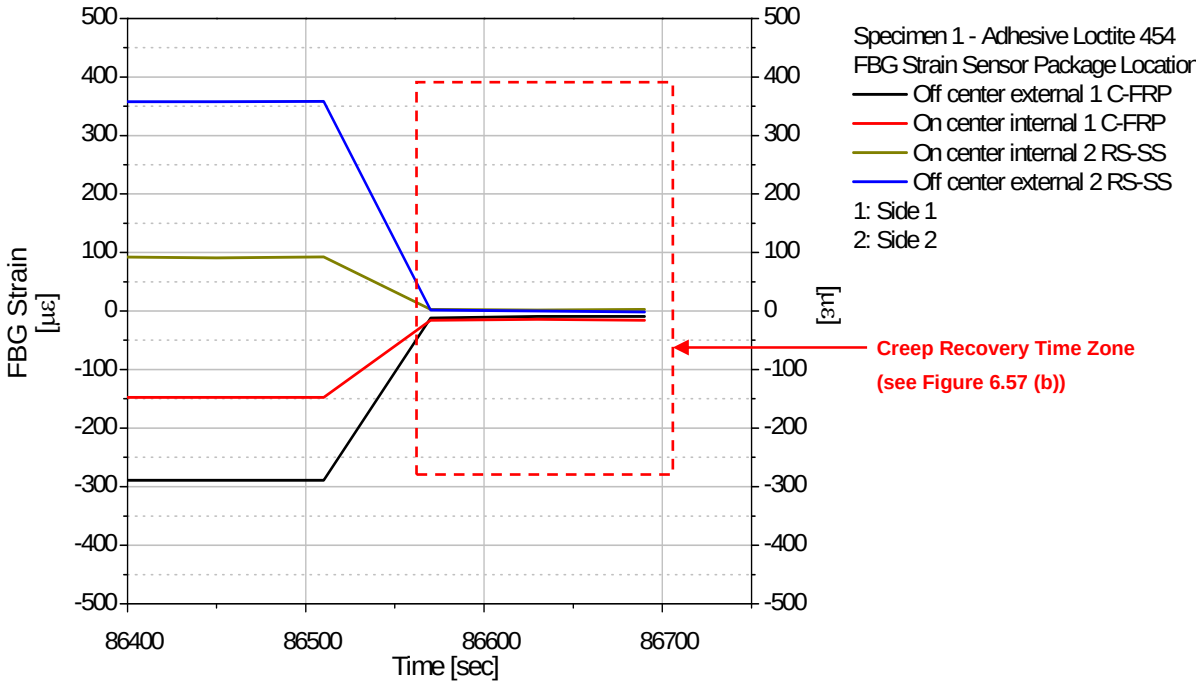

(a) Residual Strains for Specimen 1, Side 1 Loading (see Figure 6.55)

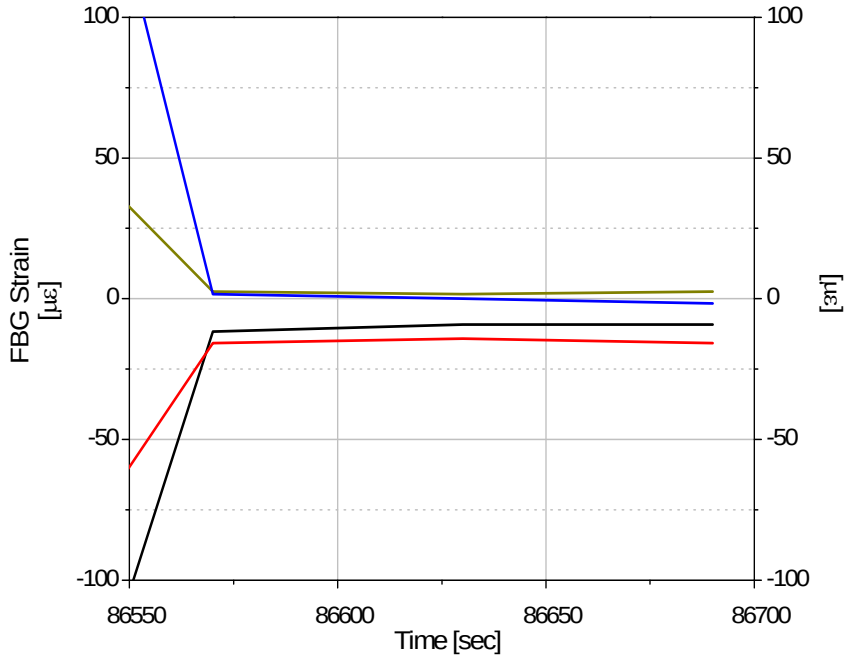

(b) Creep Recovery Time Zone (see Figure 6.57 (a))

Figure 6.57. Sustained Loading Test: Residual Strains After Unloading for Specimen 1, Side 1 Loading

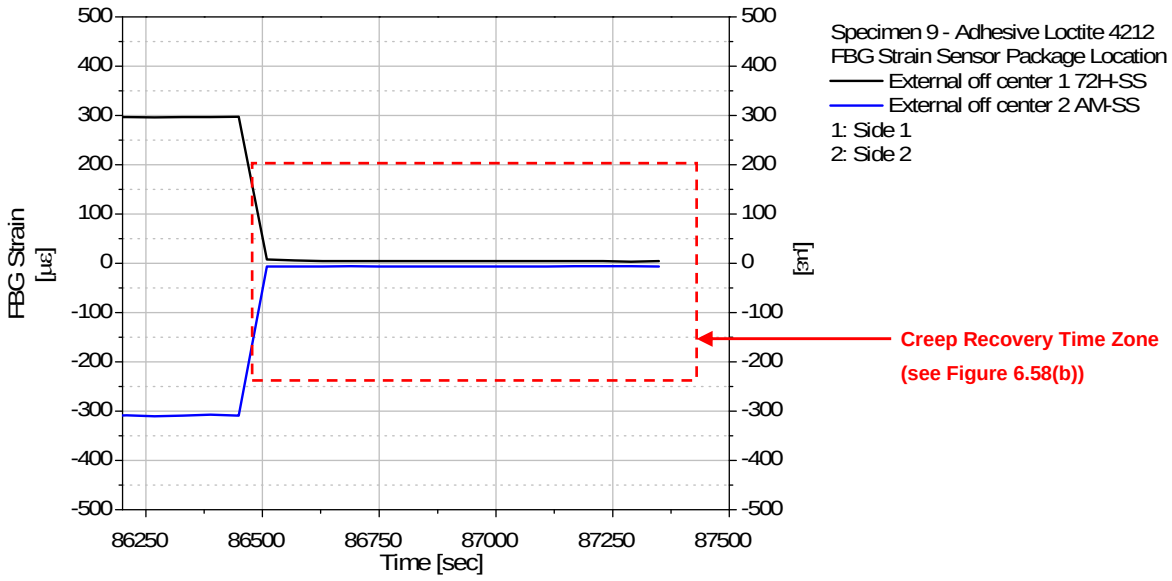

(a) Residual Strains Time Zone

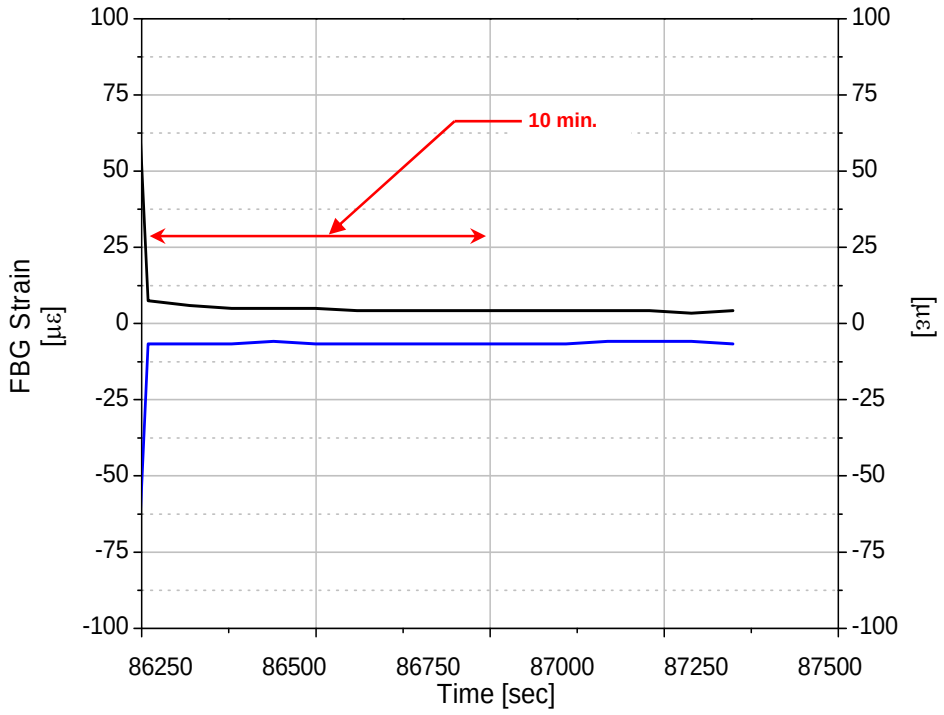

(b) Creep Recovery Time Zone

Figure 6.58. Sustained Loading Test: Residual Strains After Unloading for Specimen 9, Side 2 Loading

From the evaluation of the rate of recovery, six FBG sensor packages with positive rates of recovery that resulted in residual strains between 1.7 με and 26.7 με were identified for the Side 1 sustained loading tests. Though in the residual strains for the Side 2 sustained loading test were

larger (i.e., between 4.2 με and 45.0 με), the rates of recovery indicated the possible recovery of the packages. The six FBG sensor packages are given in Table 6.17 for further information.

Table 6.16. Sustained Loading Test: Residual Strains After 24 hours and Rate of Recovery per Hour for Specimens 1, 5 and 7

Specimen	Loading Side	External FBG 1		Internal FBG 1		Internal FBG 2		External FBG 2	
		Rate of Recovery	Res. Strain	Rate of Recovery	Res. Strain	Rate of Recovery	Res. Strain	Rate of Recovery.	Res. Strain
		[με/hr.]	[με]	[με/hr.]	[με]	[με/hr.]	[με]	[με/hr.]	[με]
1	1	11.5	-9.2	7.7	-14.2	0.0	2.5	-19.2	-2.5
	2	*-15.4*	*-59.2*	*-15.4*	*-15.0*	*-3.8*	*31.7*	*-23.1*	*58.3*
3	1	15.6	1.7	9.4	-11.7	6.3	0.0	---	---
	2	-16.7	5.0	-6.7	-8.3	13.3	-15.8	---	---
9	1	4.0	0.8	---	---	---	---	2.0	2.5
	2	15.4	4.2	---	---	---	---	0.0	-6.7

Note. - "---" indicates an inoperative FBG sensor.

Table 6.17. Sustained Loading Test: Selected Structural FBG Sensor Packages

Specimen	Structural Package	Side 1 Loading		Side 2 Loading	
		Rate of Recovery	Residual Strains	Rate of Recovery	Residual Strains
		[με/hr]	[με]	[με/hr]	[με]
4	External C-FPP – Loctite 426	42.3	-1.7	35.7	5.0
4	External RS-SS – Loctite 426	69.2	2.5	50.0	-31.7
8	External IS-SS – Loctite 4212	18.8	10.0	33.3	-45.0
9	External 72H-SS – Loctite 4212	4.0	0.8	15.4	4.2
3	Internal AM-SS – Loctite 454	6.3	0.0	13.3	-15.8
4	Internal RS-SS – Loctite 426	26.9	26.7	28.6	-15.8

All external FBG sensor packages were visually inspected to detect any physical deterioration. No damage was observed confirming the accuracy of the strain reading during and after loading.

From the Sustained Loading Tests, the following observations were drawn:

- The comparison of the bending and sustained loading strains confirmed that the FBG structural packages had similar EI values. Only for Specimen 1, Side 2 Loading, the low strains for all FBG sensors could be possibly explained by either the structural package bonding line weakening or data collection errors.

- Strain levels varied with uncontrolled laboratory temperature fluctuations. The linear correlations indicated that the sustained load strain data and temperature variation were partially related.
- The viscoelastic behavior was present in the adhesive (i.e., part of the strain deformation during the 24 hour loading and residual strains after the load removal). Only six packages, after completing the Side 1 and Side 2 sustained loadings showed creep recovery over periods below 10 minutes. The evaluation of the rate of recovery was a useful tool to predict the creep recovery of the structural FBG sensor packages.
- No sign of deterioration/damage was observed in the packages.

6.3.3.1.2. **Accelerated Loading Test**

The accelerated loading tests were intended to understand the behavior of the adhesive bond on the FBG sensors subjected to an initial accelerated loading. The main objective of these tests was to evaluate the viscoelastic behavior of the FBG structural packages subjected to 2500 lbs with three different rates of accelerated loadings (i.e., varying from 1 minute, 30 seconds and 1 second), followed by a constant sustained loading of twenty minutes before the removal of the load. Three different rates of loading were applied varying from the level of the bending test of 2500 lbs/min, increasing to 5000 lbs/min and to an instantaneous pulse of 2500 lbs/sec.

In Figure 6.59, the typical FBG strain history for an initial rate of loading of 2500 lbs/sec along with the load and ambient temperature is presented. In the accelerated loading time zone (see Figure 6.59), the applied accelerated load increased in two steps. During the first six seconds, the load increased to approximately 200 lbs and the rest of the effective load was applied in one second. As observed, the strain levels increased along with the peak load, stabilized in the following 3 to 6 seconds and remained constant to a load of 2500 lbs for another 15 minutes. For the 2500 lbs/min and 5000 lbs/min accelerated loading tests, strains increased in one step and stabilized in less than 2 seconds (see Figure 6.60 “Accelerated Loading Time Zone”). In the laboratory, the ambient temperatures fluctuated in the range of +/-0.6 ^{o}F, inducing strain levels in the range of the sensor precision (+/-2.0 $\mu\varepsilon$).

The impact of the accelerated loading tests on the FBG sensor packages was studied as follows:

- Comparison of the 2500 lbs/min accelerated loading with the bending loading tests to assess the initial conditions of the packages (EI parameter).

- Comparison of the 2500 and 5000 lbs/min accelerated loading peak strains for the purpose of evaluating the conditions of the packages (EI parameter) after accelerated loadings.
- Comparison of the 2500 lbs/min and 2500 lbs/sec accelerated loading results for evaluating the conditions of the packages upon a higher loading rate (EI parameter).
- Evaluation of the FBG sensor package final conditions after completing the accelerated loading test program through residual strain values and visual inspection.

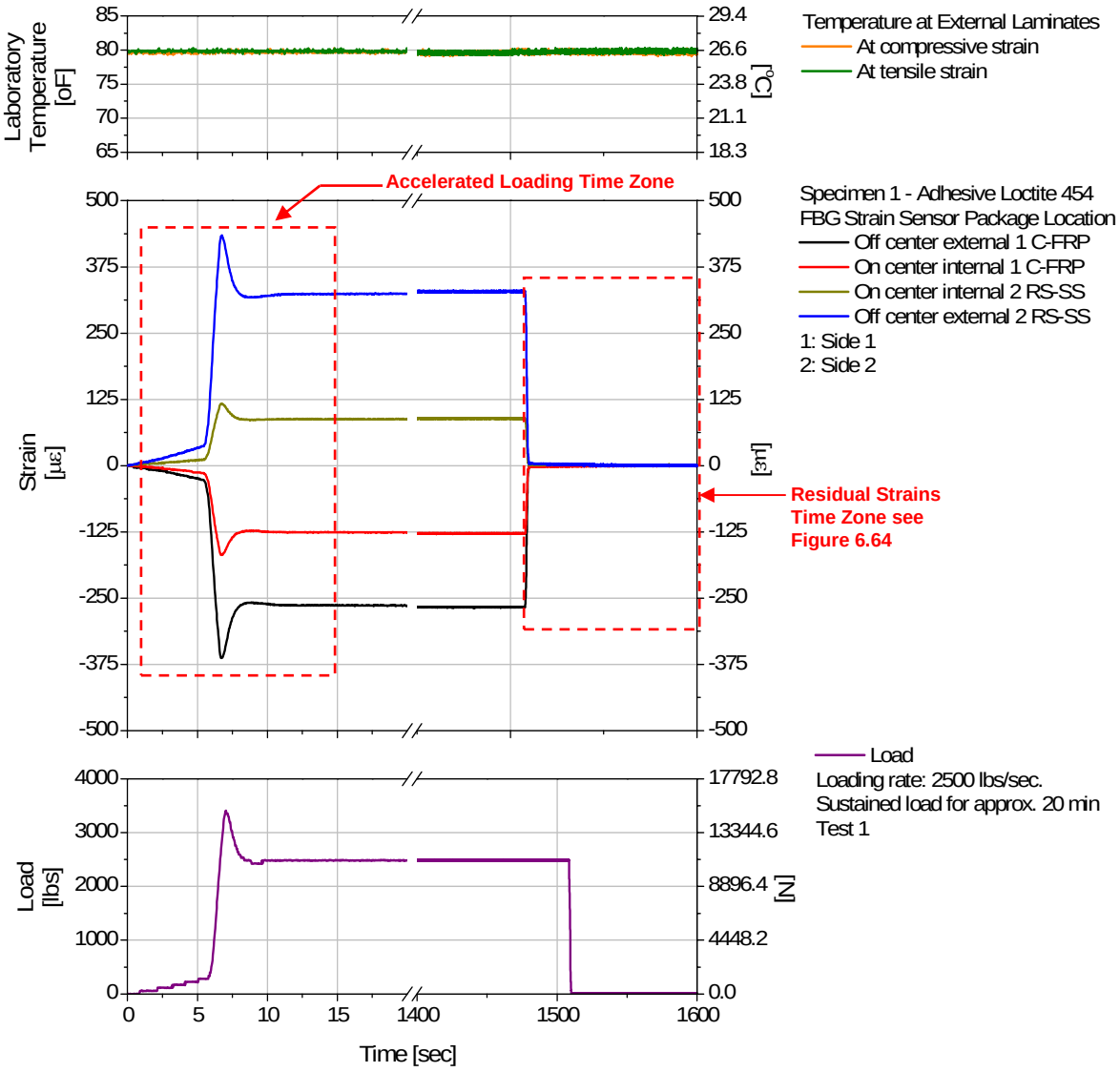

Figure 6.59. Accelerated Loading Test – 2500 lbs/sec: Load, Strain and Temperature vs. Time for Specimen 1, Side 1 Loading

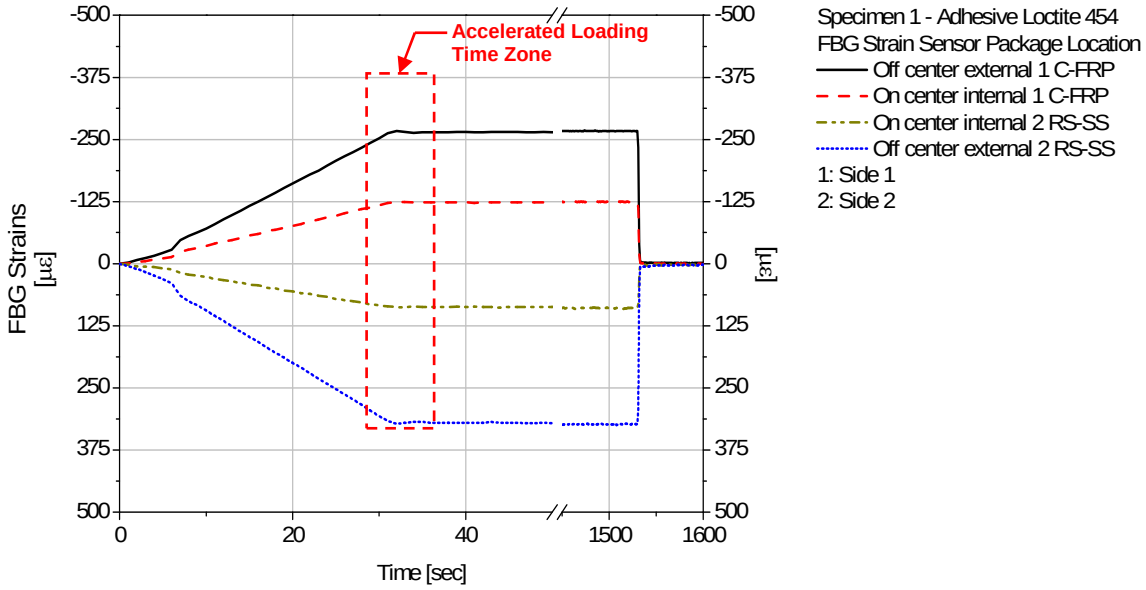

Figure 6.60. Accelerated Loading Test – 5000 lbs/min: Strain vs. Time for Specimen 1, Side 1 Loading

Comparison of the 2500-lbs/min Accelerated Loading and Bending Loading Test. Average strains determined in both tests were compared for purpose of verifying the repeatability of sensor response. Note that for the 2500 accelerated loading test, Specimen 6 with inoperative FBG sensors was not tested. After completing the Side 1 Loading test series, Specimen 2 was not operative (specimen damaged during handling on the testing machine). During the constant sustained loading, the strain dispersions were in the order of the sensor precision, which indicated the strain data were stable. In Figure 6.61, the bending loading and accelerated loading results are presented for Specimens 1, 4 and 7.

The following observations summarize the conditions of the FBG structural packages subjected to the 2500 lbs/min accelerated loading with respect to the bending results:

- For the Side 1 Loading, the accelerated loading average strains were on the order of the bending average values; the strain differences ranged from 2 με to 14 με. However, for the Specimen 1, external FBG 2 sensor, the accelerated loading strains were 41 με lower than the bending loading value. Possible changes in the EI parameter on the package could be attributed to the adhesive bonding line. No visible damage was observed.
- For the Side 2 Loading, the strain differences were in most cases lower than 15 με. In Specimen 1, the four FBG sensors had higher compressive and tensile strains at the 2500 lbs/min accelerated loading test, which could indicate changes in the adhesive bonding line.

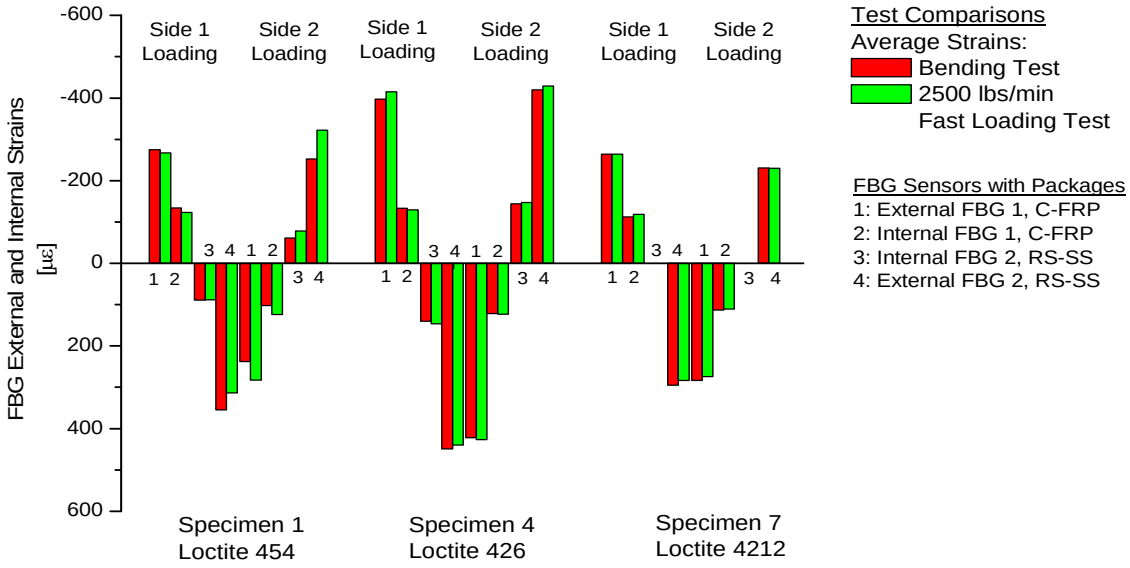

Figure 6.61. Comparison of the 2500 lbs/min Accelerated Loading Test and Bending Test Results for Specimens 1, 4 and 7

Based on the test 2500-lbs/min accelerated loading results, with exception of Specimen 1, the rest of FBG sensor packages had similar strain levels (EI parameter) than the previous bending test results.

Comparison of the 2500 and 5000 lbs/min Accelerated Loading Tests. After applying the load of 2500 lbs at rates for 2500 and 5000 lbs/min, both strains and load were found to be stable in less than two seconds (see see Figure 6.60 "Accelerated Loading Time Zone"). In Figure 6.62, peak strains compared to their respective average strains are plotted for accelerated loading rates of 2500 lbs/min and 5000 lbs/min. Typically, strain differences between the peak strains and average strains were found to be below 6 με, for both accelerated loading tests. During the constant sustained loading, the average strains had standard deviations below +/- 3.0 με.

Based on both test comparisons, the FBG sensors possessed similar strain levels indicating that the packages have consistent EI parameters for the two different loading rates. After removing the load, residual strains were observed at the end of both loading tests in all packages. For the 2500 lbs/min, the residual strains were less than 15.8 με; while for the 5000 lbs/min, the strain levels were less than 7.0 με. When inspecting each strain history, the strain recovery was observed in all tests confirming the viscoelastic behavior of the packages.

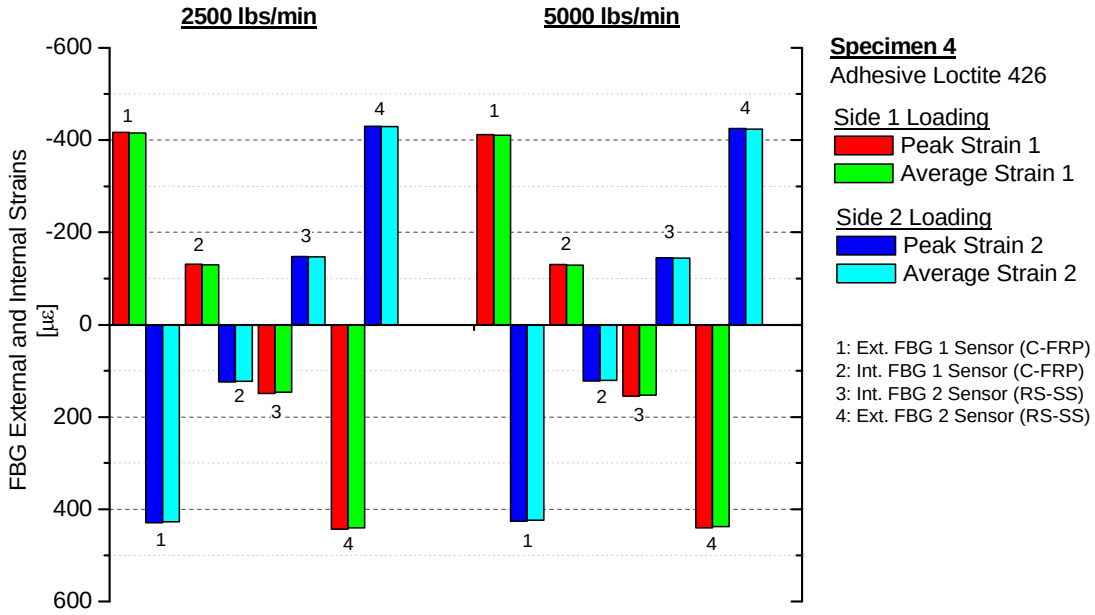

Figure 6.62. Representative Peak and Average Strain Comparisons for 5000 lbs/min and 2500 lbs/min Accelerated Loading Tests for Specimen 4

Comparison of the 2500 lbs/min and 2500 lbs/sec Accelerated Loading Tests. In Figure 6.63, strain comparisons for both accelerated loading tests are presented for Specimen 4; and in Table 6.18, the strain results for the selected FBG structural packages are given. As observed in Figure 6.59 ("accelerated loading time zone"), higher strain levels were instantaneously obtained per sensor packages upon the 2500 lbs/sec accelerated loading. Peak strains were above 30% higher than the average strain values (see Table 6.18). In each specimen, the 2500 lbs/sec accelerated loading test was repeated twice and the strain reproducibility was verified in all specimens. The strain dispersions for the 2500 lbs/sec tests were in the range of +/-3 με, indicating that the strain levels were stable during the constant loading. The average strain levels for the 2500 lbs/sec accelerated loading test were compared to the 2,500 lbs/min test values. The differences between both average strains were less than 7.0 με. (e.g., see Table 6.18). In general, strain differences between average strains indicated that the sensor packages had similar EI parameters after subjecting the specimens to 2500 lbs/min and 2500 lbs/sec accelerated loading tests.

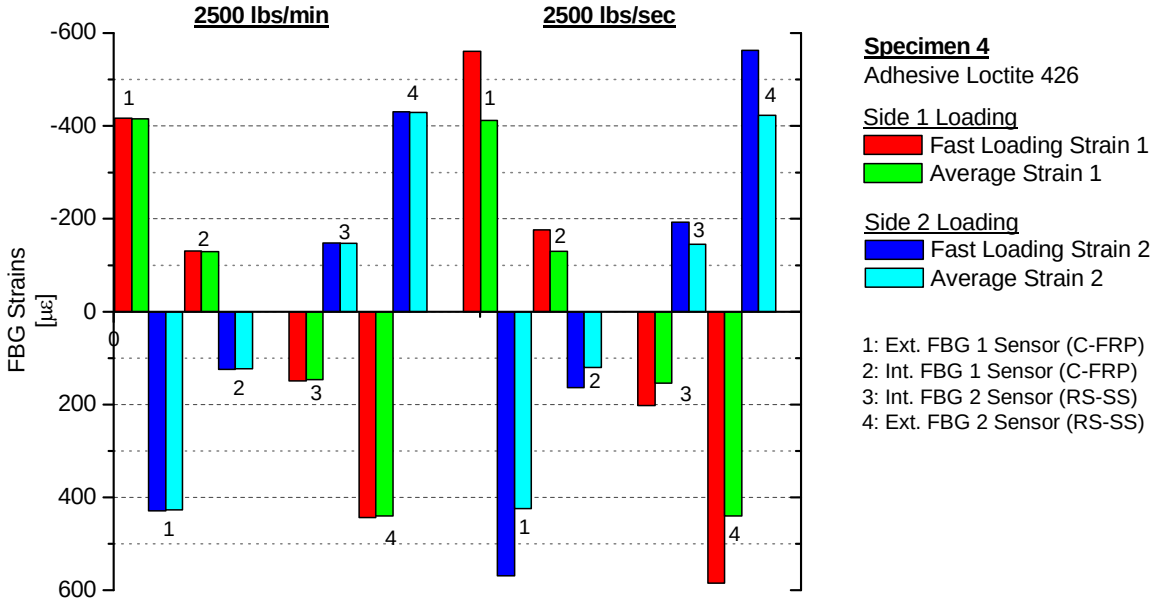

Figure 6.63. Comparison of 2500 lbs/min and 2500 lbs/sec Accelerated Loading Tests: Peak and Average Strains for Specimen 4

Table 6.18. Comparison of 2500-lbs/min and 2500-lbs/sec Accelerated Loading Test for the Selected FBG Structural Packages

FBG Sensor (Package)	Loading Side	Rate of Loading	Peak Strain	Average Strain	Increment	Std. Dev.	Residual Strain
			[με]	[με]	[%]	[με]	[με]
Specimen 4	1	2500 lbs/min	-416.7	-415.4	0%	0.8	-1.7
Ext. FBG 1 Sensor		2500 lbs/sec	-560.8	-412.2	36%	0.5	0.0
(C-FRP Loctite 426)	2	2500 lbs/min	429.2	427.3	0%	1.6	9.2
		2500 lbs/sec	568.3	424.4	34%	1.1	5.8
Specimen 4	1	2500 lbs/min	443.3	439.9	1%	2.6	6.7
Ext. FBG 2 Sensor		2500 lbs/sec	585.0	440.1	33%	1.6	3.3
(RS-SS Loctite 426)	2	2500 lbs/min	-430.0	-428.7	0%	1.2	-5.8
		2500 lbs/sec	-562.5	-422.9	33%	1.6	9.2
Specimen 8	1	2500 lbs/min	359.2	357.3	1%	1.3	15.8
Ext. FBG 2 Sensor		2500 lbs/sec	466.7	357.2	31%	1.0	4.2
(IS-SS Loctite 4212)	2	2500 lbs/min	-351.7	-350.7	0%	0.8	-0.8
		2500 lbs/sec	-504.2	-355.1	42%	1.2	-3.3
Specimen 9	1	2500 lbs/min	-308.3	-306.5	1%	0.8	0.0
Ext. FBG 1 Sensor		2500 lbs/sec	-433.3	-308.3	40%	0.9	-3.3
(RS-SS Loctite 4212)	2	2500 lbs/min	297.5	296.2	0%	1.1	3.3
		2500 lbs/sec	418.3	291.7	43%	0.7	1.7
Specimen 3	1	2500 lbs/min	134.2	132.4	1%	0.9	3.3
Int. FBG 2 Sensor		2500 lbs/sec	185.0	132.0	40%	0.9	2.5
(RS-SS Loctite 454)	2	2500 lbs/min	-138.3	-136.7	1%	0.5	-0.8
		2500 lbs/sec	-235.8	-137.8	71%	0.6	0.0
Specimen 4	1	2500 lbs/min	149.2	146.4	2%	1.5	5.0
Int. FBG 2 Sensor		2500 lbs/sec	202.5	153.5	32%	1.3	3.3
(RS-SS Loctite 426)	2	2500 lbs/min	-147.5	-147.0	0%	0.5	-0.8
		2500 lbs/sec	-193.3	-145.3	33%	0.8	4.2

Final Conditions of the Structural FBG Sensor Packages. To evaluate the structural condition of the packages after removing the load, the residual strains were assessed. In Figure 6.64, the residual strains are presented for Specimen 1 after being subjected to a 25000 lbs/sec accelerated loading over three minutes. The residual strain levels were less than 2.5 με. For the 2500 lbs/min accelerated tests, the residual strains for the six selected packages ranged between 0.8 and 15.8 με (noted in Table 6.18). While for the 2500 lbs/sec accelerated loading tests, the residual strains varied from 0.0 με to 9.2 με. Therefore, the residual strains for all specimens after the accelerated loading tests were small. Once the testing program was completed, the structural FBG sensor packages were visually inspected. No sign of deterioration was observed in any package.

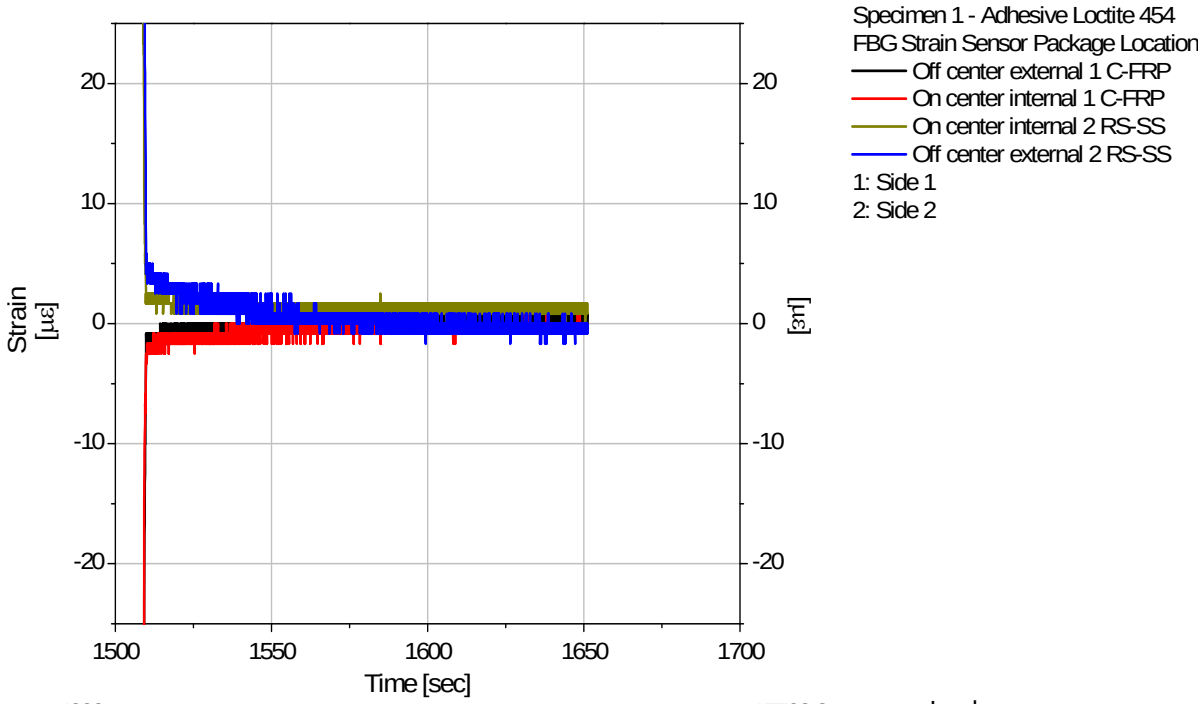

Figure 6.64. 2500-lbs/sec Accelerated Loading Test: Residual Strains for Specimen 4, Side 2 Loading (See "Residual Strains Time Zone in Figure 6.59)

From the accelerated loading testing program, the following observations were made:

- With exception of the Specimen 1, similar average strains between the 2500 lbs/min accelerated loading and the bending test results confirmed that the structural FBG sensor packages had similar EI parameters.

- The 2500 lbs/min and 5000 lbs/min accelerated loading tests had similar impact in the FBG structural packages. For both accelerated loading tests, the differences between the peak strains and respective average strains were less than 6 με.
- Higher peak strains resulted from the 2500 lbs/sec accelerated loading tests. After the stabilized loading, the strain levels at a constant sustained loading of 2500 lbs were comparable to the 2500 lbs/min accelerated loading test results. The average strain differences were below 7 με. For all specimens, the package EI parameters were maintained after completing the accelerated testing protocol.
- For the three accelerated loading tests, the residual strains after four to six minutes decreased to less than 15.8 με. The consistent viscoelastic behavior of the package adhesive was present.
- FBG sensor packages were undamaged.

6.3.3.1.3. **Pseudo** C**yclic Loading Test**

Pseudo cyclic loading tests were defined as repetitive loading of the specimens subjected to 2500 lbs over short periods of 40 min and 15 min. Each pseudo cyclic loading test consisted of 10 cycles with rates of loading and unloading of +/-1250 lbs/min and +/-5000 lbs/min, applied on each specimen bending side The ramping rates were selected based on the bending test rate of loading (1250 lbs/min) and increased four times (similar to the 5000 lbs/min accelerated loading test).

In Figure 6.65, a representative pseudo cyclic FBG strain history and applied load for Specimen 1 is shown. As observed, the strains varied along with the cyclic loading. Peak strains were approximately constant. The ambient laboratory temperature fluctuations were less than +/-0.4^{o}F. In this test program, Specimen 6 and 2 were inoperative due to damage on the sensors and specimen after the Side 1 Loading, respectively.

In-service conditions, structural bridge members are frequently subjected to repetitive truck loadings. In this context, limited cyclic load was applied to the small glulam specimens to examine the viscoelastic behavior of the structural packages; in particular, if any phase lag response upon loading and after the removal of the applied load have occurred. For this purpose, peak strains were examined for reproducibility. In addition, the residual strains were evaluated to verify creep recovery of the structural FBG sensor packages.

The viscoelastic behavior in each structural package was evaluated by comparing both +/-5000 and +/-1250 lbs/min pseudo cyclic loading tests as follows:

- Comparison of the strain results for the +/-1250 lbs/min pseudo cyclic loading test with the bending test to verify reproducibility.
- Comparison of the average peak strains of both cyclic and bending results.
- Evaluation of the residual strains at the cyclic loading.

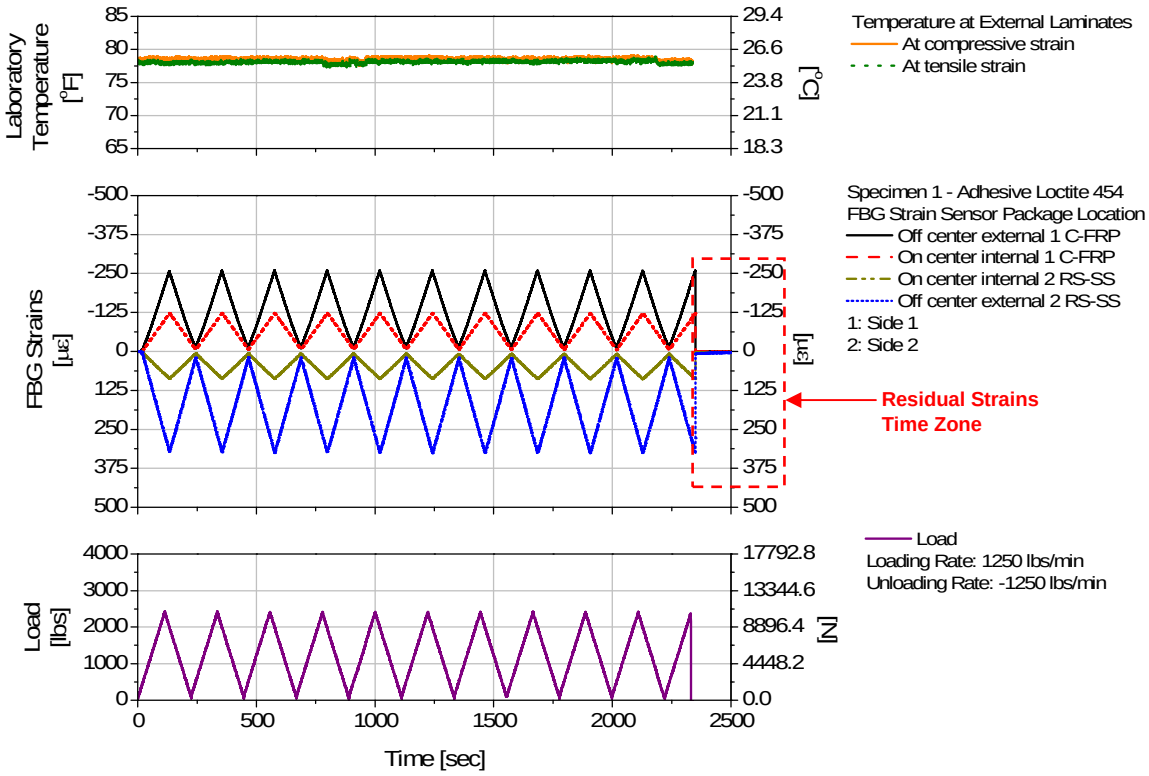

Figure 6.65. Representative Pseudo Cyclic Loading Test: Rate of loading +/-1250 lbs/min

Comparison of the Strain Results for Bending Tests and +/-1250 lbs/min Pseudo Cyclic Loading Tests. In Figure 6.66, the peak strains are plotted for Specimens 1, 4 and 7. Note that the Specimen 1, Side 2 Loading under similar rates of loading, the strain levels for pseudo cyclic loading tests were larger than the bending test results. Strain differences were between 21.5 με and 46.9 με. Similar higher strain differences were found in the 2500 lbs/min accelerated loading test results. The four sensor packages at Specimen 1 could have possibly changed their EI parameters, associated to the adhesive bonding line. No visible damage was observed on the four packages. For the other specimens, the peak strain differences were lower; differences varied from 0.7 με to 20.2 με.

Comparison of Strain Results for Both Pseudo Cyclic Loading Tests: Both +/-5000- and +/-1250- lbs/min test results were compared at the level of average peak strains, per specimen. In Figure 6.67 and Figure 6.68, average peak strains for Specimens, 1, 2, 4, 5, 7 and 8 are plotted for both pseudo cyclic loading tests. Typically, the external average peak strains for a loading rate of +/- 1250 lbs/min were less than the values obtained at the +/-5000-lbs/min test results. The average peak strain differences were between 3 με and 12 με. For the internal packages, the peak strain differences were smaller.

In both tests, the associated standard deviations for average strains were less than +/-3με. FBG sensors typically have a precision of +/-2 με. In this context, the peak strains per pseudo cyclic loading test were similar to the initial peak strain value. In Table 6.19, the summary of the pseudo cyclic loading test results is given for the selected six FBG structural packages

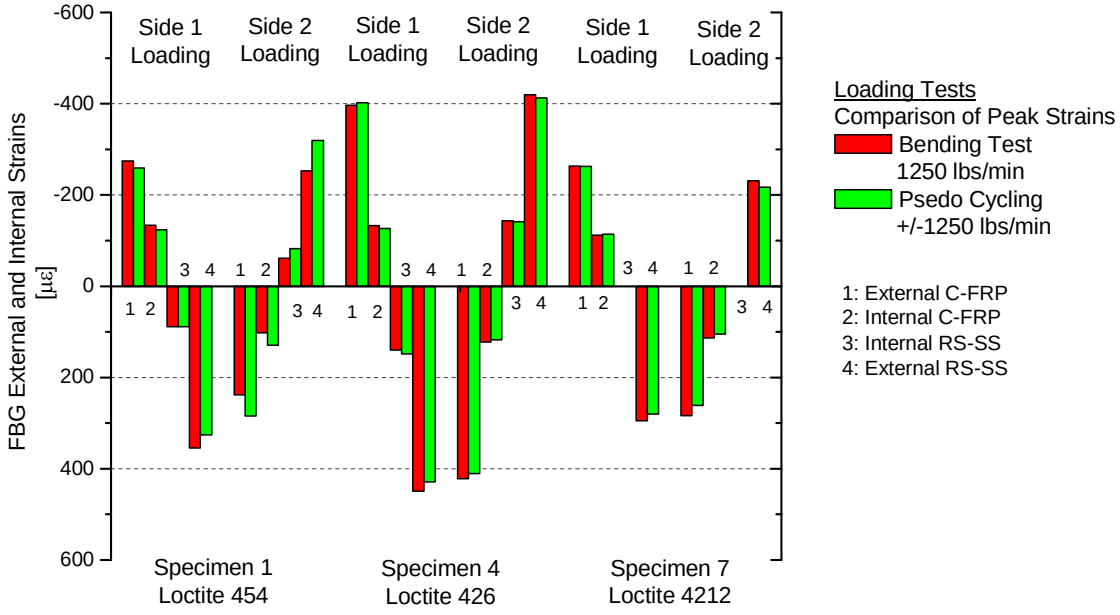

Figure 6.66. Comparison of Strain Results for Bending Tests and +/-1250 lbs/min Pseudo Cyclic Loading Tests: Specimens 1, 4 and 7

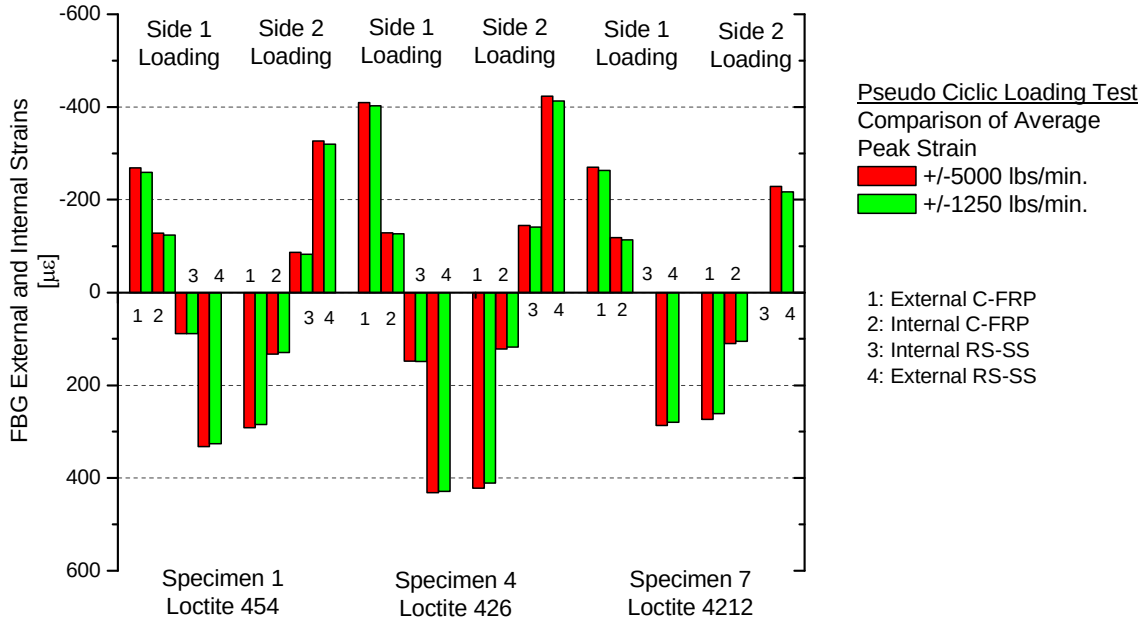

Figure 6.67. Pseudo Comparison of Strain Results for +/-5000 lbs/min and +/-1250 lbs/min Pseudo Cyclic Loading Tests: Specimens 1, 4 and 7

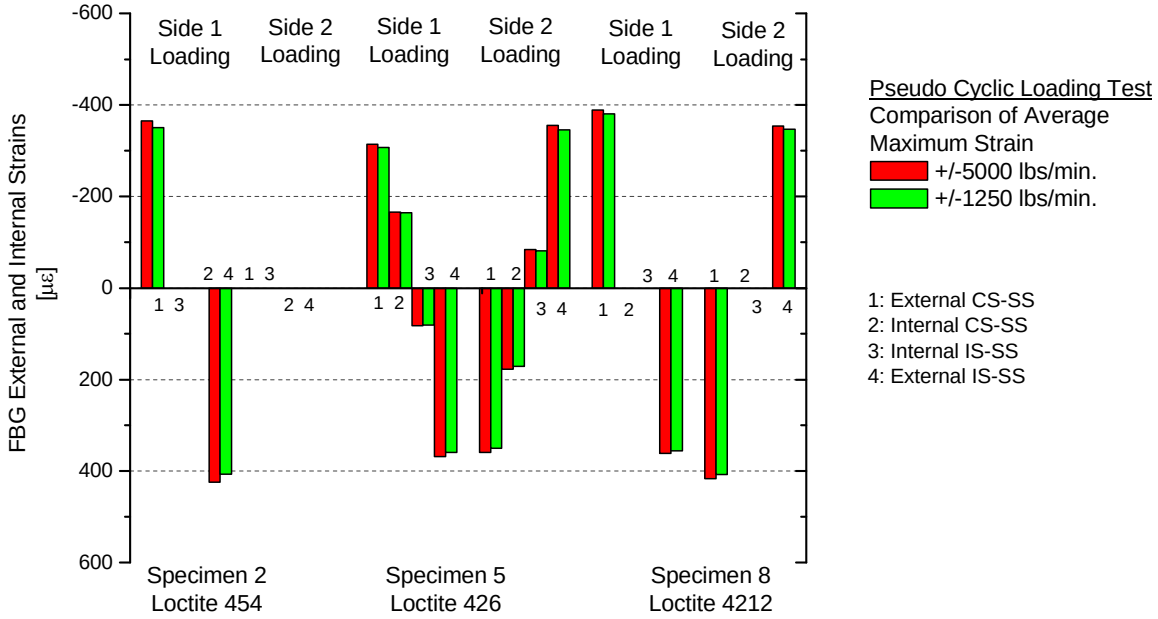

Figure 6.68. Pseudo Comparison of Strain Results for +/-5000 lbs/min and +/-1250 lbs/min Pseudo Cyclic Loading Tests: Specimens 2, 5 and 8

Final Conditions of the FBG Structural Packages. After removing the load, the residual strains gradually decreased within three minutes to values ranging from 0.0 με to 10 με (see Table

6.19). In Figure 6.69, the residual strains curves are shown for Specimen 8, Side 2 Loading when completed the +/-5000 lbs/min pseudo cyclic tests. The residual strains after 1.3 min (75 sec) were negligible (less than 0.8 με). The data plots for all specimens showed that all sensor residual strains decreased over periods of 1 to 3 minutes (short term creep recovery).

When completing the test protocol, the FBG sensor packages were visually inspected; no sign of deterioration was observed.

Test results show that:

- The residual strains were minimal indicating that the selected FBG structural packages had a consistent viscoelastic behavior (short term creep recovery).

Table 6.19. Pseudo Cyclic Loading Tests: Results for Selected FBG Structural Packages

FBG Sensor (Package)	Side Loading	Rate of Loading [lbs/min]	Average Strain [με]	Std. Dev. [με]	Residual Strain [με]
Specimen 4	1	+/-1250	-402.7	1.0	0.0
Ext. FBG 1 Sensor		+/-5000	-409.4	0.8	-1.7
(C-FRP Loctite 426)	2	+/-1250	410.5	1.3	0.8
		+/-5000	421.9	1.3	0.0
Specimen 4	1	+/-1250	428.8	1.9	4.2
Ext. FBG 2 Sensor		+/-5000	431.8	1.0	3.3
(RS-SS Loctite 426)	2	+/-1250	-413.0	2.8	-4.2
		+/-5000	-423.3	2.7	-1.7
Specimen 8	1	+/-1250	355.5	1.5	1.7
Ext. FBG 2 Sensor		+/-5000	361.5	1.3	1.7
(IS-SS Loctite 4212)	2	+/-1250	-346.8	1.2	0.8
		+/-5000	-354.2	1.6	0.8
Specimen 9	1	+/-1250	-303.3	0.3	0.8
Ext. FBG 1 Sensor		+/-5000	-309.5	0.7	-10.0
(RS-SS Loctite 4212)	2	+/-1250	288.6	1.4	4.2
		+/-5000	-309.5	0.7	-10.0
Specimen 3	1	+/-1250	132.0	2.2	6.7
Int. FBG 2 Sensor		+/-5000	132.0	0.7	1.7
(RS-SS Loctite 454)	2	+/-1250	-135.6	0.4	-0.8
		+/-5000	-139.1	0.3	-0.8
Specimen 4	1	+/-1250	148.7	1.9	3.3
Int. FBG 2 Sensor		+/-5000	147.6	0.3	2.5
(RS-SS Loctite 426)	2	+/-1250	-141.1	2.8	-1.7
		+/-5000	-144.8	2.7	-1.7

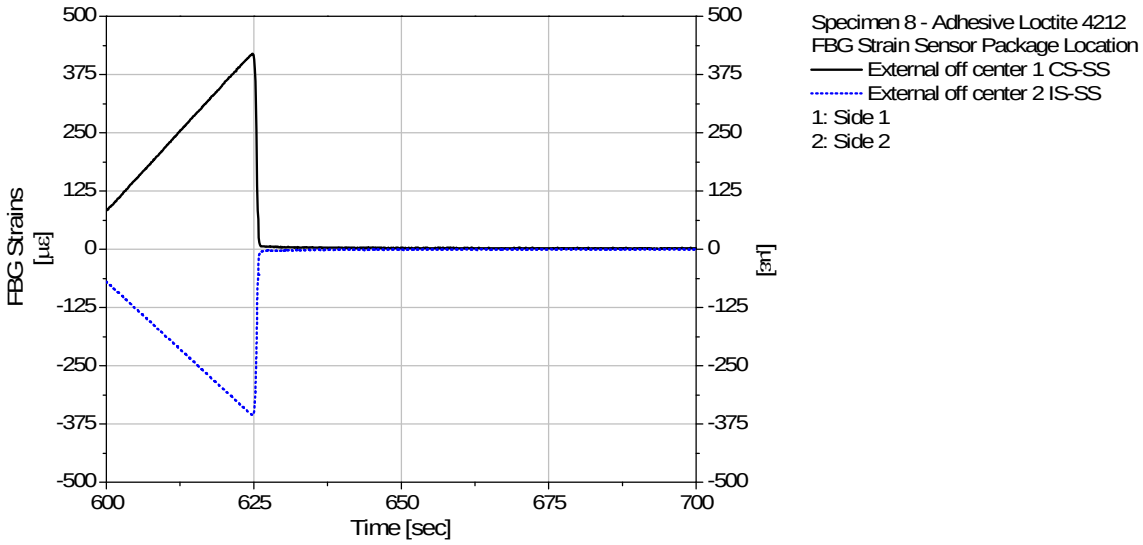

Figure 6.69. Pseudo Cyclic Loading Test: +/-5000 lbs/min Residual Strains for Specimen 8, Side 2 Loading

- The pseudo cyclic loading tests (rates of +/-1250 lbs/min and +/-5000 lbs/min) show the strain phase lag to be negligible.
- In all cases, the packages had not deteriorated.

6.3.3.1.4. **Heat and Sustained Loading Test**

The specimens were subjected to combined heat and sustained loading for 24 hours to evaluate the viscoelastic behavior of the FBG packages during and after loading. After testing, structural FBG sensor packages were examined to detect physical damage. The strain data were analyzed as follows:

- Performance of the FBG structural packages.
- Temperature versus strain evaluation.
- Residual strain evaluation.
- Final conditions of the FBG structural package.

Prior to testing, the moisture content of the glulam specimens was measured. For all specimens, the moisture contents were approximately 6%. The specimen was confined into a heat box and loaded for 24 hours with a sustained load of 2500 lbs. After 20 min, the heat source was connected (see Section 6.2.8.1.2.5). At the end of the 24 hours, the specimen was unloaded and after 10 minutes, the heat source was disconnected. Additional strain and temperature data were collected for a minimum of 3 hr. Only seven operative specimens were laboratory tested. In Specimen 5, the

external IS-SS Loctite 426 package was inoperative after handling the specimen on the testing fixture (damage in the FBG leads).

Strain Performance of the FBG Structural Packages. In Figure 6.70 (a), a representative time plot is shown for strains, applied load and temperature variations for 24 hours and unloading time of 25 min (total of 87900 sec). The strain levels increased along with the load of 2500 lbs and remained constant for the "sustained loading over 20 min" (Figure 6.70 (b)). For all specimens, the strain standard deviations during this period were less than 3 με, while temperature variations were approximately +/-0.5^{o} F.

When comparing the average strains for the 20 min sustained loading and the bending loading tests results, the average strain differences were small. For Specimen 5, Side 1 Loading, the average strain differences varied from 1 με to 7 με (see Figure 6.70 (b)). In contrast, for Specimen 1, Side 2 Loading (Figure 6.71), the average strain differences between initial sustained loading and bending tests varied from 31 με to 118 με (e.g., RS-SS Loctite 454 noted in). For the other specimens, the averages strains for the sustained loading tests were between 0.8 με and 105 με lower than the bending tests results. The relatively low strain levels could be attributed to the modification of loading testing fixture (use of a pin support instead of a roller support) and/or changes in the EI parameter of the package adhesive.

Immediately after connecting the heat source, the temperature increased non linearly for all sensors. In general, the specimens were subjected to temperatures above 100^{o} F and below 125^{o} F (e.g., see Figure 6.70 (a) and Figure 6.71 (a)). While the external strain levels increased along with the temperatures increments, the internal strain levels slowly increased. The observed strain lags could be possibly attributed to the thermal expansion lag due to the insulation properties of the wood specimen.

After 24 hours, the load was removed and the strains immediately decreased for all specimens (see Figure 6.70 (b) and Figure 6.71 (b)). The residual strain levels were above 80 με after removing the load (noted in both figures as "load removal time zone"). The heat source was connected for another 10 min. After 15 minutes of cooling the specimens, the residual strains decreased in a minimum of 10 με (noted in figure as "cooling off time zone"). The residual strains are assessed later in this section.

Temperature and Strain Evaluation. As observed in Figure 6.70 (a) and Figure 6.71 (a), the temperature fluctuation had visible influenced the strain variations. In Table 6.20, the summary of the linear regression R^2 coefficients are presented for the external FBG sensor packages of seven specimens. In addition, temperature fluctuations are given.

As observed, R^2 coefficients varied from 0.247 to 0.974. Only the Specimen 9, 72H-SS Loctite 4212 package had good correlations between strains and temperature fluctuations in both tests (i.e., 0.974, 0.955). For Specimens 1 and 7, Side 1 Loading with temporary temperatures above 150^o F when (see Table 6.20), two FBG 2 sensors were closest to the heat of source, the linear regression R^2 coefficients were 0.685 and 0.771, respectively. For correlations less than 0.95, the viscoelastic behavior of the package adhesives could be also influenced by creep due to the sustained loading and larger temperature increments.

The biomass of the wood composed mainly of lignin, hemicelluloses and cellulose decompose at temperatures between 392^o F and 932^o F. At these elevated temperatures, cellulose decomposes in 400 s, while hemicelluloses and lignin decompose at 100 s. In these conditions, structural changes in forms of both shrinkage and cracking are expected to occur (Shen et al, 2009). For all specimens, the external surfaces at temperatures above 150^o F were not structurally damaged (e.g., Specimens 1 and 7). Note that the oven drying temperatures for wood requires 215^o F to 217^o F (Wengert, 2008); therefore, when the temperatures were between 104.5^o F and 173.4^o F, the moisture content of 0% was not attained. However, the initial moisture content of all specimens could have potentially decreased after the first test (Side 1 Loading). In general, wood that contains moisture (i.e., 6% in all specimens before testing), first expands when heated and then gradually shrinks due to the lost of moisture. Even in the longitudinal direction (grain), dimensional changes due to shrinkage predominate over the dimensional changes due to thermal expansion after prolonged heating (Wood Handbook, 1999). In contrast, for very dry wood (perhaps 3% or 4% moisture content of less), the thermal expansion coefficients are positive in all directions (1.7 to 2.5 x 10^{-6} /^{o} F). In addition, wood is a good insulator and does not respond rapidly to temperature changes in the environment. Therefore, wood thermal expansion and contraction lag substantially behind temperature changes (Ritter, 1992). It should be noted that the linear regression R^2 coefficient with values less than 0.95 could indicate that influence of the wood thermal expansion lag for specimens that were dry (i.e., moisture content less than 6%).

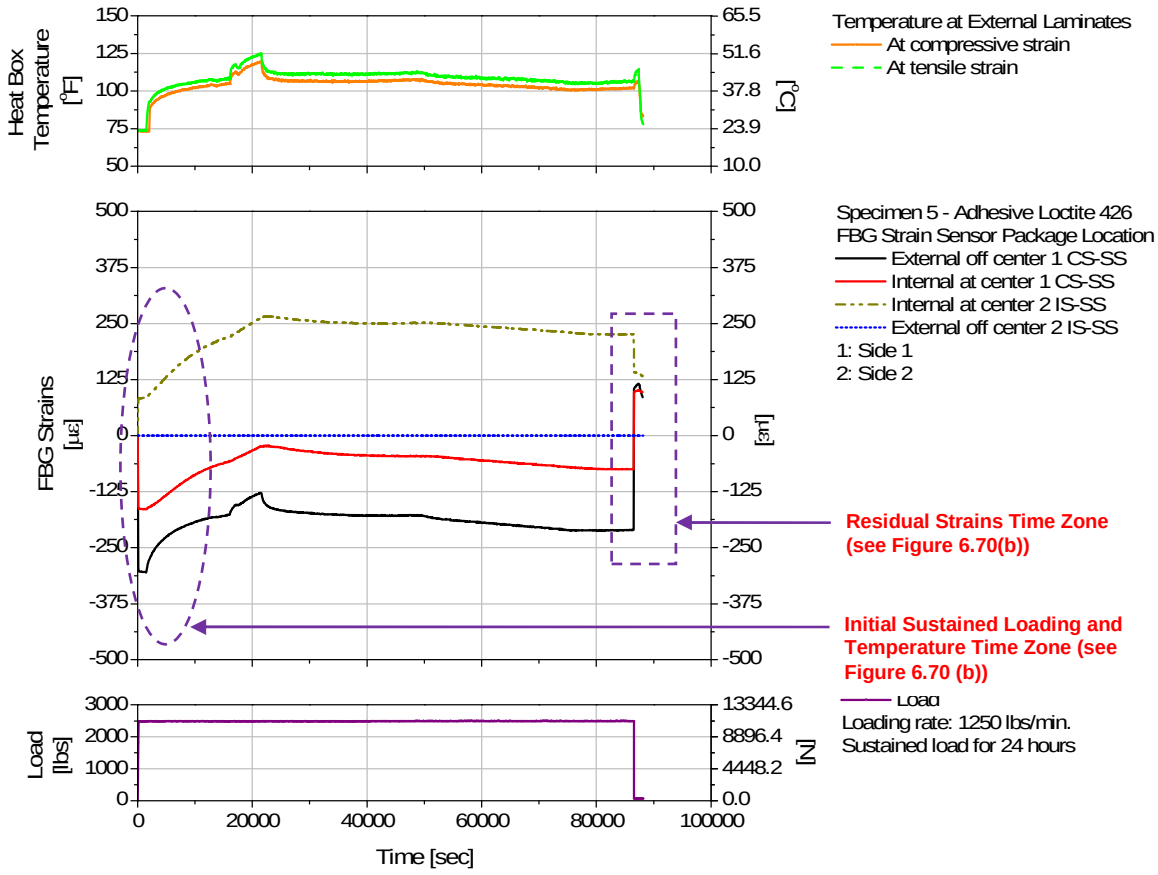

(a) Side 1 Loading

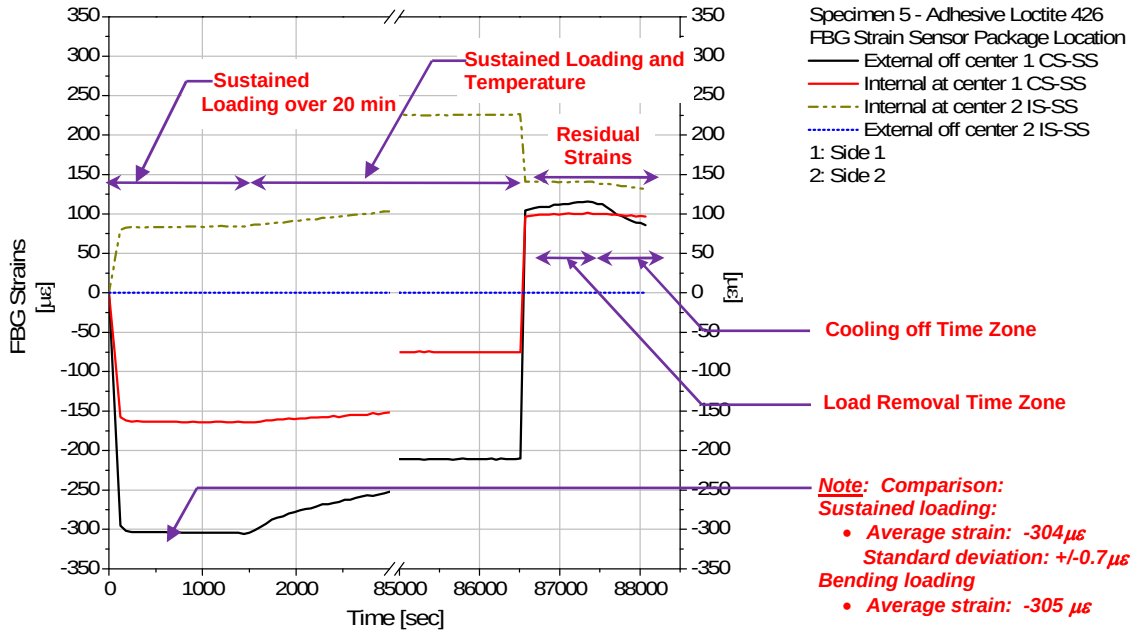

(b) Close up of Figure 6.70 (a): Initial and Final Loading

Figure 6.70. Heat and Sustained Loading Tests: Specimen 5, Side 1 Loading

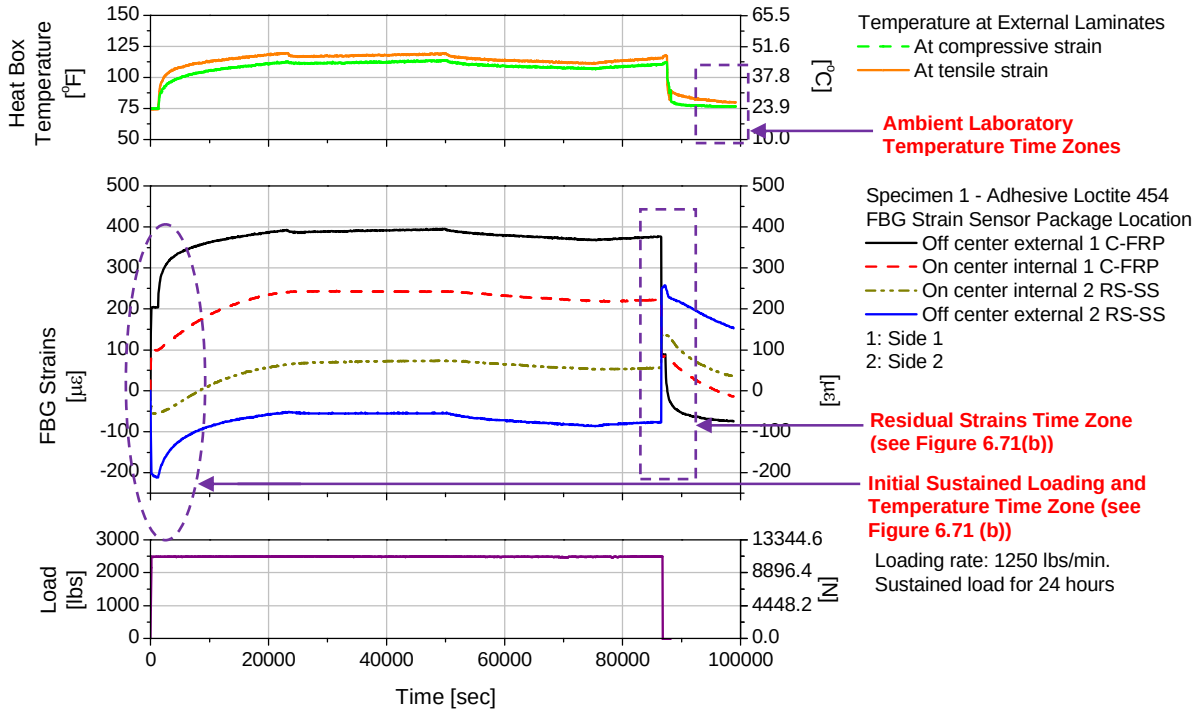

(a) Side 2 Loading

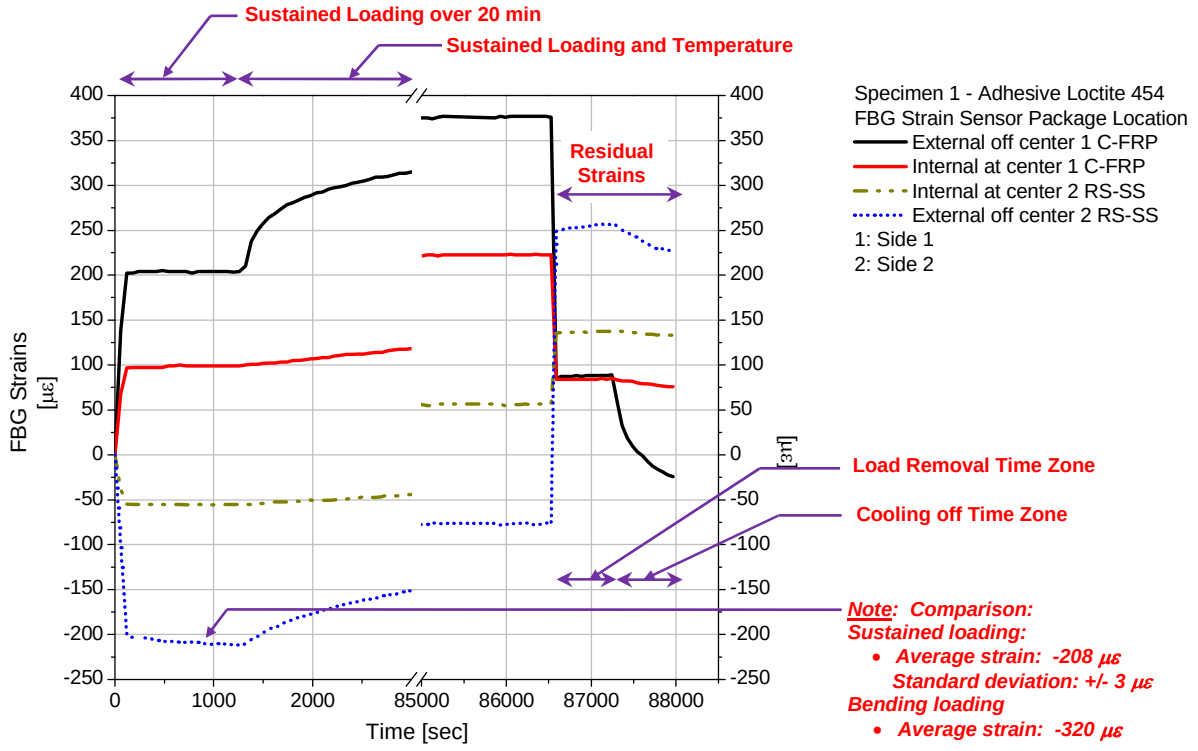

(b) Close up of Figure 6.71 (a)

Figure 6.71. Heat and Sustained Loading Tests: Specimen 1, Side 2 Loading

Table 6.20. Heat and Sustained Loading Test: Linear Regression for External Strains and Temperatures

Spec.	Sensor Type	Package	R^2 Side 1 Loading	Temperature Min. – Max. [°F]	R^2 Side 2 Loading	Temperature Min. – Max. [°F]
1	FBG 1	C-FPP – Loct. 454	0.834 (C)	66.3 – 147.9	0.918 (T)	74.9 – 112.6
	FBG 2	RS-SS – Loct. 454	*0.685 (T)*	*66.8 – 173.4*	0.958 (C)	74.6 – 119.5
4	FBG 1	C-FPP – Loct. 426	0.629 (C)	77.2 – 105.3	0.829 (T)	75.1 – 106.0
	FBG 2	RS-SS – Loct. 426	0.247 (T)	77.2 – 116.4	0.731 (C)	75.3 – 118.5
7	FBG 1	C-FPP – Loct. 4212	0.942 (C)	77.7 – 125.9	0.781 (T)	79.1 – 126.7
	FBG 2	RS-SS – Loct. 4212	*0.771 (T)*	*77.7 – 165.9*	0.692 (C)	79.8 – 130.0
5	FBG 1	CS-SS – Loct. 426	0.931 (C)	73.3 – 119.3	0.923 (T)	73.8 – 111.5
	FBG 2	IS-SS – Loct. 426	---	73.6 – 123.6	---	73.5 – 106.8
8	FBG 1	CS-SS – Loct. 4212	0.926 (C)	75.3 – 108.3	0.844 (T)	79.6 – 113.8
	FBG 2	IS-SS – Loct. 4212	0.603 (T)	76.6 – 112.6	0.916 (C)	84.4 – 116.8
3	FBG 1	72H-SS – Loct. 454	0.917 (C)	77.1 – 105.9	0.345 (T)	76.9 – 113.8
	FBG 2	AM-SS – Loct. 454	---	76.9 – 112.4	---	79.3 – 129.1
9	FBG 1	72H-SS – Loct. 4212	*0.974 (C)*	*70.6 – 104.9*	*0.955 (T)*	*71.0 – 106.3*
	FBG 2	AM-SS – Loct. 4212	0.695 (T)	70.1 – 112.1	0.947 (C)	70.1 – 102.3

Note. - Spec.: specimen, Min.: minimum, Max.: maximum, Loct.: Loctite adhesive.

Residual Strains. After removing the load, the residual strains in all specimens were larger than 80 με. The heat box was removed and the specimens were allowed to cool for a minimum of three hours to ambient temperatures (see "ambient laboratory temperature time zones" in Figure 6.72).

For all specimens, the residual strains gradually decreased over time (see "residual strains time zone" in Figure 6.72). For Specimen 8, Side 2 Loading, the strains visibly decreased after five hours (time point of 110,000 sec); at that time, the residual strains were -15 με and -2 με, for CS-SS Loctite 4212 and IS-SS Loctite 4212 packages, respectively.

For Specimen 1, Side 2 Loading, the residual strains for four operative sensors are shown in Figure 6.73. After cooling the specimen for three hours up to the ambient laboratory temperatures, the external strains were still -75 με and 153 με for the C-FRP and RS-SS Loctite 454 packages, respectively. In contrast, the residual strains for the internal packages were smaller (i.e., -14 με and 35 με).

For all specimens, the sensor packages had residual strain levels that were larger than 20 με after cooling the specimen more than four hours. The large residual strains could be attributed to the

thermal contraction (cooling) lag due to the wood insulation properties of the glulam specimen and/or the creep in the package adhesive due to the elevated temperatures and/or the combination of all.

Final Conditions of the Structural Packages. At the end of each test, the packages were visually examined to determine their final conditions. In general, when the specimens were subjected to under temperatures between 100° F and 125° F, the packages showed no damage. However, some damage occurred for temperatures larger than 125° F. For Specimen 1, Side 1 Loading (Figure 6.74), the temperature increased from the ambient conditions (66.8° F) to 173.4° F in a period of four hours, which is close to the adhesive manufacturer's recommended operating temperature of is 180° F. The temperature was gradually decreased to less than 125° F until the end of the test. Both external strain levels increased in some proportion to the temperature fluctuations (see "high temperatures and strains time zone" in Figure 6.74).

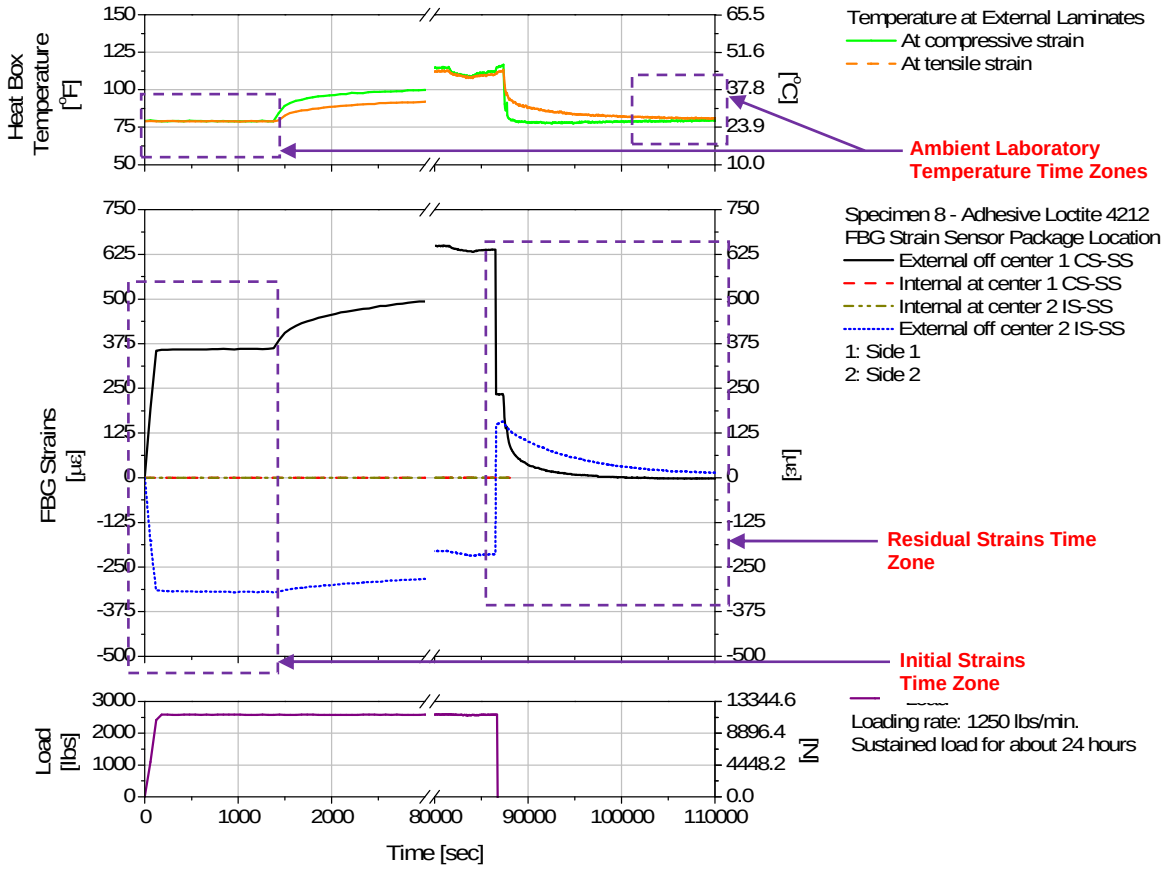

Figure 6.72. Heat and Sustained Loading Test: Close Up of Initial and Final Time Zones for Temperatures and Strains for Specimen 8, Side 2 Loading

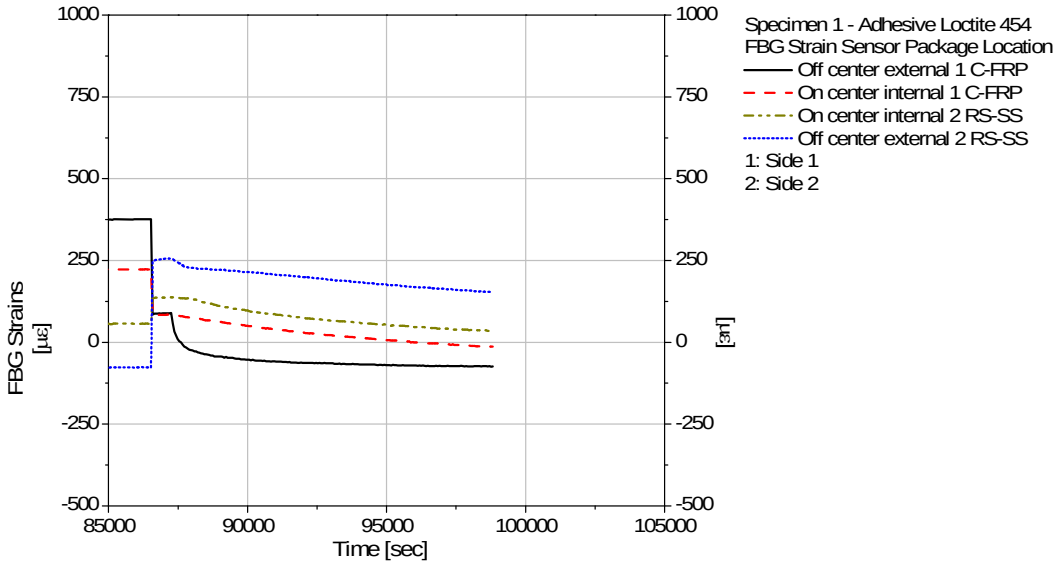

Figure 6.73. Heat and Sustained Loading Test: Residual Strains for Specimens 1, Side 2 Loading after Cooling Off for 3 hours (see Figure 6.71)

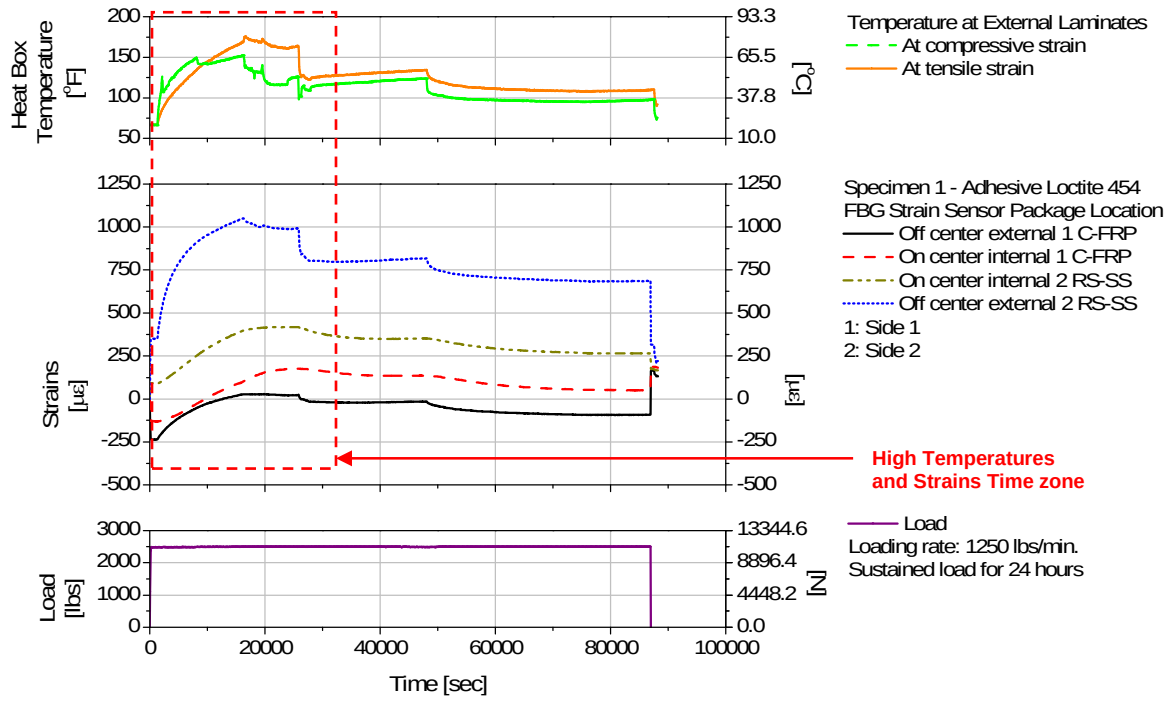

Figure 6.74. Heat and Sustained Loading Test: Temperature, Strain and Load History for Specimens 1, Side 1 Loading

After the Side 1 Loading test, delamination occurred at one end of the Specimen 1RS-SS Loctite 454 package (see Figure 6.75 (a)). After the Side 2 Loading test, the package detached when

removing the specimen from the testing fixture. An alternating failure mode type was identified by the signs of remaining adhesive on the package backing material (see Figure 6.75 (b)). In this failure type, the tensile stresses within the plane of the adhesive can destabilize a growing debond (adhesive cracking path), causing it to alternate from one adherend to the other (Dillard, 2005). In the same specimen, the C-FRP Loctite 454 package showed no sign of delamination.

In Specimen 7, Side 1 Loading, the temperature on Side 2 exceeded 165^{o}F for approximately 5 hours. After this period, the temperature was gradually stabilized to 120^{o} F, approximately. In both external C-FRP and RS-SS Loctite 4212 packages, no physical damage was observed. One advantage of these packages over the delaminated RS-SS Loctite 454 package was the use of the Loctite 4212 adhesive which can operate at temperatures up to 250^{o}F (manufacturer's recommendations).

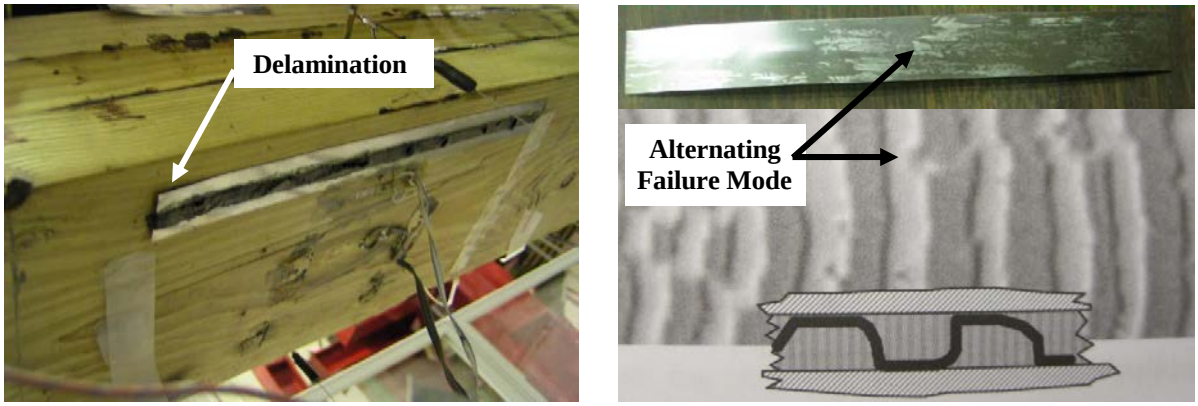

(a) Side 2: Delamination after the Side 1 Loading

(b) Detached RS-SS package backing material and associated alternating failure mode (Dillard, 2005)

Figure 6.75. Heat and Sustained Loading Test: Specimen 1, Side 1 Loading – Package Delamination

From the heat and sustained loading test, the following observations were outlined:

- Before applying heat, the 20 min sustained loading strains were smaller than the bending test results. Large strain differences were observed in Specimen 1, Side 2 Loading; changes in the FBG structural packages were attributed to the EI parameters.
- Elevated temperatures visibly affected the strain levels. The linear regression between the temperature and the external strain data varied from 0.247 to 0.974. Correlations less than 0.95 could be attributed to either the viscoelastic behavior of the package adhesive (creep due to

sustained loading and temperature) or the wood thermal expansion lag or the combination of both.

- The presence of residual strains could be also attributed to the package adhesive viscoelastic behavior and/or the wood thermal contraction (cooling the specimen) lag.
- The elevated temperatures may potentially reduce the remaining moisture content in the glulam specimens. The moisture content at the end of the testing program was unknown.
- With the exception of the RS-SS Loctite 454 package, most of the FBG structural packages subjected to temperatures under 125^{o}F had no damage after completing the bending test. The selected six FBG structural packages were capable of resisting the entire test program.

When completing the test, Specimens 1 lost both internal and external RS-SS Loctite 454 packages. In Specimen 8, the CS-SS Loctite 4212 package lost both connectors at the end of the Side 2 Loading test (handling).

6.3.3.1.5. **Cold and Sustained Loading Test**

This test program was conducted for the purpose of evaluating the effect of cold temperatures and 24 hour sustained loading on the viscoelastic behavior of the FBG structural packages. The evaluation of the strain data was as follows:

- Performance of the FBG structural packages during the sustained loading.
- Temperature and strain comparison during loading.
- Residual strains.
- Final conditions of the structural FBG sensor packages and specimens.

The process of testing the specimens with cold and sustained load is described in Section 6.2.8.1.2.1. At the beginning of the test program, the moisture content readings for seven specimens were not detected by the two-prong resistance moisture meter.

Strain Performance of the Structural FBG Sensor Packages. In Figure 6.76 (a), an example of the FBG strain history, temperature variations, and the 24-hour load are shown. Typically, dry ice pellets were placed near the packages and surrounding the specimen, on top of the specimen and on bottom of the cold box. After sealing the specimen, the load was applied with a loading rate of 1250 lbs/min. As observed in Figure 6.76 (b), the tensile and compressive strains increased upon loading and were decreasing with cold temperatures maintained inside the box cold.

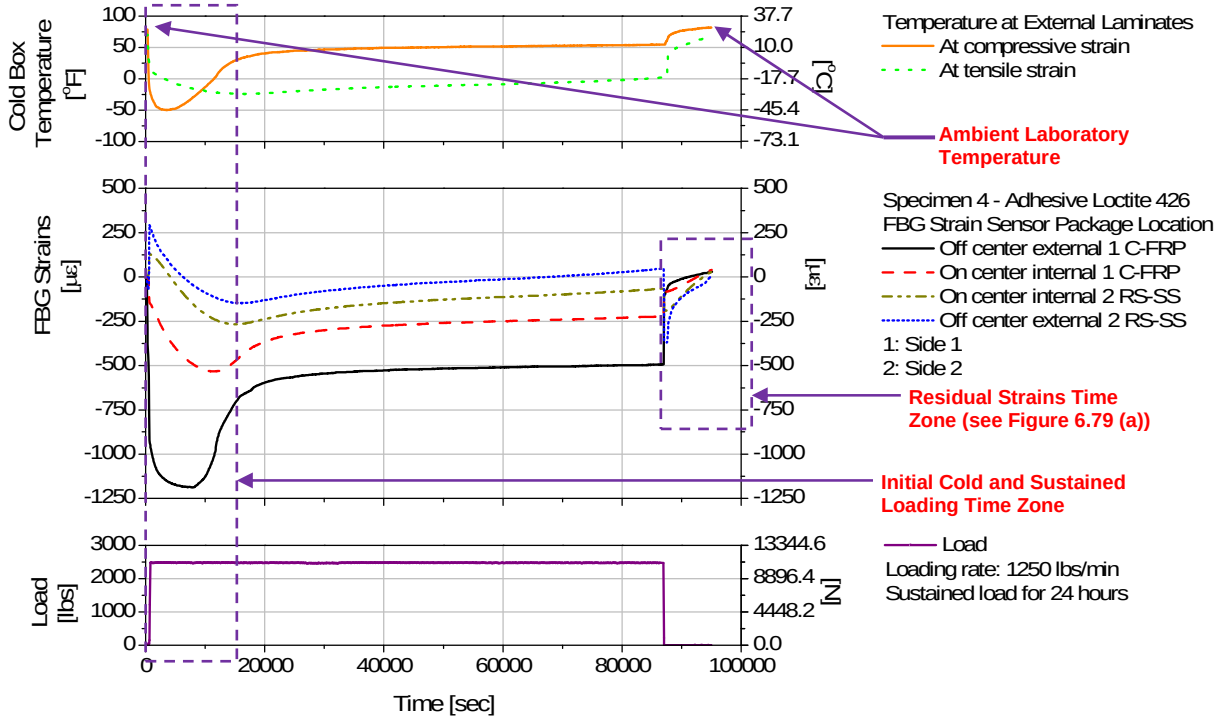

(a) Strains, Load and Temperature vs. Time

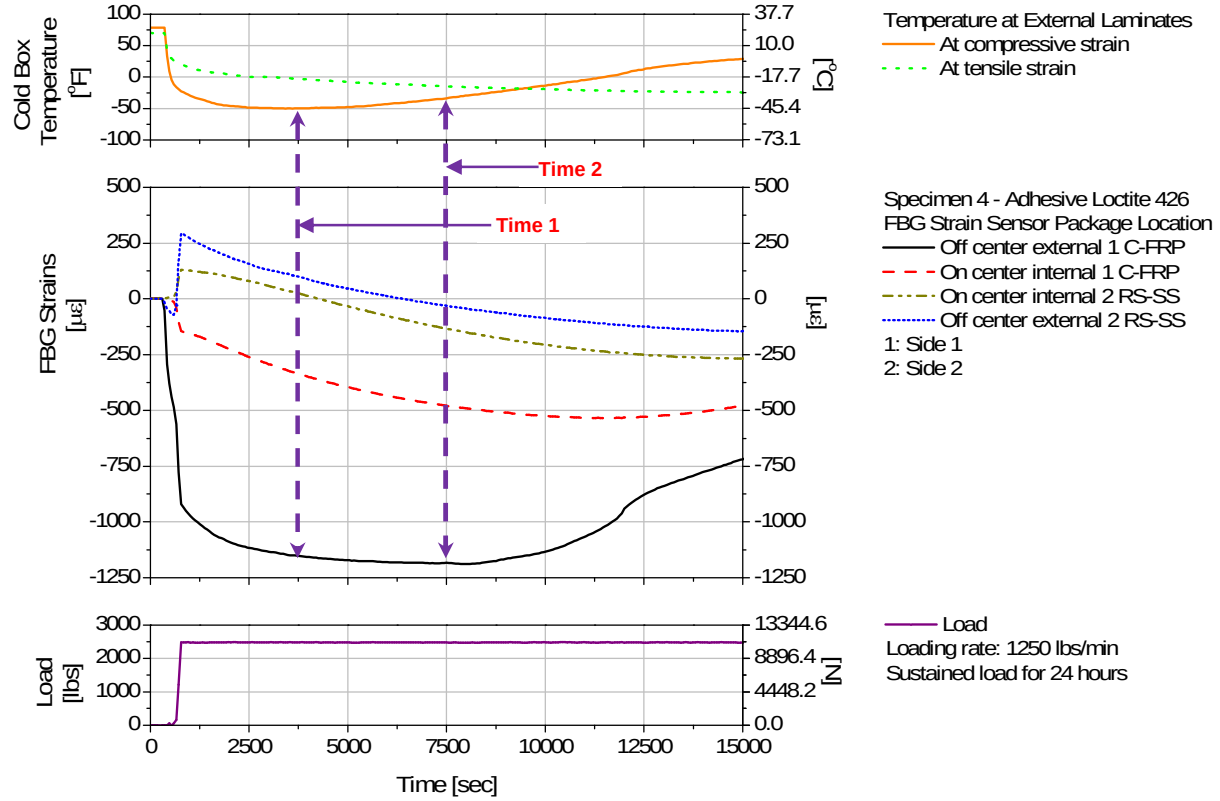

(b) Close up of Initial Cold and Sustained Loading Time Zone for Strains and Temperatures

Figure 6.76. Cold and Sustained Loading Test Results for Specimen 4, Side 1 Loading

For Specimen 4, Side 1 Loading, the temperatures in the compressive side were lower than -50°F during the first hour and gradually increased to approximately 50°F (Figure 6.76 (a)). The tensile bending surface was subjected to temperatures below 0°F for during the 24 hour loading. Consequently, variable temperature gradients were imposed to the specimen that could have affected the internal strain levels. In addition, a close up of the initial cold and sustained loading is shown in Figure 6.76 (b). For the C-FRP Loctite 426 package, the Time 1 and Time 2 strains and temperatures were compared under the sustained load of 2500 lbs. For Time 1 (3750 s), for a strain level of -1152.5 με, the temperature was -49.4° F; while for Time 2 (7500 s), for a strain level of -1184.2 με, the temperature was -33.5° F.

By comparing both time results, the larger strains for lower temperatures (Time 2) indicated the presence of other factors altering the strain response. When comparing the strain results from the previous tests, the following was observed:

- Due to a bending loading, the expected strain level was -396 με.
- For the sustained loading test under ambient laboratory temperatures (7500 s), the strain level was -393 με, on the order of the bending test result.
- However, when subjecting the specimen to cold temperatures and sustained load, the viscoelastic behavior of the package adhesive could have induced large compressive strains.
- In the previous test, heat and sustained loading, the wood thermal insulation property indicated to possibly have influenced the strain response of the FBG sensor packages during heating for 24 hours and cooling of the specimens. Similarly, the thermal contraction lag due to the cold temperatures could have added lag strains in the FBG package strain response.

For all sensor packages, the strain responses were expected to be affected by both viscoelastic behavior of the package and the temperature contraction lag during the 24 hour test.

Note that the surface mountable FBG sensor with C-FRP backing material, the minimal operating temperature was -40° F (manufacturer's specifications); while for the bare FBG strain sensor for all other packages the operating temperature for cold conditions was -85° F. As for the adhesive, the operating temperature recommended by the manufacturer was -65° F. In this test program, the minimal operating temperatures of various materials were exceeded and are assessed in the following sections.

Temperature and Strain Evaluation. As previously noted (e.g., Figure 6.76 (b)), the effect of the temperature variations in the stains levels could have a retarded effect due to the insulation wood properties. In this case, no linear regression calculation was made because it would not realistically represent the correlation between strains and temperatures at real time.

In the Side 1 Loading 1 tests, all FBG sensor packages were functioning under variable cold temperatures (e.g., Figure 6.76). However, in the Side 2 Loading tests, "abnormal" strains were observed in several sensor packages. In Figure 6.77, an example of "abnormal strains" was observed for the Specimen 4, external RS-SS Loctite 426 package during the first 10,000 sec (2.8 hr). "Abnormal" strains were observed immediately after applying the ice and when the temperature decreased to -63^{o} F (see "abnormal strains (out of range)) and warming up (see "abnormal strains (spikes)").

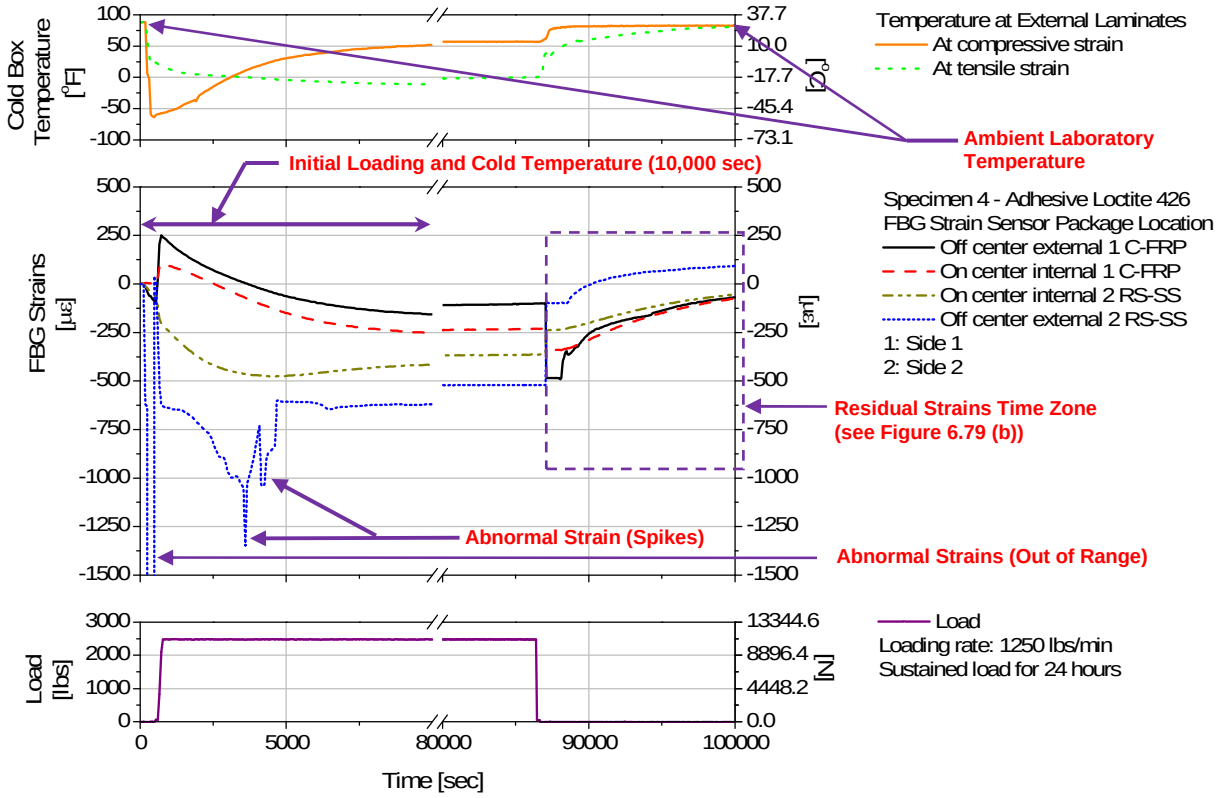

Figure 6.77. Cold and Sustained Loading Test: Strains, Load and Temperature vs. Time for Specimen 4, Side 2 Loading

Four external structural packages located at Specimens 3, 4, 5 and 7 showed flawed strains under temperatures between -10 °F and -93 °F. For Specimen 5, Side 2, "abnormal strains were observed while initially loading and applying cold temperatures (similar to Figure 6.77). However, for Specimens 3, Side 2, "abnormal" strains were observed at different times of loading when the cold temperatures were warming up. For Specimen 7, Side 2 (Figure 6.78), "abnormal" strains (out of range) were observed after 3 hr (12060 sec) and disappeared immediately after removing the load. The reason of the "abnormal" strains is unknown. Factors that generated the erroneous readings could be attributed to effect of the cold temperatures either in the bare FBG sensor and/or package adhesive bonding line.

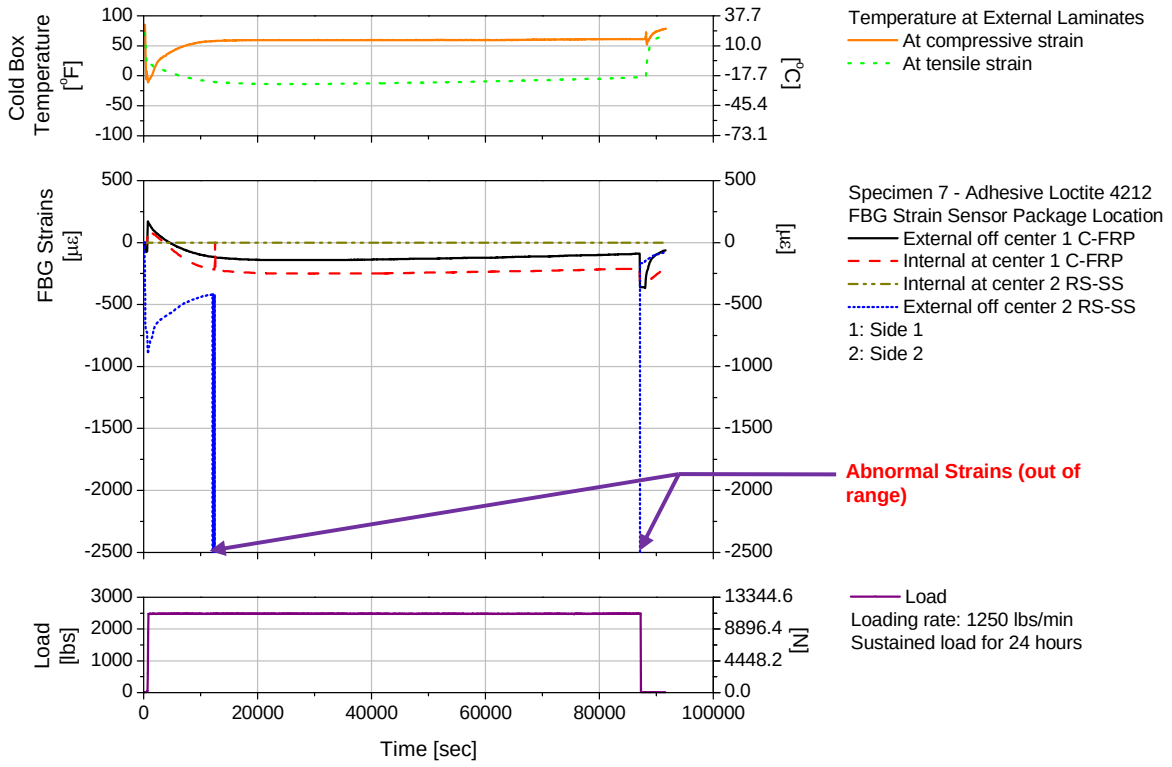

Figure 6.78. Cold and Sustained Loading Test: Strains, Load and Temperature vs. Time for Specimen 7, Side 2 Loading

Residual Strain Evaluation. After completing the loading test, the cold box was disassembled and the specimen was warmed for a minimum of two hours with the assistance of a fan until the specimen was subjected to similar ambient laboratory temperatures. Additional strain and temperature data were collected to examine the strain recovery of the packages. After unloading, the residual strain levels for most specimens were between 25 με and -500 με (e.g., Figure 6.79). In

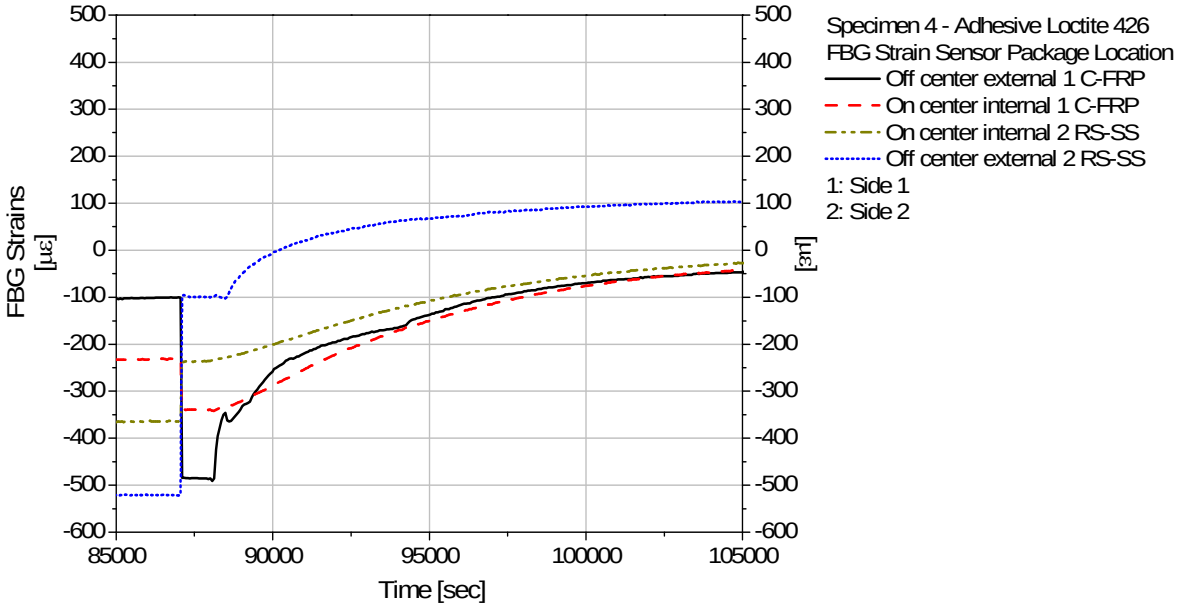

(a) Side 1 Loading (See Figure 6.76 (a))

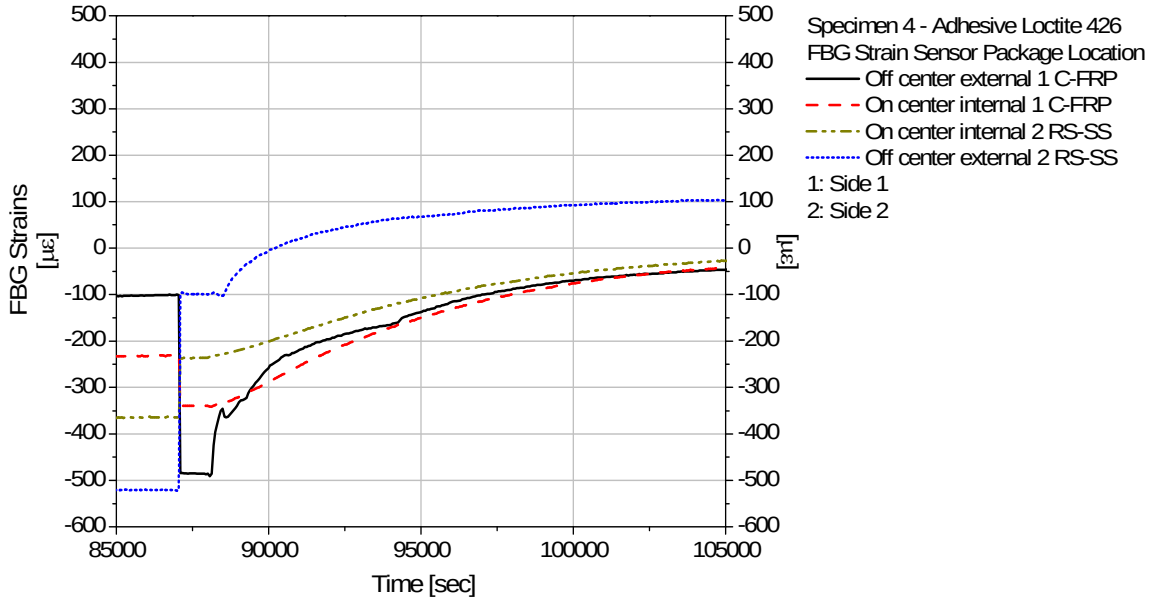

(b) Side 2 Loading (See Figure 6.77)

Figure 6.79. Cold and Sustained Loading Test: Residual Strains for Specimen 4

general, the strain levels decrease over time. After warming the specimen to the initial ambient laboratory temperatures, some packages had strain levels that varied from 5 με to 400 με.

The residual strains of the three of six selected packages are presented in Figure 6.79 for Specimen 4 (i.e., external and internal RS-SS and external C-FRP Loctite 426 packages). In Figure

6.79 (a), the external residual strains after more than 2 hr (8053 sec) were 5.8 με to 28.3 με; while for the internal FBG packages, the residual strains were 31.6 με and 40.8 με. Note that the internal strains could be affected by the thermal contraction/expansion lag and/or creep recovery of the adhesive. In Figure 6.79 (b), the residual strains for three packages after approximately 5 hr (17,940 s) varied from 27.5 με to 46.7 με. Only for the external RS-SS Loctite 426 package with "abnormal" strains during testing, the residual strain was 103.3 με.

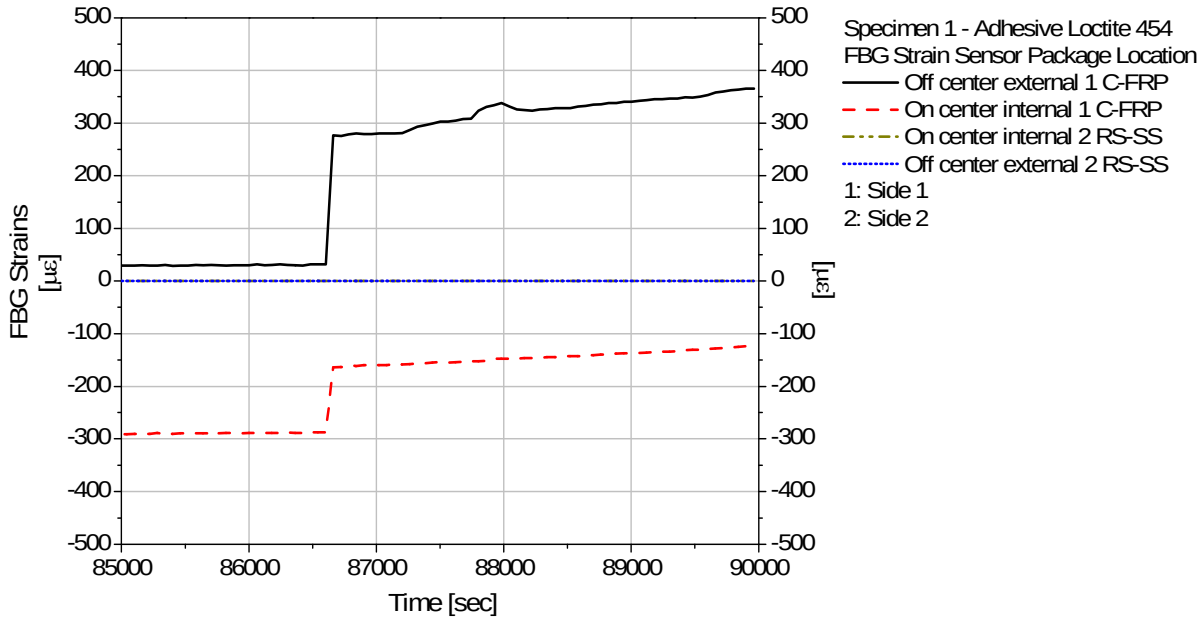

Figure 6.80. Cold and Sustained Loading Test: Residual Strains for Specimen 1, FBG 1 Sensor

In Figure 6.80, the final strain levels are shown for two operative sensor packages at Specimen 1, Side 1. After removing the load and cold box and warming up the specimen for almost an hour, the residual strains for both external and internal C-FRP Loctite 454 packages were 360 με and -120 με, respectively. In the strain plots, no sign of strain recovery was observed for these packages after the specimen reached the ambient temperatures.

In general, the level of residual strains could be attributed to the viscoelastic behavior of the package adhesive and/or the wood thermal contraction and expansion lag (changing from cold to warm temperatures), or the combination of all. The large residual strains and slow strain recovery were observed in some packages with "abnormal" strains during the cold and sustained loading testing.

Final Conditions of the structural FBG Sensor Packages and Specimens. In general, all operative FBG sensor packages remained in place after completing the test program. Only the glulam specimens were observed relatively dryer than at the beginning of the testing program. In Figure 6.81 and Figure 6.82, photos for Specimen 1 and 4 show the conditions of the Side 2 bending surfaces before the bending loading test and after completing the cold and sustained loading tests. For Specimen 1, Side 2, after the RS-SS Loctite 454 package delamination, only one cold and sustained loading test was performed on Side 1. The regions at the sensor locations showed the external dry condition of the specimen (Figure 6.81 (b)). For Specimen 4, Side 2, the test protocol was completed. The dry appearance of the specimen was less than the Specimen 1, Side 2 bending surface. In general, all specimens had dry appearance similar to the Specimen 4, Side 2.

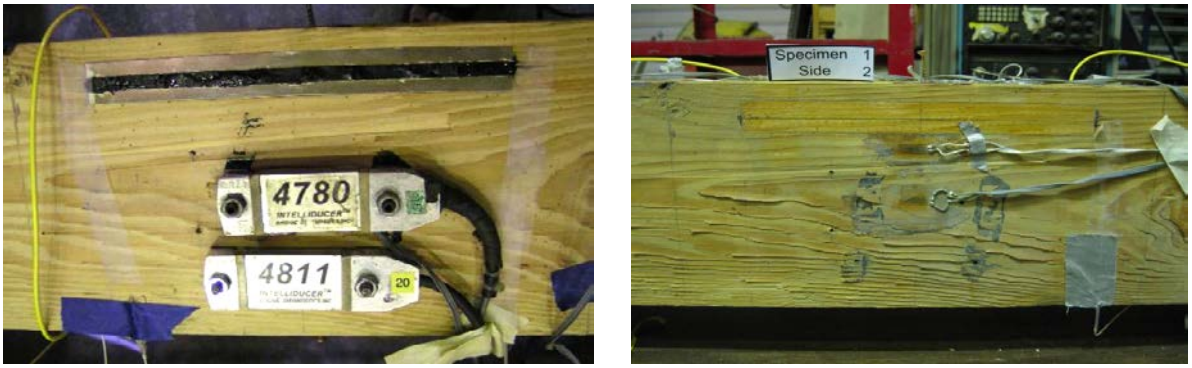

(a) Before Bending Test (b) After Hot and Sustained Loading

Figure 6.81. Bending Surface Before and After Testing Program for Specimen 1, Side 2

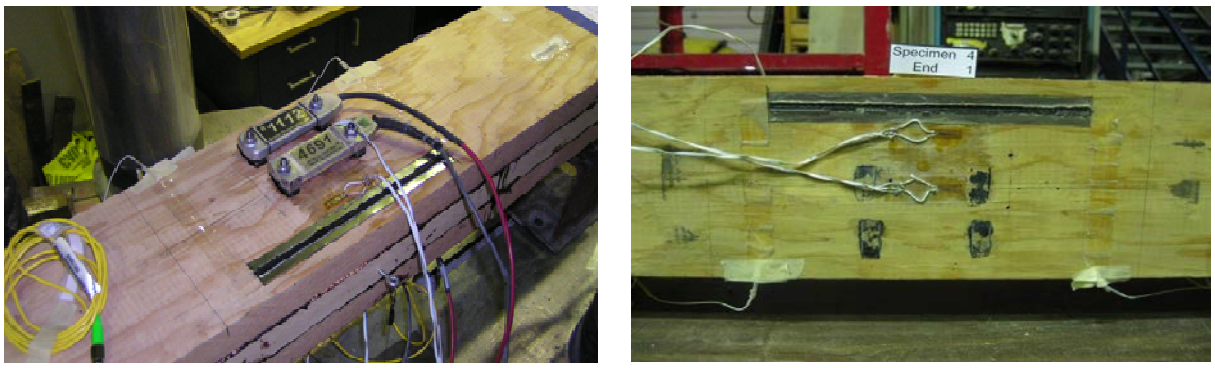

(a) Before Bending Test (b) After Hot and Sustained Loading

Figure 6.82. Bending Surface Before and After Testing Program for Specimen 4, Side 2

After the evaluation of the cold and sustained loading tests, the following comments were outlined:

- During Side 1 Loading, the strain responses decreased along with the cold temperatures. However, the lowest strains (compressive flexural strains) did not correspond to the coldest temperature. The effect of the thermal contraction lag due to the thermal insulation properties could have affected the total strain levels along the test.
- The presence of "abnormal" strains indicated that erroneous readings which could be attributed to effect of the cold temperatures either in the bare FBG sensor and/or package adhesive bonding line.
- The residual strains could be attributed to the viscoelastic behavior of the package adhesive and/or the wood thermal contraction and expansion lag (changing from cold to warm temperatures), or the combination of both.
- After testing, most specimens appeared relatively dry

Based upon all tests, six structural sensor packages were selected for further evaluation in the full scale glulam beam. They consisted of the C-FRP plus Loctite 426, the RS-SS plus Loctite 426, the IS-SS plus Loctite 4212, the 72H-SS plus Loctite 4212, the AM-SS plus Loctite 454, and the RS-SS Loctite 426. These packages were selected for their generally superior performance and corroboration with other sensor types.

6.3.4. NON-STRUCTURAL PACKAGE

In this section, the experimental results of bending tests performed on the five small-scale glulam specimens with embedded non-structural FBG sensor packages are presented.

6.3.4.1. MODIFIED BENDING TEST EVALUATION

Wood is a durable structural bridge material when properly engineered (i.e., design, fabrication and installation process). However, when timber bridge members are subjected to extended service periods may decay and/or deteriorate due to the exposure to deleterious environmental and biologic factors (Phares et al, 2005). In this context, the development of sensors and health monitoring techniques are required for assessing the condition of the timber bridge structures, by measuring factors associated with the decay/deterioration (i.e., moisture content, corrosion and ultraviolet light degradation). In the present investigation, non-structural package techniques for isolating embedded sensors for non-structural purposes were developed, installed in small scale glulam specimens and evaluated.

Bending tests were performed to assess five non-structural package techniques by measuring mechanical strains in the embedded FBG sensors (Section 6.2.8.2.2.1). Note that zero strain readings would indicate the perfect isolation. Otherwise, if the package techniques were not efficient, the experimental strains were expected to vary between +/-177 με and +/-133 με, for assumed moduli of elasticity of 1500 ksi and 2000 ksi, respectively. In Figure 6.83, the typical sensor instrumentation is shown. Non-structural FBG 1 and FBG 2 sensors were placed in recess areas of 1 1/2 x 6 in. and 3 x 6 in., respectively, protected by non-structural packages. In addition, two external strain transducers were attached to the external bending surfaces as references. Strain values were expected to be in the range of the theoretical values (i.e., +/-530 με and +/-398 με).

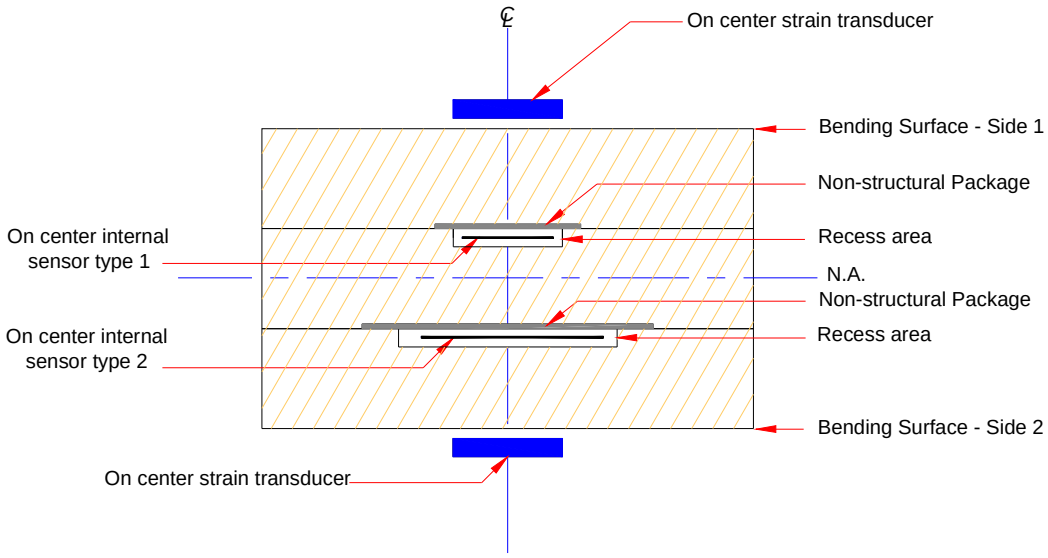

Figure 6.83. Typical Cross Section Sensor Instrumentation at Mid Span for Glulam Specimens

In Figure 6.84, a representative strain and load history is presented for the Non-Structural Specimen 3 (NS3). For all specimens, the modified bending test consisted in applying 2500-lbs loadwith a loading rate of 500 lbs/min, sustained for 5 min and remove with an unloading rate of 500 lbs/min. As observed, no mechanical strains were detected by both FBG sensors during the loading and unloading process. After removing the load for minimum of 1.5 min, “residual” strains due to the “free” sensor were still present.

A summary of the strain results during the 5-min sustained load is presented in Table 6.21 for Specimen NS3 shown in Figure 6.84. Strain levels during loading increased between -2.5 με and -5

με. During the sustained loading, noise due to the testing machine was detected in form of strains (standard deviations less than 1 με). After unloading, the strain levels were between 3.3 με and 5.8 με.

In general, the external strains varied from +/-200 με to +/-341 με, being lesser than the theoretical lower bound (i.e., +/-398 με).

The following general observations were made based on modified bending test results of five non-structural specimens:

- For the non-structural FBG 1 sensors, the strain levels less than 3.3 με, while the residual strains were between 0.8 με and 5.0 με.
- For the non-structural FBG 2 sensors, the strain levels ranged from 1.7 με to 8.0 με. The residual strains were between 0.0 με and 5.8 με.

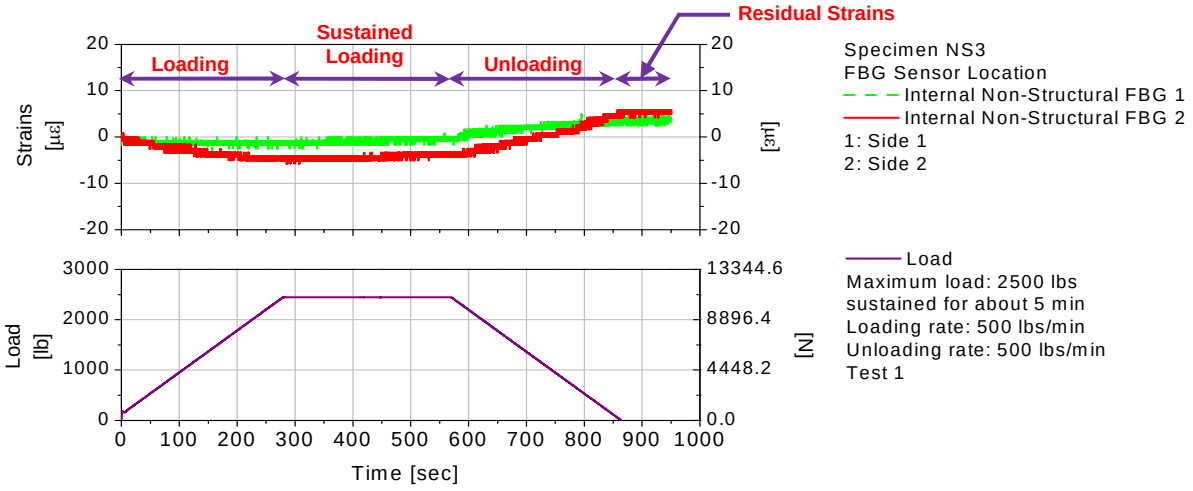

Figure 6.84. Modified Bending Test: Specimen NS1, Side 1 Loading – Strains and Load vs. Time

Table 6.21. Modified Bending Test: Summary of the Results for Specimen NS3, Side 1

	Internal FBG 1 Sensor	Internal FBG 2 Sensor
	[με]	[με]
Initial	-2.5	-5.0
End	-3.3	-5.8
Average	-2.4	-5.4
Standard Deviation	0.6	0.6
Residual Strains	3.3	5.8

- The presence of strains during loading and after the removal of the load could be attributed to the noise of the testing machine.
- Only the FBG 2 sensor embedded in Specimen NS2 registered internal average strains of 81.5 με (see Figure 6.85), being lower than the estimated theoretical lower bound strain of 133 με. The source of error was attributed to the package adhesive that may have bled in the recess area and partially attached the sensor to the recess area.

During the 5-min sustained loading, the strain standard deviations were lower than +/-1 με, indicating the stability of the sensor readings during maximum loading. After removing the load, the residual strains varied from 0.0 με to 5.8 με indicating that possible friction between the wood recess area and the lose FBG sensor may have occurred.

Based on the strain levels and the non-structural package installation, the following observations were made:

- In all cases, the techniques used to install the non-structural packages were proved to be easily implemented in any wood member.
- At the load of 2500 lbs, small mechanical internal strains were obtained in the non-structural packages isolating the sensors from structural response.
- The presences of residual strains confirmed that the sensors relatively moved inside the recess area. Further investigation of materials to support the sensors into the recess areas while isolating them from strain may be investigated with developed FBG sensors for non-structural sensing.

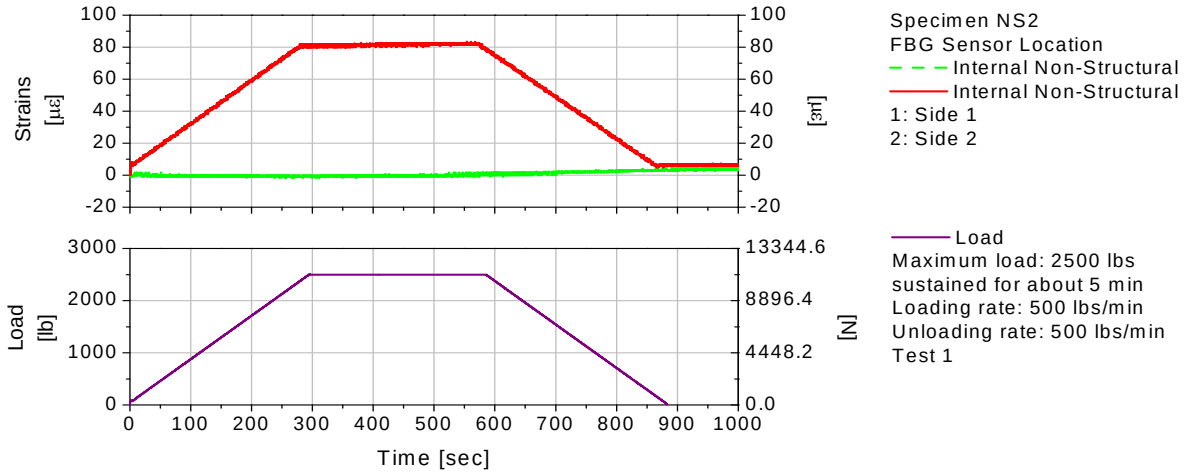

Figure 6.85. Modified Bending Test: Specimen NS2, Side 1 Loading – Strains and Load vs. Time

From the results, two non-structural package types were selected to be evaluated in the full scale glulam girder. The non-structural packages constructed with aluminum foil and Loctite 454 adhesive, and the one constructed with stainless steel shim and 3M VHB tape were selected to be installed in the full scale glulam girder because they exhibited the best strain isolation characteristics.

6.4. FULL SCALE GLULAM SPECIMEN

In the preceding chapter, FBG sensor packages for structural and non-structural purposes were selected based on the analysis of a series of bending tests performed on small scale glulam specimens. Before final selection of sensor package types, a full scale glulam girder was assembled at the manufacturing plant utilizing laminates previously instrumented with FBG sensor packages. It was found that after assembling and handling the girder, some of the internal FBG sensors did not survive. In the laboratory, other external FBG sensor packages and strain sensors were externally attached for comparison. The girder was tested with two-point loading simulating typical service truck levels for the purpose of evaluating the FBG sensor packages. A bending test was performed to establish the bending behavior. The girder was also tested in bending while varying the duration of the applied load and the cycle of the loading.

6.4.1. CONSTRUCTION OF THE SPECIMEN

The following section presents the construction of the full scale glulam specimen. In Chapter 3, four external and two internal structural FBG sensor packages were selected as was described previously to be installed in a full scale glulam specimen (girder) because of their consistent viscoelastic behavior. For non-structural packages, two types of packages were selected based upon their easy installation process and demonstrated ability to be strain isolated.

6.4.1.1. GLULAM GIRDER SELECTION

The selected girder represented a single girder from a fictitious double lane timber bridge with a 24-ft roadway width. The fictitious bridge superstructure was assumed to consist of seven 31-foot long glulam girders typically spaced at 44 in. with a cross section of 27 1/2 x 6 3/4 in. supporting a 5 1/8 in. thick transverse glulam deck (Wacker et al, 2001). The layup of the girder consisted of twenty Douglas-Fir laminates symmetrically balanced in lumber quality and strength through the depth. In Figure 6.86, the specimen cross section is shown. This balanced girder layup was selected for the

purpose of loading both bending surfaces, Side 1 and Side 2, to obtain both compressive and tensile flexural strains on each sensor.

Prior to assembling wood members and installing both internal and external packages, the laminates were visually inspected for surface irregularities. Encased and intergrown knots as well as finger joints were preferably avoided at the FBG sensor packages locations but still allowed in the vicinity of the sensors. The full-size glulam beam specimen was fabricated with a beam layup of 24F-V8 (DF/DF) by a glulam manufacturer located in Albert Lea, Minnesota.

(a) Selected laminates for girder assembling

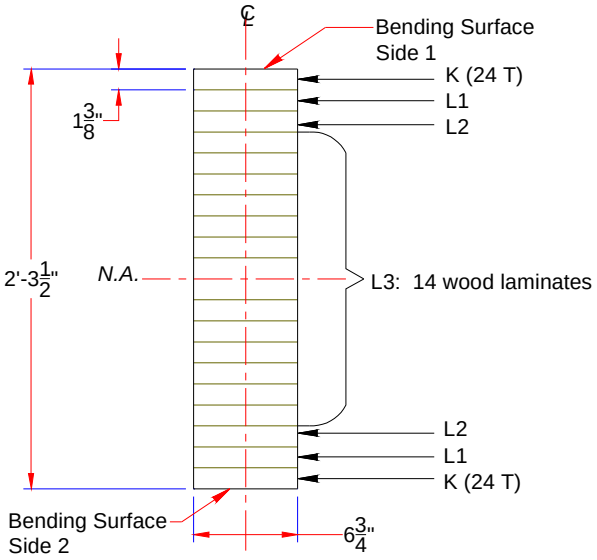

(b) Laminate distribution of glulam girder

Figure 6.86. Cross Section of the 24F-V8 DF/DF Glulam Girder

6.4.1.2. INSTALLATION OF THE EMBEDDED STRUCTURAL AND NON-STRUCTURAL FBG SENSOR PACKAGES

Two internal L1 and L2 graded laminates were instrumented with ten FBG sensors utilizing six structural and four non-structural packages. The FBG sensors were placed in three predetermined cross sections; one at mid span of the girder and two lateral ones at 7ft – 3 in. from the center (Figure 6.87); hereafter, the cross sections are referred as mid span, west and east sections respectively.

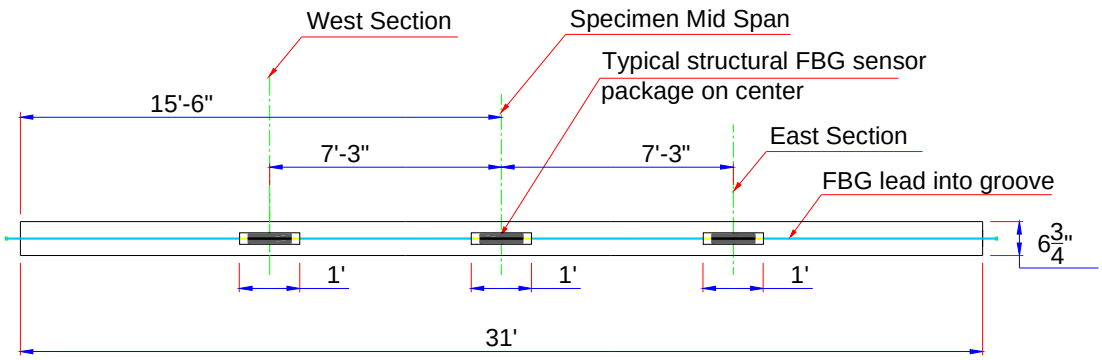

Figure 6.87. Typical Laminate Instrumentation: Plan View

For the L1 laminates, the structural FBG sensor packages were placed at each of the three cross sections. The L1 Side 1 and L1 Side 2 laminates were instrumented with the AM-SS Loctite 454 structural packages and the RS-SS Loctite 426 packages, respectively.

Similarly, the L2– Side 1 and Side 2 laminates were instrumented with two types of non-structural packages at the west and east sections. For the L2 – Side 1 and Side 2 laminates, the FBG sensors were protected with non-structural packages which consisted of aluminum foil bonded using 3M™ VHB™ – 5915 adhesive tape and stainless steel shim and Loctite 454 adhesive, respectively.

In Table 6.22, the location and material configuration utilized to fabricate the structural and non-structural packages per laminate are summarized.

Table 6.22. Location and Configuration of the Internal Structural and Non-Structural Packages

Laminate – Package Type	West Section	Mid Span	East Section
L1 Side 1 – Structural package	AM-SS with Loctite 454 adhesive	AM-SS with Loctite 454 adhesive	AM-SS with Loctite 454 adhesive
L2 Side 1 – Non-structural package	Aluminum foil bonded with Loctite 454 adhesive / FBG sensor stuffed with cotton fiber	---	Aluminum foil bonded with Loctite 454 adhesive / FBG sensor stuffed with foam
L2 Side 2 – Non-structural package	Stainless steel shim bonded with 3M VHB adhesive tape / FBG sensor stuffed with cotton fiber	---	Stainless steel shim bonded with 3M VHB adhesive tape / FBG sensor stuffed with foam
L1 Side 2 – Structural package	RS-SS with Loctite 426 adhesive	RS-SS with Loctite 426 adhesive	RS-SS with Loctite 426 adhesive

For the structural FBG sensor packages, the embedding technique given previously was followed. An additional 1/8-in. deep recess area was prepared to house the packaged FBG sensor and part of the

bare FBG strands with the purpose of reducing the possibility of crushing the FBG strand and lead (Figure 6.88). Grooves were routed 1/8 in. deep and 1/8 in. wide to host the FBG leads. For the RS-SS Loctite 426 packages, the recess area was 1 in. long x 12 in. wide; while for the AM-SS Loctite 454, the recess area was approximately 1 5/8 in. x 12 in.

Using the same technique as in the small specimens, 1/4 in.-deep recess areas and grooves were routed in the longitudinal direction for the non-structural packages. Two 12-in. long recess areas were routed 1/2 in. wider than the packaged sensor. In Figure 6.89, the recess area, the packaged FBG sensor, the leads and the position of the backing material are shown. The non-structural backing materials consisted of two pairs of aluminum foils and stainless steel shim sheets that were prepared 1 in. wider than the recess areas (i.e., 1 3/8 x 12 in. and 2 x 12 in.). Both aluminum foils and stainless steel shim were bonded surrounding the recess area utilizing the selected adhesive tape or adhesive. The embedding of the non-structural was completed as discussed previously.

Bare FBG strain sensors with total lengths of 32 ft. were manufactured in series of three and two sensors spaced at approximately 7 ft. 3in. and 14 ft 6 in., for the structural and non-structural packages respectively. The FBG sensor spacing was coincident with the cross sections to be instrumented. In all cases, the FBG sensors were manufactured in SMF 28-compatible fiber type and coated with polyimide (see Section 6.2.1). The grating length was approximately 1/2 in. centered in the bare portion of the fibers. Each set of FBG sensors were manufactured with two FC/APC connectors.

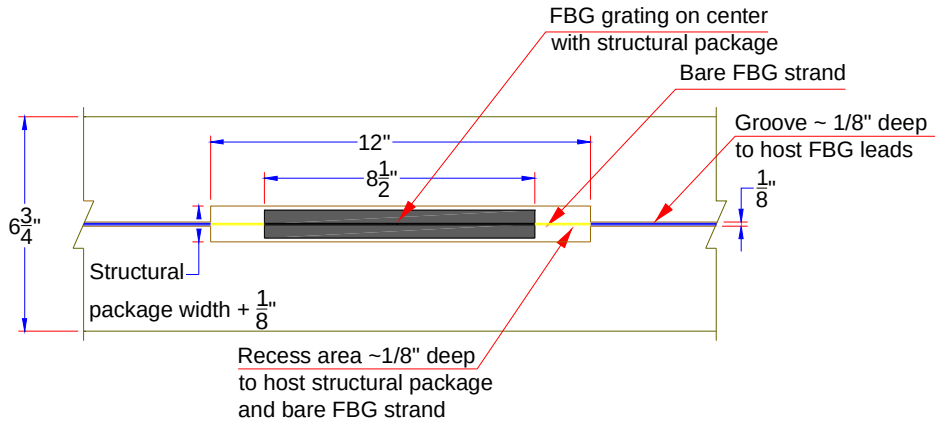

Figure 6.88. L1 Laminate Instrumentation: Detail of Structural FBG Sensor Package

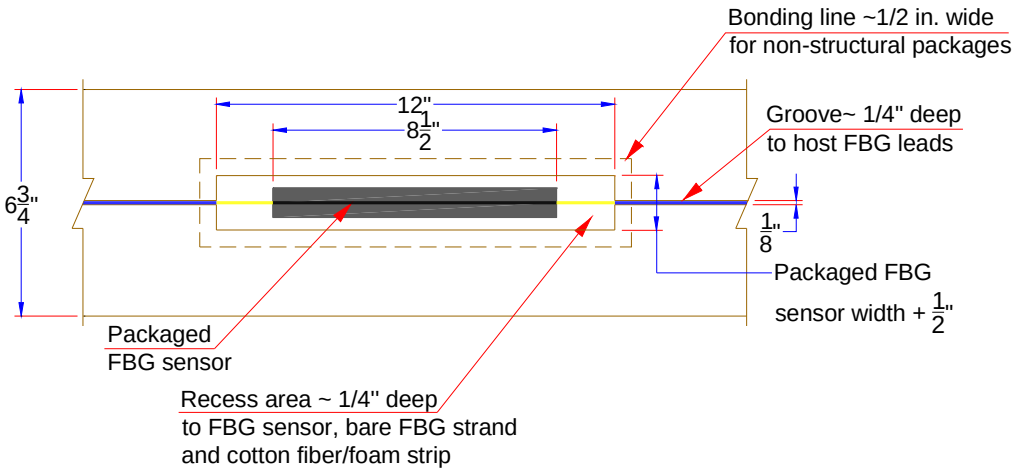

Figure 6.89. L2 Laminate Instrumentation: Detail of Non-Structural FBG Sensor Package

As shown in Figure 6.90, the recess areas were prepared for the respective structural FBG sensor packages. After bonding the AM-SS Loctite 454 and RS-SS Loctite 426 backing materials, the central FBG sensor was bonded in accordance with the procedure previously discussed; later, the lateral sensors were placed at the west and east sections located at 7ft. 3in. from centerline (see Figure 6.91). All structural adhesives were cured for a minimum of 24 hours.

For the non-structural FBG sensor packages, the FBG sensors were accommodated in the recess area (see Figure 6.92) following the methodology discussed previously. In Figure 6.93, both non-structural packages are shown. The adhesives and adhesive tapes were cured for 24 and 72 hours respectively, as specified by the manufacturers. After installing the sensors, the FBG leads were secured in grooves which were filled with a commercially available silicone (see Figure 6.94).

To complete the internal instrumentation, the FBG connectors were inserted into a 5/8 in.-deep recess area routed at both ends of the laminates (see Figure 6.95 (a)). Backing material was then inserted to protect the FBG connectors from the glulam adhesive. As shown in Figure 6.95 (b), a stainless steel shim covered the recess area and aluminum foil was partially bonded to the stainless shim and free at the laminate end to allow access the FBG connectors after girder laminating.

Wavelength readings were obtained in the ten installed FBG sensors indicating that all sensors were operative before assembling the laminates. In all cases, the wavelength repeatability ranged within +/- 2με (i.e., sensor precision).

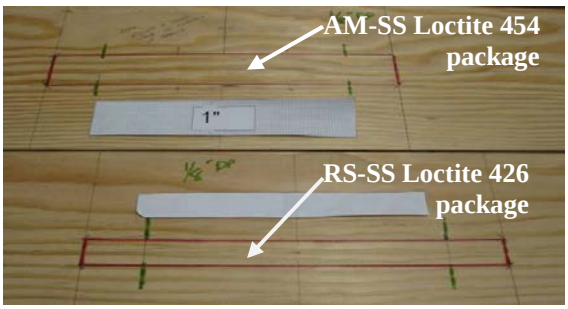

(a) Outlining the recess areas

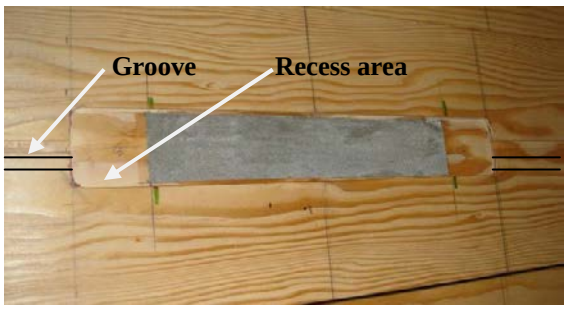

(b) Recess area and groove for backing material and FBG leads

Figure 6.90: Preparation of the Laminate

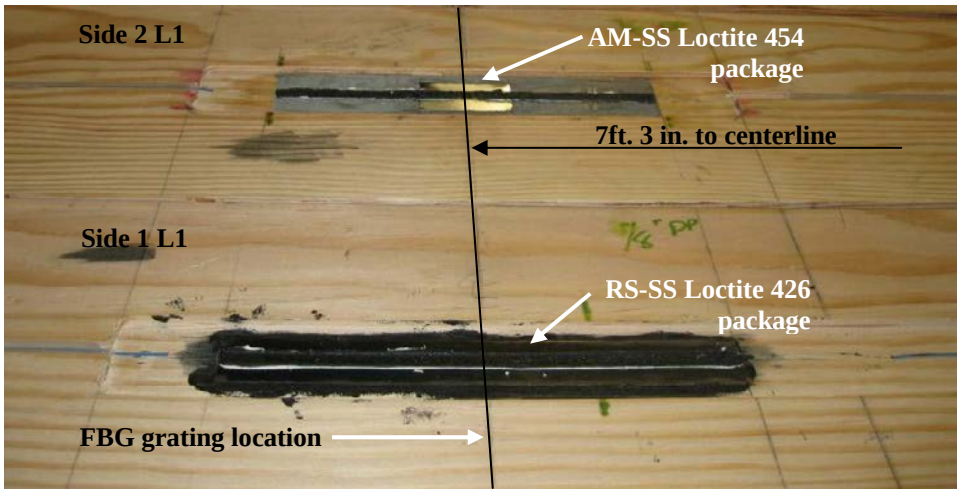

Figure 6.91. Internal Instrumentation of Laminates L1 with FBG Sensors with Structural Packages

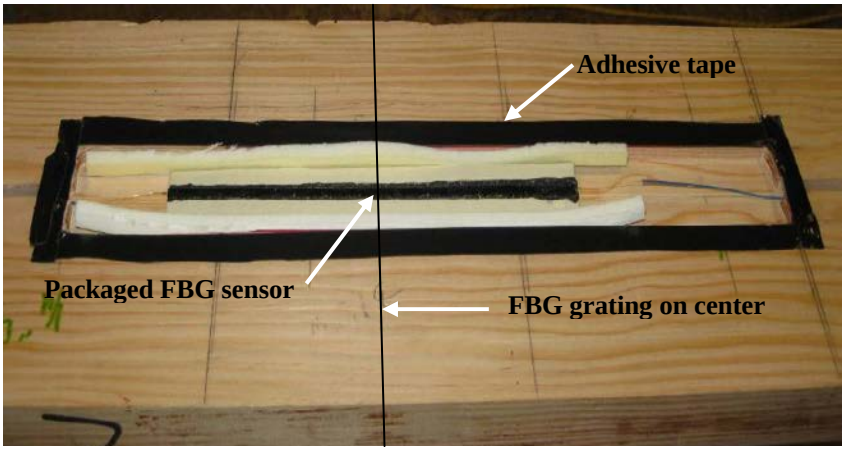

Figure 6.92: Installation of the FBG sensor and Adhesive Tape

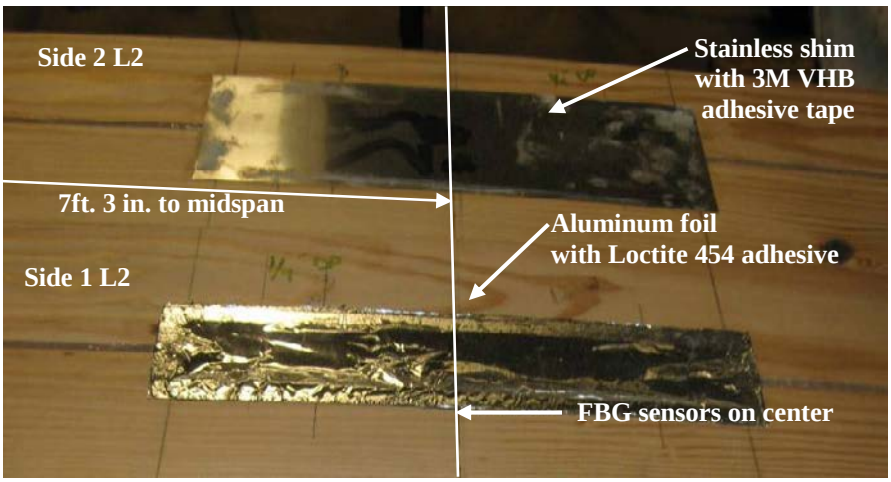

Figure 6.93: Installation of Non-Structural Packages

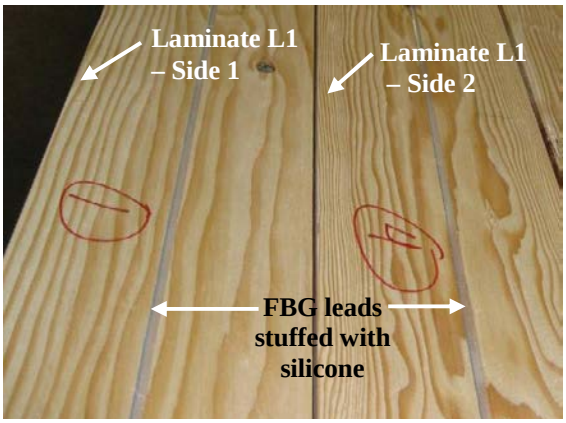

Figure 6.94: Protection of the FBG sensor leads

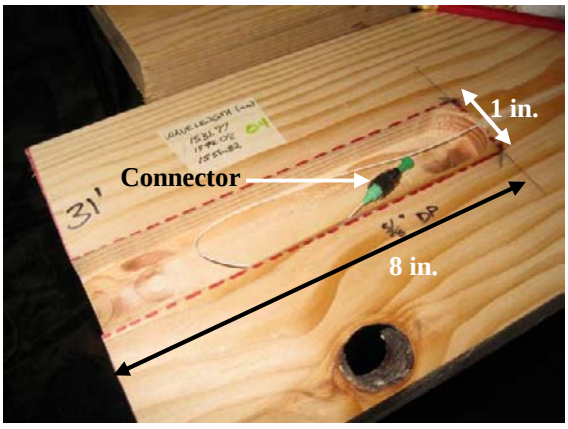

(a) 5/8 in.-deep recess area to host the FBG connector

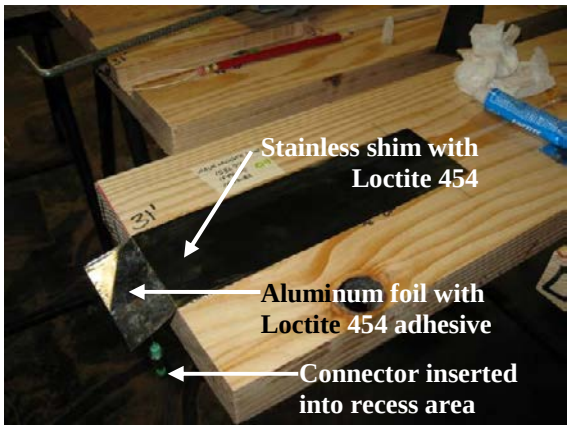

(b) Stainless shim and aluminum foil for protecting the FBG connector

Figure 6.95: Protection of the FBG connectors

6.4.1.3. GLULAM GIRDER ASSEMBLING

After completing the internal instrumentation, the 31-foot long laminates were assembled at the manufacturing plant. Each laminate was inserted in the bonding machine at a speed of 390 ft/min with glue lines spaced at approximately 1/4 in. (Figure 6.96 (a)). For the instrumented L1 and L2 laminates, the bonding speed was reduced to one half with the purpose of providing double volume of adhesive and less pressure in an effort to avoid damaging the bare portion of the FBG sensors if exposed (Figure 6.96 (b)). Each of the recently glued laminates was manually placed on its narrow edge (see Figure 6.96 (c)), laterally aligned and pounded against the steel frame with very heavy weights. Clamps spaced at 16 in. on center were manually bolted and fastened using a torque wrench to a clamping pressure of approximately 100 psi (see Figure 6.96 (d)). Once again, wavelength readings were taken confirming that all ten sensors were operative.

(a) Glue application

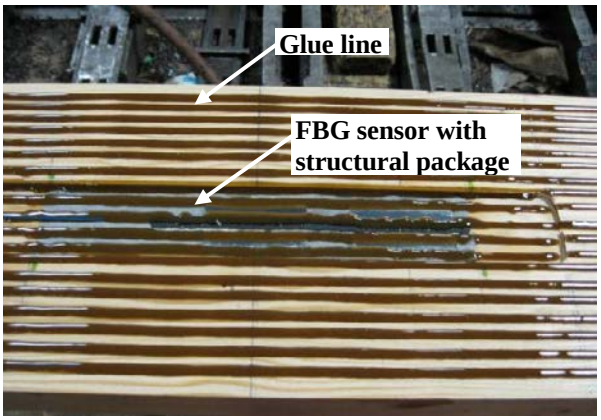

(b) Close up of the glue application

(c) Manually placing one laminate L3

(d) Fastening the clamps

Figure 6.96: Assembling of the Wood Laminates

The clamping force on the glulam girder was maintained for 48 hours. The clamps were released one by one with the torque wrench. To complete the manufacturing process, the girder was laterally surfaced to the width of 6 3/4 in. The girder was packaged and transported to the Iowa State University Structures Laboratory (Figure 6.97). No wavelength data were gathered during these activities. Immediately upon arrival, wavelength readings from the ten internal FBG sensors were taken. At this stage, two of the six FBG sensors with structural packages and two of the four FBG sensors for non-structural purposes were operative. Many sources that could have damaged the FBG sensors were suspected (i.e., during unclamping, lateral resurfacing, packaging for delivery, transportation, lifting, etc); however, no one source could be clearly identified.

Figure 6.97: Full Scale Glulam Girder at the Laboratory

6.4.1.4. INSTALLATION OF THE ATTACHED STRUCTURAL PACKAGES

A total of six external FBG strain sensors were installed on bending surfaces Side 1 and Side 2 using four packages selected from Chapter 3 and summarized in Table 6.23. The external instrumentation followed the developed attaching technique presented previously.

Table 6.23. Location and Configuration of the External Structural Packages

Location	West Section	Mid Span Section	East Section
Side 1	C-FRP Loctite 426	C-FRP Loctite 426	72H-SS Loctite 4212
Side 2	RS-SS Loctite 426	RS-SS Loctite 426	IS-SS Loctite 4212

Prior to attaching the external FBG structural packages, each bending surface was cleaned from wood slivers with a brush. All structural packages were directly bonded to the bending surface and

only routed along the length of the FBG leads. An additional piece of steel shim was bonded to protect the exposed bare fiber (see Figure 6.98(a)). All adhesives were cured for 24 hours. The backing materials were cleaned and taped to form a reservoir which was smoothed and cleaned. The bare FBG sensor was submerged into the Loctite 410 adhesive as shown in Figure 6.98 (b). After completing the curing time, the tape was removed and the packages were cleaned with acetone. Wavelength readings were taking before and after the installation confirming that all FBG sensors were operative.

In addition to the above mentioned external sensors, commercially available Stainless Steel Mounted (SSM) FBG strain sensors (Figure 6.99 (a)) were installed near the Side 1 FBG sensors with custom design packages (Figure 6.99 (b)). These manufactured FBG sensors are manufactured from a single mode fiber SMF28 compatible fiber optic coated with polyimide. The grating length is protected by a 302-stainless steel package, which provides an effective gage length of approximately 0.87 in. According to the manufacturer's specifications, these FBG sensors have an estimated strain sensitivity of 0.0014nm/με within a range of +/- 2500με and can be thermally compensated. The locations of the FBG sensors with structural and non-structural packages that were embedded in and attached to the full scale glulam girder are shown in Figure 6.100 (a). The position of the sensors within the three cross sections is indicated in Figure 6.100 (b).

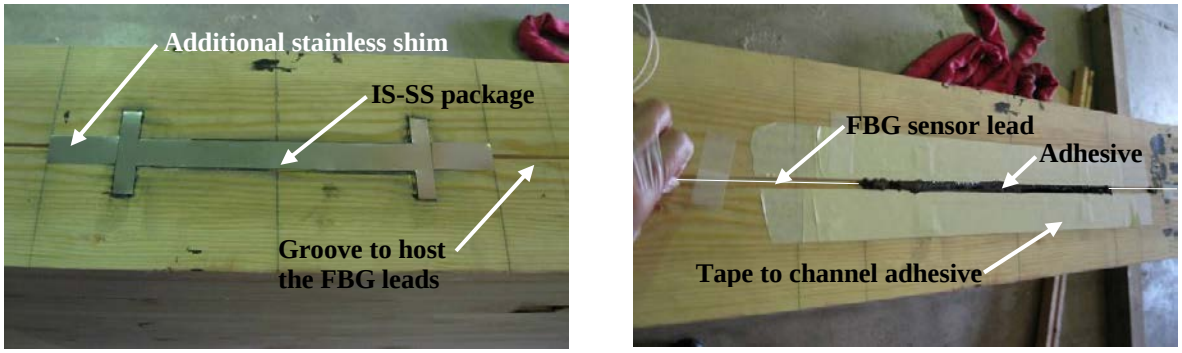

(a) Bonding of the package (b) Installation of the bare FBG strain sensor

Figure 6.98: External Structural Package and FBG Sensor Installation

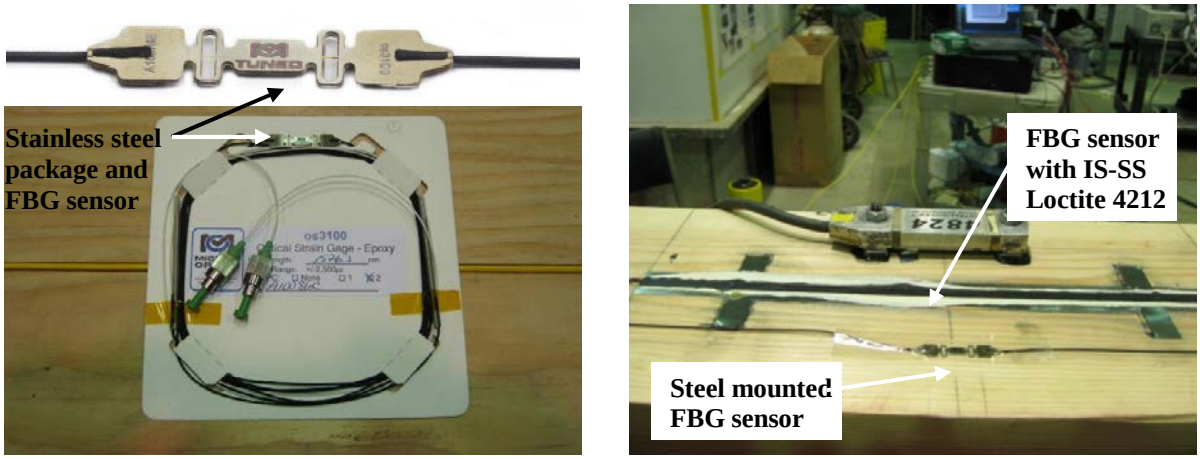

(a) Detail of the stainless steel package and FBG sensor (b) Location of the sensors on Side 1

Figure 6.99: Steel mounted FBG strain sensor for epoxy

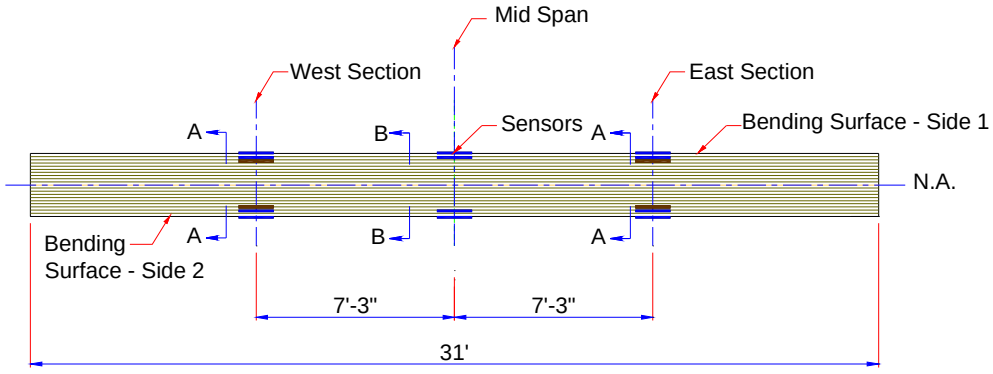

(a) Location of FBG Sensors along the glulam girder

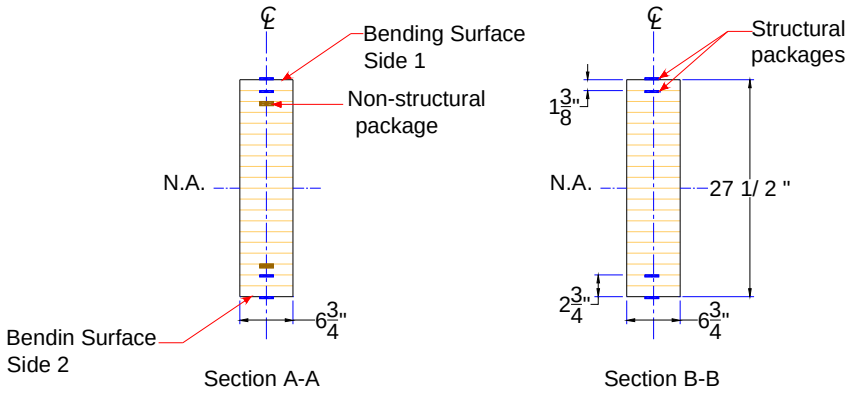

(b) Scheme of the cross sections

Figure 6.100. Location of the FBG Sensor Instrumentation at the Full Scale Glulam Girder

6.4.2. FULL SCALE GLULAM GIRDER: MECHANICAL PROPERTIES

According to the published graded 24F-V8 DF/DF girder characteristics for loads applied perpendicular to the wide faces of the laminations, the modulus of elasticity was estimated to be 1800 ksi (APAEWS, 2004). Thus, theoretical strains were calculated using basic beam theory formulas, assuming that the girder is loaded in the elastic range and both compressive and tensile flexural properties are the same. In Table 6.24, the estimated strains at each sensor location under codified design conditions are summarized per cross section. Theoretical vertical displacements at mid span and at the loading sections were estimated also to be 0.96 in. and 0.91 in., respectively.

Table 6.24. Theoretical Strain Levels due to Bending at the FBG Sensor's Locations

Laminate	Mid Span	West/East Section
	[με]	[με]
External laminate – K	974	719
Internal laminate – L1	877	647
Internal laminate – L2	799	575

6.4.3. STATUS OF THE FBG SENSORS

The internal FBG strain sensors were operative during and immediately after girder fabrication. In the plant, the girder was unclamped after 48 hours, surfaced to the final dimensions and wrapped for delivery to the laboratory.

In the laboratory, four of the six FBG sensors with structural packages and two of the four FBG sensors for non-structural purposes were found to be working following delivery. After placing the girder on Side1, one of the internal FBG sensors located on Side 1 stopped working. Similarly, when the girder was positioned on Side 2, one internal sensor on Side 2 stopped working. Of the four internal operative sensors, two structural and two non-structural sensor packages were operative. After preloading the girder with a total of 2000 lbs to verify the operability of the sensors and load cells, two internal FBG sensors for structural purposes stopped working. In Table 6.25, the status of the operative FBG sensors at the time of testing is summarized.

6.4.4. TESTING PROGRAM

A testing program was conducted to verify the performance of the sensor packages in and on the manufactured girder. Before testing, a frame test setup was constructed and additional instrumentation was installed. The girder was subjected to bending tests with a total load of 23,680 lbs to evaluate the behavior of the FBG sensor packages under:

Table 6.25. FBG Sensors with Structural and Non-Structural Packages – Status of the FBG Sensors

Laminate Location	West Section		Mid Span Section		East Section	
	Package	Status	Package	Status	Package	Status
Ext. Laminate K	C-FPR Loctite 426	O	C-FPR Loctite 426	O	IS-SS Loctite 4212	O
Int. Laminate L1	AM-SS Loctite 454	X	AM-SS Loctite 454	X	AM-SS Loctite 454	X
Int. Laminate L2	Aluminum foil with Loctite 454	X	---	---	Aluminum foil with Loctite 454	O
Int. Laminate L2	Stainless steel shim with 3M VHB adhesive tape	X	---	---	Stainless steel shim with 3M VHB adhesive tape	O
Int. Laminate L1	RS-SS Loctite 426	X	RS-SS Loctite 426	X	RS-SS Loctite 426	X
Ext. Laminate K	RS-SS Loctite 426	O	RS-SS Loctite 426	X	72H-SS Loctite 4212	X

Note.- "O" denotes that the FBG sensor is operative; "X" denotes that the FBG sensor is inoperative.

- Loading and unloading of the girder with four step loadings of 25%, 50%, 75% and 100% of the total load (23,680 lbs).
- Sustained loads (eight hours) under uncontrollable laboratory temperatures.
- Short term pseudo cyclic loadings.
- In addition, the strain readings were recorded due to laboratory temperature variations to establish a relationship between sensor readings and temperatures.

6.4.4.1. TEST SETUP

The full scale specimen was tested in bending by the two-point loading method. The 31-ft. girder was supported by one pin and one roller located 6 in. from each girder end. To apply the load at two points, two steel load frames were constructed and positioned at 4 ft. 6 in. from the mid span. In Figure 6.101 and Figure 6.102, details of the typical bending test configuration are shown.

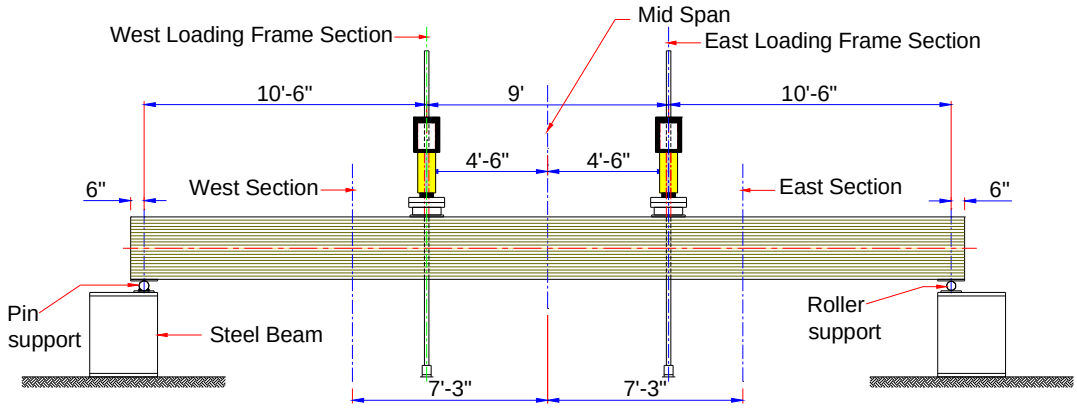

Figure 6.101. Full Scale Glulam Girder

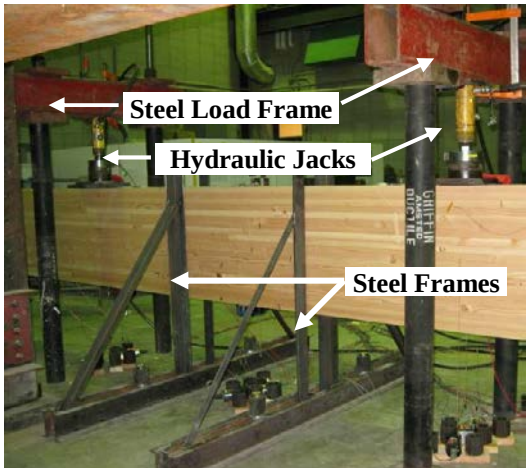

(a) At mid span: Two inverted T frames spaced at 4 ft to prevent instability

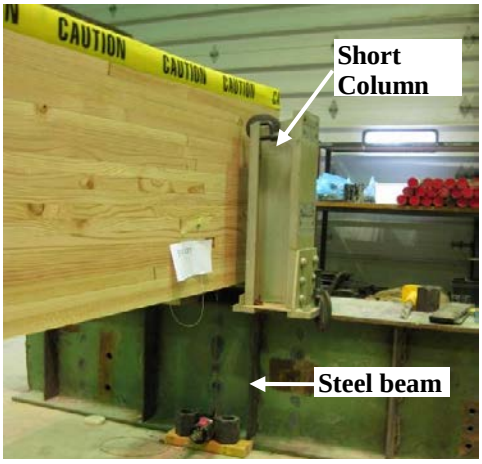

(b) At the support: view of one lateral short column to prevent instability

Figure 6.102: Typical Bending Test Configuration

6.4.4.2. ADDITIONAL SENSORS AND OTHER TESTING EQUIPMENT

In addition to the FBG sensors, the girder was externally instrumented with six foil strain gages and six strain transducers located near the FBG strain sensors. These sensors were laterally placed at 1 1/2 in. from the edge at mid span as well as at the west and east sections. The foil strain gages were centered with respect to the FBG sensor grating and topped with a strain transducer (see Figure 6.103) as was described in previous section.

Differential current displacement transducers (DCDTs) were connected to the bottom and mid depth of the girder to measure the deflections. Five DCDTs were centered on the girder coincident with load frames, at mid span, and near the supports. In addition, three pairs of DCDTs were placed at mid depth at the load locations and at mid span. In Figure 6.104, the locations of the DCDTs are presented. Photographs of typical DCDTs are shown in Figure 6.105.

6.4.4.3. TEST PROTOCOLS

As previously mentioned, the girder was tested using the two point loading method. All data were collected at a frequency of 1 Hertz. Three series of bending tests were conducted similar to the small specimens' test protocols and adapted from the ASTM 198-05a provisions (ASTM 198-05a, 2005). Bending tests were performed to evaluate the general behavior. A sustained loading test was performed for eight hours to evaluate the viscoelastic behavior of the packages during and after loading. In addition, a pseudo cyclic loading was conducted to evaluate the energy dissipation capabilities of the sensors. All bending tests were first performed on Side 1, and repeated on Side 2.

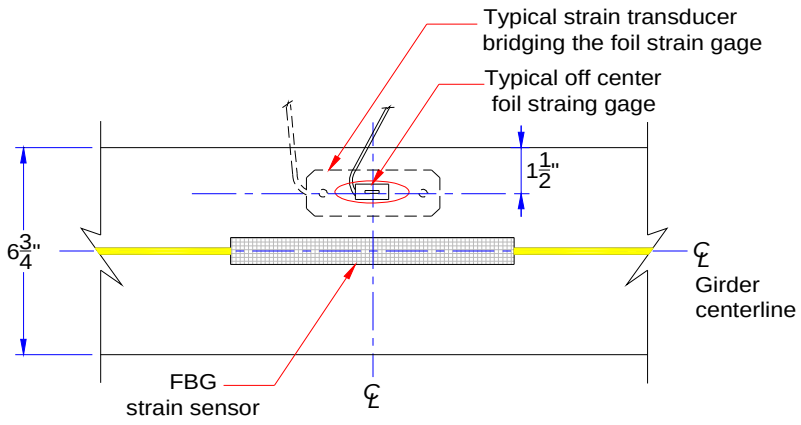

Figure 6.103: Location of the Foil Strain Gages and Strain Transducer

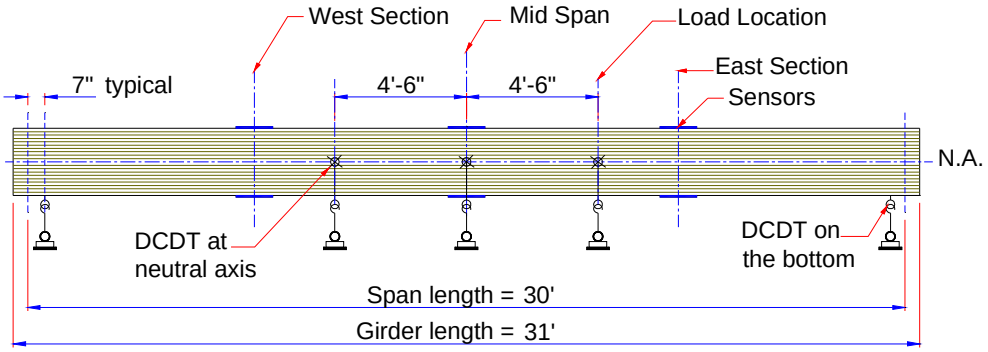

Figure 6.104: Location of the DCDTs

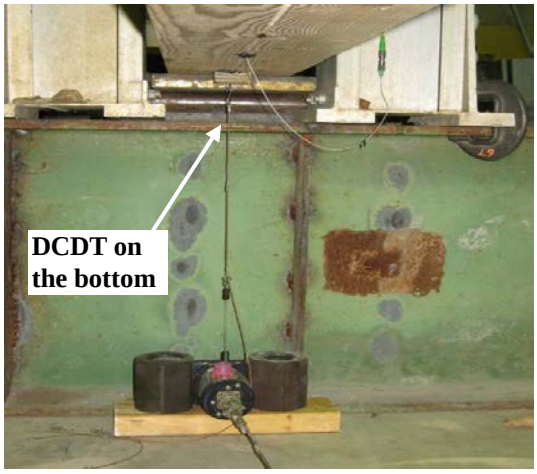

(a) DCDT on the bottom at one girder end

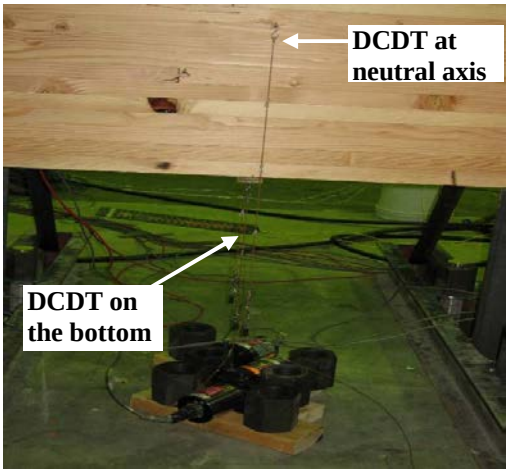

(b) DCDTs at mid span

Figure 6.105: View of DCDTs

6.4.4.3.1. **Bending Test**

The bending test was performed to evaluate the strain levels in the structural and non-structural FBG sensor packages under minimal and maximum service loads. In addition to this, experimental FBG strains were compared to theoretical values and to the foil strain gages and strain transducers' data, where possible.

For the bending test, the girder was subjected to four load steps with total loads equivalent to 25%, 50%, 75% and 100% of 23,680 lbs. In each step, the load was applied with a loading rate of approximately 3000 lbs/min, maintained constant for three minutes and removed for another three minutes. After applying the four load levels, strain data were continuously collected for another 30 minutes. The test was repeated to verify the reproducibility of the results.

6.4.4.3.2. **Sustained loading Test**

Sustained loading tests were performed to evaluate the elastic and viscoelastic behavior of the structural FBG sensors packages and the loading effect in the non-structural FBG sensor packages. In addition to the strain instrumentation, three thermocouples were installed near the Side 1 sensor locations. After loading the girder with a rate of approximately 4000 lbs/min, the total load of 23,680 lbs was maintained constant for eight hours. After unloading, strain data were collected for at least eight hours to investigate the residual strains. The test was performed twice to verify the reproducibility of the strain data. The same test protocol was repeated on Side 2.

6.4.4.3.3. **Pseudo Cyclic Loading Test**

The main objective of this test was to evaluate the viscoelastic behavior of the adhesive through strain phase lag and residual strains. In addition, the capability of the non-structural packages to isolate the structural response under pseudo cyclic loading was evaluated. The girder was loaded and unloaded with a manually controlled electric pump. Each test consisted of twelve cycles to a total load 23,680 lbs applied in intervals of approximately one minute. After the twelve cycles, data were collected for 30 minutes to allow for stabilization of the sensors. The test was repeated to verify its reproducibility.

6.4.4.3.4. **Temperature Effect Test**

Temperature effects on the FBG sensors with structural packages were evaluated by comparing the readings and the temperature fluctuations under no load. The ambient temperatures were modified by introducing cool temperatures to the laboratory. In the first hour, ambient laboratory

temperature and strain data were gathered. In the second hour, the specimen was subjected to the environmental cold temperatures. Following this, the girder was warmed for an additional hour. The temperature test was performed before the sustained loading test. Data were obtained for Side 1 and later for Side 2 sensors.

6.4.5. EXPERIMENTAL RESULTS

In this section, the analyses of the results are presented. In addition, comparisons to theoretical values are made, when applicable.

6.4.5.1. BENDING TEST

The objective of this bending test was to evaluate the behavior of both the structural and non-structural FBG sensor packages when the girder was subjected to four gradual and consecutive loadings and unloading up to service levels. The strain levels were examined to verify each sensor readings' consistency and behavior. In addition, the strain levels were compared to the theoretical values and other sensor responses, where applicable.

6.4.5.1.1. **Structural Packages**

The FBG sensor packages' strains were evaluated to verify the consistency of the readings during loading, at the maximum load and after removing the load as follows:

- Comparison of the modulus of elasticity (MOE) per package and each step loading. In addition, the evaluation of the apparent MOE based on the ASTM D 198 – 05a provisions.
- At each load step, the location of the neutral axis was investigated.
- At constant loading, the consistency of the strain levels was assessed per package.
- Assessment of the residual strains.

In Figure 6.106, a typical strain and load history is presented. Note that in the plot, the applied load (i.e., 25% through 100%) was sustained of approximately three minutes and removed for a minimum of three minutes. After removing the load, small residual strains were present.

MOE Evaluation. Experimental MOEs were determined per FBG sensor package at each load step to verify the consistency of the readings and linear elastic behavior of the packages under short term loading. In Figure 6.107, an example of the MOEs for the four-step loadings with respect to the West C-FRP Loctite 426 sensor is shown. As observed, the calculated MOE values were similar

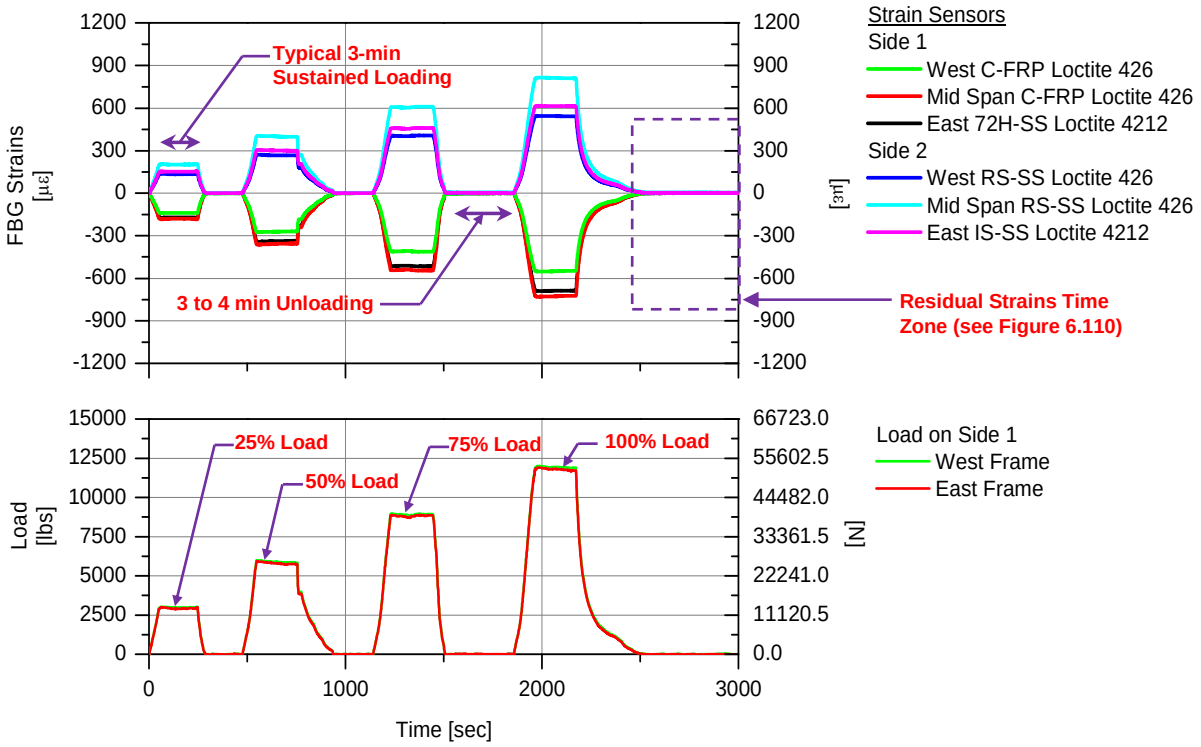

Figure 6.106. Bending Test: Typical FBG Strain and Load History

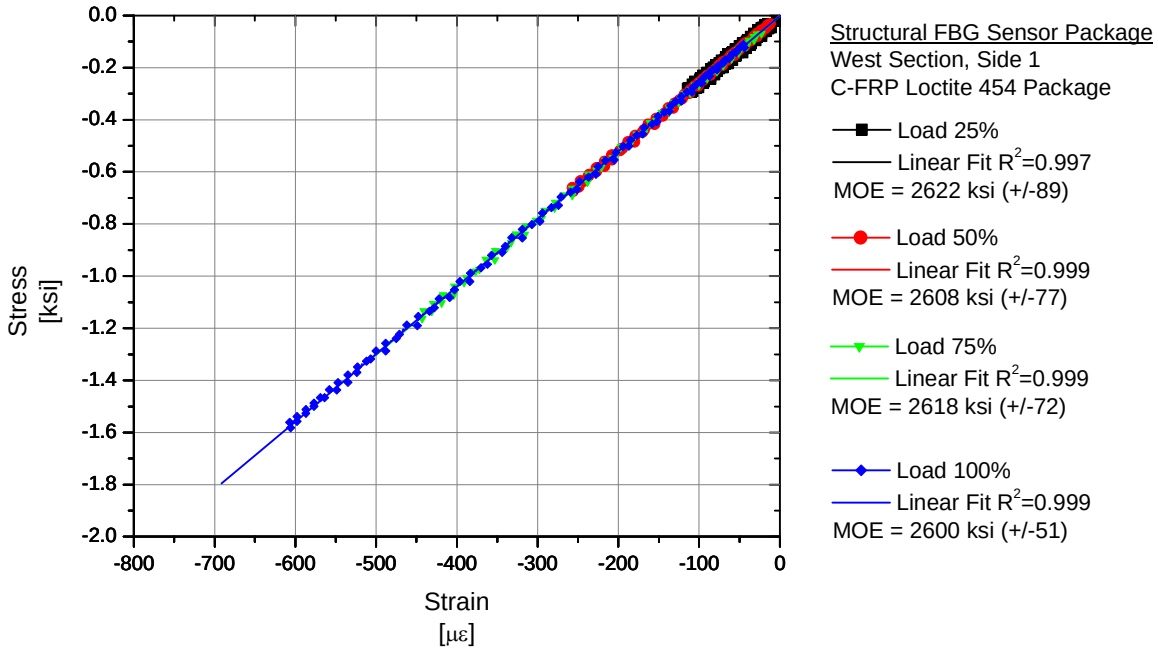

Figure 6.107. Bending Test: Strains vs. Stress Comparison – Side 1 Loading

during all load steps indicating consistency in response. Overall, most FBG sensor readings resulted in MOE values that were consistent at all loadings; differences of only 8% with respect to the maximum loading were calculated. However, the West SSM FBG sensor had variable MOEs that varied from 3918 ksi (+/-133) for the 25% loading to 4708 ksi (+/-461) for the 100% loading. The MOE differences were attributed to localized factors such as a knot hole.

In Table 6.26, MOEs are summarized for the nine structural packages with respect to the 100% load. For the custom design packages on Side 1, the compressive MOEs were larger than the tensile values by at least 11%. The Side 2 FBG sensors had similar MOE values; differences of up to 3% were attributed to the minor surface irregularities.

In addition, the apparent MOE was calculated using the deflections at midspan and then compared to the calculated MOE values (ASTM D 198 – 05, 2005). For the Side 1 and 2 loadings, the MOEs calculated from the deflections were 2043 ksi and 2037 ksi, respectively. When comparing the apparent MOEs to the midspan experimental values, the differences were between 4% and 20% (see Table 6.26).

Table 6.26. Bending Test: Summary of Average Modulus of Elasticity and Standard Deviation

Side Loading	Side	Sensor Package Type	West Section		Midspan Section		East Section	
			Avg. MOE	Std. Dev.	Avg. MOE	Std. Dev.	Avg. MOE	Std. Dev.
			[ksi]	[ksi]	[ksi]	[ksi]	[ksi]	[ksi]
1	1	Custom Design	(2600)	51	(2452)	48	(3222)	70
	1	SSM	(4708)	461	(2203)	46	(2945)	71
	2	Custom Design	3273	77	2184	48	2857	73
2	1	Custom Design	2340	102	2260	83	2890	111
	1	SSM	3403	114	1712	74	2232	90
	2	Custom Design	(3218)	120	(2119)	71	(2884)	98

Note.- Avg. MOE.: stands for Average Modulus of Elasticity, Std. Dev.: stands for Standard Deviation, ( ): corresponds to the compressive Avg. MOE.

Maximum Loading – Experimental Neutral Axis Comparison. At the three cross sections, the position of the neutral axis based on the external FBG strains per load step was determined and compared to the other loadings' positions. As an example, in Figure 6.108 and Figure 6.109 the neutral axis positions for four step loadings are shown for the midspan section Side 1 and 2 loadings,

respectively. Note that for each side loading, the neutral axis position was basically the same at each of the four load steps. In all cases, the compressive and tensile strains at each load level were different due to the dissimilar MOE. Consequently, the neutral axis location was not coincident with the geometric center of gravity. At the midspan section, the distance between the neutral axis and the center of gravity was 0.5 in. and 0.7 in., with respect for Side 1 and Side 2 loadings. For the west and east sections, the neutral axis positions per side loading were also comparable for all step loadings. The distance between the neutral axis and center of gravity of the cross section was between 0.0 and 2.1 in.

Short-Term Strain Consistency. After each step loading, the load was maintained constant for three minutes. During this interval, the strain data dispersions were calculated to evaluate the consistency of each FBG sensor reading. In all cases, the strain dispersions were less than +/-3 με.

Residual Strains. After completing the bending program, the strain levels decreased over the period 30 min. As observed in Figure 6.110, the residual strains for all FBG sensors were small, typically varying from 1.7 με to 3.3 με.

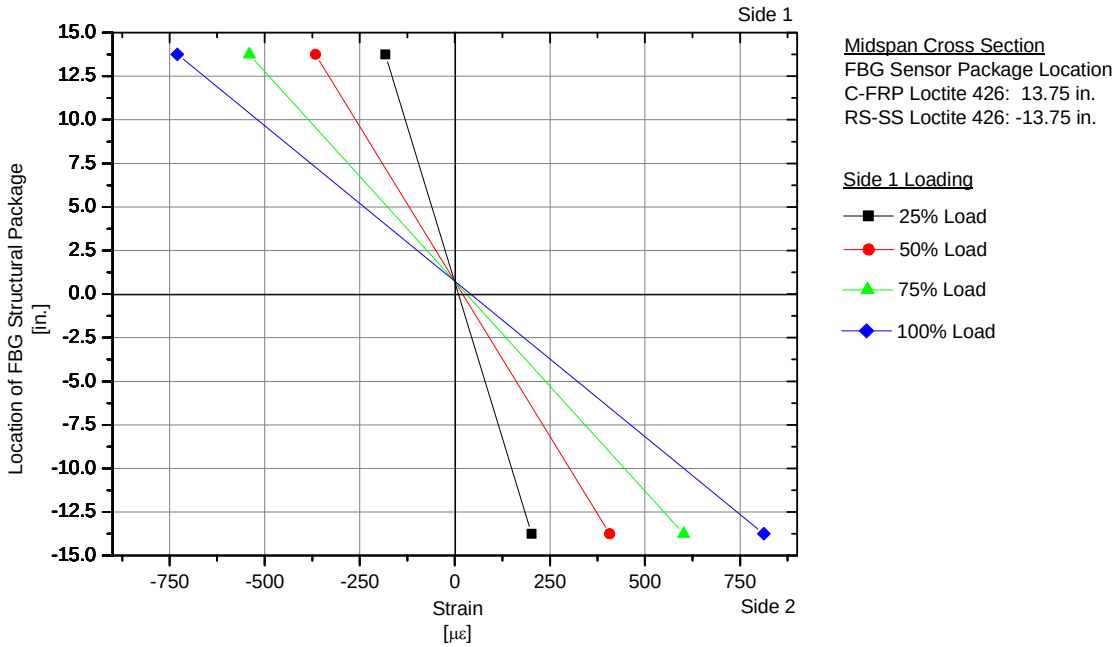

Figure 6.108. Bending Test: Neutral Axis Locations – Midspan Section, Side 1 Loading

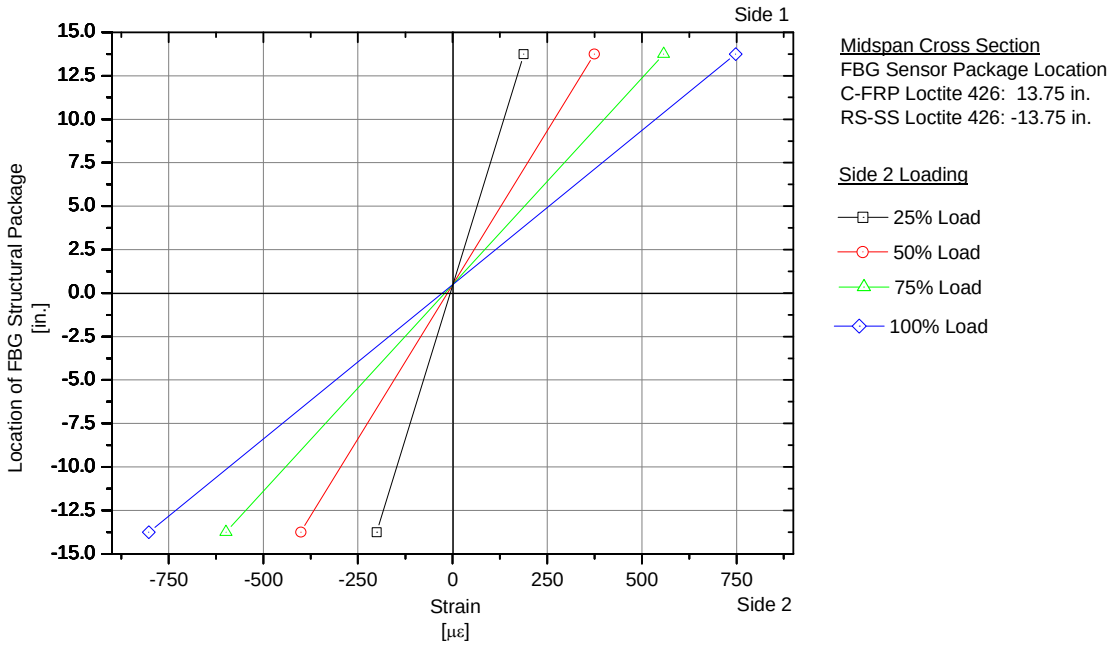

Figure 6.109. Bending Test: Neutral Axis Location – Midspan Section, Side 2 Loading

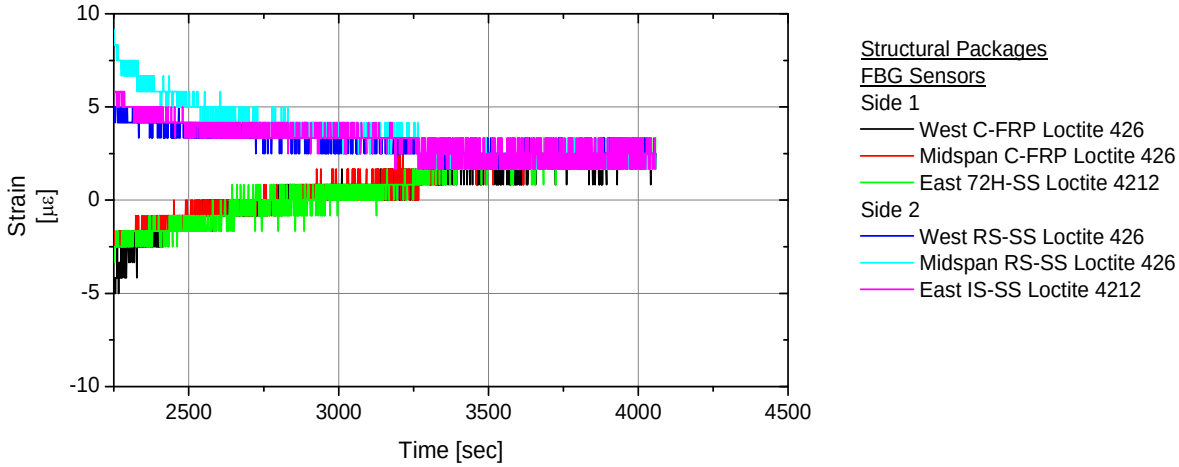

Figure 6.110. Bending Test: Typical Residual Strain Responses (see Figure 6.106)

STRAIN COMPARISONS. The operability of the FBG sensor packages was evaluated by the following comparisons:

- Experimental FBG strains and associated deflections were compared to theoretical values.
- Experimental FBG strains were compared to the other installed sensors' responses.

Theoretical Strain Comparison. In each loading phase, the experimental strain levels were observed to be consistently lower than the theoretical values. As an example, the strains for an

applied load of 23,680 lbs (100% loading) are shown for the three cross sections in Figure 6.111. The differences between the experimental and theoretical strains ranged from minimal to 300 με. The largest differences were observed in the West SSM FBG strains.

Theoretical Deflection Comparison: Each set of experimental deflection data were compared to their respective theoretical values. Typically, the average deflections were lower than their respective theoretical values. In Table 6.27, the average deflections at the three main locations for a total load of 23,640 lbs and their respective theoretical deflections are presented for comparison. When comparing Side 1 and 2 loading deflection levels, both values were consistently on the same order.

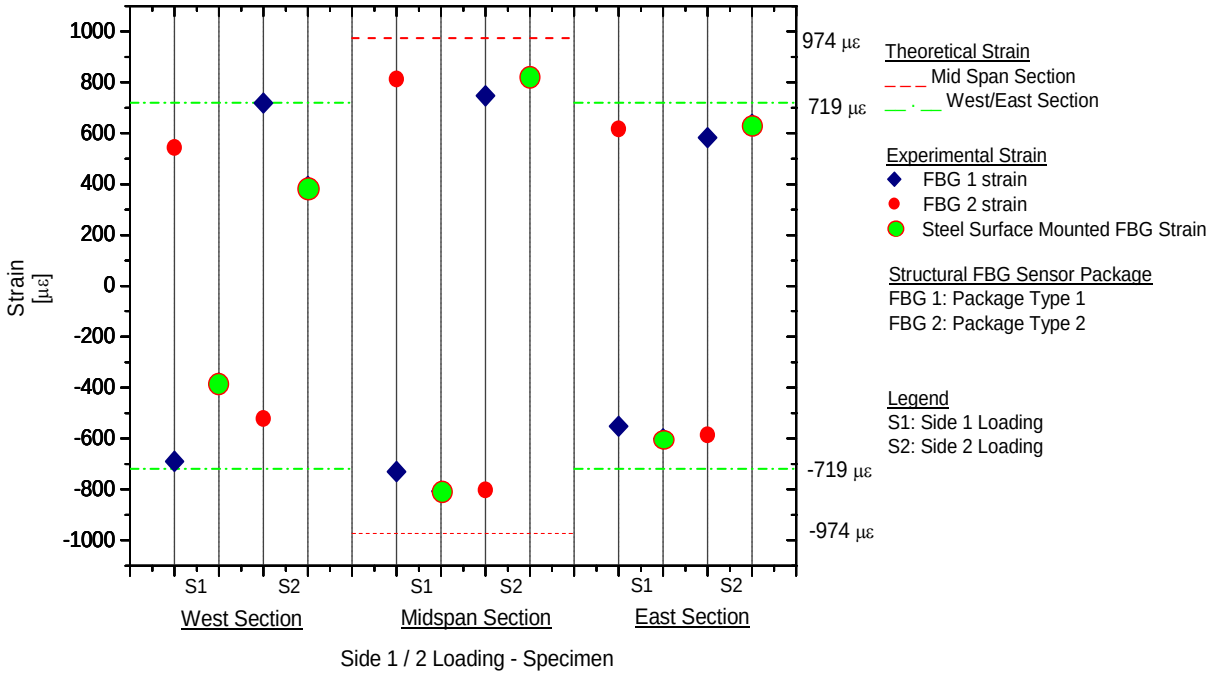

Figure 6.111. Bending Test: Comparison of Theoretical and Experimental External FBG Strains

Table 6.27. Bending Test: Deflections at the Maximum Loading

Bending Load	Side Loading	West Load Frame	East Load Frame	Theoretical Deflection	Mid Span	Theoretical Deflection
100%	S1	0.767	0.762	0.910	0.849	0.960
	S2	0.761	0.760		0.850	

Foil Strain Gages and Strain Transducers Comparison. At maximum loading, both structural FBG sensor package types were compared to readings from the foil strain gages and strain transducer. In addition, the FBG sensors were compared to the average strain of all sensors to determine the consistency in measurements.

Sensor Strain Comparison. In Figure 6.112, the comparisons of the west section sensors (including FBG sensors, foil strain gages and strain transducers) and theoretical strains are presented for both Side 1 and 2 loadings. In this plot, the FBG sensors with custom design packages had strain levels on order of the foil strain gages and strain transducers, with strain differences of approximately 70 με. Conversely, the SSM FBG sensor had compressive and tensile strain values below 400 με. At the midspan and east sections, sensor strain differences below 80 με were observed (see Figure 6.113).

Average Strain Comparison. To further assess the performance of the FBG sensors, the average strains were calculated for each location and compared to the individual FBG sensor readings. In Table 6.28, the compressive and tensile FBG strains at the maximum load of 23,680 lbs and average strains are presented. In addition, the associated standard deviation and strain differences in percentage are indicated.

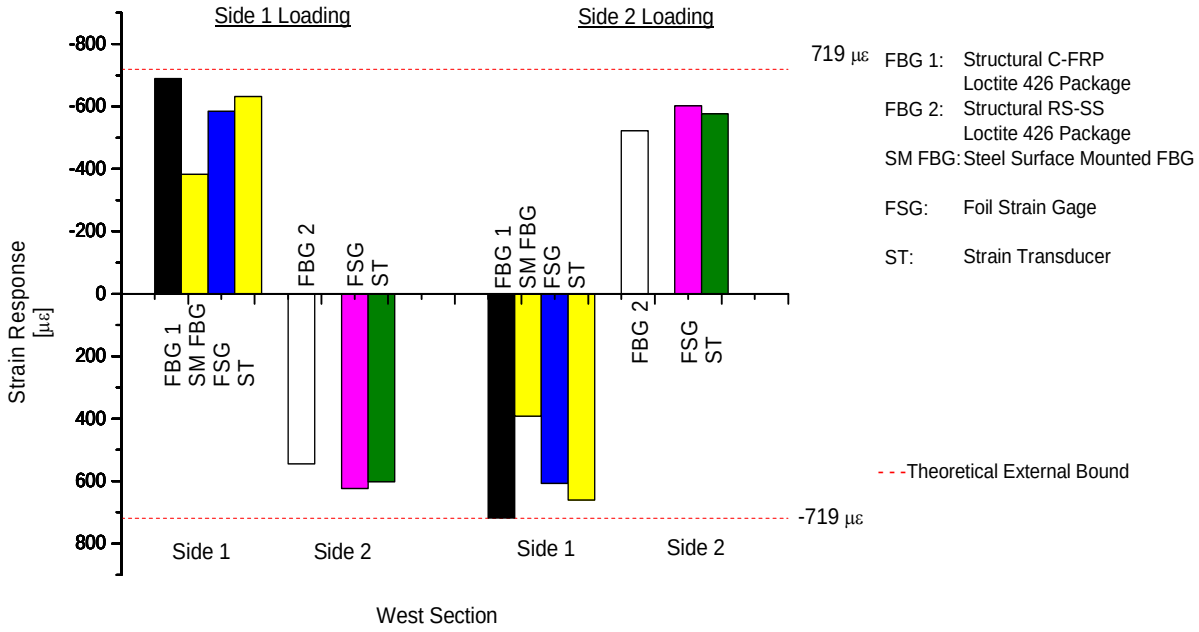

Figure 6.112. Bending Test: Strains at Maximum Loading – West Section, Side 1 and 2 Loadings

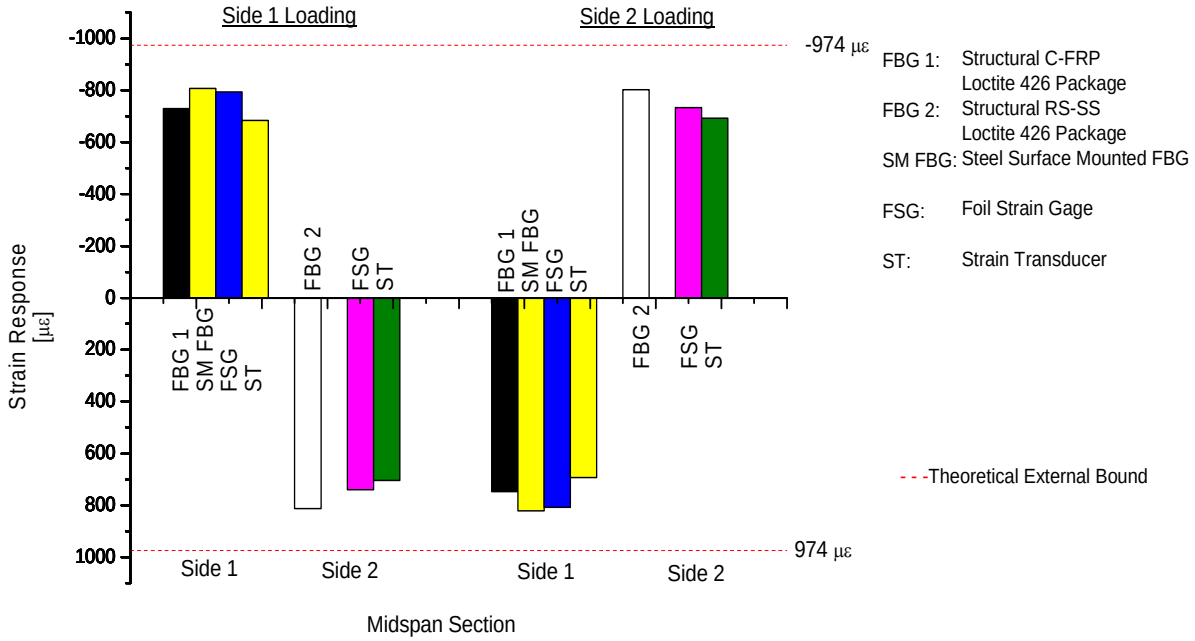

Figure 6.113. Bending Test: Strains at Maximum Loading – Mid Span Section, Side 1 and 2 Loadings

Table 6.28. Bending Test: External FBG Sensor vs. Average Strain

Sensor Location	Structural Package	Loading Side	FBG Strain [με]	Avg. Strain (Std. Dev.) [με]	Difference %
West section – S1	C-FPP – Loctite 426	1	-689	-572 (133)	20%
		2	718	595 (143)	21%
	Steel Surface Mounted	1	-383	-572 (133)	-33%
		2	392	595 (143)	-34%
Midspan section – S1	C-FPP – Loctite 426	1	-730	-753 (57)	-3%
		2	748	767 (59)	-3%
	Steel Surface Mounted	1	-806	-753 (57)	7%
		2	820	767 (59)	7%
East section – S1	IS-SS – Loctite 4212	1	-552	-553 (34)	0%
		2	583	585 (35)	0%
	Steel Surface Mounted	1	-601	-553 (34)	9%
		2	635	585 (35)	9%
West section – S2	RS-SS – Loctite 426	1	544	590 (41)	-8%
		2	-522	-567 (41)	-8%
Midspan section – S2	RS-SS – Loctite 426	1	813	752 (55)	8%
		2	-802	-743 (56)	8%
East section – S2	72H-SS – Loctite 4212	1	617	578 (42)	7%
		2	-586	-550 (37)	7%

As expected, the largest differences were observed at the West Side 1 sensors location (i.e., between 20% and 33%). By analyzing the results at this location, the difference between the C-FRP Loctite 426 package and the other sensors (i.e., foil strain gage and strain transducer) would be

reduced to 8% (not considering the SSM FBG sensor response). Note that all sensors installed on a wood surface with minor surface irregularities and straight to diagonal grain orientation, had lower strain differences (i.e., ranging from 0% to 9%). Statistically, the FBG strains were either contained or in the vicinity of the standard deviation of the average strains.

6.4.5.1.2. **Non-Structural Packages**

At each load step, the FBG sensors protected by the non-structural packages detected some strain levels (see Figure 6.114). To verify the level of the isolation, the experimental strains were compared to the corresponding theoretical strains. In the non-structural package S2, the maximum strains were up to 40 με, 7% of the theoretical strain for an applied service load of 23,680 (i.e., 575 με, see Table 6.24). In the other package S1, the maximum strain was up to 15 με, (3%). After removing the load, residual strains ranged from 2.5 με to 15 με.

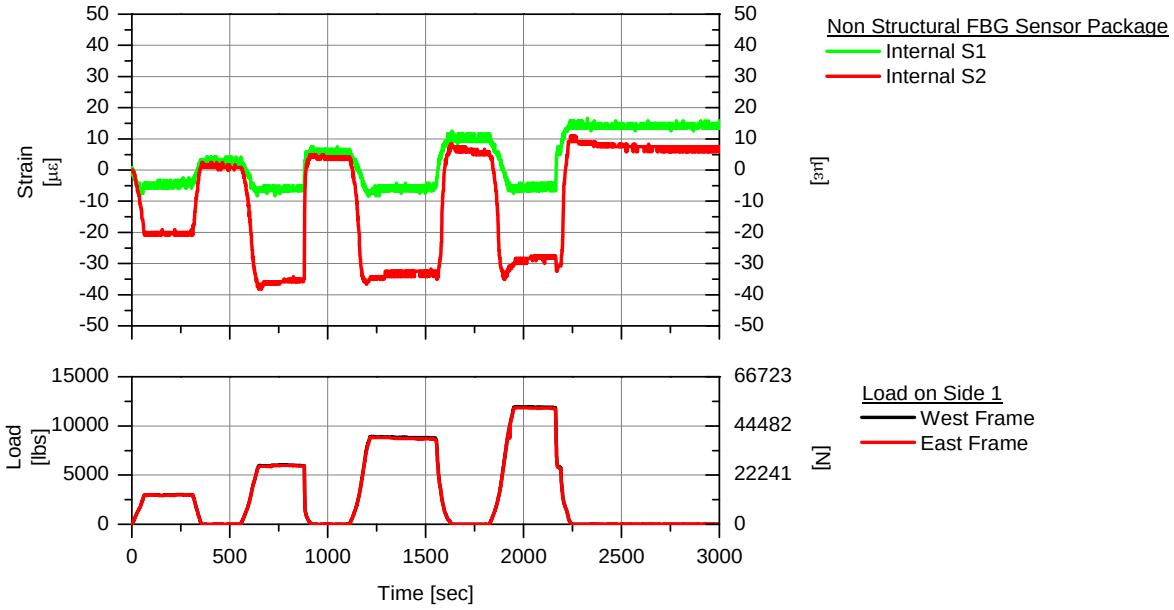

Figure 6.114. Bending Test: Strain and Load vs. Time – Side 1 Loading

6.4.5.2. SUSTAINED LOADING TEST

The objective of the sustained loading test was to verify the viscoelastic response of the structural FBG sensor packages during and after 8 hours of constant loading and uncontrolled ambient laboratory conditions. In addition, the further study of the effectiveness of non-structural packages in isolating mechanical strains was completed.

6.4.5.2.1. **Structural Packages**

In Figure 6.115, FBG strains, load and temperature data are plotted against time. At the maximum loading, the strain levels along with the uncontrolled laboratory temperatures. After removing the load, small residual strains were present.

For the structural packages, the FBG sensor strains were analyzed as follows:

- Short term strain comparison between the sustained loading strains and the bending test at a total load of approximately 23,680 lbs.

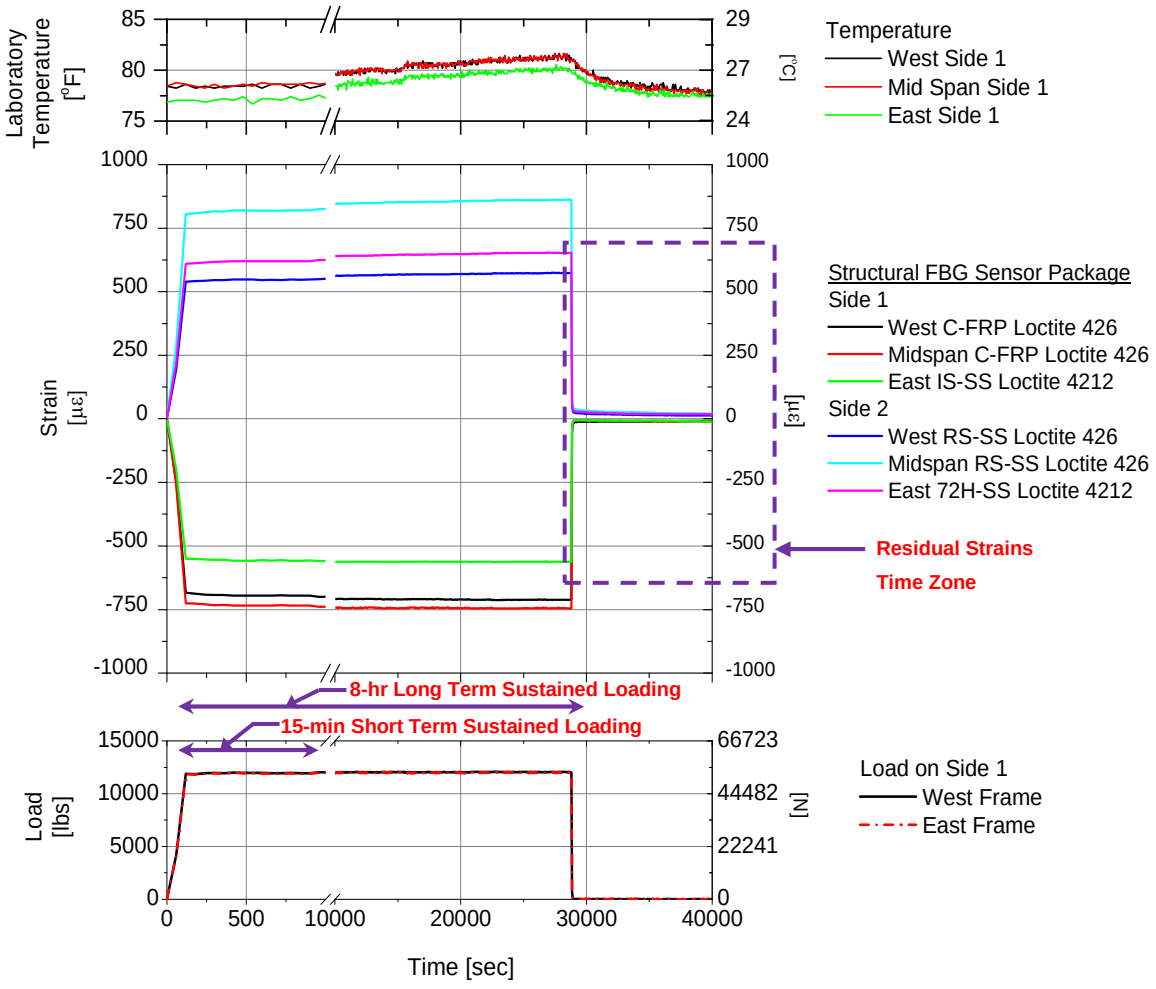

Figure 6.115. Sustained Loading Test: Typical FBG Strains, Temperature Load vs. Time Responses

- At maximum loading, the relationship between temperature and strain data was investigated.
- Assessment of the residual strains.

Short Term Strain Comparison: For the sustained loading, average strains were determined in the interval of 15 minute strain data. In this interval, strain dispersions were up to 5.4 με; during that same period, temperature fluctuated in the range of +/-0.2 ^{o}F. Due to temperature fluctuations, strains were minimal (+/-1 με). Other factor that may have affected the strain dispersions was that fact that the load was constantly decreasing and had to be adjusted. Nevertheless, the strain levels for initial sustained loading were on the order of the bending tests' results (see Figure 6.116); for most sensors, the strain levels differed by a maximum of 8 με.

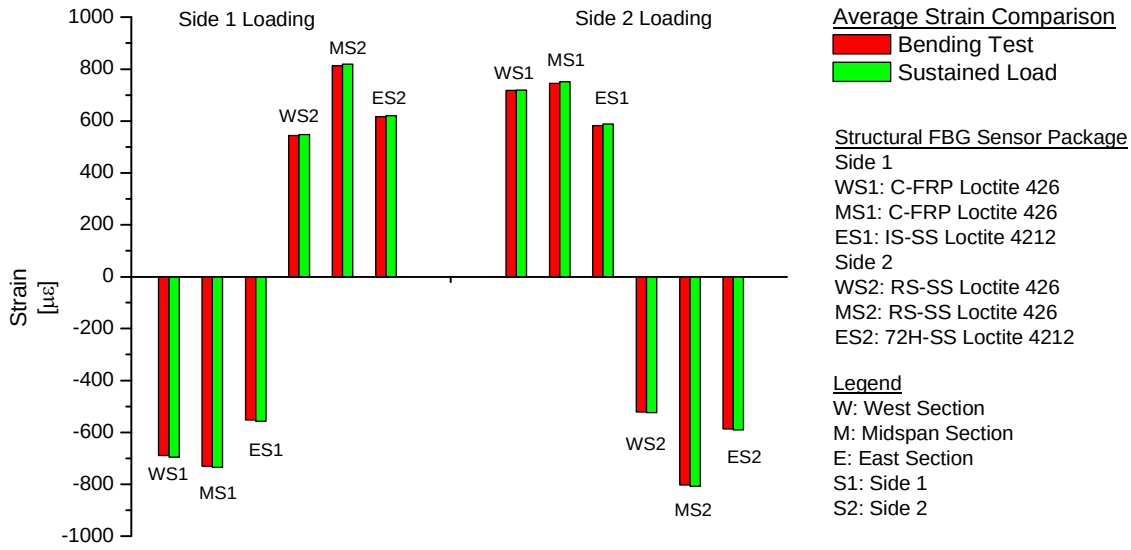

Figure 6.116. Sustained Loading Test: Comparison of Bending and Sustained Loading FBG Strains

Strain and Temperature Relationship: Before testing, the moisture content of the girder was assessed. At the west and east sections, the moisture content was 9%, while at midspan, this value was 11%. As anticipated from the testing described in Chapter 3, all FBG sensor packages were found to be impacted by temperature fluctuations. In Figure 6.115, the strain levels during the constant loading were observed to vary with the temperature variations. A linear regression fit was determined between each set of temperature and strain data to measure the degree of the linear relationship degree. From the evaluation, the R^2 coefficients ranged from 0.00 to 0.90 (see Table 6.29). The linear regression R^2 coefficients less than 0.95 indicated that the influence of the temperature had only partially affected the strain variation. The rest of the variation might be explained by creep deformation of the package adhesive.

Table 6.29. Sustained Loading Test: Linear Regression between Strains and Temperatures

Sensor Location	Structural Package	Side 1 Loading		Side 2 Loading	
		R^2 Coefficient	Temp. Std. Dev. [°F]	R^2 Coefficient	Temp. Std. Dev. [°F]
West section – S1	C-FPP – Loctite 426	0.34	0.9	---	---
	Steel Surface Mounted	0.90	0.9	---	---
Midspan section – S1	C-FPP – Loctite 426	0.71	0.9	---	---
	Steel Surface Mounted	0.81	0.9	---	---
East section – S1	IS-SS – Loctite 4212	0.00	0.9	---	---
	Steel Surface Mounted	0.41	0.9	---	---
West section – S2	RS-SS – Loctite 426	---	---	0.05	0.5
Midspan section – S2	RS-SS – Loctite 426	---	---	0.35	1.2
East section – S2	72H-SS – Loctite 4212	---	---	0.63	1.3

Residual Strain Evaluation. After loading for eight hours and then unloading, the residual strains were less than 40 με, which represented 5% of maximum strain. As observed in Figure 6.117, the residuals strains gradually decreased over one hour (see "residual strains decreasing over constant temperature zone"). After that, the strains were varied along with the temperature fluctuations.

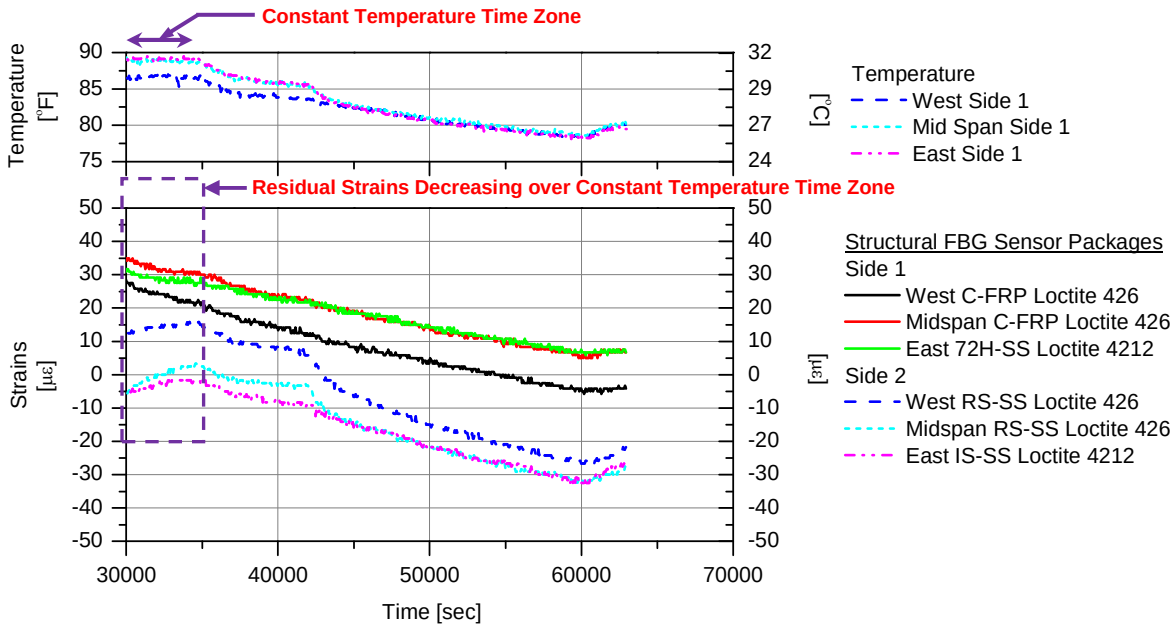

Figure 6.117. Sustained Loading Test: Residual FBG Strains – Side 2 Loading

6.4.5.2.2. **Non-Structural Packages**

In the sustained loading test, two FBG sensors with non-structural packages at internal Side 1 and Side 2 were impacted by the external loading as observed in Figure 6.118 (see "15-min short term

sustained loading" for Internal S1 and Internal S2 sensors). The measured strain levels varied between 16.7 με and -28.3 με upon loading. During the "8-hr long term sustained loading", the strains increased between 21 με and 41.6 με.

When removing the load, strain levels instantly decreased and decreased impacted by the unloading. Residual strain levels were to 35 με and decreased to values between -5 με and 10 με. The strain recovery of the sensors was observed to be slow (see "residual strains time zone" in Figure 6.118); the relative FBG sensor movement in the recess area was suspected to retain the induced residual strains. In addition, thermal effects were suspected to affect the final strains. At the end of the data collection, the residual strains were -5 με and 15 με.

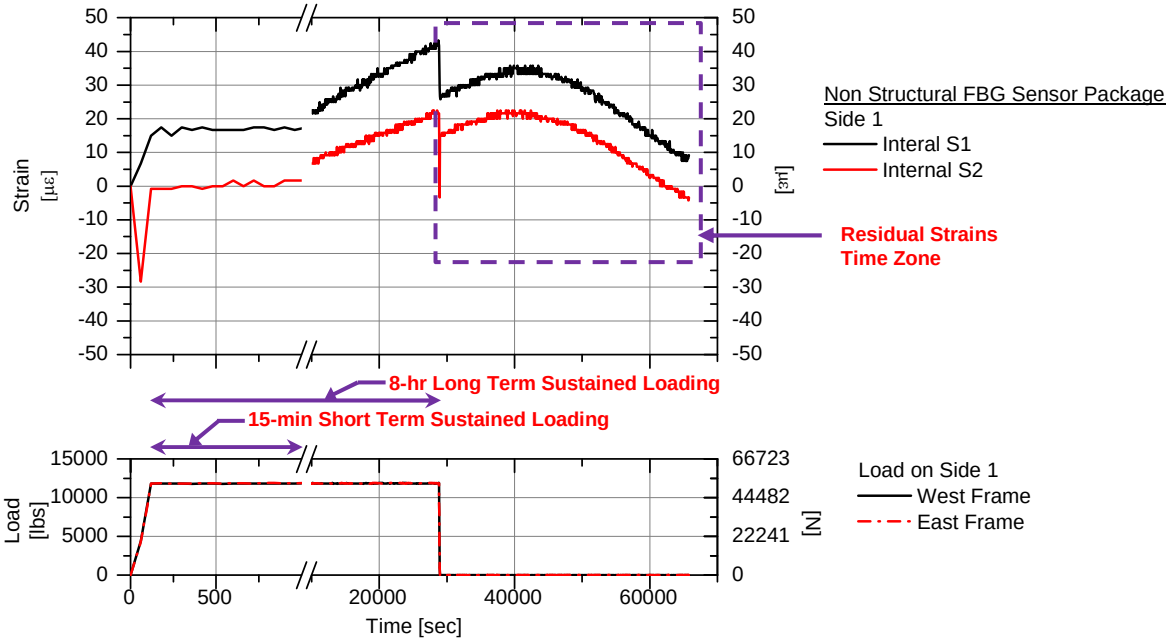

Figure 6.118. Sustained Loading Test: Non Structural FBG Strains and Load History

6.4.5.3. PSEUDO CYCLIC LOADING TEST

Limited cyclic loads were applied to the full scale girder to assess the viscoelastic behavior of the packages, particularly to assess any strain phase lag upon consecutive loadings. In this context, peak strains were compared for reproducibility. In addition, the viscoelastic behavior of the structural FBG sensor packages was investigated through the creep recovery of the packages (i.e., residual strains decreasing to minimal values). In the non-structural packages, sensor strain data were further assessed to determine the sensitivity of the package to mechanical strains.

6.4.5.3.1. **Structural Packages**

The performance of the FBG sensor packages was evaluated:

- Evaluation of the FBG sensor package strain levels.
- Comparison of strain results for bending test and pseudo cyclic loading test results.
- Assessment of the residual strains.

Evaluation of the FBG sensor package strain levels: The peak strains for twelve cyclic loadings were averaged and the associated peak strain dispersion was determined per sensor package. In Figure 6.119, an example of the pseudo cyclic loading and strains against time is presented. Similar variability between load and strain plots can be observed. During the tests, temperature fluctuations were below +/-0.5 ^{o}F.

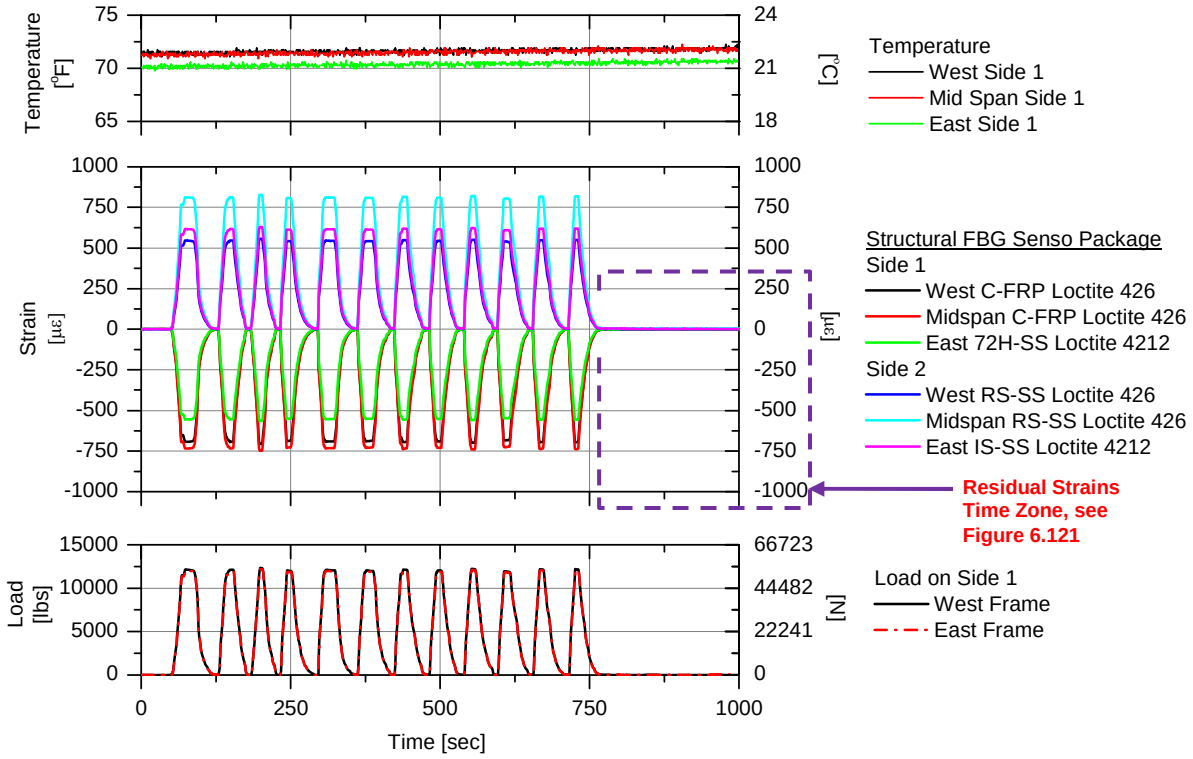

Figure 6.119. Pseudo Cyclic Loading Test: Typical FBG Strains, Temperature, Load vs. Time Responses

The average peak strains and respective standard deviations are summarized in Table 6.30. As observed, the standard deviations were between 4 με and 8 με, less than 1% of the average peak

strains. The strain standard deviations were small; strain differences could be attributed to the variable rate of loading and unloading.

Comparison of the Strain Results for Bending Tests and Pseudo Cyclic Loading Tests. The averages of the peak strain levels for the pseudo cyclic loading tests were compared to the bending average strains as shown in Figure 6.120. For all sensors, the differences between both tests results were less than +/-6 με.

Table 6.30. Pseudo Cyclic Loading Test: Peak Strains and Standard Deviation [με]

Sensor Location	Structural Package	Side 1 Loading		Side 2 Loading	
		Peak Avg.	Std. Dev.	Peak Avg.	Std. Dev.
West section – S1	C-FPP – Loctite 426	-694.4	5.5	714.4	7.1
	Steel Surface Mounted	-416.7	5.1	411.4	4.3
Midspan section – S1	C-FPP – Loctite 426	-735.1	5.7	745.9	7.5
	Steel Surface Mounted	-812.4	6.2	815.9	8.2
East section – S1	IS-SS – Loctite 4212	-555.8	4.2	582.7	5.7
	Steel Surface Mounted	-607.3	4.6	633.9	6.3
West section – S2	RS-SS – Loctite 426	546.9	4.0	-524.7	5.3
Midspan section – S2	RS-SS – Loctite 426	814.2	6.0	-798.0	7.9
East section – S2	72H-SS – Loctite 4212	617.8	4.7	-585.6	6.0

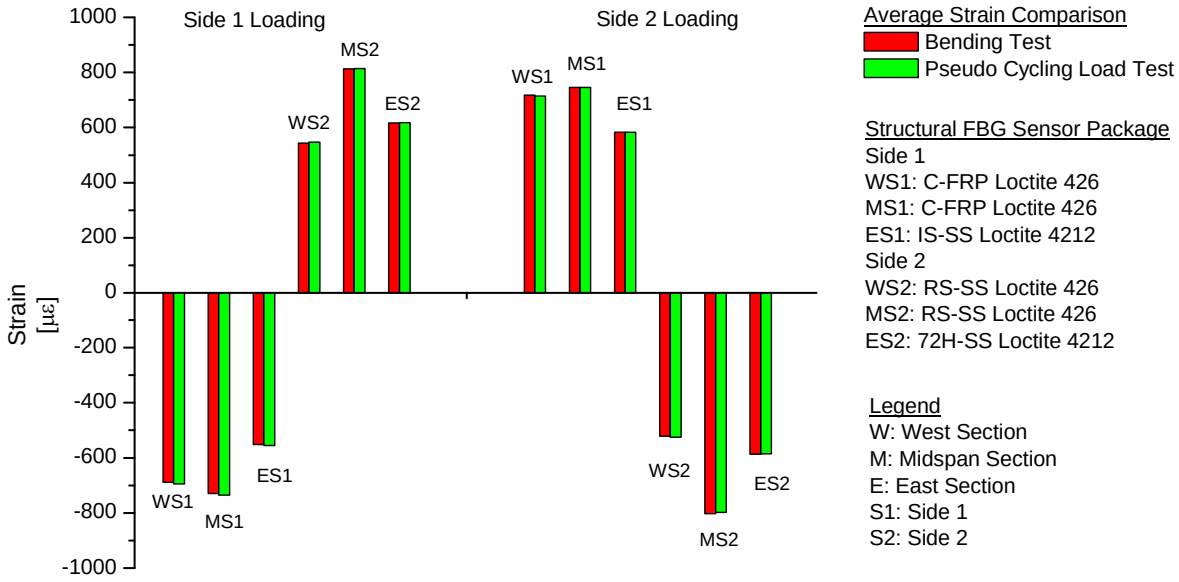

Figure 6.120. Pseudo Cyclic Loading Test: Comparison of Average Strain Results for Bending and Pseudo Cyclic Loading Test Results

Residual Strains. After removing the load, residual strain data were collected for approximately 25 minutes (see Figure 6.121). For all FBG sensor packages, the residual strains decreased over time and at the end of the recording period were between zero and 4 με. These results indicated that the sensors had a consistent viscoelastic behavior after pseudo cyclic loadings.

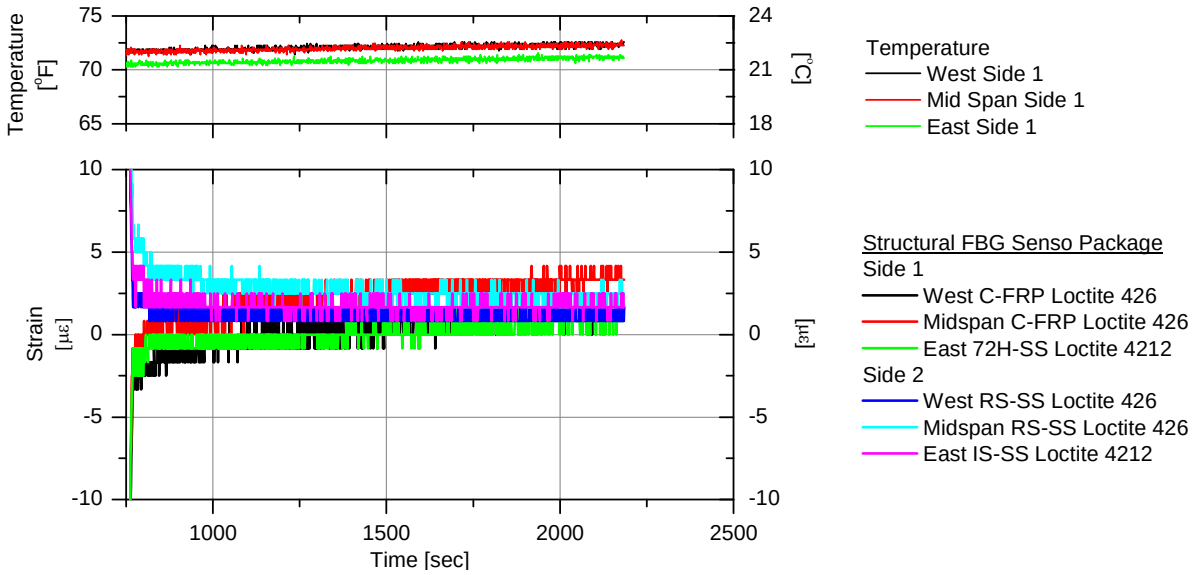

Figure 6.121. Pseudo Cyclic Loading Test: Residual Strains After Pseudo Cyclic Loading

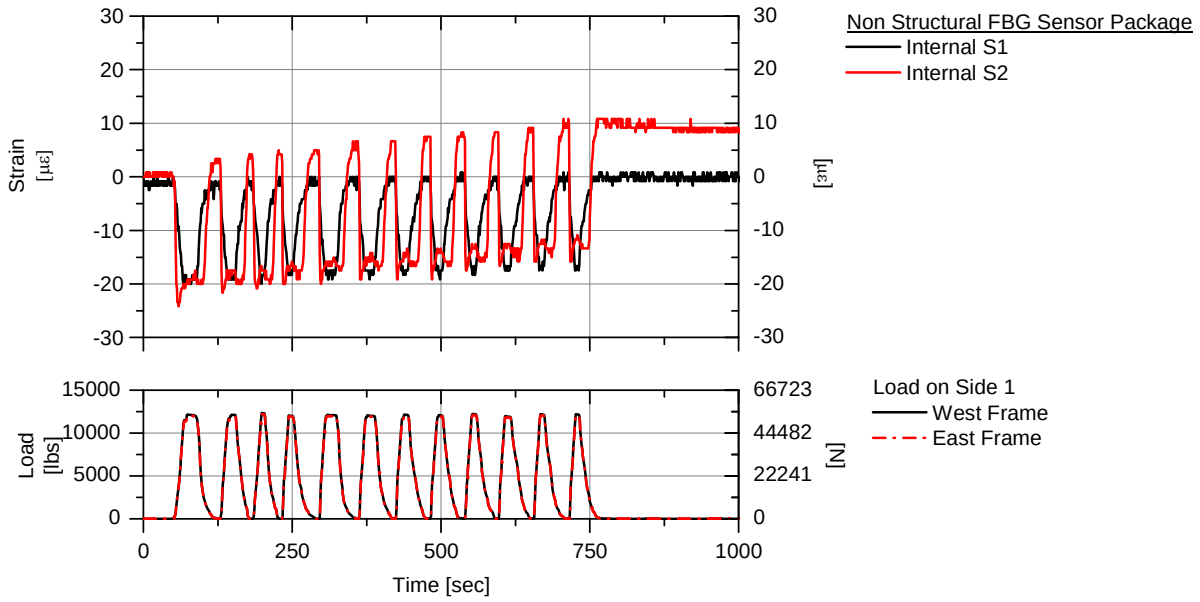

Figure 6.122. Pseudo Cyclic Loading Test: Non Structural Packages – Typical FBG Strains, Temperature Load vs. Time Responses

6.4.5.3.2. **Non-Structural Packages**

As expected, the pseudo cyclic loading induced strain levels that ranged from 15 με to 30 με, which was equivalent to 5% of the theoretical (see Figure 6.122) strain at the gage location.

After the load removal, the residual strains were between 0 με and 16 με. The residual strains were also assumed to be part of the friction between FBG sensor and the recess area.

6.4.5.4. TEMPERATURE EFFECT TEST

Strain and temperature data were collected for the external structural FBG sensor packages to evaluate if a linear correlation existed. The laboratory temperatures were increased and decreased at approximately +/- 8 ^{o}F per hour. In Figure 6.123, strains and temperature against time are presented for the custom design IS-SS Loctite 426 package and the commercially available SSM FBG sensor at the east section. Both FBG sensor strains showed variabilities with respect to the temperature fluctuations; however, the custom design package showed a more pronounced temperature influence. Similarly, the West and Mid SSM FBG sensors' strain patterns showed a relatively lower temperature variation than the IS-SS Loctite 4212 and C-FRP FBG Loctite 426 sensor packages.

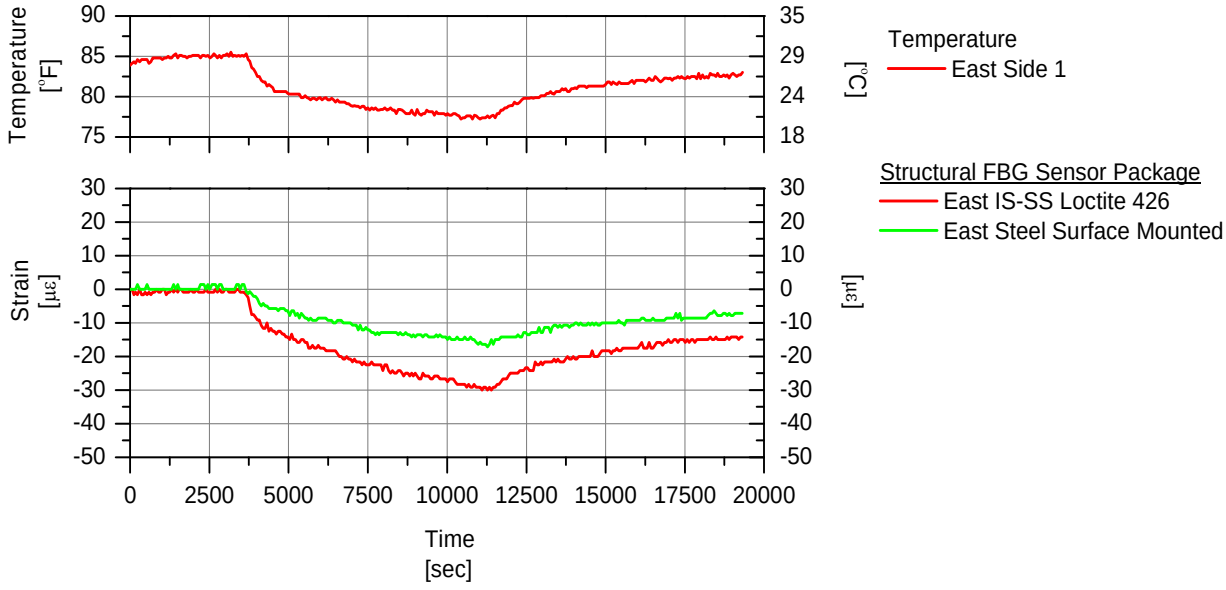

Figure 6.123. Temperature Test: Residual FBG Strains – Side 2 Loading

Using a linear regression model, the quality of the fit was measured by the R^2 coefficients (see Table 6.31). For the custom design packages, the linear correlation was above 0.95 showing that the bare FBG sensor has a predominant temperature influence over the other package materials. Conversely, the SSM FBG sensors had R^2 coefficients that were between 0.77 and 0.87.

Table 6.31. Temperature Test: Linear Regression between Strains and Temperatures

Sensor Location	Structural Package	Side 1 Loading		Side 2 Loading	
		R^2 Coefficient	Temperature Min. – Max. [°F]	R^2 Coefficient	Temperature Min. – Max. [°F]
West section – S1	C-FPP – Loctite 426	0.99	78.6 – 86.6	---	---
	Steel Surface Mounted	0.87		---	---
Midspan section – S1	C-FPP – Loctite 426	0.95	78.1 – 86.2	---	---
	Steel Surface Mounted	0.77		---	---
East section – S1	IS-SS – Loctite 4212	0.95	77.4 – 85.0	---	---
	Steel Surface Mounted	0.77		---	---
West section – S2	RS-SS – Loctite 426	---	---	0.95	80.9 – 89.5
Midspan section – S2	RS-SS – Loctite 426	---	---	0.95	80.6 – 88.9
East section – S2	72H-SS – Loctite 4212	---	---	0.98	80.5 – 88.5

6.5. SUMMARY, CONCLUSIONS AND RECOMMENDATIONS

6.5.1. SUMMARY

In this work, techniques for embedding and attaching FBG sensor packages for monitoring structural and non-structural attributes of timber bridges were investigated through the construction and testing of glulam specimens. Two sets of packages were developed and deployed on/in small scale glulam specimens. One set of packages served to protect the FBG strain sensor as well as to provide mechanical connectivity between the FBG sensor and glulam member for measuring structural response. The other set was intended to isolate the sensor from structural responses. Initial package designs were installed in fourteen small scale glulam specimens for testing and evaluation. From this study, a group of structural and non-structural FBG sensor packages were selected and installed in a manufactured full scale glulam girder to test and further verify their performance.

The internal and external structural FBG sensor package conceptually consisted of a backing material and a bare FBG strain sensor bonded together. The resulting package system was either attached to an exposed wood surface or embedded between the laminates of glulam members. In this work, five new backing material configurations were developed utilizing either stainless steel shims

or aluminum mesh sheets. These custom designed structural packages were dimensioned to resist the horizontal shear stresses and to allow for the redistribution of localized strain irregularities between the package and the wood laminates. In addition to the bare FBG strain sensors, one commercially available surface mounted FBG strain sensor bonded to a C-FRP package was evaluated. Three structural adhesives were selected to bond the backing material to the wood surface.

The non-structural FBG sensor package conceptually consisted of a backing material and adhesive or adhesive tape that isolated the FBG sensor from load induced structural response. In that sense, no physical attachment between the FBG sensor and wood laminate was desired. These sensors were inserted in a recess area in the wood laminate. Ten non-structural packages were prepared with a combination of stainless steel shims and aluminum foil as backing materials which were bonded to the edge of a recess area with two different types of adhesives and two adhesive tapes.

Under a typical third-point-loading test fixture, the nine small specimens instrumented with structural FBG sensor packages were tested in bending to evaluate the performance of the packages. With the same total load, six series of bending tests were performed by varying the rates of loading, cycling loadings and sustained loadings under uncontrolled ambient temperatures as well as imposed heat and cold temperature conditions. Each specimen was loaded on each bending surface (Side 1 and 2) to obtain the compressive and tensile flexural response in each package.

The strain data indicated that the developed sensor packages were operating within predicted values and were compatible to other installed sensor types. Strain recovery was evident in all packages indicating that the viscoelastic behavior was consistent. In a 24-hour sustained loading, creep deformations and uncontrolled ambient temperature changes were found to significantly influence the FBG sensor packages' strain levels in the long term loading and after unloading (residual strains).

Thermal changes in the form of heat above 110 ^{o}F and cold below 0 ^{o}F were applied to the specimens under a sustained load verified that most FBG sensor packages operate in extreme environmental conditions while loaded and recover to their previous state. When cooling and loading Side 2, the specimens subjected to a sustained loading and temperatures below -50 ^{o}F showed suspect strain levels. These inconsistent strains in few packages indicated that changes in the mechanical properties of either the wood or sensor packages occurred.

After completing the small-scale testing program, the following packages were selected for their generally superior performance and corroboration with other sensor types:

- External structural FBG sensor packages:
  - C-FRP Loctite 426.
  - RS-SS Loctite 426.
  - IS-SS Loctite 4212.
  - 72H-SS Loctite 4212.
- Internal structural FBG sensor packages are:
  - AM-SS Loctite 454.
  - RS-SS Loctite 426.

Specimens with non-structural packages tested in bending demonstrated that the developed packages isolated the FBG sensors from structural strains. Only one package had an installation error which resulted high strain levels. From the non-structural package evaluation, two packages were selected for further evaluation:

- Aluminum foil and Loctite 454.
- Stainless Steel shim and adhesive tape 3M VHB.

With the selected structural and non-structural FBG sensor packages, a full scale glulam girder was instrumented by the research team and assembled at a commercial manufacturing plant. In a selected balanced 24F-V8 DF/DF layup girder type, two outer internal L1 and L2 graded laminates were instrumented. In two L1 graded laminates, structural packages were installed at three cross sections separated 7 ft 3 in. from midspan. Two pairs of non-structural packages were installed in two L2 graded laminates. The processes of instrumenting the laminates and assembling the girder were satisfactory and six structural and four non-structural packages were operative. However, additional activities that occurred after clamping such as handling, resurfacing and delivering were suspected to have damage the fragile bare fiber. Before testing, only two internal non-structural FBG sensor packages were working. Externally, four-custom design and five commercially available structural FBG sensor packages were successfully installed using the respective attaching technique.

The full-scale girder was symmetrically loaded at two points with an equivalent service load to verify the operability of both the structural and non-structural FBG sensor package types. Bending tests were performed by gradually increasing the load, modifying the load duration, and cycling the load up to the pre-determined service load. The girder was loaded on both bending surfaces to obtain

the compressive and flexural strains per package. In the four-step bending tests, each external structural package was verified for strain consistency. When comparing the experimental strains to the beam theory values and the other strain sensors, all structural packages were operating within the theoretical limits and the other sensors response (i.e., in the range of 9%). For the short term pseudo-cyclic loading, strain levels were consistent. In the short term bending tests, residual strains per package were lower than 4 με. In the sustained loading bending tests, creep and affected the strain pattern over the 8-hour loading. After unloading, residual strains were observe to be below 50 με. The strain recovery was evaluated over a short period with a relatively constant temperature. Temperature evaluations of each package show that the custom designed sensor packages had an estimated linear response to temperature fluctuations; in contrast, the manufactured steel surface mounted packages had a lower linear response. Most non-structural packages indicated no sign of structural strain levels.

6.5.2. CONCLUSIONS

The general conclusions of the study are:

- Techniques for embedding and attaching FBG sensor packages for structural monitoring in small scale specimens worked adequately immediately after set up. However, survivability of the sensors decreased when the specimens were released from the assembly fixture (unclamping) and handled for testing. In general, sensor damage occurred at the fragile bare strand transition between the packaged bare FBG sensor and the leads.
- Macroscopic wood characteristics affected the measured strains in Specimen 1 due to intergrown knot and spiral grain orientation. After each test evaluation, strain levels at maximum load were different with respect to the previous test. The FBG packages performed consistently and strain levels were constant over time during each bending test.
- The consistent performance of the FBG sensor packages was proven through the reproducibility of the bending strain data while varying the duration of the load (i.e., bending tests, up to twenty minutes sustained loading, stabilized accelerated loading and average peak strains for the pseudo cyclic loading results). In all cases, minimal strain differences were observed among average strain levels.
- Viscoelastic behavior of the FBG sensor packages was verified by residual strain levels decreasing in time. In the short term tests (less than twenty minutes), the residual strains varied from 0 to 9 με.

- Sustained loadings at ambient laboratory temperatures as well as adding hot/cold temperatures modified the viscoelastic behavior of the packages, retarding the strain recovery over time. In the cold and sustained loading, dryer conditions of the specimens added thermal contraction lags that retarded the strain recovery process. Most packages proved to operate and resist the imposed thermal conditions (i.e., heat and cold temperatures) during sustained loading; after unloading, strain recovery was slow but evident over time.
- In the small specimens, the developed non-structural FBG sensor packages and associated embedding technique were satisfactorily applied. With the exception of one sensor that registered strain levels, all packages were effective at isolating the sensor from strain.
- In the full scale glulam girder, the improved installation process and assembly of both sets of internal structural and non-structural packages was satisfactory. However, additional manufacturing activities were found to damage the internal FBG sensors. In this context, the sensor installation technique needs to be improved to be suitable for manufacturing.
- In the full scale girder, the external structural sensor packages were successfully installed. In the experimental program, all structural packages confirmed to be behaving consistently upon loading and unloading, being suitable for future deployment.
- The non-structural packages generally were not affected by the structural response; however, some vibrations of the “free” sensor resulted in extraneous readings.

6.5.3. RECOMMENDATIONS FOR CONTINUED STUDY

As previously noted, both structural and non-structural FBG sensors package types were adequately operating in the small scale glulam specimens. Damage in the internal packages was associated to the assembling and handling of the specimens as well as the fragile nature of the bare FBG sensor. In the full scale girder, although all internal FBG sensor packages were successfully installed, FBG sensor packages were damaged during the final manufacturing process (i.e., unclamping, surfacing, handling, etc.). In this context, supplementary assessment and improvement in the embedding and attaching techniques are required to ensure the bare FBG sensors protection and operability. Additionally, testing of other sensor types should evaluate if they have better survivability. To address the possible sources of damage as well as to evaluate the resulting FBG sensor packages’ techniques, the following list of recommendations for future research work is presented:

- A review of available deterioration-type sensors (moisture, ferric ion, lignin loss) should be conducted to ensure that the general types of non-structural packages can be adapted. Where

appropriate the identified deterioration-type sensors should be evaluated in small scale specimens that are fabricated at a commercial facility. Testing should be conducted under variable environmental conditions.

- A constructability review of various sensor types should be conducted. Unlike the work described in this report, testing should look at electrical-type gages and the above mentioned deterioration-type sensors in addition to the previously evaluated optical sensors. As with the above mentioned small-scale specimens, this testing should be completed on specimen(s) fabricated in a commercial facility.
- The adhesive and package combination should be evaluated for its fatigue performance. Specifically, a full-scale beam should be tested under service levels of load for up to 1,000,000+ cycles.
- Develop alternative encasement procedures for improved protection during manufacturing of fragile FBG leads.

6.6. REFERENCES

1. American Association of State Highway and Transportation Officials. (2005) "AASHTO LFRD Bridge Design Specifications Customary U.S. Units Second Edition." Washington D.C. 2000.

2. American Instituted of Timber Construction (2004). "AITC 117 - 2004 – Standard Specifications for Structural Glued Laminated Timber of Softwood Species." 68 pp.

3. American Standards for Testing Materials (2005). "Standard Test Method for Apparent Shear Strength of Single-Lap-Joint Adhesively Bonded Metal Specimens by Tension Loading (Metal-to-Metal)." ASTM International, West Conshohocken, PA 19428-2959, ASTM 1002-05, 5 pp.

4. American Standards for Testing Materials (2005). "Standard Tests Methods of Static Tests of Lumber in Structural Sizes." ASTM International, West Conshohocken, PA 19428-2959, ASTM 198-05a, 26 pp.

5. American Standards for Testing Materials (2006). "Standard Test Method for Shear Adhesion of Pressure-Sensitive Tapes." ASTM International, West Conshohocken, PA, 19428-2959, ASTM D3654/D3654M-06, 6 pp.

6. Barbosa, C., Costa, N., Ferreira, L. A., Araujo, L. A., Varum, H, Costa, A., Fernandes, C. and Rodrigues, H. (2008). "Weldable Fibre Bragg Grating Sensors for Steel Bridge Monitoring." Measurement Science and Technology. 19 (2008) 125305, 10 pp. © 2008 IOP Publishing Ltd. UK.

7. Casas, J. R. and Cruz, P. J. S. (2003). "Fiber Optic Sensors for Bridge Monitoring." Journal of Bridge Engineering © ASCE, November/December 2003, Issue 6, pp. 362-373.

8. Childers, B. A., Froggatt, M. E., Allison, S. G., Moore, T. C., Sr., Hare, D. A., Batten, C. F. and Jegley, D. C. (2001). "Use of 3000 Bragg Grating Strain Sensors Distributed on Four Eight-Meter Optical Fibers During Static Load Tests of a Composite Structure." Proc. SPIE 4578, pp. 8-18.

9. Claus, R. O., Holton, C. E, and Zhao, W. (1998). "Performance of Optical Fiber Sensors Embedded in Polymer Matrix Composites for Fifteen Years." SPIE Conference on Sensory Phenomena and Measurement Instrumentation for Smart Structures and Materials, San Diego, CA. SPIE Vol. 3330, pp. 8-11.

10. Dillard, D. A. (2005). "Stress Distribution: Mode of Failure." Handbook of Adhesion, Edited by Parham, 2nd Edition, John Willey & Sons, West Sussex, England.

11. Doornink, J. D. (2006). Monitoring the Structural Condition of Fracture-Critical Bridges Using Fiber Optic Technology. Dissertation in Partial Fulfillment of the Requirements of the degree of Doctor of Philosophy, Iowa State University, Ames, Iowa.

12. Doyle, D., Drow, J., and McBurney, R. (1946). "Elastic Properties of Wood." Forest Product Laboratory, Reports No. 1528 and 1528, A to H.

13. Funke, R. W., Jr. (1986). "Behavior of Longitudinal Glued Laminated Timber Deck Bridges." Thesis submitted in partial fulfillment of the requirements for the degree of Master of Science. Iowa State University, Ames, Iowa.

14. Gangopadhyay, T. K., Majumder, M., Chakraborty, , A. K., Dikshit, A. K. and Bahttacharya, D. K. (2009). "Fibre Bragg Grating Strain Sensor and Study of its Packaging material for use in Critical Analysis on Steel Structure." Sensors and Actuators A 150 (2009), pp. 78-86 © Elsevier B. V.

15. Hao, J. H., S. Takahashi, Z. H, Cai, J. H., NG, X. F., Yang, Z. H., Chen, C. Lu (2006). "Packaging Effects on Fiber Bragg Grating Sensor Performance." Acta Automatica Sinica, Vol. 32, No. 6, pp. 999-1007.

16. Henkel ® (2005). "Adhesive Source Book ® - Complete Directory of Loctite ® Products for Assembly, Manufacturing and Maintenance." Henkel Corporation ® Vol. 5, 149 pp.

17. Hexion (2010). "Product Bulletin – Cascophe ® LT-5210J and Cascoset FM-6210 or FM 6210(s) – Phenol-Resorcinol Adhesive System." http://www.hexitherm.com/pdf/LT-5210J_FM-6210%28S%29.pdf. Accessed in August 2010.

18. Hill, K. O. and Meltz, G. (1997). "Fiber Bragg Gratin, Technology Fundamentals and Overview." Journal of Lightwave Technology, Vol. 15, No. 8, August 1997, pp. 1263-1276.

19. Hill, K. O., Fuji, Y., Johnson, D. C. and Kawasaki, B. S. (1978). "Photosensitivity in optical fiber waveguides: Aplication to reflection fabrication." Appl. Physics Lett., Vol. 32, pp. 647-649.

20. Hill, K. O., Malo, B., Bilodeau, F., Johson, D. C and Albert, J (1993). "Bragg gratings Fabricated in Monomode Photosentive Optical fiber by UV exposure through a phase mask." Appl. Phys. Letters, Vol. 62, pp. 1035-1037, 1993.

21. ISIS - Intelligent Sensing for Innovative Structures. (2001) "Guidelines for Structural Health Monitoring – Design Manual No. 2." University of Manitoba, Winnipeg, Manitoba 2001.

22. Kreuzer, M. (2007). "Strain Measurement with Fiber Bragg Grating Sensors." http://www.hbm.com/fileadmin/mediapool/techarticles/2007/FBGS_StrainMeasurement_en.pdf Accessed in July 2010.

23. Kuenzy, E., and Kommers, W. (1942). "Method of Measuring the Shear Moduli in Wood." Forest Product Laboratory, Report No. 1301.

24. Lefebvre, P., Vincelette, A., Allard, S. and Carbonneau, S. (2006). "Reliability Characterization of Fiber Bragg Grating." Optical Society of America 2006. http://www.lxdata.com/en/technology/white-papers/Reliability-Technology-White-Paper.pdf Accessed in July 2010.

25. Li, H. N., Li, D. S, and Song, G. B. (2004). "Recent Applications of Fiber Optic Sensors to Health Monitoring in Civil Engineering." Engineering Structures 2004, Vol. 26, pp. 1647-1657.

26. Lin, Y. B., Chan, K. C., Chern, J. C. and Wang, L. A. (2005). "Packaging Methods of Fiber-Bragg Grating Sensors in Civil Structure Applications." IEEE Sensors Journal, DOI 10.1109/JSEN.2005.844539

27. Meltz, G., Morey, W. W. and Glenn, W. H. (1989). "Formation of Bragg gratings in optical fiber by a transverse holographic method." Optical Society of America, August 1st 1989, Vol. 14, No. 15, Optic Letters.

28. Merzbacher, C. I., Kersey, A. D. and Friebele, E. J. (1996). "Fiber Optic Sensors in Concrete Structures: A Review." Journal of Smart Materials and Structures, Vol. 5, No. 2, pp. 196-213.

29. Moyo, P., Brownjohn, J. M. W., Suresh, R., and Tjin, S. C. (2005). "Development of Fiber Bragg Grating Sensors for Monitoring Civil Infrastructure." Engineering Structures 2005, Vol. 27, pp. 1828-1834.

30. Phares, B. M., Wipf, T. J. and Deza. U. (2007). "A 5-year Research Plan for the Development of a Smart Glue-laminated Timber Bridge" Bridge Engineering Center – CTRE – Iowa State University.

31. Radcliffe, B. M. (1955). "A Method for Determining the Elastic Constants of Wood by Means of Electric Resistance Strain Gages." Forest Product Journal, Vol. 5, No. 1, Feb. 1955, pp. 77-80.

32. Rao, M. B., Bhat, M. R., Murthy, C. R. L., Madhav, K. V. and Asokan, S. (2006). "Structural Health Monitoring (SHM) Using Strain Gages, PVDF Film and Fiber Bragg (FBG) Sensors: A Comparative Study." Proc. National Seminar on Non-Destructive Evaluation, 2006, Hyderabad, NDE-2006, 333-337.

33. Ritter, M. A. (1992) "Timber Bridges: Design, Construction, Inspection and Maintenance." United States Department of Agriculture, Forest Service, Approved for reprinting August 1992, EM 7700-B, Washington, DC, 970 pp.

34. Shen, D. K, Gu, S., Luo, K. H. and Bridgwater (2009). "Analysis of Wood Structural Changes under Thermal Radiation." American Chemical Society, Energy and Fuels 2009, Vol. 23, pp. 1081-1088.

35. Sanders, W. W., Jr, Klaiber, F. W. and Wipf, T. J. (1985). "Load Distribution in Glued Laminated Longitudinal Timber Deck Highway Bridges." Report No. ERI-85441. Iowa State University, Ames, Iowa.

36. Satori, K., Fukuchi, K., Kurosawa, Y. and Hongo, A. (2001). "Polyimide-Coated Small-Diameter Fiber Sensors for Embedding in Composite." Proceedings SPIE, Vol. 4328, 285 (2001). Newport Beach, CA.

37. Tahir, B. A., Ali, J. Rahman, A. (2005). "The Functionability of Fiber Bragg Grating Sensor Compared to that of Foil Gage." American Journal of Applied Science 2 (12) 2005, pp. 1600-1605.

38. Tennyson, R. C., Mufti, A. A., Rizkalla, S., Tadros, G. and B. Benmokrane, B. (2001). "Structural Health Monitoring of Innovative Bridges in Canada with Fiber Optic Sensors." Journal of Smart Materials and Structures, Vol. 10, No. 2, p.p. 560-573.

39. Tingley, D. A., Gilham, P. C. and Kent, S. M. (1996). "Long Term Load Performance of FPR Reinforced Glulam Bridge Girders." National Conference on Wood Transportation Structures, Ed(s). Ritter, M. A., Duwadi, S. R., Lee, P. D. H. Madison, WI, Product Forest Laboratory, pp. 201-206.

40. Udd, E. (1991). "The Emergence of Fiber Optic Sensor Technology." Fiber Optic Sensors–An Introduction for Engineers and Scientists." Edited by E. Udd, John Wiley & Sons, USA, Inc., 1991, 496 pp.

41. Vohra, S. T., Johnson, G. A. and Todd, M. D. (1999). "Strain Monitoring During Construction of a Steel Box-Girder Bridge with Array of Fiber Bragg Gratin Sensors." Naval Research Laboratory, NRL/MR/5670-99-8390. Washington, DC 20375-5320, 51 pp.

42. Wengert, Gene (2008). "Oven-Drying Wood for Moisture Content Testing." http://www.woodweb.com/knowledge_base/OvenDrying_Wood_for_Moisture.html. Accessed in August 2010.

43. Wipf, T. J., Phares, B. M. and Doornink, J. D. (2007). "Evaluation of Steel Bridges – Volumen I: Monitoring the Structural Condition of Fracture-Critical Bridges Using Fiber Optic Technology." Final Report – Center for Transportation Research and Education, Iowa State University, Ames, Iowa, 157 pp.

44. Wnuk, V. P., Mendez, A., Fergurson, S. and Graver, T. (2005). "Process for Mounting and Packaging of Fiber Bragg Grating Strain Sensors for use in Harsh Environment Applications." Smart Structures Conference 2005, SPIE paper 5758-6.

45. Youngquist, W. G. (1957). "Performance of Bonded Wire Strain Gages on Wood." University of Wisconsin – Madison. Forest Products Laboratory, Madison, Wisconsin. Forest Service, U. S. Department of Agriculture. Report No. 2087, pp. 43.

46. 3MTM Structural Adhesive (2010). "Structural Adhesive – Technical Sheet." http://multimedia.3m.com/mws/mediawebserver?mwsId=66666UuZjcFSLXTtmxfVM8T6EVuQEcuZgVs6EVs6E666666--. Accessed in August 2010.

47. 3MTM VHBTM Tapes (2010). "Tapes Technical Sheet." http://multimedia.3m.com/mws/mediawebserver?mwsId=66666UuZjcFSLXTtnxMtLXs6EVuQEcuZgVs6EVs6E666666--. Accessed in August 2010.

CHAPTER 7. SUMMARY, CONCLUSIONS AND RECOMMENDATIONS FOR FUTURE WORK

7.1. SUMMARY

The main effort of this series of investigations was focused on the integration of sensors and smart systems for structural monitoring of critical highway bridge types.

After the construction of the first of three precast, segmental pedestrian bridges, the need for structural monitoring was clear due to two factors. One factor was the unusual nature of the structural system, which combined post-tensioned match-cast concrete deck panels suspended from the steel arch ribs using high strength steel rods. The other factor involved the presence of a considerable number of panel cracks in the vicinity of the hanger rods. As a result, hanger loads needed to be monitored during the construction of two nearly identical pedestrian bridges (see Chapter 3). In this monitoring, two sensing systems were implemented for comparison. Externally-mounted accelerometers and attached bare fiber optic strain sensors were installed to obtain hanger forces in each stage of deck assembly and after bridge construction was completed. Unfortunately, some of the fiber optic sensors were damaged during the construction (i.e., handling issues). However, forces calculated from the undamaged fiber optic sensors were comparable to the forces obtained using accelerometers. Necessary load adjustments for the hanger rods were possible due to the real-time evaluation of collected data at different construction stages. Consequently, deck panel cracking caused by unexpected forces during construction were minimized. Immediately after completion of the bridge construction and after one year of service, the hanger loads were evaluated.

The use of FRP composites as an innovative material has been promoted through the FHWA's Innovative Bridge Research and Construction program. In a specific example, the City of Bettendorf constructed a three-span bridge composed of steel reinforced concrete, glass FRP reinforced concrete and a FRP panel bridge deck that is composite with prestressed concrete (PC) girders, the latter deck type being the first of its kind. Short-term and long term monitoring evaluations were conducted to investigate the structural performance of the composite bridge superstructure and were presented in Chapter 4. For the short-term monitoring, the bridge was instrumented with strain transducers to monitor strain levels on the top and bottom flanges of the twelve PC girders, and on the bottom of the FRP panels at four locations. For comparison, strain levels were also collected on six PC girders that supported the steel reinforced concrete deck. From the field monitoring for two consecutive years, it

was found that the FRP panels appear to behave elastically, and the PC girder strains levels remained similar over the test period. Other bridge parameters such as load distribution coefficients were calculated and compared to the AASHTO specifications (i.e., Standard and LRFD) confirming that no significant changes occurred. The neutral axis location, based on the gage location and strain field data, indicated that some intermediate girders may not have fully attained composite action with the FRP deck. However, the measured strains were below the design strains in all cases. From field inspections, signs of deck overlay cracking, aligned with the FRP panel components in the transverse direction of the traffic, were present. In general, the FRP panel deck performed adequately. Only serviceability issues due to debonding after the first year were observed. With respect to the long-term monitoring, strains to detect any possible large load event were collected for approximately 2 years.

In addition, the design, fabrication of FRP panels, construction and field load testing of a temporary bypass bridge was presented in Chapter 4. Due to the deterioration condition of existing steel temporary bridge, FRP deck bridges were investigated as an alternative, due to the light weight for transporting and with few components likely to deteriorate. Prior to field implementation, the novel bridge was load tested using transducers to measure deflection and strain. A load test was performed on the bridge prior to field implementation. Not long after traffic was allowed on the detour bridge, delamination of the deck was observed. The FRP bypass bridge end details at the bridge approach allowed initiation of deck edge damage from tire impact and possibly other environmental factors (i.e., moisture).

There has been particular focus in the area of structural health monitoring on steel and concrete bridges but limited work has been conducted for timber structures. The goal of the work presented in Chapter 5 was to establish a research plan with multiple phases or tasks to develop a smart timber bridge. This conceptual smart timber bridge will monitor all structural materials including the superstructure composed of glulam stringers and transverse glulam deck. Among other sensor types considered, existing and newly developed fiber optic sensors will be attached and/or embedded to the timber members for detecting structural response and damage and/or deterioration. The monitoring system will include a communication system and data reporting. This smart timber bridge approach would supplement current on-site inspections and evaluations specified by the National Bridge Inspection Program. The developed monitoring systems will include beta testing and final deployment of the system.

Only an initial phase of the overall five-year plan was completed. Techniques were developed for embedding and attaching FBG sensors to glulam members and are presented in Chapter 6. Two sets of packages were designed, installed and tested. One set was developed to monitor structural response while the other was developed to isolate the sensor from mechanical strains and to allow for monitoring of deterioration parameters such as moisture content, corrosion, and wood deterioration. Small-scale glulam specimens were internally and externally instrumented with the sensor packages. Nine specimens instrumented with internal and external structural sensor packages were laboratory tested under different loading rates and temperature conditions. Five specimens with non-structural sensor packages were tested under bending loading to verify the lack of connectivity. These tests aided in the selection of appropriate FBG sensor packages. After completing the small-scale specimen testing program, six structural FBG sensor packages and two non-structural packages were selected for further study on a full scale specimen. In the manufacturing of the full scale glulam girder, the installation process and assembly of both sets of internal structural and non-structural packages was improved. Though all sensors were working, additional manufacturing actions caused damage to some of the internal FBG sensors.

7.2. CONCLUSIONS

The previous studies have included field and laboratory tests of bridge members in which sensors were integrated for performance quantification of critical highway bridges successfully monitored the bridge condition. From these studies, the following was concluded:

- For the pedestrian bridge:
  - A sensor system based on fiber optic (FO) was developed for real time feedback during the construction process. Load levels in the bridge were successfully monitored in real time to provide quality control. Some FO sensors were damaged during the bridge assembling activities.
  - With an improved sensor technique installation, this FO sensor system was also implemented for evaluation of a second bridge. Alternatively, surface mountable accelerometers were installed for comparison, corroborating the accuracy of this FO sensing system, where applicable.
- For the FRP panel deck compositely constructed with prestressed concrete girders, the implementation of short-term and long-term field test monitoring systems allowed the

performance evaluation of this innovative state-of-the-art bridge. From both evaluations, the following was noted:

  - For the short-term monitoring, strain and displacement transducers were used to compare the results of field tests over two years. The bridge parameters (e.g., strains, displacements, load distribution factors, etc.) indicated that the bridge performance was consistent over time.
  - During the long-term monitoring period, no unusually large loads were detected by the specialized strain monitoring system. With these results, the bridge performance was also proved to be invariable over time.

- For the FRP panel temporary bypass bridge, the measured strain performance prior and after installation was satisfactory.
- For the smart timber bridge member development, embedded and attached FO sensor packages (systems) for long term and structural health monitoring were developed. The following aspects were highlighted for structural and non-structural sensor package evaluation:
  - The structural FBG sensor packages were generally found to perform consistently in the short term loading tests. Strain levels were lower than predicted and comparable with other conventional sensor systems (i.e., foil strain gages, strain transducers).
  - After long term loading and temperature variation tests, viscoelastic behavior for most structural sensor packages was predominant and consistent. Strain recovery was observed.
  - The non-structural sensor packages performed effectively.

7.3. RECOMMENDATIONS FOR FUTURE WORK

Additional research is recommended based upon the established conclusions:

- Embedded mechanical strain sensors should be installed before manufacturing high-strength hanger rods or cables for segmental construction of bridge superstructures. In addition, the manufacturer should be involved with the installation of fiber optic sensors or other specialized sensors, development of these smart members, and package installation technique design. Specimens should be evaluated for performance to select the sensor and package type. Results of the tests should be compared to the proven test methodology presented in this work (i.e., use of externally mounted accelerometer, vibration test protocol) before deployment.
- Testing of the Bettendorf Bridge span composed of FRP deck panels and prestressed girders indicate that the composite action was partially attained. Additionally, the sensors used for long

term monitoring were influenced by uncontrolled air temperature, varying the maximum strain levels obtained under ambient traffic. Due to these issues, the following is recommended:

- Improve the level of the composite action. Shear pocket spacing should be decreased along the length of the girder top flange. For laboratory testing, additional embedded sensors should be installed in the transition between the panel and the grout to verify the integrity of the composite cross section.
- Improve the long-term monitoring system by using new sensor technology capable to compensate or correct the temperature variations. Develop software for performance evaluation and reporting.

- To address the possible sources of damage and survivability of the sensor packages studied in the smart timber bridge member development, the following is recommended:
  - A review of available sensors for measuring structural (strains) and deterioration (moisture, ferric ion, lignin loss) parameters should be conducted to ensure that the general types of structural and non-structural packages could be adapted. With the appropriate identified sensor types, small scale specimens should be fabricated at a commercial facility. A testing program including bending tests with variable rate of loading and temperatures to evaluate the sensor packages performance should be conducted. Testing of the specimens with variable environmental conditions should be performed.
  - Evaluation of the constructability for various sensor types should be conducted. Testing should also include the installation of electrical-type gages and the above mentioned structural and deterioration-type sensors. This testing should be completed on small scale specimens fabricated in a commercial facility.
  - To complete the investigation, adhesive and package combinations should also be evaluated for fatigue performance. A full-scale beam instrumented and fabricated at the commercial facility should be tested under service levels of load for up to 1,000,000+ cycles.

ACKNOWLEDGMENTS

The author would like to express her deepest gratitude to Dr. Terry Wipf and Dr. Brent Phares for their continuous help and guidance, without them this dissertation would not have been possible. The author would like to thank the committee members, Dr. Wayne Klaiber, Dr. Loren Zachary and Dr. Douglas Stokke, for their special interest and input in this work. Thanks also to Mr. Douglas Wood, ISU Research Laboratory Manager, for his field and laboratory assistance during diverse stages of this work. Thanks to the Iowa Department of Transportation, City of Bettendorf and Forest Product Laboratory for their contribution to the different projects. Finally, the author also likes to thank to her parents, Emma and Nestor, and to her husband, Dr. Travis Konda, for their valuable dedication.